DISSERTATION

FACTORS WHICH AFFECT AND LIMIT THE PERFORMANCE OF SUBSTITUTED TRIS(BIPYRIDINE)COBALT(II) COMPLEXES IN DYE-SENSITIZED SOLAR CELLS

Submitted by

Jeremy J. Nelson

Department of Chemistry

In partial fulfillment of the requirements

for the Degree of Doctor of Philosophy

Colorado State University

Fort Collins, CO

Fall 2007

COLORADO STATE UNIVERSITY

October 12, 2007

WE HEREBY RECOMMEND THAT THE DISSERTATION PREPARED UNDER OUR SUPERVISION BY JEREMY NELSON ENTITLED "FACTORS WHICH AFFECT AND LIMIT THE PERFORMANCE OF SUBSTITUTED TRIS(BIPYRIDINE)COBALT(II) COMPLEXES IN DYE-SENSITIZED SOLAR CELLS" BE ACCEPTED AS FULFILLING IN PART THE REQUIREMENTS FOR THE DEGREE OF DOCTOR OF PHILOSOPHY.

Committee on Graduate Work

Prof. Eugene Chen

Prof. Bruce Parkinson

Prof. James Sites

Prof. Grzegorz Szamel

Prof. C. Michael Elliott, Advisor

Prof. Anthony Rappé, Department Chair

ABSTRACT OF DISSERTATION

FACTORS WHICH AFFECT AND LIMIT THE PERFORMANCE OF SUBSTITUTED TRIS(BIPYRIDINE)COBALT(II) COMPLEXES IN DYE-SENSITIZED SOLAR CELLS

Significant efforts were made towards the development of a novel, solid state dye-sensitized solar cell (DSSC) with a thin layer of cobalt redox polymer on the surface of the photoanode. The intent was to utilize atom transfer radical polymerization (ATRP) to grow a surface-bound polymer based on a cobalt tris(bipyridine) type complex which was only 1-10 monolayers thick. Ultimately, a thin cobalt redox polymer film was successfully grown in a surface-initiated polymerization. However, it is unlikely that the polymerization reaction proceeded in a controlled/living manner or, in fact, that it occurred by way of an ATRP-type mechanism at all. SEM and XPS experiments suggest that the polymerization was initiated at the surface by the dye, but that the active radical was typically not well-deactivated, resulting in isolated regions of uncontrolled polymer growth. Over time (approximately 10 hours), these islands of polymer merged, forming a fairly pinhole-free film on the macroscopic surface of the titania layer. Although reproducible, the film impaired photoanode performance in DSSC iV experiments. Whether it did so because of a reduced photoactive surface area or because of an intrinsic electrical resistance on the part of the polymer remains unclear.

A suite of DSSC characterization experiments was developed which could be rapidly performed on a standard two electrode sandwich cell. In combination with a novel technique for mediator replacement without cell disassembly, this suite was utilized

to probe the influence of a variety of parameters on DSSC functioning in order to elucidate the processes limiting performance in cells mediated by cobalt complexes. The results of this study clearly implicate diffusion of cobalt(III) to the cathode as frequently being rate-limiting. Strategies to alleviate this condition include increasing the cobalt(III) concentration as well as lowering the solvent viscosity. A somewhat unexpected result of the flow-through study is that TiO_2 underlayers or $TiCl_4$ treatments have a surprisingly small effect on the performance of DSSCs, despite their dramatic effect on dark currents. This may be a further indication that diffusion of cobalt(III) – and not recombination across the FTO surface – is performance-limiting in cobalt mediated DSSCs.

A novel three electrode DSSC experiment, modified from two existing techniques, was devised and implemented in order to study cathode behavior in cobalt-mediated DSSCs. The new experiment incorporated a split photoanode in conjunction with a customized potentiostat circuit to allow for simultaneous monitoring of cathode potential, photoanode potential and cell current while still maintaining the thin electrode separation of the standard sandwich cell configuration. Interestingly, DSSCs with poor cathodes, characterized by decreased photocurrent and/or fill factor, exhibited only modest charge transfer overpotentials (or none at all) on the cathode. Even more perplexing, mass transfer overpotentials were not observed, even in clearly diffusion-limited cases. Whether these results are due to a deficiency in the experiment or are a consequence of the DSSC system being extremely sensitive to very small overpotentials is still uncertain.

The possibility of mass transfer limitations in typical cobalt-mediated DSSCs was examined from a theoretical standpoint. Although conventional electrochemical models

do not predict mass transfer of cobalt(III) to be a problem, actual DSSCs are likely more complicated than standard models of relatively simple systems. Two hypotheses were developed and examined. The first supposed that catalytic "islands" on the cathode were responsible for observed photocurrents but were simply not sufficiently numerous to provide adequate surface area for cobalt(III) reduction. However, experiments using cathodes intentionally fabricated to behave in this manner (catalytic gold nanoclusters on relatively inert FTO glass) did not support this hypothesis. The second hypothesis reasoned that diffusion of cobalt(III) through the mesoporous titania layer of the cell was hampered by the layer's small pore size, tortuosity, or both. Preliminary experiments using a modified rotating disk electrode indicate that this is very likely the case. Although further research is required to accurately quantify the effect, initial considerations and results suggest that the effective diffusion coefficient (uncorrected for porosity) of cobalt bipyridine complexes through mesoporous titania films is on the order of 1×10^{-7} cm^2 s^{-1} or less.

Jeremy Nelson
Chemistry Department
Colorado State University
Fort Collins, CO 80523
Fall 2007

ACKNOWLEDGEMENTS

Obviously, the research presented herein benefited greatly from a good number of persons, both directly and indirectly. Naturally enough, I would like to first and foremost acknowledge the help of my advisor, Prof. C. Michael Elliott, not just for his scientific expertise (which is considerable) but also for his character. In my book, "character" takes on a meaning less similar to "eccentric" and more akin to "integrity" and "quality of person," and in this regard Mike has an overwhelming abundance of the stuff.

Of course, I would also like to acknowledge the assistance given to me by the other members of my research group, both scientific and otherwise (i.e., helping to keep me sane – relatively, at least). Other professors here have also been of assistance (Prof. Bruce Parkinson, in particular), as have all of the scientific support staff (Mr. Pat McCurdy, Mr. Elden Burk and Mr. Chris Rithner, among others). The incredibly helpful secretarial staff has also been a real boon.

Lastly, but just as importantly, I would like to thank my friends and family, not so much for their direct contributions to my research, but for their presence in my life and the influence they have had in shaping me as a person. We are the company we keep, and I feel I have kept some pretty damn good company. In particular, I would like to thank my parents: for their love, their grammar, and for showing me what character is all about.

And briefly, to the normally lackluster fortune-cookie people, for their inspiration that "commitment is the daily triumph of integrity over skepticism." And to ol' Murph, for always being there...

TABLE OF CONTENTS

LIST OF SYMBOLS AND ABBREVIATIONS

$A_{1OH}N3$	"Amphiphilic N3"-type dye with two 1-carbon chains terminating in an alcohol
$A_{7OH}N3$	"Amphiphilic N3"-type dye with two 7-carbon chains terminating in an alcohol
$A_{7\alpha BE}N3$	"Amphiphilic N3"-type dye with two 7-carbon chains terminating in an αBE
APCE	Absorbed photo-to-current conversion efficiency
ATRP	Atom transfer radical polymerization
CB	Conduction band
CMRP	Cobalt-mediated radical polymerization
cP	Centipoise
CRP	Controlled/"living" radical polymerization
dAb	Diacrylate bipyridine
dcb	Dicarboxy bipyridine
DCM	Dichloromethane
diol	Dialcohol bipyridine (7-carbon chain)
$diol_{1C}$	Dialcohol bipyridine (1-carbon chain)
dMA	Dimethacrylate bipyridine
DMB	4,4'-dimethyl-2,2'-bipyridine
dtb	Di(tert-butyl) bipyridine
D_x	Diffusion coefficient of species X
E_F	Fermi energy
EtOH	Ethanol
E_{xx}	Potential of xx
$E_{xx,yy}$	Potential of xx, relative to potential of yy
FF	Fill factor
FTO	Fluorine-doped tin(IV) oxide

GBL	γ-Butyrolactone
HOMO	Highest occupied molecular orbital
hν	Photon of light
i	Current
IMPS	Intensity modulated photocurrent spectroscopy
IMVS	Intensity modulated photovoltage spectroscopy
IPCE	Incident photon-to-current conversion efficiency
ITO	Indium/tin oxide
iV	Current-voltage
J_{sc}	Short circuit current density
LDA	Lithium diisopropyl amide
LUMO	Lowest unoccupied molecular orbital
MEHQ	Monomethyl ether hydroquinone
MeOH	Methanol
MMA	Methyl methacrylate
NMP	Nitroxide-mediated polymerization
NMR	Nuclear magnetic resonance spectroscopy
OCVD	Open circuit voltage decay
PC	Propylene carbonate
PN	Propionitrile
PRE	Persistent radical effect
RAFT	Reversible addition-fragmentation transfer polymerization
RDE	Rotating disk electrode
RTIL	Room temperature ionic liquid
SEM	Scanning electron microscopy
TBP	tert-Butylpyridine
terpy	2,2':6',2''-Terpyridine
THF	Tetrahydrofuran
UV	Ultraviolet
V_{oc}	Open circuit voltage
XPS	X-ray photoelectron spectroscopy

αBE-bpy	Di(α-bromoester) bipyridine
αBE-dye	$Ru(dcb)_2(\alpha BE\text{-}bpy)(PF_6)_2$
δ	Hydrodynamic boundary layer thickness
η	Efficiency of DSSC; overpotential of electrode
η_{CT}	Charge transfer overpotential
η_{MT}	Mass transfer overpotential
λ	Wavelength

Chapter 1

A Brief Introduction to Dye-Sensitized Solar Cells

Introduction

With over 10^{12} terajoules of sunlight striking the surface of the earth every year, the potential of the sun to meet the world's current and future energy demands is, for all practical purposes, limitless.[1] One strategy for harvesting this energy is the direct conversion of sunlight to electrical power (e.g., photovoltaic technology).[2, 3] Although power conversion efficiencies of electrical solar cells have risen dramatically over the last few decades, the development of cost-efficient cells has proven difficult.[2, 4] In 1991, O'Regan and Grätzel announced the realization of a new type of solar cell which may

potentially offer reasonable power conversion efficiency at relatively low cost.[5] Dubbed the "dye-sensitized solar cell" (DSSC), it has continued to attract much interest, with the result that significant progress has since been made towards improving the performance and understanding the underlying principles of this novel photovoltaic device.[6-8]

Current scientific efforts are mainly directed along two separate lines of inquiry: refinement of the solar cell so that it is better suited for eventual commercialization and fundamental studies to more fully understand the complex mechanisms that govern the operation of the cell.[4, 8] The goals of the commercialization strategy are primarily to lower the manufacturing cost of the cell and improve the operation lifetime of the device.[9, 10] Strategies for lowering DSSC cost include the substitution of the more expensive components of the cell (e.g., ruthenium and platinum metals, transparent conducting glass) as well as the development of low-cost manufacturing processes (such as roll-to-roll processing of titania photoanodes).[9, 11, 12] An approach directed towards the goal of extended device lifetimes is the development of a solid state DSSC, thereby eliminating the leakage and sealing issues problematic of the current manifestation of the DSSC which utilizes a volatile, solution-phase hole transport material.[10, 13, 14] The aims of the second line of investigation include a better understanding of the charge separation mechanisms and the origin of the photovoltage produced by the cell.[6, 8, 15, 16]

The research presented herein is similarly directed along the same two lines. In the second chapter, efforts to fabricate a solid state DSSC containing a thin polymer film based on tris(bipyridine)cobalt(II) are detailed. The remaining chapters describe studies focused on elucidating the fundamental operation and shortcomings of solution-phase tris(bipyridine)cobalt(III) complexes in DSSCs. Before delving into this work, a brief

introduction to the construction of DSSCs, their mechanism of operation and their present limitations is in order.

Components of DSSCs

Overview

A dye-sensitized solar cell comprises three primary components: a photoanode (PA), a dark cathode (DC) and a redox mediator (M).[17] This is shown pictorially in **Figure 1**. Illumination is nearly always directed through the photoanode, which itself is composed of three parts: a transparent conducting oxide (TCO) glass substrate, a thin layer of nanocrystalline TiO_2 and a monolayer of a light absorbing dye.[17] In DSSCs, the photoanode is the most innovative component of the cell and is where the "magic" of the cell really lies.[18] Dye molecules on the surface of the titania absorb incident photons and inject the photoexcited electrons into the conduction band (CB) of the titania.[18] It has been demonstrated that the titania film, by virtue of its small nanoparticles (~20 nm on average) and the liquid electrolyte, is not capable of supporting a macroscopic electric field.[19] Therefore, the excited electrons, once injected, diffuse towards the TCO substrate in a so-called random walk fashion.[20] Upon arrival at the TCO substrate, the electrons experience the electric bias of the cell and are free to travel through the circuit as electric current. After traveling through the circuit, electrons arrive at the dark cathode and are transferred to the oxidized mediator (i.e., the mediator is reduced at the cathode).[5] The dark cathode is simply a conducting surface on which the reduction of oxidized mediator is facile (typically platinum metal).[12, 21] The third component of the cell, the redox mediator serves to electrically connect the photoanode and dark cathode by shuttling

electrons (or, in solid state DSSCs, holes) between the two electrodes.[22] Reduced mediator (formed at the cathode) diffuses into the porous, nanocrystalline photoanode and reduces the photooxidized dye, thereby completing the electrical circuit. In this way, DSSCs are able to convert light into electrical power.

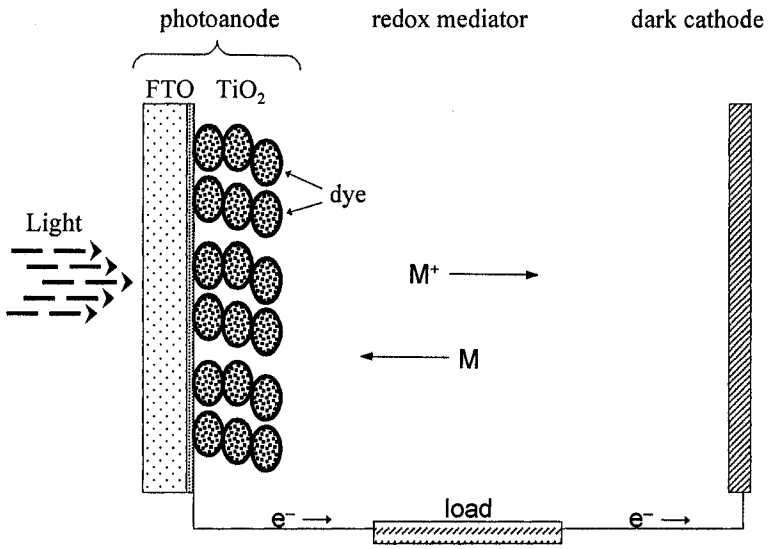

Figure 1. The major components of a DSSC (not to scale).

Transparent conducting oxide glass

As previously mentioned, illumination is generally directed through the cell from the photoanode side.[17] Therefore, a transparent substrate is required to allow as much light as possible to reach the light-absorbing dye. Transparent conducting oxide (TCO) glass substrates are ideal for this purpose as they are nearly as transparent as regular SiO_2 glass and are sufficiently conductive so as to serve as electrical leads to the exterior circuit. TCO glass is primarily SiO_2 glass, but with a thin layer of a conducting oxide on

its surface. In DSSCs, fluorine-doped tin(IV) oxide (FTO) is the conducting oxide most frequently used, although indium/tin oxide (ITO) may also be used.[17]

Nanocrystalline titania

A thin film of nanocrystalline titania (TiO_2) is deposited onto the TCO substrate and consists of a network of randomly distributed spheres of anatase TiO_2 with an average diameter usually on the order of 10-20 nm.[17, 23] Although difficult to quantify, the pores which result are generally assumed to be on the order of 2-50 nm and, as such, the film is usually regarded as being mesoporous.[23, 24] The total film thickness of the titania varies, but is usually between 4 and 10 μm.[20, 23, 25] The usual method for fabricating this film is to "doctor-blade" (a method akin to screen-printing) a thin layer of colloid using two strips of adhesive tape as spacers to control the thickness.[9, 23] Once the colloid is fairly dry, the tape is removed and the anode is baked at 450 °C to remove organic components of the colloid and sinter the TiO_2 particles.

The primary function of the TiO_2 film is to serve as a high surface-area scaffold for the light-absorbing dye.[5] As the dye is adsorbed as a monolayer on the titania surface, a large surface area is required for maximal light absorption and power conversion efficiency. An unforeseen consequence of the mesoporous film is that it does not support any macroscopic electric fields when wetted with liquid electrolyte (i.e., redox mediator), a fact which likely facilitates efficient redox mediation and may have important ramifications for DSSCs with solid state mediators.[19]

Dye

As the light absorbing component of the cell, the dye serves a critical role and must meet several criteria.[18] Firstly, the dye must possess a high molar extinction coefficient (i.e., it must absorb light efficiently) for wavelengths in the visible portion of the spectrum, preferably extending well into the longer wavelengths of the red. The most popular, N3-type (defined below) dyes possess extinction coefficients on the order of 14,000 M^{-1} cm^{-1}.[17] Secondly, the energy levels of the dye ground (D^+/D) and excited states (D^+/D^*) must be appropriately aligned so that charge injection from D^+/D^* into the CB of the TiO_2 is thermodynamically favorable, but not so large in magnitude that a significant portion of the photovoltage is lost during the charge injection reaction. Thirdly, the oxidized dye must react slowly with injected electrons in the TiO_2 CB and rapidly with the redox mediator in order to minimize counterproductive charge recombination within the cell (*vide infra*).

By far, the most common and successful dyes in DSSCs are based on ruthenium polypyridyl complexes and may be categorically referred to as "N3-type" dyes, named for the N3 dye which was used nearly exclusively ca. 15 years ago and continues to be among the most popular today.[17, 18] The N3 dye, *cis*-di(thiocyanato)bis(2,2'-bipyridyl-4,4'-dicarboxylate)ruthenium(II), and related compounds adsorb strongly to the TiO_2 surface through one or more carboxylate groups on the bipyridine rings.[18] They feature broad absorption peaks in the visible region of the spectrum (peak maximum at 535 nm for N3) and inject photoexcited electrons on pico- to femtosecond time scales (often <100 fs) with near quantum efficiency, due largely to the first excited state orbitals (or LUMO) being located on the bipyridine ligands (i.e., the lowest energy electronic transition is a

metal-to-ligand-charge-transfer, or MLCT band).[18, 26, 27] Conveniently, the HOMO is localized away from the TiO_2 surface (calculated to be shared by both the metal and thiocyanato ligands), a fact which is likely responsible for the slow recombination kinetics of these dyes with photoinjected electrons and may also facilitate their reduction by solution-phase mediators.[18, 28]

Cathode

Generally speaking, the cathode is the component of the cell with the fewest requirements and the lowest degree of specialization. The function of the cathode is simply to reduce the oxidized form of the mediator.[21, 25] Therefore, the only *a priori* requirements are that the cathode be conductive and that it possess sufficiently fast heterogeneous electron transfer kinetics with the redox mediator so that photogenerated cell currents may be delivered with a minimum of overpotential required.[21, 25] In addition, as the illumination is typically from the photoanode side, a reflective cathode is typically used in order to maximize light absorption in the cell.[17, 21]

Due to the prevalence of the I^-/I_3^- redox couple in DSSCs (discussed below), cathodes based on platinum metal are used almost exclusively for the simple reason that no other surfaces exhibit comparable catalytic activity for the reduction of I_3^-.[29] As already stated, typically a mirrored platinum cathode is used for enhanced light absorption. However, FTO cathodes with platinum nanoclusters have also been used, primarily with the intent of lowering cell cost by decreasing overall platinum loading.[21] As cost is the main disadvantage of platinum cathodes, some effort has also been made to

investigate the use of carbon-based cathodes, which show moderate but generally not sufficient catalytic activity for I_3^- reduction.[21, 29]

Redox mediator

The function of the mediator (M) is to shuttle electrons from the cathode to the oxidized dye on the photoanode surface.[6, 30, 31] Alternately, the mediator may be described as the hole-transport material, responsible for conducting positively charged holes (generated in the form of a photooxidized dye molecule) to the cathode.[31, 32] Either way, its function is the same and the thermodynamic requirements for this task are not difficult to meet.[22, 33, 34] The reduction potential of the mediator (M^+/M) should be negative of (higher in energy than) the reduction potential of the dye (D^+/D) by an amount sufficient to drive the electron transfer from M to D^+ at a fast rate – quick reduction of the dye is important in order to avoid recombination of the photoinjected electron with oxidized dye.[22, 34] However, it is important that the reduction potential of the M^+/M redox couple not lie too far negative (too high in energy) as the maximum attainable voltage of the cell is dependent, in part, on the reduction potential of the mediator and decreases as the reduction potential becomes more negative.[22] Broadly speaking, finding compounds that meet these two thermodynamic parameters is not particularly difficult.

Far more demanding are the contrasting kinetic traits required for proper DSSC functioning.[33] As already stated, reduction of the mediator at the cathode should be rapid, as should the oxidation of the mediator at the photoanode (alternately stated, the reduction of the photooxidized dye). These two processes are necessary for efficient

DSSC operation, however other processes are possible within the cell but are undesirable as they impede cell performance.[29, 33, 34] Accordingly, the rates of these undesirable reactions will ideally be very slow. The two reactions of greatest concern are the reduction of the oxidized mediator by electrons in the TiO_2 CB and by electrons in the FTO CB.[33] Both of these reactions are often referred to as "recombination" reactions, a term borrowed from the study of semiconductor photovoltaics to describe the undesirable annihilation of a previously photoseparated electron/hole pair. Due to the deliberately high surface area of the TiO_2, the reaction of its CB electrons is particularly important.[33] Recombination through exposed regions of FTO is also a concern, despite the fact that relatively little of the FTO surface is not covered by TiO_2, as the concentration of electrons is particularly high at the FTO surface.[33] These kinetic constraints are summarized below:

a.	$M^+ + e^-_{DC} \rightarrow M$	(fast)
b.	$M + D^+ \rightarrow M^+ + D$	(faster than **e.**)
c.	$M^+ + e^-_{TiO2} \rightarrow M$	(slow)
d.	$M^+ + e^-_{FTO} \rightarrow M$	(slow)
e.	$D^+ + e^-_{TiO2} \rightarrow D$	(slower than **b.**)

With such demanding criteria required of a redox mediator, it is hardly surprising that few chemical species have been found that are capable of serving in this capacity.[12, 33, 34] In fact, nearly all DSSCs utilize I^-/I_3^- as the redox mediator as it is far and away the best mediator known.[12, 22, 23, 34] Other halogens and pseudohalogens have also been studied but remain inferior.[22] Recently, in our group as well as others, certain cobalt(II) complexes coordinated with polypyridine derivatives have been found to function reasonably well in the role of mediator but still fall short of the high standard attained by I^-/I_3^-.[12, 34]

Despite the superior performances of I^-/I_3^-, it is not without several shortcomings, most of which are related to the eventual commercialization and widespread distribution of DSSCs.[10, 33] Iodide/triiodide requires the use of platinum as a cathode material simply because no other surfaces are sufficiently catalytic towards the reduction of I_3^-.[21] As previously mentioned, platinum is an expensive metal which increases the cost of the DSSC. Furthermore, I^-/I_3^- is corrosive towards gold and other metals, making it difficult to implement current collectors within the cell (desirable as the resistivity of FTO, while low, is significant over areas larger than ~1 cm^2).[33] In addition, I^-/I_3^- requires careful, long-term sealing of the cell in order to prevent the loss of volatile components.[10, 33] Typical DSSCs utilize I^-/I_3^- dissolved in a high-boiling-point organic solvent which nevertheless has a non-zero vapor pressure and will evaporate over time.[10, 35] Furthermore, I_3^- exists in an equilibrium ($I_3^- \leftrightarrow I^- + I_2$) with I_2, a volatile species itself.[33] The most successful efforts to alleviate these sources of volatility utilize room temperature ionic liquids, which introduce new concerns with environmental safety and still require hermetic sealing.[35] Another disadvantage of I^-/I_3^- is that its reduction potential, while adequate, is not as positive (lower in energy) as would be ideal.[22] As previously stated, a too negative reduction potential unnecessarily limits the maximum voltage attainable by the cell. A final disadvantage of I^-/I_3^- is that it is not modifiable.[33] Whereas reduction potentials and other properties of cobalt complexes, for example, may be rationally tuned through adjustment of their ligands, no such mechanism exists with I^-/I_3^-.[12] This has disadvantages for both commercialization (no ability to optimize the reduction potential) as well as for fundamental studies of essential redox mediator properties (size, reduction potential, heterogeneous electron transfer kinetics, etc.).

Additives to the electrolyte

In addition to the redox mediator, various other compounds have been added to the liquid electrolyte in an effort to increase cell performance. Two of the most common are lithium ion (Li^+) and 4-*tert*-butylpyridine (TBP). The addition of Li^+ has been shown to facilitate charge injection into the conduction band of the TiO_2 through a mechanism involving intercalation of Li^+ into the titania nanoparticles and subsequent shifting of the titania flatband potential to more positive values.[36] This effect is especially important for dyes with excited states very close in energy to the flatband potential of TiO_2.[36] DSSCs with TBP in the electrolyte frequently exhibit enhanced performance through improved fill factors (FFs, *vide infra*) and larger open circuit voltages (V_{oc}, *vide infra*).[17, 37] The mechanism by which TBP improves cell performance is not well understood and remains a subject of investigation and debate. Proposed mechanisms include: reduced recombination at the photoanode surface due to a steric blocking effect caused by adsorption of TBP onto the surface,[17, 38, 39] negative shift of the TiO_2 flatband potential due to basicity of TBP,[40, 41] reduced recombination resulting from interaction of TBP with I_3^- which lowers concentration of I_3^- at the photoanode surface,[42] effective shifts of TiO_2 flatband potentials through interactions with Li^+ which prevent its adsorption onto the titania surface,[43, 44] and stabilization of N3 dye through suppression of the thiocyanato ligand (SCN^-) loss mechanisms[42] (anecdotally, the vast array of hypotheses underscores the incredible complexity of the DSSC system and the multitude of often interdependent kinetic processes which must conspire to result in a functioning cell). Of course, other additives have been researched but are less common and will not be covered here.

Titania underlayers

Although not common, the use of a compact (i.e., not nanocrystalline) layer of titania has been experimented with in an effort to reduce losses due to recombination pathways at the FTO surface.[45-47] The underlayer is applied as a uniform coating over the FTO surface prior to deposition of the nanocrystalline TiO_2 layer. The most common method utilizes the spray pyrolysis technique developed by Kavan and Grätzel.[48] The resulting films are typically 50-500 nm in thickness, sufficient to block the direct electron transfer from FTO to solution-phase redox mediators.[45, 47] Generally speaking, these films are not necessary with I^-/I_3^- mediated cells but have been found useful with some alternative mediators based on cobalt(II) coordination complexes.[47, 49]

Light-scattering layers

Although not commonly employed for basic research purposes, optimized DSSCs may include a light-scattering layer of larger titania nanoparticles, typically with an average diameter of 200-400 nm.[46, 50, 51] The primary purpose of this layer is to increase light absorption by lengthening the effective pathlength of light through the cell.

Spacers

Most frequently, DSSCs are constructed with the photoanode and cathode placed directly onto one another.[17, 23] More recently, DSSC assemblies have often included the use of a plastic spacer in the cell between the cathode and photoanode.[46, 49, 52, 53] This serves both to seal the cell as well as to prevent direct contact of the photoanode with the

cathode, useful for eliminating electrical shorts between the two electrodes.[54] The spacers are kept thin (1-100 microns), however, so as to not overly exacerbate any performance limitations due to diffusion of mediator across the cell.

DSSC Evaluation

The iV experiment

While a variety of techniques exist for the evaluation of DSSCs, the most frequently performed experiment is the current-voltage experiment (iV).[7, 27, 55] In this experiment, a DSSC is assembled in the so-called "sandwich cell" configuration, which is done by simply placing the cathode onto the photoanode (with or without a spacer).[7, 23] Mediator solution is subsequently introduced to the cell, typically by applying a few microliters to the edge of the cell and allowing capillary action to wick the solvent into the volume between the electrodes. More complicated methods may also be utilized, especially when sealing of the cell is desired.[46]

Once assembled, the cell is illuminated and an external device, such as a sourcemeter or potentiostat (wired to behave as a sourcemeter), is used to control the voltage difference across the cell while simultaneously monitoring the current. The resulting data are plotted as shown in **Figure 2**, with applied voltage on the horizontal axis and current or current density on the vertical axis. From one iV curve, several different parameters are extracted. The point at which the curve crosses the x-axis is referred to as the open circuit voltage (V_{oc}) and represents the maximum photovoltage that the cell is capable of generating. Likewise, the y-intercept is the point of maximum photocurrent, termed the short circuit current density (J_{sc}). A third parameter, the fill

factor (FF), is calculated by dividing the point of maximum power density (P_{max} = V x J) by the theoretical maximum power density that the cell is capable of (P_{theo} = V_{oc} x J_{sc}). The fill factor is useful as a way to quantify the shape of the iV curve (*vide infra*). The fourth parameter is the maximum efficiency of the cell (η). This is calculated by dividing the point of maximum power density (P_{max}) by the incident light power density (most often calibrated to AM 1.5 (1 sun), equal to 1000 W m^{-1} or 100 mW cm^{-2}).

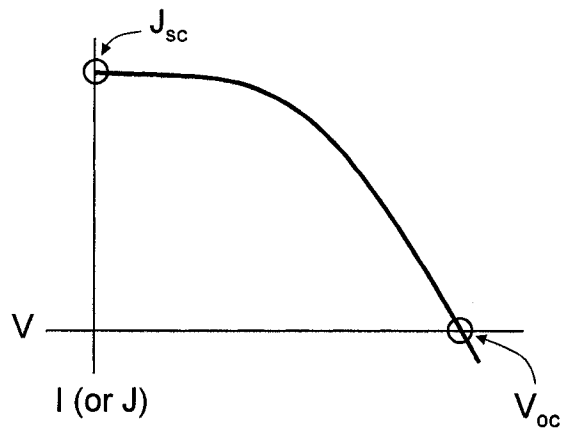

Figure 2. A sample iV curve. The x-axis is potential, the y-axis is current (I) or current density (J).

Together, the four parameters do an excellent job of quickly evaluating DSSC performance but do not generally yield specific information about individual mechanisms within the cell. In this respect, the iV experiment is somewhat analogous to cyclic voltammetry in that both are invaluable tools for the quick (but less quantitative) characterization of their respective systems. Maximum efficiency is the parameter which best reflects the bottom-line performance of the cell and is of greatest concern for the real world application of the cell (aside from cost).[4] The much-touted target efficiency of any solar conversion device is 10%. Although the best recorded efficiencies meet or exceed

this value (10-11%), typical devices do not.[1, 2, 4] Furthermore, scale-up is a very large issue with DSSCs and generally results in even lower values for η.[1] Comparison of V_{oc} and J_{sc} values is entirely straightforward: the larger the better. Typical DSSCs have a V_{oc} around 700 mV, while J_{sc} ranges more widely (3-15 mA cm^{-2}).

The least intuitive parameter is the fill factor. It quantifies the deviation of the shape of the actual iV curve from an ideal iV curve.[46] In the absence of recombination and significant resistances both internal and external to the cell, the shape of the iV curve would be a perfect rectangle.[46] Real DSSCs, without exception, suffer from one or more of these phenomena and display an iV curve with a rounded corner at higher voltages. The extent of this rounding is reflected by the FF, which decreases from 1 as the recombination and/or resistance gets worse. An excellent realistic FF is 0.7-0.8 but FFs between 0.5 and 0.7 are still very acceptable. For calibration, a straight line between the J_{sc} and V_{oc} results in a FF of 0.25 and is very poor.

Other experiments

Other experiments may be conducted to better elucidate one or more processes occurring within the cell. As a broad category, these experiments frequently do not utilize the sandwich cell configuration and are generally focused on a particular aspect of the DSSC (e.g. charge injection efficiency, recombination kinetics). The number of reported techniques is too large to list comprehensively here, but they include IPCE[17, 56], APCE[57], transient absorbance[22, 58], OCVD[54, 59], IMVS[41], IMPS[60, 61], impedance spectroscopy[19], cyclic voltammetry[12] and transient cell experiments[46] (acronyms are defined in the List of Symbols and Abbreviations, page *x*). Space considerations prohibit

further description of these experiments here, but the introduction to Chapter 3 covers select experiments in somewhat greater detail. Also, more information about specific experiments is easily obtained by consulting the cited references.

Cobalt Complexes in DSSCs

Previous research

Clearly, the sizable list of undesirable properties of I^-/I_3^- underscores the need for research into alternative redox mediators for DSSCs (*vide supra*) However, few compounds display the appropriate kinetics to serve adequately in this capacity.[33, 34] Of this select group are certain coordination complexes of cobalt(II).[12, 34] Early efforts with cobalt complexes were, for the most part, disappointing.[34, 62] Nusbaumer et al. were able to achieve very good efficiencies with one cobalt species (~7%), but only at low illumination intensities (1/10 sun) and only with a synthetically complicated ligand.[34] More recently, Sapp et al. reported achieving DSSC performances (at full 1 sun illumination) with certain polypyridine complexes of cobalt that were approximately 80% of the performances displayed by I^-/I_3^- in otherwise identical cells.[12] Although the results were encouraging, maximum efficiencies were still only 1.3%, far below the best DSSCs to date.

Advantages of tris(bipyridine) cobalt(II)

Despite the fact that tris(bipyridine) cobalt(II) complexes have not outperformed I^-/I_3^- to date, they retain a few key advantages over iodide/triiodide. First and foremost, they are modifiable, generally through relatively straightforward synthetic procedures.[12]

The substituents on the 4 and 5 positions of each ring may be customized to rationally affect properties of the entire cobalt(II) complex, including the reduction potential and size of the cation. Therefore, unlike I^-/I_3^-, polypyridyl complexes of cobalt(II) may be fine-tuned to both optimize cell performance and to advance our fundamental understanding of redox mediation processes within a DSSC.

From a practical perspective, tris(bipyridine) cobalt(II) complexes offer other advantages, such as being non-volatile and non-corrosive.[12] Admittedly, the non-volatility of these complexes is somewhat mitigated by the fact that they are still dissolved in a volatile organic phase, but with modification of the polypyridyl ligands so readily conducted, the possibility of redox polymer films based on cobalt is one way to achieve true non-volatility of the redox mediator (see Chapter 2). The non-corrosiveness of cobalt(II) complexes is especially valuable as it allows for research into previously restricted materials (e.g., gold, carbon) for use within the cell. The potential for cheaper cathodes as well as for current collectors within the cell hold advantages for the scale-up and eventual commercialization of DSSCs as well.[12, 33]

Why cobalt(II) complexes work

Phenomenologically, there are two principles reason why cobalt(II) complexes function well as mediators in DSSCs. Firstly, the reduction potential of polypyridyl cobalt(II) complexes is well-suited for use within DSSCs based on N3-type dyes.[12] Secondly, and more importantly, these complexes exhibit an unusual surface dependence with respect to their heterogeneous electron transfer kinetics (regarding the +3/+2 couple only).[12] Specifically, these kinetics are exceptionally slow on metal oxide surfaces,

including the FTO and TiO_2 which constitute the photoanode. On surfaces such as gold, glassy carbon, and platinum, the complexes frequently display very rapid, "quasi-reversible" electron transfer kinetics. This surface dependence makes cobalt(II) complexes, as a class of materials, ideally suited for use within DSSCs.

The origin of this atypical surface dependence is not well understood.[12] It has been known for some time that cobalt(II) complexes typically exhibit extraordinarily slow rates of self-exchange (i.e., $Co^{II} + Co^{III} \rightarrow Co^{III} + Co^{II}$), with a rate constant of 18 M^{-1} s^{-1} for tris(bipyridine)cobalt(II).[63-65] The likely explanation for this lies in the realm of Marcus theory.[66] Cobalt(II) is a d7 metal and, when ligated by polypyridyl-type ligands, adopts a high-spin electron configuration (**Figure 3**).[67] Upon oxidation, the complex assumes a low-spin configuration, a shift which involves a change in bond lengths (due to the depopulation of anti-bonding e_g^* orbitals and increased population of the t_{2g} orbitals) and a concurrent reorganization of the surrounding solvation sphere (Marcus reorganization parameter, λ).[67] Given the extensive reorganization involved, as well as the energy barriers for doing so, it seems reasonable that the reaction occurs relatively slowly. Accordingly, the self-exchange reaction should also occur slowly, as should the heterogeneous electron transfer reaction (essentially just ½ of a self-exchange reaction), which is the relevant reaction in the case of DSSCs.

Nevertheless, while this hypothesis is sufficient to explain why electron transfer may be expected to be slow for cobalt(II) complexes, it does not explain why it is slow on some surfaces and dramatically faster on others (i.e., the surface dependence). The work of Sapp and coworkers may provide a hint.[12] They found that only cobalt complexes with bulky substituents on the pyridine rings were efficient mediators in DSSCs, perhaps

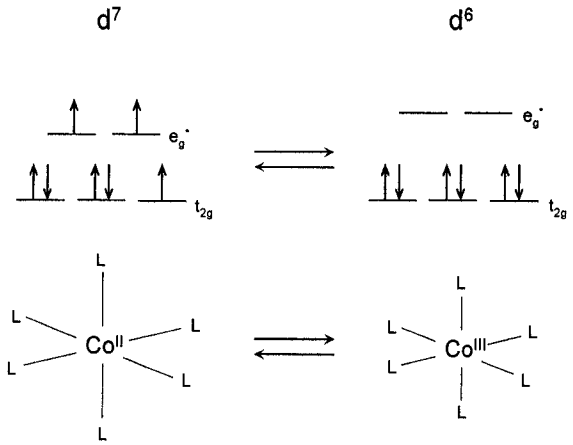

Figure 3. Diagram illustrating the electronic and physical rearrangements which occur upon oxidation of (left) cobalt(II) complexes and reduction of (right) cobalt (III) complexes.

indicating that the degree of electronic coupling between the complex and the electrode surface (hindered with bulkier substituents) may play a significant role in determining the electron transfer kinetics. Still, the question remains as to why other surfaces (such as gold, glassy carbon, and platinum) are affected to such a lesser degree by the steric properties of the polypyridyl ligands.

The answer almost certainly is related to the properties of each surface. In the course of my own research, it has become evident that surface characteristics as well as surface *history* play a large role in determining cobalt(II) behavior. On gold, in particular, cobalt(II) behavior can be influenced by time, polishing procedure, flame, and the phase of the moon (or so it has appeared, at times).[68] In addition, the electron transfer kinetics on platinum are influenced to a large degree by the presence of Li^+ ion (they become even slower).[68] Furthermore, it has been recently discovered that FTO and ITO surfaces become catalytic to the oxidation and reduction of tris(bipyridine) cobalt(II) complexes when their surface is modified by the adsorption of other metal complexes.[69-71] All of these observations indicate that the electrode surface may be the dominant

factor in determining the heterogenous electron transfer kinetics of cobalt complexes, presumably by such characteristics as nanoscopic surface morphology or the thickness of the oxide layer.

Given that a relatively large energy barrier exists for the oxidation and reduction of polypyridyl cobalt(II) complexes (*vide supra*) and that these complexes frequently display extraordinarily slow heterogenous electron transfer kinetics (often to the extent of being effectively chemically inert on the surface), it may be best to regard their oxidation/reduction reactions as *catalytic* processes.[69] As such, electrodes on which cobalt complexes exhibit nearly ideal electron transfer kinetics should be thought of as catalytic surfaces which, through some currently unknown means, avoid/reduce/tunnel through an intrinsic energy barrier for electron transfer and speed up this otherwise very slow reaction.[69]

My Research

The research presented herein comprises two separate lines of investigation, each with its own goals and intentions. The second chapter details efforts to take the first step toward the realization of solid state, cobalt-mediated DSSCs. Taking advantage of the ease with which tris(bipyridine)cobalt(II) may be modified, significant effort was made to integrate these complexes into DSSCs as a redox polymer film. Unfortunately, this effort was not successful, primarily due to the requirement that the film be exceedingly thin and uniform.

The second line of inquiry is described in the subsequent chapters. An array of experimental techniques was utilized in order to identify and understand the factors

which limit the performance of cobalt-based mediators in DSSCs. Insights into the peculiar behavior of tris(bipyridine)cobalt(II) gained from these studies narrow the possible models for describing the fundamental operation of solution-phase cobalt complexes and indicate that mass transfer of cobalt(III) to the cathode is often rate-limiting in this system.

Bibliography

1. Grätzel, M., Photoelectrochemical cells. *Nature* **2001,** 414, 338.

2. Lewis, N. S., Toward Cost-Effective Solar Energy Use. *Science* **2007,** 315, (5813), 798-801.

3. Turner, J. A., A Realizable Renewable Energy Future. In *Science*, 1999; Vol. 285, pp 687-689.

4. Tributsch, H., Dye sensitization solar cells: a critical assessment of the learning curve. *Coordination Chemistry Reviews* **2004,** 248, 1511-1530.

5. O'Regan, B.; Grätzel, M., A low-cost, high-efficiency solar cell based on dye-sensitized colloidal TiO_2 films. *Nature* **1991,** 353, 737-739.

6. Bisquert, J.; Cahen, D.; Hodes, G.; Rühle, S.; Zaban, A., Physical Chemical Principles of Photovoltaic Conversion with Nanoparticulate, Mesoporous Dye-Sensitized Solar Cells. *Journal of Physical Chemistry B* **2004,** 108, 8106-8118.

7. Grätzel, M., Perspectives for dye-sensitized nanocrystalline solar cells. *Prog. Photovoltaics* **2000,** 8, (1), 171-185.

8. Gregg, B. A., Excitonic Solar Cells. *Journal of Physical Chemistry B* **2003,** 107, 4688-4698.

9. Lindström, H.; Holmberg, A.; Magnusson, E.; Lindquist, S.-E.; Malmqvist, L.; Hagfeldt, A., A New Method for Manufacturing Nanostructured Electrodes on Plastic Substrates. *Nano Letters* **2001,** 1, (2), 97-100.

10. Nogueira, A. F.; Longo, C.; De Paoli, M.-A., Polymers in dye sensitized solar cells: overview and perspectives. *Coordination Chemistry Reviews* **2004,** 248, 1455-1468.

11. Hara, K.; Kurashige, M.; Ito, S.; Shinpo, A.; Suga, S.; Sayama, K.; Arakawa, H., Novel polyene dyes for highly efficient dye-sensitized solar cells. *Chem. Commun.* **2003**, 252-253.

12. Sapp, S. A.; Elliott, C. M.; Contado, C.; Caramori, S.; Bignozzi, C. A., Substituted Polypyridine Complexes of Cobalt(II/III) as Efficient Electron-Transfer Mediators in Dye-Sensitized Solar Cells *Journal of the American Chemical Society* **2002,** 124, (37), 11215-11222.

13. O'Regan, B.; Lenzmann, F.; Muis, R.; Wienke, J., A Solid-State Dye-Sensitized Solar Cell Fabricated with Pressure-Treated P25-TiO_2 and CuSCN: Analysis of Pore Filling and IV Characteristics. *Chemistry of Materials* **2002,** 14, 5023-5029.

14. Peter, K.; Wietasch, H.; Peng, B.; Thelakkat, M., Dual-functional materials for interface modifications in solid-state dye-sensitised TiO_2 solar cells. *Applied Physics A - Materials Science & Processing* **2004,** 79, 65-71.

15. Gregg, B. A., Interfacial processes in the dye-sensitized solar cell. *Coordination Chemistry Reviews* **2004,** 248, 1215-1224.

16. Kron, G.; Rau, U.; Werner, J. H., Influence of the Built-In Voltage on the Fill Factor of Dye-Sensitized Solar Cells. *Journal of Physical Chemistry B* **2003,** 107, 13258-13261.

17. Nazeeruddin, M. K.; Kay, A.; Rodicio, I.; Humphry-Baker, R.; Müller, E.; Liska, P.; Vlachopoulos, N.; Grätzel, M., Conversion of Light to Electricity by *cis*-X_2Bis(2,2'-bipyridyl-4,4'-dicarboxylate)ruthenium(II) Charge-Transfer Sensitizers ($X = Cl^-, Br^-, I^-, CN^-$ and SCN^-) on Nanocrystalline TiO_2 Electrodes. *Journal of the American Chemical Society* **1993,** 115, 6382-6390.

18. Hagfeldt, A.; Grätzel, M., Molecular Photovoltaics. *Accounts of Chemical Research* **2000,** 33, 269-277.

19. Zaban, A.; Meier, A.; Gregg, B. A., Electric Potential Distribution and Short-Range Screening in Nanoporous TiO_2 Electrodes. *Journal of Physical Chemistry B* **1997,** 101, 7985-7990.

20. Nelson, J.; Chandler, R. E., Random walk models of charge transfer and transport in dye sensitized systems. *Coordination Chemistry Reviews* **2004,** 248, 1181-1194.

21. Papageorgiou, N., Counter-electrode function in nanocrystalline photoelectrochemical cell configurations. *Coordination Chemistry Reviews* **2004,** 248, 1421-1446.

22. Oskam, G.; Bergeron, B. V.; Meyer, G. J.; Searson, P. C., Pseudohalogens for Dye-Sensitized TiO_2 Photoelectrochemical Cells. *Journal of Physical Chemistry B* **2001,** 105, 6867-6873.

23. Barbé, C. J.; Arendsa, F.; Comte, P.; Jirousek, M.; Lenzmann, F.; Shklover, V.; Grätzel, M., Nanocrystalline Titanium Oxide Electrodes for Photovoltaic Applications. *J. Am. Ceram. Soc.* **1997,** 80, (12), 3157-3171.

24. Rouquerol, J.; Avnir, D.; Fairbridge, C. W.; Everett, D. H.; Haynes, J. H.; Pernicone, N.; Ramsay, J. D. F.; Sing, K. S. W.; Unger, K. K., Recommendations

for the Characterization of Porous Solids. *Pure and Applied Chemistry* **1994,** 66, (8), 1739-1758.

25. Zaban, A.; Zhang, J.; Diamont, Y.; Melemed, O.; Bisquert, J., Internal Reference Electrode in Dye Sensitized Solar Cells for Three-Electrode Electrochemical Characterizations. *Journal of Physical Chemistry B* **2003,** 107, 6022-6025.

26. Anderson, N. A.; Lian, T., Ultrafast electron injection from metal polypyridyl complexes to metal-oxide nanocrystalline thin films. *Coordination Chemistry Reviews* **2004,** 248, 1231-1246.

27. Ellingson, R. J.; Asbury, J. B.; Ferrere, S.; Ghosh, H. N.; Sprague, J. R.; Lian, T. Q.; Nozik, A. J., Dynamics of Electron Injection in Nanocrystalline Titanium Dioxide Films Sensitized with [Ru(4,4'-dicarboxy-2,2'-bipyridine)$_2$(NCS)$_2$] by Infrared Transient Absorption. *Journal of Physical Chemistry B* **1998,** 102, 6455-6458.

28. Rensmo, H.; Lunell, S.; Siegbahn, H., Absorption and electrochemical properties of ruthenium(II) dyes, studied by semi-empirical quantum chemical calculations. *Journal of Photochemistry and Photobiology A: Chemistry* **1998,** 114, 117-124.

29. Papageorgiou, N.; Liska, P.; Kay, A.; Grätzel, M., Mediator Transport in Multilayer Nanocrystalline Photoelectrochemical Cell Configurations. *Journal of the Electrochemical Society* **1999,** 146, (3), 898-907.

30. Pelet, S.; Moser, J.-E.; Grätzel, M., Cooperative Effect of Adsorbed Cations and Iodide on the Interception of Back Electron Transfer in the Dye Sensitizationof Nanocrystalline TiO_2. *Journal of Physical Chemistry B* **2000,** 104, 1791-1795.

31. Kron, G.; Egerter, T.; Werner, J. H.; Rau, U., Electronic Transport in Dye-Sensitized Nanoporous TiO_2 Solar Cells - Comparison of Electrolyte and Solid-State Devices. *Journal of Physical Chemistry B* **2003,** 107, 3556-3564.

32. Grant, C. D.; Schwartzberg, A. M.; Smestad, G. P.; Kowalik, J.; Tolbert, L. M.; Zhang, J. Z., Characterization of nanocrystalline and thin film TiO_2 solar cells with poly(3-undecyl-2,2'-bithiophene) as a sensitizer and hole conductor. *Journal of Electroanalytical Chemistry* **2002,** 522, 40-48.

33. Gregg, B. A.; Pichot, F.; Ferrere, S.; Fields, C. L., Interfacial Recombination Processes in Dye-Sensitized Solar Cells and Methods To Passivate the Interfaces. *Journal of Physical Chemistry B* **2001,** 105, 1422-1429.

34. Nusbaumer, H.; Moser, J.-E.; Zakeeruddin, S. M.; Nazeeruddin, M. K.; Grätzel, M., $Co^{II}(dbbip)_2^{2+}$ Complex Rivals Tri-iodide/Iodide Redox Mediator in Dye-Sensitized Photovoltaic Cells. *Journal of Physical Chemistry B* **2001,** 105, 10461-10464.

35. Wang, P.; Zakeeruddin, S. M.; Comte, P.; Exnar, I.; Grätzel, M., Gelation of Ionic Liquid-Based Electrolytes with Silica Nanoparticles for Quasi-Solid-State Dye-Sensitized Solar Cells. *Journal of the American Chemical Society* **2003,** 125, (5), 1166-1167.

36. Kelly, C. A.; Farzad, F.; Thompson, D. W.; Stipkala, J. M.; Meyer, G. J., Cation-Controlled Interfacial Charge Injection in Sensitized Nanocrystalline TiO_2. *Langmuir* **1999,** 15, 7047-7054.

37. Huang, S. Y.; Schlichthörl, G.; Nozik, A. J.; Grätzel, M.; Frank, A. J., Charge Recombination in Dye-Sensitized Nanocrystalline TiO_2 Solar Cells. *Journal of Physical Chemistry B* **1997,** 101, 2576-2582.

38. Hara, K.; Dan-oh, Y.; Kasada, C.; Ohga, Y.; Shinpo, A.; Suga, S.; Sayama, K.; Arakawa, H., Effect of Additives on the Photovoltaic Performance of Coumarin-Dye-Sensitized Nanocrystalline TiO2 Solar Cells. *Langmuir* **2004,** 20, (10), 4205 - 4210.

39. Shi, C.; Dai, S.; Wang, K.; Pan, X.; Kong, F.; Hu, L., The adsorption of 4-*tert*-butylpyridine on the nanocrystalline TiO_2 and Raman spectra of dye-sensitized solar cells in situ. *Vibrational Spectroscopy* **2005,** 39, 99-105.

40. Hara, K.; Tachibana, Y.; Ohga, Y.; Shinpo, A.; Suga, S.; Sayama, K.; Sugihara, H.; Arakawa, H., Dye-sensitized nanocrystalline TiO2 solar cells based on novel coumarin dyes. *Solar Energy Materials & Solar Cells* **2003,** 77, 89-103.

41. Schlichthörl, G.; Huang, S. Y.; Sprague, J.; Frank, A. J., Band Edge Movement and Recombination Kinetics in Dye-Sensitized Nanocrystalline TiO_2 Solar Cells: A Study by Intensity Modulated Photovoltage Spectroscopy. *Journal of Physical Chemistry B* **1997,** 101, 8141-8155.

42. Greijer, H.; Lindgren, J.; Hagfeldt, A., Resonance Raman Scattering of a Dye-Sensitized Solar Cell: Mechanism of Thiocyanato Ligand Exchange. *Journal of Physical Chemistry B* **2001,** 105, (27), 6314-6320.

43. Nakade, S.; Kanzaki, T.; Kubo, W.; Kitamura, T.; Wada, Y.; Yanagida, S., Role of Electrolytes on Charge Recombination in Dye-Sensitized TiO2 Solar Cell (1): The Case of Solar Cells Using the I^-/I_3^- Redox Couple. *Journal of Physical Chemistry B* **2005,** 109, (8), 3480-3487.

44. Nakade, S.; Kanzaki, T.; Kambe, S.; Wada, Y.; Yanagida, S., Investigation of Cation-Induced Degradation of Dye-Sensitized Solar Cells for a New Strategy to Long-Term Stability. *Langmuir* **2005,** 21, (5), 11414 - 11417.

45. Peng, B.; Jungmann, G.; Jäger, C.; Haarer, D.; Schmidt, H.-W.; Thelakkat, M., Systematic investigation of the role of compact TiO_2 layer in solid state dye-sensitized TiO_2 solar cells. *Coordination Chemistry Reviews* **2004,** 248, 1479-1489.

46. Nusbaumer, H. Alternative Redox Systems for the Dye-Sensitized Solar Cell. Doctor of Philosophy, École Polytechnique Fédérale de Lausanne, Lausanne, 2004.

47. Cameron, P. J.; Peter, L., M., Characterization of Titanium Dioxide Blocking Layers in Dye-Sensitized Nanocrystalline Solar Cells. *Journal of Physical Chemistry B* **2003,** 107, 14394-14400.

48. Kavan, L.; Grätzel, M., Highly efficient semiconducting TiO_2 photoelectrodes prepared by aerosol pyrolysis. *Electrochimica Acta* **1995,** 40, (5), 643-652.

49. Cameron, P. J.; Peter, L., M.; Zakeeruddin, S. M.; Grätzel, M., Electrochemical studies of the Co(III)/Co(II)(dbbip)$_2$ redox couple as a mediator for dye-sensitized nanocrystalline solar cells. *Coordination Chemistry Reviews* **2004,** 248, 1447-1453.

50. Rothenberger, G.; Comte, P.; Gratzel, M., A contribution to the optical design of dye-sensitized nanocrystalline solar cells. *Solar Energy Materials and Solar Cells* **1999,** 58, (3), 321-336.

51. Zhang, Z.; Ito, S.; O'Regan, B.; Kuang, D.; Zakeeruddin, S. M.; Liska, P.; Charvet, R.; Comte, P.; Nazeeruddin, M. K.; Pechy, P.; Humphry-Baker, R.; Koyanagi, T.; Mizuno, T.; Gratzel, M., The electronic role of the TiO_2 light-scattering layer in dye-sensitized solar cells. *Zeitschrift fuer Physikalische Chemie (Muenchen, Germany)* **2007,** 221, (3), 319-328.

52. Klein, C.; Nazeeruddin, M. K.; Di Censo, D.; Liska, P.; Grätzel, M., Amphiphilic Ruthenium Sensitizers and Their Applications in Dye-Sensitized Solar Cells. *Inorganic Chemistry* **2004,** 43, 4216-4226.

53. Wang, P.; Klein, C.; Humphry-Baker, R.; Zakeeruddin, S. M.; Grätzel, M., A High Molar Extinction Coefficient Sensitizer for Stable Dye-Sensitized Solar Cells. *Journal of the American Chemical Society* **2005,** 127, 808-809.

54. Bisquert, J.; Zaban, A.; Greenshtein, M.; Mora-Seró, I., Determination of Rate Constants for Charge Transfer and the Distribution of Semiconductor and Electrolyte Electronic Energy Levels in Dye-Sensitized Solar Cells by Open-Circuit Photovoltage Decay Method. *Journal of the American Chemical Society* **2004,** 126, 13550-13559.

55. Cahen, D.; Hodes, G.; Grätzel, M.; Guillemoles, J. F.; Riess, I., Nature of Photovoltaic Action in Dye-Sensitized Solar Cells. *Journal of Physical Chemistry B* **2000,** 104, 2053-2059.

56. Argazzi, R.; Bignozzi, C. A.; Heimer, T. A.; Castellano, F. N.; Meyer, G. J., Enhanced Spectral Sensitivity fro Ruthenium(II) Polypyridyl Based Photovoltaic Devices. *Inorganic Chemistry* **1994,** 33, 5741-5749.

57. Ferrere, S., New Photosensitizers Based upon $[Fe(L)_2(CN)_2]$ and $[Fe(L)_3]$ (L = Substituted 2,2'-Bipyridine): Yields for the Photosensitization of TiO_2 and Effects on the Band Selectivity. *Chemistry of Materials* **2000,** 12, 1083-1089.

58. Frank, A. J.; Kopidakis, N.; van de Lagemaat, J., Electrons in nanostructured TiO_2 solar cells: transport, recombination and photovoltaic properties. *Coordination Chemistry Reviews* **2004,** 248, 1165-1179.

59. Zaban, A.; Greenshtein, M.; Bisquert, J., Determination of the Electron Lifetime in Nanocrystalline Dye Solar Cells by Open-Circuit Voltage Decay Measurements. *ChemPhysChem* **2003,** 4, 859-868.

60. de Jongh, P. E.; Vanmaekelbergh, D., Investigation of the Electronic Transport Properties of Nanocrystalline Particulate TiO2 Electrodes by Intensity-Modulated Photocurrent Spectroscopy. *Journal of Physical Chemistry B* **1997,** 101, (14), 2716-2722.

61. Dloczik, L.; Ileperuma, O.; Lauermann, I.; Peter, L. M.; Ponomarev, E. A.; Redmond, G.; Shaw, N. J.; Uhlendorf, I., Dynamic Response of Dye-Sensitized Nanocrystalline Solar Cells: Characterization by Intensity-Modulated Photocurrent Spectroscopy. *Journal of Physical Chemistry B* **1997,** 101, (49), 10281-10289.

62. Bonhôte, P.; Grätzel, M.; Jirousek, M.; Liska, P.; Pappas, N.; Vlachopoulos, N.; Von Planta, C.; Walder, L. In *Abstract C2*, Presented at the 10th International Conference on Photochemical Conversion and Storage of Solar Energy (IPS-10), Interlaken, Switzerland, 1994; Interlaken, Switzerland, 1994.

63. Glick, M. D.; Schmonsees, W. G.; Endicott, J. F., Structural Evidence for Variations in the Franck-Condon Barrier to Electron Transfer between Low-Spin Cobalt(II) and Cobalt(III). *Journal of the American Chemical Society* **1974,** 96, (17), 5661-5662.

64. Endicott, J. F.; Brubaker, G. R.; Ramasami, T.; Kumar, K.; Dwarakanath, K.; Cassel, J.; Johnson, D., Electron-Transfer Reactivity in Some Simple Cobalt(III)-Cobalt(II) Couples. Franck-Condon vs. Electronic Contributions. *Inorganic Chemistry* **1983,** 22, 3754-3762.

65. Sutin, N., Theory of Electron Transfer Reactions: Insights and Hindsights. In *Progress in Inorganic Chemistry*, Taube, H.; Lippard, S. J., Eds. John Wiley & Sons, Inc.: 1983; Vol. 30, pp 441-498.

66. Marcus, R. A., Electron Transfer Reactions in Chemistry: Theory and Experiment (Nobel Lecture). *Angewandte Chemie International Edition* **1993,** 32, (8), 1111-1222.

67. Billing, R.; Benedix, R.; Stich, G.; Hennig, H., Calculation of the cobalt(III)/low-spin cobalt(II) reduction potentials of selected amine and diimine complexes. *Zeitschrift für Anorganische und Allgemeine Chemie* **1990,** 583, 157-162.

68. Nelson, J. J.; Elliott, C. M., Unpublished results.

69. Elliott, C. M.; Caramori, S.; Bignozzi, C. A., Indium Tin Oxide Electrodes Modified with Tris(2,2'-bipyridine-4,4'-dicarboxylic acid) Iron(II) and the Catalytic Oxidation of Tris(4,4'-di-tert-butyl-2,2'-bipyridine) Cobalt(II) *Langmuir* **2005,** 21, (7), 3022-3027.

70. Xue, D.; Elliott, C. M.; Gong, P.; Grainger, D. W.; Bignozzi, C. A.; Caramori, S., Indirect Electrochemical Sensing of DNA Hybridization Based on the Catalytic Oxidation of Cobalt (II). *Journal of the American Chemical Society* **2007,** 129, (7), 1854-1855.

71. Scott, M. J.; Nelson, J. J.; Caramori, S.; Bignozzi, C. A.; Elliott, C. M., Cis-Dichloro-bis(4,4'-dicarboxy-2,2'-bipyridine)osmium(II)-Modified Optically Transparent Electrodes: Application as Cathodes in Stacked Dye Sensitized Solar Cells. *Inorganic Chemistry (submitted for publication)* **2007**.

Chapter 2

Research Directed Towards Incorporation of a Cobalt Redox Polymer into Dye-Sensitized Solar Cells

Abstract

This chapter describes efforts to take the first step towards a novel, solid state DSSC with a thin layer of cobalt redox polymer on the surface of the photoanode. The intent was to utilize atom transfer radical polymerization (ATRP) to grow a surface-bound polymer based on a cobalt tris(bipyridine) type complex which was only 1-10 monolayers thick. Ultimately, a thin cobalt redox polymer film was successfully grown in a surface-initiated polymerization. However, it is unlikely that the polymerization reaction proceeded in a controlled/living manner or, in fact, that it occurred by way of an

ATRP-type mechanism at all. SEM and XPS experiments suggest that the polymerization was initiated at the surface by the dye, but that the active radical was typically not well-deactivated, resulting in isolated regions of uncontrolled polymer growth. Over time (approximately 10 hours), these islands of polymer merged, forming a fairly pinhole-free film on the macroscopic surface of the titania layer. Although reproducible, the film impaired photoanode performance in DSSC iV experiments. Whether it did so because of a reduced photoactive surface area or because of an intrinsic electrical resistance on the part of the polymer remains unclear.

Introduction

Solid state DSSCs

From a commercialization standpoint, one of the greatest drawbacks of DSSCs is the utilization of a liquid phase electrolyte in the cell. Liquid phase components require careful sealing of the cell in order to prevent loss of the liquid through leaking or evaporation.[1-3] Although possible, long-term sealing is problematic and creates additional steps in device fabrication, adding unwanted cost and complexity to device manufacture. Also, depending on the nature of the solvent, the array of possible glues and sealants may be limited by chemical reactions with the solvent.[4]

Accordingly, there has been much interest in the development of a solid state redox mediator. Truly solid state devices based on p-n type heterojunctions utilizing inorganic hole conductors were among the first solid state DSSCs investigated.[5] In particular, CuSCN was found to successfully transport holes to the back cathode contact, although device efficiencies were still well below those of liquid state mediators.[5, 6] Solid

state organic hole conductors have also been explored.[7, 8] Other solid state cells were fabricated with a poly(thiophene) derivative as both dye and hole transporter.[9] Devices incorporating p-type polymer materials, such as polythiophene and polypyrrole, have also been investigated, although with limited success.[10-12] Research into ion-conducting polymers has been similarly disappointing.[1, 13, 14] Recently, attention has focused onto quasi-solid state DSSCs utilizing room-temperature ionic liquids (RTILs), primarily those incorporating iodide ions.[2] Despite their high viscosity, RTILs have been shown to be surprisingly apt ion conductors in DSSCs. Although conversion efficiencies remain slightly below that of solution based DSSCs, devices with reasonable efficiencies (7%) have been fabricated.[2] Unfortunately, however, RTILs still necessitate sealing of the device and in addition are extremely toxic to the environment.[2]

Redox polymers (conductive polymers incorporating redox-active metal centers) are noticeably absent from the solid state DSSC literature. Much of the research in this field has focused on solid state electrolytes with I^-/I_3^- ion conducting properties.[3] This is hardly surprising as I^-/I_3^- continues to be used almost exclusively in liquid state devices and therefore presents the most logical starting point for solid state research. Recently, two novel DSSC systems have been reported which utilize cobalt complexes as redox mediators.[15-17] Sapp et al. found that 4,4'-substituted tris(bipyridine)cobalt(II) complexes performed well in DSSCs, yielding conversion efficiencies up to 80% of a comparable cell with I^-/I_3^-.[16] Although tris(bipyridine)cobalt complexes offer several advantages to I^-/I_3^-, perhaps the most exciting is that they are modifiable.[18] Whereas I^-/I_3^- is simply I^-/I_3^-, a near limitless number of tris(bipyridine)cobalt complexes can be synthesized by varying the substituents at either the 4 or 5 positions on the pyridine rings. Most relevant

to solid state research, polymerizable groups may be added to these positions, enabling the introduction of redox polymers into DSSCs.

Redox polymers, especially those of iron, osmium and ruthenium, have been well characterized.[19-21] Reduction potentials of redox polymer films are generally very similar to those of the constituent monomer. Accordingly, as alkyl-substituted tris(bipyridine)cobalt complexes have a reduction potential well-suited for use in a DSSC, so too should a redox film composed of such units. Conductivity in redox polymers is dependent upon the mobility of both the counterions and the electrons throughout the medium. Counterion mobility is a function of counterion size as well as the degree of cross-linking in the polymer matrix. Electron mobility is determined primarily by the rate at which electrons are transferred from metal center to metal center.[22] The rate constant for this reaction in the polymer corresponds closely to a metal complex's rate constant for self-exchange in solution, although a lack of polymer segmental motion may also inhibit conductivity.[22-24] Unfortunately, the +3/+2 self-exchange rate for tris(bipyridine)cobalt is exceedingly slow (18 $M^{-1} s^{-1}$).[25] Consequently, it is predicted that a redox polymer based on Co(III)/Co(II) will be considerably resistive.

Nevertheless, a tris(bipyridine)cobalt redox polymer may still prove useful in a DSSC. The primary function of the polymer will be to control the electron transfer kinetics at the photoanode/electrolyte interface. For the most part, the greatest difficulty in developing alternative redox mediators for use in DSSCs is finding a redox couple with the appropriate electron transfer kinetics, i.e. one which quickly reduces the oxidized dye but is only slowly reduced by electrons from either the nanoporous titiania or conducting glass surface of the photoanode. As tris(bipyridine)cobalt complexes in

solution have demonstrated these rare kinetics, a tris(bipyridine)cobalt redox polymer may very well exhibit similar kinetics in a solid state DSSC. Although cobalt polymers can be expected to be inherently resistive, the overall resistance arising from the polymer film can be controlled by keeping the polymer layer thin. Using the Dahms-Ruff relation, we have estimated that the thickness of a cobalt III/II redox film must be kept within 10 or so monolayers in order to ensure that it is sufficiently conductive to provide the milliamp currents produced in DSSCs.[26]

Obviously, a 10 monolayer thick redox polymer film will not be sufficient to reach the back cathode. A second, more conductive electrolyte will be required to transport the photogenerated holes from the backside (towards the cathode) of the cobalt polymer to the cathode. As the kinetic requirements of this co-mediating polymer are very straightforward (i.e. simply be conductive), nearly any hole-conducting polymer with the appropriate energetics should serve.

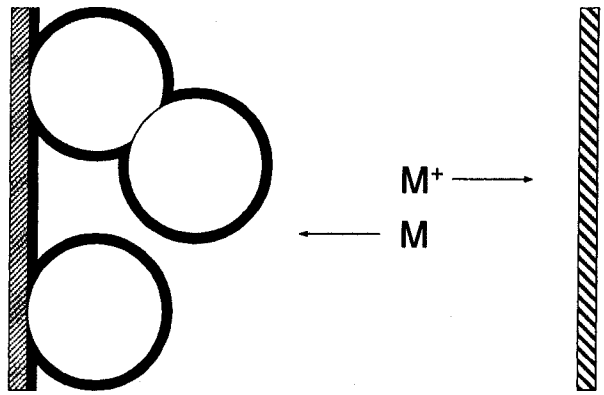

Figure 1. DSSC with a thin, tris(bipyridine)cobalt film (thick black lines) covering the photoanode surface (left side). A second mediator (M) would be required to transport holes to the cathode (right side).

However, deposition of a several-monolayers thick, cross-linked polymer film onto a porous, nanocrystalline surface is a challenging endeavor. While such thicknesses

can be attained relatively easily on flat substrates with conventional techniques, the high degree of roughness of the photoanode surface (commonly estimated at approximately 1000:1 actual surface area to projected surface area) presents a significant challenge.[27] With flat substrates, spin-coating, drop-coating, and electrochemical polymerization techniques are all commonly employed to produce thin, tris(bipyridine)metal redox films. Drop-coating involves the application of a small volume of dilute monomer solution to a substrate, followed by slow evaporation of the solvent. Spin-coating similarly involves application of a monomer solution, but evaporation is assisted by spinning the substrate at high speeds. In both cases, polymerization and cross-linking of the residual monomer film are performed subsequent to solvent evaporation, typically with heat or UV light. Electrochemical growth of vinylbipyridines has also been exploited, and involves application of a negative potential to an electrode in monomer solution.[28-30] Polymer film growth occurs at the surface of the working electrode and is easily controlled by either the number of voltage cycles or the duration of the voltage pulse. Unfortunately, the chemisorption of carboxylate-bound dyes (such as those most commonly used in DSSCs) has been found to be unstable at negative potentials, making electrochemical growth of metal-vinylbipyridines an impossibility.[31, 32] As will be described below, both spin- and drop-coating methods were attempted, but both were found to yield unsatisfactory results.

Controlled/living radical polymerization

Controlled/living radical polymerization (CRP) presents an attractive alternative to simple "coat and heat" methods. Whereas methods such as spin- and drop-coating regulate final polymer thickness through painstakingly control of the amount of monomer

delivered to the substrate, CRP allows for control within the polymerization process itself.[33, 34] This control is achieved by virtue of CRP's first order kinetics with respect to monomer concentration in combination with a linear relationship between degrees of polymerization (DP) and conversion.[35] Accordingly, in the case of surface-bound polymers, polymer thickness may be controlled straightforwardly through regulation of reaction time.[33, 36] As removal of the photoanode substrate from the monomer solution is all that is required to end the reaction, CRP offers a considerable advantage over "coat and heat" methods.

Controlled/living radical polymerizations are fundamentally distinct from other radical polymerization techniques in that the propagating radical exists in a dynamic equilibrium between active and dormant states.[37] In the active state, the growing polymer chain is terminated by a free radical which is capable of reacting with monomer, a result which represents propagation of the polymer chain. Importantly, the free radical may also react with another type of species present in solution, yielding a dormant, or deactivated state. This reaction is reversible, and a catalyst and/or heat is employed to optimize the equilibrium between the dormant and active states of the radical. Although a desirable equilibrium typically will favor the dormant state, the rate of deactivation must be on the order of the propagation rate so that reaction of the active radical with monomer is competitive with deactivation. Successful CRP reactions generally require conditions where one or less propagation steps occur per activation cycle (i.e. dormant-active-dormant).[37, 38] Activation of the radical is usually much slower than either propagation or deactivation, and consequently polymer chains spend most of their time in a dormant state.[37] It should be noted that this discussion of CRP does not pertain to

reversible addition-fragmentation transfer (RAFT) polymerization - or any other technique based on degenerative transfer - which, although a very successful CRP technique, operates on slightly different principles.[37]

Although it greatly slows polymerization, weighting the equilibrium towards a dormant radical is the source of many of CRP's advantages over other radical polymerizations.[37] Reaction of two chain-end, propagating radicals is a major termination pathway in conventional radical polymerizations. With CRP, on the other hand, most radicals exist in the dormant state so that, at any one time, the concentration of active radicals is small and radical-radical termination is drastically reduced, typically to levels below 10%.[37] Conventional polymerizations often proceed very quickly, with initiation-propagation-termination cycles frequently lasting less than one second.[37] In contrast, CRP reactions may take hours to days to achieve comparable DPs and, in some respects, never achieve termination as the dormant species (usually fairly stable) may be reintroduced to polymerization conditions at any point and continue propagating.[37] Advantages of CRP reactions include lower polydispersities, linear increases in DP with monomer conversion, and greater overall control of molecular weight.[37] The stability of the dormant species is especially advantageous in the synthesis of well-defined block copolymers, as it allows growing polymer chains to be transferred from one monomer solution to another during the course of the reaction.

The field of controlled/living radical polymerization has been advanced considerably within the last two decades.[37] There now exist several mature CRP techniques, with the most successful being: atom transfer radical polymerization (ATRP), nitroxide-mediated polymerization (NMP), reversible addition-fragmentation

transfer (RAFT), and cobalt-mediated radical polymerization (CMRP). Although each technique has been well-demonstrated to yield polymers with low polydispersities and controlled molecular weights, not all techniques are suitable for all types of monomers in all conditions. Perhaps the most versatile of the currently known CRP methods, ATRP has been used to polymerize a wide variety of monomer types under an extraordinarily broad range of reaction conditions.[33, 37] In addition, there are a variety of functionalities capable of initiating ATRP, most of which are commercially available and easily incorporated into a variety of initiator molecules, further adding to the technique's versatility.[37] Furthermore, ATRP has been successfully employed by several groups to grow surface-bound polymers.[35, 36, 39, 40] For these reasons, ATRP was the CRP technique selected for this project.

In atom transfer radical polymerization, the active radical is deactivated by the reversible transfer of a halogen atom to the propagating polymer chain by a catalyst, typically a transition metal coordination complex (**Figure 2**). Suitable monomers include styrenes, acrylates, methacrylates, acrylonitriles acrylamides methacrylamides, acrylic acids, methacrylic acids, and 4-vinyl pyridines as well as a few other miscellaneous monomers.[41] Initiator functionalities generally resemble the halogenated form of the monomer, although interestingly they may also resemble the halogenated form of a different type of monomer from that being employed (eg. a benzylic halide initiator – resembling halogenated styrene – in conjunction with a methacrylate monomer).[38, 41] Accordingly, types of initiators employed include halogenated alkanes, benzylic halides, α-haloesters, α-halonitriles, and sulfonyl halides.[41] It is also possible to use conventional radical initiators such as azobisisobutryonitrile (AIBN) in the presence of deactivator (the

reduced form of the catalyst), a technique referred to as reverse ATRP.[41] For both normal and reverse ATRP, a variety of transition metal catalysts have been employed, but by far the most popular are those based on copper.[41] Polydentate ligands are employed, usually two- to four- coordinate, and are generally either polypyridines or branched, aliphatic amines.[41] ATRP may be performed in bulk or in solvent, with solvents ranging in polarity from toluene to water.[33, 38, 41] Reaction temperatures also vary dramatically; some systems require 120 °C while others proceed rapidly at room temperature. Although all ATRP reactions are conducted in air-free environments, the procedure is fairly O_2 tolerant, especially in comparison to other techniques such as anionic and cationic polymerizations.[33]

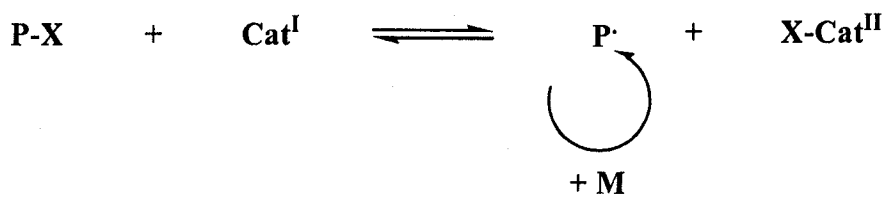

Figure 2. Popagation process in atom transfer radical polymerization. P = growing polymer chain, M = monomer, X = halogen, Cat = catalyst.

The persistent radical effect (PRE) is the name given to a phenomenon of crucial importance to ATRP and most other controlled/living radical polymerization techniques (excluding RAFT).[37] In ATRP reactions, the catalyst is added to the reaction mixture in its reduced form and in this state may be referred to as an "activator." Its primary function is to catalyze the transition of the propagating radical from a dormant to an active state. It does so by abstracting the chain-end halogen atom, with the central metal of the catalyst simultaneously experiencing a +1 change in its formal oxidation state.

This oxidized form of the catalyst is responsible for the return of the active radical to a dormant state, and as such is sometimes referred to as a "deactivator." Since the catalyst is generally added only in its reduced form, the initial concentration of deactivator is very low (approximately zero). Although the deactivator concentration increases once the polymer chain radical has been activated, it is still very small in the early stages of the reaction. Accordingly, deactivation is less efficient and termination between propagating chains occurs with greater frequency. However, for every termination event, two molecules of deactivator are generated (one from each chain) and the deactivator concentration quickly increases until it reaches a level where deactivation proceeds with sufficient rapidity to prevent further termination events. In most cases, only very low concentrations of deactivator are required, so termination is maintained at tolerable levels, usually less than 10%.[37] This series of events has been dubbed the persistent radical effect (PRE) and is frequently exploited in controlled/living radical polymerizations.

Surface-initiated ATRP

Considering the high degree of flexibility of ATRP, it is hardly surprising that several groups have investigated its use in fabricating well-defined, surface-bound polymers.[35, 36, 39, 40] There are two distinct approaches to the preparation of surface-bound polymers (commonly referred to as "polymer brushes"): a "grafting to" approach wherein the preformed polymer is attached to the surface and a "grafting from" approach with a surface-bound species initiating the reaction and subsequent polymer growth being directed away from the surface.[33, 34] Although initial research in this field was focused on

"grafting to" methods, polymer brush densities and thicknesses were limited by the approach. Steric crowding of adsorption sites by non-linear polymer chains limited attainable brush densities while thicknesses were restricted by the minimal solubility of high molecular weight polymers.[33] The "grafting from" approach (also referred to as "surface-initiated polymerization") alleviates both problems and has become method of choice for most polymer brush syntheses.[33, 34] While any of the major classes of polymerization techniques may be used, CRP – and ATRP, in particular – is especially amenable to polymer brush synthesis due to the wide variety of available monomer types, less stringent reaction conditions and greater control over molecular weight.[33]

Notably, there is no literature precedent for the surface-initiated ATRP of cross-linked redox polymers, although reasons for optimism can be found. While the vast majority of ATRP reactions are conducted on monomers with a single polymerizable functionality (yielding straight-chain polymers), effort has been directed recently towards the synthesis of cross-linked films via the polymerization of certain difunctional monomers.[42-45] The fabrication of cross-linked polymer brushes presents unique challenges and several different techniques have arisen to address them.

Catalyst systems, in particular, have required adjustment in order to maintain a desirable persistent radical effect. As mentioned previously, the PRE is responsible for generating the baseline deactivator concentration necessary for a proper equilibrium between the active and dormant states of the propagating radical. When ATRP is conducted in a homogenous medium, the initial concentrations of initiator and catalyst are high enough that this baseline is reached quickly and with only a minimal percentage of polymer chains being lost to termination. Surface-initiated ATRP, on the other hand,

presents a situation where the overall number of initiating sites is inevitably much lower.[43] Further exacerbating the problem, the heterogeneous nature of the reaction leads to a concentration imbalance: a localized density of propagating radicals on the surface (requiring a high concentration of deactivator) and a "dilution" of the solvated deactivor as it diffuses away from the polymer chains. In the surface-initiated ATRP reactions of straight-chain polymers, this dilemma is easily addressed through the use of "sacrificial" initiator in solution.[33, 46] Deactivator concentrations are restored to appropriate levels and propagation is controlled. Although this results in polymer growth in solution as well as on the intended surface, the substrate may be easily extracted from the reaction medium and rinsed of all ungrafted polymer. When grafting cross-linked polymers, however, the polymerization reaction generally must be confined to the surface as the low solubility of cross-linked polymers causes them to irreversibly precipitate onto the substrate.[33, 43] One technique used to avoid this situation is to suspend the substrate in the reaction medium such that most precipitate deposits somewhere other than the substrate surface.[44] Although success with this approach has been reported, gelation of the entire reaction medium may also occur and renders the polymerization useless.[43] A more common technique is to add the deactivating form of the catalyst to the reaction solution.[33, 36, 43] The most significant drawback to this technique is that reaction rates are dramatically slowed if deactivator concentrations become too high.[35] Nevertheless, a balance may be achieved and the addition of deactivator has become a popular tool for controlling the surface-initiated growth of cross-linked polymers.

Another approach to the fabrication of cross-linked polymer brushes is to first grow a straight chain polymer appended with sidechain functional groups.[43] These

functional groups may then be utilized in a second reaction to cross-link the surface-bound polymer. A common strategy is to use a radical polymerization for the first reaction, followed by a condensation reaction with a difunctional cross-linker for the second. Another strategy is to react a preformed, spin-coated film of covalently-linked bipyridines with free metal ions in solution, generating a cross-linked film upon coordination of the bipyridine ligands with the redox-active metal.[24] A concern with this approach is that if the degree of cross-linking at the polymer brush surface is too high, further penetration of the metal cross-linker into the film may become impossible. In this case, an unevenly cross-linked polymer brush results, and a high electrical resistance across the inner portion of the film can be expected due to the absence of redox-active centers.

Experimental

4,4'-bis(7-bromoheptyl)-2,2'-bipyridine

To a 3-necked flask under N_2, cooled to -78 °C with a dry ice/acetone bath and containing approximately 30 mL of freshly distilled THF and 7.8 mL of diisopropylamine (filtered over alumina and degassed), 28 mL of 2M *n*-butyllithium in hexanes were added. After allowing 30 min for the formation of LDA to proceed, 5 g of 4,4'-dimethyl-2,2'-bipyridine (DMB, Reilly Industries, Indianapolis), dissolved in approximately 350 mL freshly distilled THF, was added dropwise to the reaction flask. After two hours, the generation of bipyridine dicarbanion was complete, resulting in a deep red solution. Finally, 16.2 mL of 1,6-dibromohexane, filtered over hot alumina and

degassed, was added to the solution. The reaction vessel was kept under N_2 and allowed to warm to room temperature overnight. After ~15 hrs, the reaction was quenched with H_2O. THF was removed via rotary evaporation and replaced by H_2O. The resulting slurry was extracted 4 times with dichloromethane (DCM). The organic layers were combined, dried over Na_2SO_4, filtered through Whatman qualitative grade filter paper, and rotary evaporated to yield a viscous brown oil which was then purified using column chromatography (flash silica with 10% ethyl acetate in dichloromethane). ^1H NMR in $CDCl_3$ (δ in ppm, multiplicity, integration): 1.4 (m, 12H); 1.8 (m, 8H); 2.9 (t, 4H); 3.4 (t, 4H); 7.5 (d, 2H); 8.7 (d, 2H); 8.8 (s, 2H).

Synthesis of 7,7'-(2,2'-bipyridine-4,4'-diyl)bis(heptane-7,1-diyl) diacrylate (dAb)

4,4'-bis(7-bromoheptyl)-2,2'-bipyridine was divided into several fractions. Each fraction was stirred for three days in a solution of sodium acetate in glacial acetic acid. The solution was neutralized with aqueous NH_4OH and extracted with dichloromethane, which was then dried over Na_2SO_4 and removed with rotary evaporation. To the resulting solid was added approximately 200 mL of 95% EtOH and several pellets of NaOH. The reaction was refluxed overnight under N_2. The solution was then neutralized with glacial acetic acid and the ethanol removed with rotary evaporation. Another DCM/H_2O extraction was performed, with the organic layer being dried over Na_2SO_4 and rotary evaporated. After further drying under vacuum, the solid product was dissolved in Optima grade acetonitrile. Acryloyl chloride (8 mL) was added and the solution was refluxed for 6 hours under N_2. After rotary evaporation, the crude oily product was purified with a dichloromethane/aqueous Et_3N (2% v/v) extraction followed by column

chromatography (flash silica with 10% acetone in dichloromethane), resulting in a white solid product. Overall yield (based on DMB) was less than 10%. ^{1}H NMR in $CDCl_3$ (δ in ppm, multiplicity, integration): 1.4 (s, 16H); 1.7 (m, 10H); 2.8 (t, 4H); 4.1 (t, 4H); 5.7 (d, 2H); 6.1 (d of d, 2H); 6.4 (d, 2H); 7.4 (s, 2); 8.7 (m, 4H).

Synthesis of $Co(dAb)_3(ClO_4)_2$

The dAb ligand was dissolved with heat into a minimal volume of MeOH, to which was added a stoichiometric amount of $Co(ClO_4)_2$ hexahydrate. The solution quickly turned brown, but was refluxed for two hours to ensure full conversion. Once approximately 80% of the solvent had been rotary evaporated, the metal complex was precipitated with diethyl ether. The product was filtered, redissolved in acetonitrile, transferred to a scintillation vial and rotary evaporated to dryness.

Synthesis of $Fe(dAb)_3(ClO_4)_2$

The dAb ligand was dissolved in a minimal volume of MeOH, to which was added a stoichiometric amount of aqueous $Fe(NH_3)_4(SO_4)_2$. The reaction was allowed to stir at room temperature for a few minutes before an excess of aqueous $NaClO_4$ was added. The resulting precipitate was filtered and used without further purification.

Synthesis of $Zn(dAb)_3(ClO_4)_2$

The dAb ligand was dissolved in a minimal volume of MeOH, to which was added a stoichiometric amount of aqueous $ZnSO_4$ x 7 H_2O. The reaction was allowed to stir at room temperature for 30 minutes before an excess of aqueous $NaClO_4$ was added.

The flask was chilled in an ice bath and the resulting precipitate was filtered and used without further purification.

Synthesis of 7,7'-(2,2'-bipyridine-4,4'-diyl)diheptan-1-ol (diol)

A modified procedure, developed by Di Xue, was used to prepare a bulk quantity of diol.[47] The strategy was similar to that employed to synthesize the dab ligand, but a bromoalcohol was used instead of a dibromoalkane. To protect the alcohol functionality, 15 g of 6-bromohexan-1-ol and 156 mg p-toluene sulfonic acid were added to 75 mL diethyl ether. The solution was purged with N_2 and cooled to 0 °C in a ice water bath. To this, 12 mL of 3,4-dihydro-2H-pyran was added dropwise. The solution was allowed to warm and stirred overnight. The reaction solution was washed four times with 1 M NaOH, three times with H_2O and once with an aqueous saturated NaCl solution. The organic layer was dried over Na_2SO_4 and rotary evaporated to a yellow liquid, which was further purified with column chromatography (flash silica, 4% v/v diethyl ether in hexane).

To a 3-necked flask under N_2, cooled to -78 °C with a dry ice/acetone bath and containing approximately 30 mL of freshly distilled THF and 6.3 mL of diisopropylamine (filtered over alumina and degassed), 22.25 mL of 2M *n*-butyllithium in hexanes were added. After allowing 30 min for the formation of LDA to proceed, 3.72 g of 4,4'-dimethyl-2,2'-bipyridine (DMB, Reilly Industries, Indianapolis), dissolved in approximately 300 mL freshly distilled THF, was added dropwise to the reaction flask. After two hours, the generation of bipyridine dicarbanion was complete, resulting in a deep red solution. Finally, 13.4 g of the protected bromoalcohol was degassed and added

to the solution. The reaction vessel was kept under N_2 and allowed to warm to room temperature overnight. After >24 hrs, the reaction was quenched with MeOH. THF and MeOH were removed via rotary evaporation and replaced by H_2O. The resulting slurry was extracted 3 times with diethyl ether. The organic layers were combined, dried over Na_2SO_4, and rotary evaporated to yield a yellow liquid which was then purified using column chromatography (flash silica with 30% ethyl acetate in hexane).

The alcohol groups were then deprotected by refluxing the reaction product in 150 mL ethanol with 0.5 g *p*-toluenesulfonic acid for greater than 24 hrs. Solvent was removed with rotary evaporation and the product re-dissolved in chloroform, washed twice with a concentrated aqueous $NaHCO_3$ solution, three times with H_2O, and once with a saturated aqueous solution of NaCl. The organic layer was dried over Na_2SO_4 and rotary evaporated to dryness. A slightly unorthodox chromatography column was used to purify the product. The flash silica gel was packed with a 50/50 v/v acetone and dichloromethane solution to which a pipette-tip (a few microns) of Et_3N (purified over alumina to remove trace brown color and water) was added to every 100 mLs of solution. Once the reaction product, dissolved in dichloromethane, was loaded onto the column, the Et_3N treatment was stopped. Overall yield was approximately 65%, based on DMB. ^1H NMR in $CDCl_3$ (δ in ppm, multiplicity, integration): 1.4 (s, 12H); 1.6 (m, 4H); 1.7 (m, 4H); 2.7 (t, 4H); 3.7 (t, 4H); 7.2 (d, 2H); 8.3 (s, 2H); 8.6 (d, 2H).

Synthesis of dMA

Typically, ~150 mg diol was dissolved in a solution of 10-15 mL of pentene-stabilized chloroform and 600 μL of triethylamine (purified over alumina) in an oven-

dried flask. The solution was cooled to 0°C and 450 μL (a five times excess) of freshly distilled methacryloyl chloride was added. The reaction was stirred under N_2 for 30 minutes, at which point it was allowed to warm to room temperature. After another 30 minutes, the reaction was usually complete by TLC. The reaction solution was washed with a basic brine solution ($NaHCO_3$ in a NaCl-saturated H_2O) at least twice and a neutral brine solution at least once. The organic layer was dried over Na_2SO_4 and rotary evaporated to dryness. Column chromatography as described above (diol synthesis) was performed. Fractions containing the product were combined and rotary evaporated, yielding a clear oil which solidified to an off-white solid after a few hours in a freezer. The crude product was dissolved in MeOH using slight heat, shaken with decolorizing carbon and filtered through a plug of glass wool. With the careful addition of water, the purified product formed through a precipitation/crystallization process and was collected by filtration, washed with cold water, and dried under vacuum. An average yield was around 50% based on diol. ^1H NMR in $CDCl_3$ (δ in ppm, multiplicity, integration): 1.4 (s, 12); 1.7 (m, 8H); 1.9 (s, 6H); 2.7 (t, 4H); 4.1 (t, 4H); 5.5 (s, 2H); 6.1 (s, 2H); 7.1 (d, 2H); 8.2 (s, 2H); 8.6 (d, 2H).

Synthesis of 7,7'-(2,2'-bipyridine-4,4'-diyl)bis(heptane-7,1-diyl) bis(2-bromo-2-methylpropanoate) (αBE-bpy)

Diol (200 mg) was dissolved in a solution of 25 mL of pentene-stabilized chloroform and 1 mL of triethylamine (purified over alumina) in an oven-dried flask. The solution was cooled to 0 °C and 1 mL (an eightfold excess) of 2-bromoisobutyryl bromide was added. After stirring for one hour at 0 °C, the reaction was complete by

TLC. The organic layer was washed three times with an aqueous $NaHCO_3$ solution, once with neutral H_2O, and once with a NaCl-saturated aqueous solution. The organic layer was dried over Na_2SO_4, rotary evaporated to dryness and re-dissolved in a minimum of dichloromethane. A slight variation of the column chromatography as described above (diol synthesis) was performed. The flash silica column was packed with dichloromethane, treated with 50 mL of a 10% by volume solution of pyridine in dichloromethane and washed with another 50 mL of dichloromethane before the crude product was loaded. Dichloromethane was used as eluent. The product, heavily contaminated with pyridine, was eluted with dichloromethane. Rotary evaporation followed by gentle heating in a vacuum oven isolated the pure product. ^1H NMR in $CDCl_3$ (δ in ppm, multiplicity, integration): 1.4 (s, 12H); 1.7 (m, 8H); 1.9 (s, 12H); 2.7 (t, 4H); 4.2 (t, 4H); 7.2 (d, 2H); 8.3 (s, 2H); 8.6 (d, 2H).

Synthesis of $Ru(dcb)_2X_2$

Ruthenium trichloride trihydrate (0.376 g) and 0.707 g of 4,4'-dicarboxylic acid-2,2'-bipyridine (dcb) were dissolved in approximately 25 mL of anhydrous dimethylformamide (DMF) and refluxed under N_2 for 8 hours. As the dark green solution cooled to room temperature, it turned dark red, likely indicating the substitution of at least one chloride ligand by a water or hydroxide group. The majority of solvent was removed by rotary evaporated at high temperature, and a 1:1 acetone-to-diethyl ether solution was added to remove the remainder of solvent. The resulting sludge was filtered using a Buchner filter with Whatman filter paper and washed several times with pure

diethyl ether followed by pure acetone. The maroon-red solid was subsequently dried in a vacuum oven for several hours.

Synthesis of $Ru(dcb)_2(\alpha BE\text{-}bpy)(PF_6)_2$ (αBE-dye)

A small volume of ethylene glycol (~5 mL) was added to 0.99 g $Ru(dcb)_2X_2$ and 0.143 g αBE-bpy. The reaction vessel was heated at 100 °C for 4 hours, during which time the dark purple solution slowly became a dark brown/orange color. Once cooled, the reaction solution was diluted with ~5 mL of acetone and used to load a flash silica column, previously packed with acetone. Acetone was used to elute the ethylene glycol, unreacted αBE-bpy, and an unidentified yellow band before switching to acidic "solvent #5." Solvent #5 was prepared as normal (50% acetonitrile, 45% water, 5% aqueous solution of saturated KNO_3) and made acidic with 10 drops of concentrated (37%) HCl per 500 mL of solvent. Colored fractions were rotary evaporated to remove acetonitrile. The resulting precipitate was filtered with Celite® 545 filtering agent, washed with acidic H_2O, and redissolved in basic H_2O. Excess NH_4PF_6 was added before acidifying the solution with a few drops of HCl (pH ~ 1-2). The desired product precipitated from solution, was filtered with Celite® 545 and re-dissolved with MeOH. After rotary evaporation, a red/orange solid remained. Characterization by UV-Vis, NMR, and mass spectrometry verified the identity of the nearly pure product. ^1H NMR in CD_3OD (δ in ppm, multiplicity, integration): 1.4 (s, 12H); 1.7 (m, 8H); 1.9 (s, 12H); 2.7 (t, 4H); 4.1 (t, 4H); 7.3 (d, 2H); 7.6 (d, 2H); 7.9 (m, 8H); 8.6 (s, 2H); 9.1 (s, 4H).

Synthesis of Ru(dcb)(diol)(SCN)$_2$ ($A_{7OH}N_3$)

Ru(*p*-cymene)Cl_2 dimer and diol were dried in a vacuum chamber overnight immediately prior to being used. In an oven-dried flask, 150 mL DMF, 0.399 g Ru dimer and 0.5 g diol were stirred at 50-80 °C under N_2 for 4 hours. A stoichiometric amount of dcb (0.318 g) was then added and the reaction was brought to reflux (~145 °C), turning the previously green-brown solution a dark red. After 4 hours, excess NH_4SCN (1.38 g, previously recrystallized three times in acetonitrile) was added. The reaction was maintained at reflux for another 4 hours, at which point the reaction vessel was removed from heat and allowed to stand for at least 12 hours. The bulk of the DMF solvent was removed with rotary evaporation followed by addition of aqueous 0.2 M HNO_3 and sonication to remove the rest. The resulting sludge was filtered with Celite® 545, washed several times with H_2O followed by diethyl ether, and re-dissolved with a large quantity of MeOH. The MeOH was removed via rotary evaporation, and the residual solid re-dissolved into a minimum of DMF. A Sephadex LH-20 chromatography column with DMF as eluent was used to separate several yellow bands from the main, red band that eluted first. DMF was removed with rotary evaporation, yielding a red, rusty solid. ^1H NMR in CD_3OD (δ in ppm, multiplicity, integration): 1.3 (s, 6H); 1.6 (m, 12H); 1.9 (m, 2H); 2.7 (t, 2H); 3.0 (t, 2H); 3.6 (d of t, 4H); 7.0 (d, 1H); 7.4 (d, 1H); 7.7 (m, 2H); 7.9 (d, 1H); 8.3 (d, 1H); 8.4 (s, 1H); 8.5 (s, 1H); 8.9 (s, 1H); 9.0 (s, 1H); 9.3 (d, 1H); 9.7 (d, 1H).

Synthesis of Ru(dcb)(αBE-bpy)(SCN)$_2$ ($A_{7\alpha BE}N_3$)

A solution of THF, 0.350 g $A_{7OH}N_3$ and 0.8 mL pyridine (purified over alumina) was stirred and degassed with N_2 for 10 minutes and sonicated. A five times excess of

2-bromoisobutyryl bromide (0.512 mL) was added and the reaction solution was refluxed under N_2 for two days.

A variety of procedures were attempted in an effort to purify the presumed product. An example of perhaps the most successful procedure follows. The reaction solution was allowed to cool. THF was removed via rotary evaporation and most of the resulting solid was re-dissolved in DCM. The remaining solid was filtered off using Celite® 545 and a Buchner funnel. The filtrate was washed twice each with basic H_2O ($NaHCO_3$ solution), H_2O, acidic H_2O (dilute HBr, pH ~3) and, in the event of severe emulsification, once with a brine solution. The organic layer was subsequently removed via rotary evaporation. The red/purple solid was dissolved in a minimum of 1:1 (by volume) THF to MeOH and run through a Sephadex LH-20 column, using the same solvent as eluent. After inconclusive characterization by NMR, a variety of separation techniques were attempted, including further extractions and Sephadex LH-20 columns, but to no avail.

Synthesis of 2,2'-bipyridine-4,4'-diyldimethanol ($diol_{IC}$)

First, the ethyl ester intermediate was prepared in a reaction with ~250 mL ethanol, 3 g dcb and ~5 mL concentrated sulfuric acid. The suspension was refluxed for over 80 hours until clear. Once the reaction mixture had cooled, approximately 300 mL H_2O was added to precipitate the product. Ethanol was removed by rotary evaporation and the remaining aqueous suspension was neutralized with a sodium hydroxide solution. The precipitate was filtered, washed with H_2O and dried under vacuum. The ethyl ester intermediate (3.0 g) was suspended in 200 mL absolute ethanol. $NaBH_4$ (8.2 g) was

added and the reaction mixture was heated at reflux for 7 hours. The reaction mixture was allowed to cool and then quenched with a saturated aqueous solution of NH_4Cl, resulting in lots of white precipitate. The ethanol was removed by rotary evaporation and the remaining aqueous suspension was extracted with several aliquots (ca. 150 mL each) of ethyl acetate. Once the ethyl acetate extractions no longer tested positive for bipyridine (using a spray of $Fe(ClO_4)_2$ in water), the organic layers were combined, dried over Na_2SO_4, and rotary evaporated to yield a white solid. ^1H NMR in CD_3OD (δ in ppm, multiplicity, integration): 4.8 (s, 4H); 7.5 (d, 2H); 8.3 (s, 2H); 8.6 (d, 2H).

Synthesis of Ru(dcb)(diol$_{1C}$)(SCN)$_2$ ($A_{1OH}N_3$)

Ru(*p*-cymene)Cl_2 dimer and diol$_{1C}$ were dried in a vacuum chamber overnight immediately prior to being used. In an oven-dried flask, 150 mL DMF, 0.399 g Ru dimer and 0.281 g diol$_{1C}$ were stirred at 75 °C under N_2 for 4 hours. A stoichiometric amount of dcb (0.318 g) was then added and the reaction was brought to reflux (~145 °C), turning the previously green-brown solution a dark purple. After 4 hours, excess NH_4SCN (1.38 g, previously recrystallized twice in acetonitrile) was added. The reaction was maintained at reflux for another 4 hours, at which point the reaction vessel was removed from heat and allowed to stand for at least 12 hours. The bulk of the DMF solvent was removed with rotary evaporation, followed by addition of aqueous HNO_3 (pH 3-4) and sonication to remove the rest. The resulting sludge was filtered with Celite® 545, washed several times with H_2O followed by diethyl ether, and re-dissolved into DMF. The DMF solution was concentrated using rotary evaporation, and a Sephadex LH-20 chromatography column with DMF as eluent was used to isolate the product. Each

fraction was rotary evaporated, treated with an aqueous $HClO_4$ solution, filtered, washed again with aqueous $HClO_4$, and collected with DMF. Those fractions containing isolated product (as determined by NMR spectroscopy) were combined. ^1H NMR in CD_3OD (δ in ppm, multiplicity, integration): 4.3 (s, 2H); 5.0 (s, 2H); 7.2 (d, 1H); 7.5 (d, 1H); 7.7 (d, 1H); 7.4 (m, 2H); 8.3 (d, 1H); 8.5 (s, 1H); 8.6 (s, 1H); 8.9 (s, 1H); 9.1 (s, 1H); 9.4 (d, 1H); 9.7 (d, 1H).

Surface-initiated polymerization of $Co(dMA)_3Br_2$ – final procedure

Three separate solutions were prepared. Solution one consisted of 4.9 mg $CoBr_2$ x 6 H_2O and 23.4 mg dMA in 290 μL of acetonitrile. Solution two was prepared with 13.6 mg $CuBr_2$ and 17.7 mg dmb in 4 mL acetonitrile. The solid reagents for both solutions were weighed in an oxygen environment, placed in a low volume cell with a truncated stirbar and a scinitillation vial, respectively, and brought into an inert atmosphere glovebox. The specially-made low volume cell was fabricated from a flattened glass tube, 3.5 cm long with inner cavity dimensions of 1 cm X 4 mm and sealed on one end. Solution three was prepared in the glove box, where 12.65 mg CuBr and 26.5 mg dmb were weighed and added to a scintillation vial. Previously degassed acetonitrile was then added via syringe in the proper volumes and the solutions stirred for at least 30 minutes. Reactions were monitored by the color change of the solvent (turning from clear to dark brown, turquoise blue and red, respectively) as well as the dissolution of bipyridine. At this point, 5 μL each of solutions two and three were added to solution one and stirred for approximately one minute. The final concentrations of monomer, activator, and deactivator were 50 mM, 0.3 mM and 0.2 mM, respectively, or 100:1

monomer-to-catalyst (both forms) ratio. The stirbar was removed, a dyed photoanode inserted, and the low volume cell was closed with a customized rubber stopper (ground by hand using sandpaper to fit the low volume cell). The vial was placed in an acetonitrile-saturated chamber, which was then wrapped in Al foil and left to sit without stirring for the designated length of time. The photoanode was then extracted from the monomer solution, removed from the glovebox, and rinsed. The standard rinse procedure consisted of a rinse under a gentle spray of acetonitrile, a soak in optima-grade acetonitrile followed by a final rinse with an acetonitrile spray. An addition soak and rinse were sometimes employed. A fresh reaction solution was usually not prepared for successive polymerizations unless one or more chemical concentrations were altered, although fresh solutions were prepared after a month or less had passed or in the event that the glovebox atmosphere's integrity was temporarily lost.

Electrochemical deposition of phenol/2-allylphenol (PPO) copolymer

A 10:10:1 (v/v/v) monomer solution of 19 mL H_2O, 21 mL 95% ethanol, and 2 mL 2-butoxyethanol was prepared, to which was added 0.237 g phenol, 0.497 g 2-allylphenol and 0.447 g $LiClO_4$, yielding initial concentrations of 60 mM, 90 mM, and 100 mM, respectively. A 10 mM solution of 0.052 g tetrabutylammonium hydroxide (TBAH) in 20 mL methanol was prepared and used to adjust the monomer solution to pH 9.0. Approximately 7-8 mL were required. An electrochemical cell was assembled using a small beaker of monomer solution, a Pt auxiliary electrode, a SSCE reference electrode, and the photoanode to be passivated as a working electrode. Under dark conditions, the potential of the working electrode was scanned from 0 V to +1.5 V to 0 V forty times at a

rate of 100 mV/s. The photoanode was then rinsed with the basic methanol solution, dried under a stream of air and baked at 150 °C for 30 minutes. Photoanodes were removed from the oven and placed directly into dye solution.

Deposition of organized, mesoporous thin films of titania nanoparticles

Dropwise, 8 mL of 37% HCl was added to 12.7 g titanium (IV) ethoxide under constant stirring. Meanwhile, a separate solution was prepared by dissolving 4.0 g Pluronic P123 with 36.3 g 1-butanol. Pluronic P123 is poly(ethylene oxide)-*block*-poly(propylene oxide)-*block*-poly(ethylene oxide), a block copolymer with an approximate composition of $PEO_{20}PPO_{70}PEO_{20}$ (M_{av}=5800). These solutions were then combined and allowed to age for 3 hours at room temperature. A conducting glass (FTO) slide, previously cleaned in a basebath for at least 30 minutes and rinsed with H_2O, distilled H_2O, and 95% ethanol, was blown dry with N_2 and readied for dip-coating. Once the titanium solution had aged, the lower half of the slide was immersed and carefully withdrawn from the solution at a rate of 0.8 mm/s. The back of the slide was quickly wiped clean before being placed in a controlled 75% relative humidity chamber. The humidity chamber was prepared in a plastic centrifuge vial, into which were added two Kimwipes and a small volume of a saturated aqueous solution of NaCl. After 30 hours, the slide was removed from the incubation chamber and baked in a temperature-programmable oven. The temperature was increased at a rate of 1 °C/min and held at 350 °C for 2 hours. Films were characterized by scanning electrode microscopy.

Electrochemical experiments

All DSSC experiments were conducted using a sandwich cell configuration. The cathode (specified in each instance, but usually gold with cobalt mediators and always platinum with iodide mediators) was placed onto the photoanode and clamped together in a custom-made cell holder with an aperture of 0.385 cm^2. A few μL's of mediator solution (the exact composition of which will be specified in each instance) were applied outside the gap between the anode and cathode and were subsequently drawn into the interior of the cell by capillary action. An FTO extension (with conducting copper tape) was clamped to the anode to facilitate electrical connection.

A 75 W Xenon arc lamp was used as a source of illumination. Wavelengths lower than 400 nm were removed with a 400 nm high pass filter, but the light was not collimated. Incident light power was adjusted with the Xenon lamp focus to 1 sun (1000 $W\ m^{-1}$, or 100 $mW\ cm^{-2}$). In cases where lower intensity light was desired, neutral density filters were placed in the light path.

Early current-voltage (iV) experiments were performed with a PAR Model 173 Potentiostat/Galvanostat controlled by a PAR Model 175 Universal Programmer. Output was recorded on a Yokogawa 3023 X-Y recorder. Later iV experiments utilized a Kiethley 1400 Sourcemeter interfaced to a personal computer via a National Instruments BNC connector box. Specially-written LabVIEW software was used to perform iV experiments (both light and dark) and calculate the cell characteristics (V_{oc}, J_{sc}, FF, η).

Cyclic voltammetry was performed with a BAS 100 B Potentiostat-Galvanostat controlled by BAS 100 W software on a personal computer. A platinum counter

electrode and a saturated sodium calomel (SSCE) reference electrode were used (working electrode will be specified for each experiment).

Spectroscopic Experiments

UV-visible spectroscopy was performed using a Hewlett-Packard Model 8452 Diode Array Spectrophotometer using either a 1 cm pathlength cuvette (for solution phase samples) or simple the photoanode (with the instrument calibrated with an air blank).

Nuclear magnetic resonance (NMR) spectroscopy (^{1}H) was conducted using a Varian 300 MHz NMR instrument.

Results/Discussion

Heat-initiated polymerizations

Preliminary, "quick and dirty" experiments were conducted to asses the feasibility of spin- and drop-coating monomer solutions onto the dyed, nanocrystalline photoanode. Initially, $Fe(dAb)_3(ClO_4)_2$ was used as a monomer as the presence of an iron redox polymer film is easily discerned through visual inspection. Later experiments incorporated the target monomer, $Co(dAb)_3(ClO_4)_2$, and were conducted as follows. Spin-coating was performed by application of less than 1 mL of 0.100 M $Co(dAb)_3(ClO_4)_2$ in acetonitrile to a still substrate which was subsequently spun with an Analytical Rotator (Pine Instruments) at 2500 rpms. The photoanode was then baked at 78 °C for 30 minutes under vacuum. Although 78 °C is a relatively low temperature to induce the thermal polymerization of an acrylate species, it was found to result in an

insoluble (i.e. crosslinked) film as judged by visual inspection after extensive rinsing. Higher temperatures were also investigated, but control experiments with uncoated photoanodes indicated an adverse effect of high temperature on photoanode performance in a cell. In fact, even 80 °C generated concern over photoanode performance, and later polymerizations were conducted at an even lower temperature of 68 °C. Following polymerization and rinsing, iV experiments were conducted using the modified photoanode in a DSSC sandwich cell arrangement. Encouragingly, the iV curve showed little difference between modified and unmodified photoanodes when $Co(dtb)_3(ClO_4)_2$ was used as a co-mediator. However, when ferrocene (FeCp) was used, cell performance was abysmal. FeCp has been shown to be an adequate mediator in DSSC cells only after the photoanode surface has been adequately passivated to prevent recombination of photoinjected electrons with oxidized mediator in solution.[18] A third experiment was conducted wherein a different polymer film was applied. The new film was prepared in an identical manner using $Zn(dAb)_3(ClO_4)_2$. Zinc redox polymers have been found to be electrically insulating due to their lack of available redox states within the potential regions customarily accessible in standard electrochemical experiments. Accordingly, a thin film of Zn redox polymer should severely inhibit cell performance if uniformly present on photoanode surface. Unfortunately, iV curves with Zn-modified photoanodes behaved identically to controls. The results of all three experiments indicated that spin-coating was not adequately depositing a thin, uniform layer of monomer.

Drop-coating was also investigated. Several drops of the monomer solution (0.1 M in acetonitrile of iron, cobalt, or zinc) were applied to the still substrate. Excess solution was removed one of two ways. Initially, a glass microscope slide was used to

scrape off the solution from the macroscopic surface of the titania layer, leaving solution behind in the pores. This method was soon discarded in favor of a new method that incorporated the use of a second solvent, usually diethyl ether. As acetonitrile was soluble in diethyl ether but the monomer was not, immersion of the drop-coated photoanode into diethyl ether resulted in the rapid deposition of monomer onto the substrate as the local solvent composition shifted to nearly 100% diethyl ether. The photoanode was removed from solution, dried under a stream of N_2, and baked under vacuum at 68 °C. The drop-coating process was repeated 1-3 times, with polymer thickness ostensibly increasing with each subsequent drop-coating. DSSC iV experiments were performed with both $Co(dtb)_3(ClO_4)_2$ and FeCp as mediator. Thinner films again showed no difference with respect to unmodified control anodes, but thicker films (3 drop-coatings) displayed an unusual iV curve, shown in **Figure 3**, with cobalt redox films. Although little effort was made to understand the curve, at first glance it resembled a reduced photocurrent response with a cyclic voltammagram superimposed onto it. Non-uniform film deposition was assumed and further exploration of drop-coating was discontinued.

Semiconductor-catalyzed photoinitiation

Initial attempts to grow a polymer from the photoanode surface explored the possibility of using the nanocrystalline titania as a photocatalyst to initiate a radical polymerization. A GE ultraviolet lamp was used as a the UV light source, providing approximately 30 mW/cm^2 of power. The spectrum of an equivalent light bulb, made by Sylvania, shows that peak illumination occurs at 360, 405 and 430 nm. The 360 nm

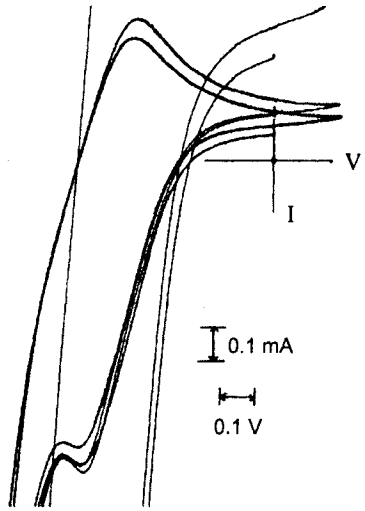

Figure 3. Result from iV experiments with thicker Co polymer films fabricated by drop-coating.

peak, with an energy of 3.44 eV, should be sufficient to excite an electronic transition across the bandgap of titania (3.2 eV).[48] Importantly, 360 nm illumination is not capable of directly exciting an electronic transition within the acrylate functionality. Any polymerization observed after UV illumination from this light source, therefore, must be due to the titania acting as a photocatalyst.

Preliminary experiments were performed to assess the feasibility of this approach. A solution of $Fe(dab)_3(ClO_4)_2$ in acetonitrile was spin-coated onto a clean glass microscope slide and covered with a microscope coverslip. The slide was exposed to UV light (30 mW/cm^2) for periods up to 20 minutes and then rinsed with acetonitrile. Assuming that any polymer formed would be cross-linked and therefore insoluble, residual red color on the slide (due to the intense red color of iron bipyridines) would indicate polymer formation. As a control, part of the microscope slide/coverslip was blocked from exposure to UV light during the experiment so that comparison could be

made between the exposed and unexposed portions. In all cases, no polymerization was observed on bare glass.

The same experiment was performed with a nanocrystalline titania photoanode. In this case, a significant amount of red color remained after the acetonitrile rinse, indicating polymer formation. Very little residual color was observed in those areas not exposed to UV light.

A similar experiment was devised, only this time a silicon rubber spacer was employed which contained a circular hole. Acting much like an O-ring, the spacer created a cavity when sandwiched between two glass slides. This cavity was filled with a solution of $Fe(dab)_3(ClO_4)_2$ monomer in acetonitrile and exposed to UV light. One side of the sandwich was always a clean microscope slide, while the other was either a microscope slide, a glass slide with a layer of compact TiO_2, or a photoanode with nanocrystalline titania. Exposure times up to 45 minutes were tried, but in all cases, polymer was only detected on the nanocrystalline titania. This was confirmed with XPS spectroscopy (using the presence or absence of an Fe peak in the spectrum).

In most cases, the detailed mechanism by which a semiconductor acts as a photocatalyst for the initiation of a radical polymerization is not fully understood. In the photocatalyzed initiation of vinyl monomers such as methyl methacrylate (MMA) by TiO_2, conflicting theories have been reported. A cationic process involving photogenerated holes, an anionic process utilizing e^-_{CB}, and a third possibility of dual e^-_{CB} and hole mechanisms have all been suggested.[49-52] Anionic initiation with MMA has been argued against on the basis of reduction potentials, as the reduction potential of MMA is approximately -1.1 V vs. NHE while that of TiO_2 is about -0.5 V vs. NHE.[49, 53,

[54] Countering this argument, the case has been made that e^-_{CB} reduce a third chemical species, creating a radical intermediary which is responsible for initiation.[49, 53, 55, 56] A cationic process utilizing a chemical intermediate has also been suggested, as has a cationic process wherein photogenerated holes react with MMA directly by abstracting a hydrogen atom, most probably from the α-methyl group.[49, 52, 57, 58] In the case of suspensions of nanoparticulate TiO_2, particle size may also play a role in determining the catalytic mechanism as so-called Q-sized ("quantum-sized," typically between 1 and 10 nm in diameter) semiconductors exhibit shifted band potentials relative to their macroscopic scale counterparts.[50, 51] Clearly, many factors influence the reaction of semiconductors in these systems, making the mechanism by which nanocrystalline TiO_2 photocatalyzes the initiation of $Co(dab)_3(ClO_4)_2$ difficult to predict.

A brief attempt to determine the initiation mechanism was made by conducting photocatalysis experiments in small (~5 mL) screwcap vials. Monomer solution (~1 mL, $Fe(dab)_3(ClO_4)_2$ in either acetonitrile or methanol) and a sliver of a nanocrystalline titiana photoanode were placed inside the vial. The vial was capped with a rubber septum and, in some cases, degassed with argon. The most polymer (darkest red residual color in the exposed area) was formed in reactions run in acetonitrile in the presence of oxygen, although the absence of oxygen did not greatly decrease the amount. With or without oxygen, very little polymer was formed during reactions run in methanol.

It has been reported that TiO_2, in the presence of water and oxygen, may produce hydroxyl radicals via an anionic mechanism with e^-_{CB} which can initiate polymerization in some systems.[49, 53, 56] In order to ascertain whether this mechanism was occurring in the cobalt system, polymerizations were also attempted with water and oxygen deliberately

introduced into the reaction solution. They were conducted in vials as just described. However, no polymerization was observed, suggesting that the reaction mechanism did not proceed through an anionic process requiring hydroxyl radical.

It is known that both acetonitrile and oxygen react rapidly with electrons in the conduction band (e^-_{CB}) of TiO_2.[49, 50, 55, 59] As neither acetonitrile nor oxygen impeded the formation of polymer, it may well be that, in this system, photocatalyzed initiation is occurring through the reaction of photogenerated holes with monomer (i.e., cationic initiation). A cationic initation is assisted by the presence of species in solution which can scavenge e^-_{CB}, preventing recombination of electron-hole pairs and thereby lengthening the hole lifetime.[50] In this system, acetonitrile and/or oxygen may play this role. Methanol, on the other hand, is known to be a hole scavenger and was observed to inhibit polymerization, indicating that it may be reacting competitively to inhibit cationic initiation.[59-61]

At this point, data from the preliminary experiments just described were reviewed and an assessment was taken in order to evaluate the likelihood that this approach would succeed in growing uniform, pin-hole free polymer films. Two major concerns still existed. Firstly, although preliminary results were encouraging, no photoanode had yet appeared dark enough to indicate a uniform polymer film across the entire surface area of the titania. Coverages seemed spotty, at best. Secondly, and more troublesome, the approach ignored the need for a monolayer of dye on the surface. Addressing the first concern, UV-Vis spectroscopy experiments indicated that, especially in the case of polymerizations conducted in glass vials, the majority of UV light was being lost to absorption by glass. Conceivably, quartz reaction vessels could reduce this amount and

improve the rate of initiation, possibly resulting in better coverages in shorter times. Also, assuming a hydrogen abstraction mechanism (*vida supra*), polymerizations of methacrylate-type monomers may be more amenable to cationic initiation than acrylates. If so, switching to a methacrylate-type monomer could also improve initiation efficiency. However, few reasonable solutions could be found to the problem of incorporating a monolayer of dye into the system. Accordingly, this line of investigation was dropped in favor of an approach utilizing ATRP.

Dye-initiated ATRP

As previously discussed, cross-linked, surface-bound polymer films must be fabricated using a "grafting from" approach due the low solubility of most cross-linked polymers. Accordingly, a surface-bound initiator is required. Fortuitously, DSSCs already have a sophisticated system in place for the application of a monolayer of dye to the titania surface. This system is based on the chemisorption of carboxylic acids to titania, and with it very dense, monolayer coverages may be attained. A sensible approach to surface-initiated polymerization in DSSCs, therefore, is to modify the dye molecule to act as both light absorber and ATRP initiator.

The development of a convenient, one-pot protocol for the synthesis of heteroleptic versions of "N3-type" dyes inspired initial designs for a complex which could fulfill the dual roles of light absorber and ATRP initiator.[62, 63] For purposes of this discussion, "N3-type" refers to ruthenium complexes with two bipyridine ligands and two thiocyanato ligands. The primary advantage that heteroleptic N3-type dyes offer is the ability to further tune the properties of the ruthenium complex via the substitution of one

of the 4,4'-dicarboxylic acid-2,2'-bipyridine ligands with another type of bipyridine (or other polypyridine). Modification of electronic properties allows for tuning of the dye's absorption spectrum, whereas other structural variations (such as hydrophobic appendages) have been shown to offer other advantages, such as longer device lifetimes, greater resistance to adventitious water, etc.[63, 64] In the case of ATRP, a heteroleptic dye would allow for the second bipyridine to contain functionalities capable of initiating the polymerization while preserving the highly desirable spectral characteristics of N3-type dyes.

Due to personal as well as group expertise, the complex chosen for the task was Ru(dcb)(αBE-bpy)$(SCN)_2$ (hereafter referred to as $A_{7\alpha BE}N_3$), where dcb = 4,4'-dicarboxylic acid-2,2'-bipyridine and αBE-bpy = 7,7'-(2,2'-bipyridine-4,4'-diyl)bis(heptane-7,1-diyl) bis(2-bromo-2-methylpropanoate. Unfortunately, the synthesis of this compound proved to be exceedingly difficult. The αBE-bpy ligand could not be chelated directly due its instability at the reaction temperatures required for the subsequent steps in the reaction (~145 °C). Accordingly, it was necessary to first synthesize Ru(dcb)(diol)$(SCN)_2$ (hereafter referred to as $A_{7OH}N_3$), where diol = 7,7'-(2,2'-bipyridine-4,4'-diyl)diheptan-1-ol, and then append the α-bromoester in a second reaction. Although all aspects of the synthesis of the $A_{7OH}N_3$ version went relatively smoothly, the isolation and characterization of $A_{7\alpha BE}N_3$ were unexpectedly troublesome.

Of particular concern was the NMR spectrum of the $A_{7\alpha BE}$N3 complex. Other heteroleptic complexes, including $A_{7OH}N_3$, behave as expected in an NMR experiment, and their spectra provide the most reliable way to identify the bipyridine ligands as well as verify product purity. In the case of $A_{7\alpha BE}N_3$, however, peak widths were dramatically

broad, so much so that peak integrations were useless and product confirmation was impossible (**Figure 4**). With the assistance of Dr. Rithner, an Inversion Recovery NMR experiment was performed to measure T_1 (or longitudinal) relaxation. The results of this experiment indicated that the T_1 parameter was within normal bounds. This suggests that the line-broadening was probably a T_2 issue, likely due to some type of kinetic exchange occurring on the timescale of the NMR experiment. Variable temperature NMR was conducted in order to both verify this conclusion and provide greater line resolution. As the compound only showed significant solubility in chloroform and dichloromethane, the accessible temperature range was somewhat limited. Standard ^{1}H NMR experiments were conducted at 50 °C and -50 °C. The spectrum of the high temperature experiment was unchanged with respect to the spectrum taken at room temperature. Surprisingly, the low temperature experiment showed only slightly greater peak resolution, despite the large difference in temperature.

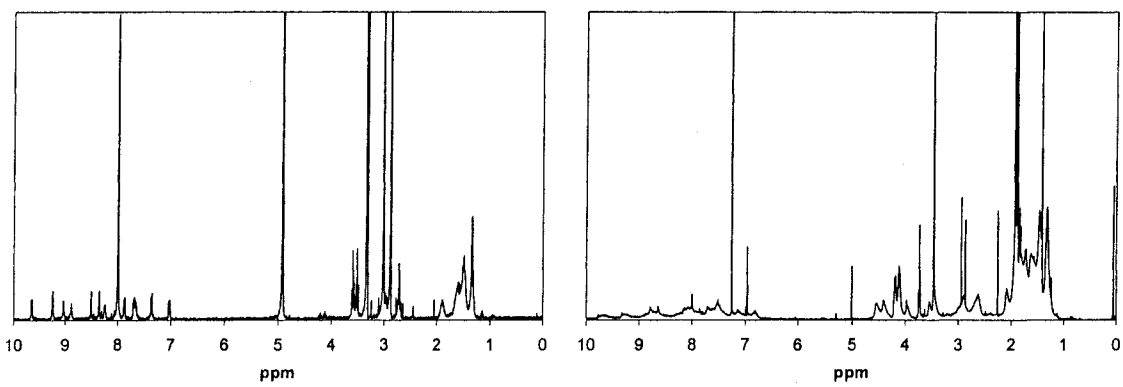

Figure 4. NMR spectra of (left) $A_{7OH}N3$ and (right) $A_{7\alpha BE}N_3$ at room temperature. Note the unusually broad lines in the right figure.

Initially, it was assumed that the kinetic exchange indicated by NMR involved transfer of a carboxylic proton, presumably either between carboxylate groups on the

same molecule or between separate molecules. HCl vapor was bubbled through a solution of $A_{7\alpha BE}N_3$ in an attempt to fully protonate the carboxylic acids, but to no effect. The influence of base on $A_{7OH}N_3$ (chosen for its normal NMR spectrum) was investigated and, although peak positions were altered, no line broadening was observed. The identity of base was unimportant, as both NaOD and Et_3N had the same effect.

Next, the possibility of bromide elimination/exchange from the α-bromoester functional group was considered. In order to eliminate such an interaction, the methacrylate analog of $A_{7\alpha BE}N_3$ was prepared. Unfortunately, the same type of line broadening was observed in the NMR spectrum.

Two final attempts were made to disrupt the kinetic exchange. In the event that the interaction was being facilitated by the length and flexibility of the carbon chain connecting the methacrylate group to the bipyridine ring, a short-chain version of the dye was synthesized. Linked to the bipyridine through a single, benzyllic carbon, the methacrylate ester should have significantly fewer degrees of freedom. However, the NMR spectrum once again indicated a kinetic exchange. Finally, an attempt was made to substitute the thiocyanato ligands with chloride ligands. Purification of the crude product was never achieved as, at this time, an alternate dye molecule was found.

Although their visible light absorption spectrum is far less desirable than that of N3-type dyes, ruthenium tris(bipyridine) species became attractive in this application due to relative ease with which they can be made. Well-studied for their optical and electrochemical properties, much is now known about the synthesis of both homo- and heteroleptic ruthenium tris(bipyridine) complexes.[65] Accordingly, $Ru(dcb)_2(\alpha BE\text{-}bpy)(PF_6)_2$ (hereafter referred to as "αBE-dye") was prepared which, although lacking a

broad UV-Vis absorption spectrum, could demonstrate proof-of-concept as an initiator for surface-initiated growth of cobalt bipyridine redox polymer. The complex was characterized with a variety of techniques, including thin layer chromatography (TLC), NMR, UV-Vis, mass spectrometry, and XPS. Although TLC seemed to indicate an impurity, NMR and mass spectrometry confirmed that the major compound present was the desired product. Photoanodes, dyed in a methanol/dye solution, were analyzed by UV-Vis and XPS (**Figure 5**). Both methods confirmed the presence of dye on the titania surface, with XPS indicating that both organic bromine and ruthenium were present.

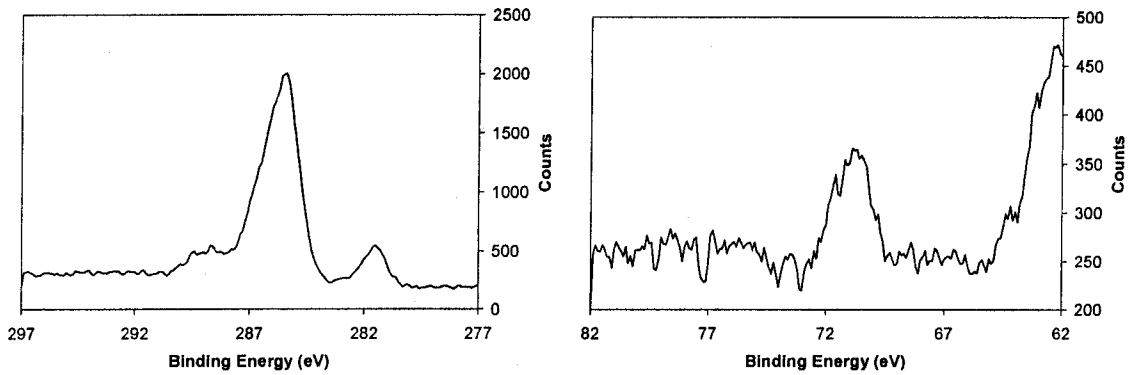

Figure 5. XPS spectra of a dyed (αBE-dye) TiO_2 photoanode: (left) peak at ~281 eV corresponds to Ru, other peaks are due to C, (right) peak at ~70 eV is from organic Br, peak at 62 eV is due to Ti. Binding energies have not been corrected.

At this point, the dyed photoanodes were used to initiate ATRP of methyl methacrylate (MMA). As precedent exists for the use of ruthenium bipyridines as initiators in the solution phase ATRP of MMA, this system was chosen to test the newly synthesized dye complex. MMA was distilled, followed by several freeze/pump/thaw cycles to remove oxygen, and brought into an inert atmosphere (N_2) glovebox. Polymerizations were conducted in toluene at two different monomer concentratios: 0.6

M MMA and 50/50 MMA/toluene (v/v). To each solution was added a nickel catalyst, dibromo-bis(triphenylphosphine)nickel(II), in an amount such that the final ratio of monomer to catalyst was either 100:1 (0.6 M solution) or 250:1 (50/50 solution). Once mixing was complete, the dyed photoanode was placed in the vial containing the reaction solution. The vial was then capped with a rubber septum, removed from the glovebox, and heated in a sandbath at ~80 °C overnight.

After 16 hours, the polymerization in the 50/50 solution was halted and the photoanode removed. The photoanode was rinsed in toluene, allowed to soak for 10 minutes in toluene, and then rinsed again with tolune to ensure removal of any unbound polymer (likely initially present as a significant amount of white solid was observed in the bottom of the vial). A white film was visible on the glass portion of the photoanode which was confirmed by XPS to be poly(MMA). Poly(MMA) was also found on the nanocrystalline titania portion (**Figure 6**), despite being invisible to the eye (not surprising given that the nanocrystalline titania appears white/blue even without the MMA film). In both cases, the presence of a strong organic bromine peak, in combination with the absence of a ruthenium peak, indicated that the film growth was proceeding in a controlled/living manner with a bromine atom capping the dormant radical chain.

After nearly 22 hours, the photoanode was extracted from the 0.6 M solution, rinsed with the same wash procedure as before, and analyzed. XPS on the titania portion indicated the presence of a thin poly(MMA) film with diminished (but still present) ruthenium peaks. No poly(MMA) was observed on the glass portion with XPS or by visible inspection. White solid, presumably polymer, was once again observed in the

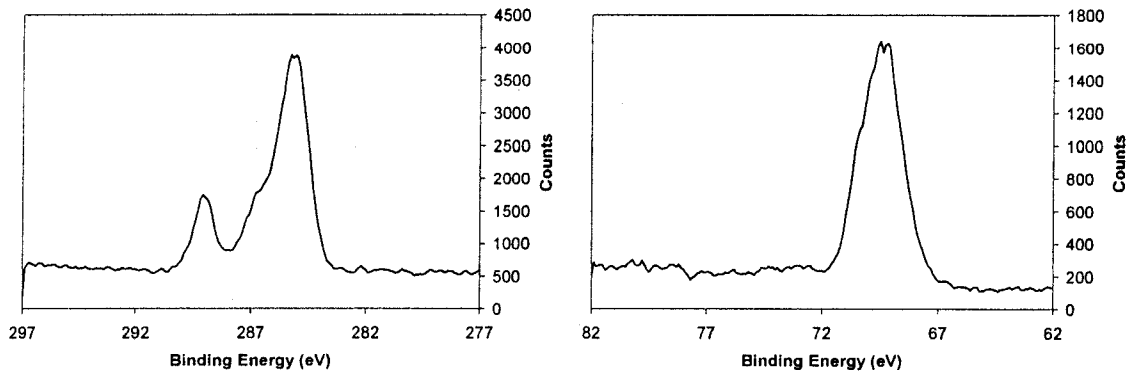

Figure 6. XPS spectra of poly(MMA) on TiO_2 photoanode: (left) Ru peak is absent, all peaks are due to C, (right) peak at ~70 eV is from organic Br, Ti peak is absent. Binding energies have not been corrected.

bottom of the reaction vial, likely indicating that polymerization was proceeding in solution as well as on the photoanode surface. Considering the vastly reduced amount of available monomer in the 0.6 M solution as well as the occurrence of polymerization in solution, the final thickness of the polymer layer on the photoanode may well have been limited by the depletion of available monomer at later reaction times. Nevertheless, both experiments demonstrated that under the proper conditions, the αBE-dye complex was capable of initiating ATRP polymerizations.

Polymerizations were then attempted with cobalt tris(bipyridine) monomer. Originally, the synthesis of $Co(dMA)_3(ClO_4)_2$ followed the same protocol as for $Co(dab)_3(ClO_4)_2$, but it was quickly discovered that isolation of $Co(dMA)_3(ClO_4)_2$ was an extremely delicate process. Premature polymerization during the rotary evaporation of MeOH was difficult to avoid, and a new strategy was adopted. The cobalt monomer was generated *in situ* in the reaction medium, eliminating losses to premature polymerization at the cost of also eliminating the ability to purify the monomer. Adventitious water, in particular, was introduced with this procedure as cobalt perchlorate hexahydrate is used as the source of free cobalt ion. Fortunately, ATRP reactions are not adversely affected

by water. In fact, reactions run in the presence of water can be significantly accelerated.[33, 43, 66-68] Free ligand was also introduced to the ATRP reaction medium, as a slight excess of dMA-bpy was used to ensure complete formation of the cobalt complex. Bis(4,4'-dimethyl-2,2'-bipyridine)copper(I) bromide was also generated *in situ*, primarily for reasons of convenience.

In the first attempted ATRP reaction, a 0.05 M solution of $Co(dMA)_3(ClO_4)_2$ in acetonitrile was prepared simply by mixing near stoichiometric quantities of $Co(ClO_4)_2$ x 6 H_2O and dMA ligand in acetonitrile using stirring with no heat. Similarly, in a second vial, a 0.005 M solution of $Cu(dmb)_2Br$ in acetonitrile was prepared, also with stirring and no heat. Within a couple of minutes, each solution became darkly colored, indicating complex formation. After ~30 minutes, 100 μL of the copper solution was added to the cobalt solution and stirred for another 5 minutes. Two dyed photoanodes were then added to the reaction solution. The reaction was allowed to proceed for 24 and 48 hours, respectively. After extensive rinsing, XPS was performed and indicated that no polymerization had occurred.

Reactions were run again, also for 24 and 48 hours, at 40 °C. No polymerization was observed. Reactions at 50 °C, however, resulted in rampant polymerization; nearly all of the solution became a brown solid (resembling mucous) that could not be re-dissolved yet was not attached to the photoanode. Only a thin, white film remained on the photoanodes after rinsing. XPS of the rinsed photoanodes indicated a loss of the ruthenium peak but no organic bromine peak (**Figure 7**). Clearly, the polymerization reaction was neither controlled nor living, and certainly not confined to the surface.

Although 50 °C is a relatively low temperature for thermally-induced polymerization of most methacrylates, it was apparently sufficient in the case of $Co(dMA)_3(ClO_4)_2$.

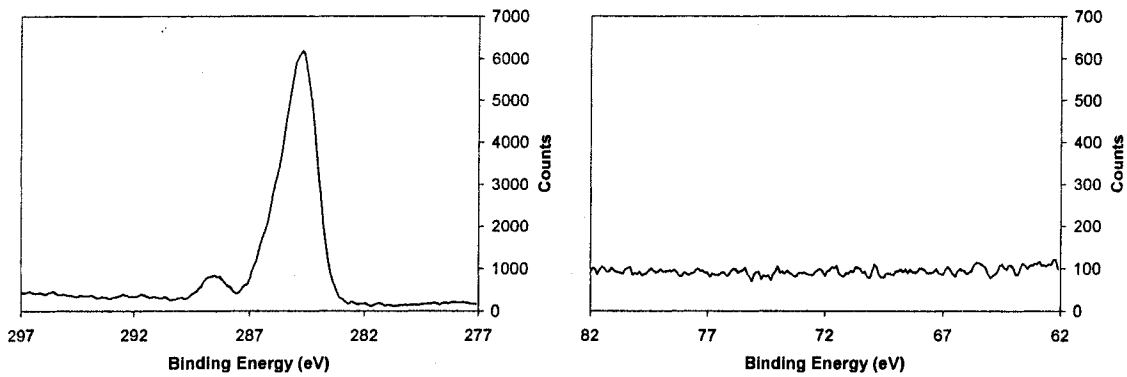

Figure 7. XPS spectra of a polymer-covered TiO_2 photoanode: (left) Ru peak is absent, both peaks are due to C, (right) neither Br nor Ti peaks are present. Binding energies have not been corrected.

The two possible strategies at this point were to either inhibit the thermal polymerization or to optimize the catalyzed ATRP reaction so that it could be performed at temperatures lower than 50 °C. Several mediocre options were possible for the former approach. Firstly, deactivator (the reduced form of the catalyst) could be added to solution. Radicals generated in solution would be passivated by transfer of a bromine atom, but the resulting dormant radical would likely continue to propagate in an ATRP fashion. Likewise, initiator could be added, increasing the efficacy of the persistent radical effect (*vide supra*) by increasing the concentration of deactivator. However, this has the same drawbacks as simply adding deactivator, i.e. ATRP would occur in solution. Thirdly, conventional inhibitors (e.g., MEHQ, catechol, quinone) could be added, but would likely inhibit both thermal and surface-initiated ATRP polymerizations. As no viable option existed for inhibiting thermal polymerization, efforts were directed towards development of ATRP at temperatures below 50 °C.

Catalyst design is of critical importance for any ATRP reaction, with novel systems often requiring modification of the catalyst.[38] In this case, it was realized that the integrity of the $Cu(dmb)_2Br$ catalyst was uncertain as an abundance of ClO_4^- anion from the cobalt monomer species was also present. Initially, this concern was ignored due to the non-nucleophilic nature of the ClO_4^- anion. As the reaction was not proceeding in an ATRP fashion, it seemed a relatively simple matter to confirm that the monomer counterion was not interfering. Accordingly, the same polymerization reaction was performed, but with $CoBr_2$ tetrahydrate rather than the perchlorate analog. After 18 hours at room temperature, the photoanode was removed from the reaction solution, rinsed well, and examined. Visual inspection revealed nothing, but XPS clearly indicated the presence of a cobalt redox film (**Figure 8**). Furthermore, the film appeared to be an ATRP-generated film as organic bromine peaks were still present.

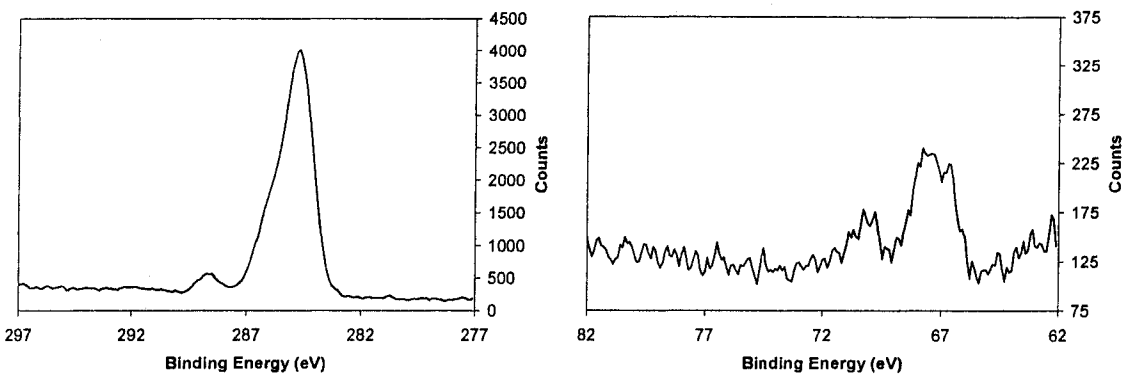

Figure 8. XPS spectra of polymer-covered TiO_2 photoanode: (left) Ru peak is absent, both peaks are due to C, (right) peak at ~70 eV is from organic Br, peak at 67 eV is due to inorganic Br, Ti peak (62 eV) is nearly gone. Binding energies have not been corrected.

Soon after this time, the αBE-dye's instability in MeOH became apparent. Dyed photoanodes, still the normal orange color, were no longer capable of initiating the

polymerization reaction. Mass spectrometry was performed and indicated that substitution of both α-bromides by methoxy groups had taken place. A solvent-screening process was begun. Although soluble in nitromethane, the αBE-dye was also not stable, quickly decomposing to a product that was never identified other than by XPS, which indicated the organic bromines had been lost. However, with extensive sonication, acetonitrile was found to be a suitable solvent.

It was also found necessary to optimize the dying procedure. Up to this point, the protocol for dying photoanodes had been to heat the photoanode in a drying oven, held at ~190 °C, for 30 minutes to an hour. The hot anodes were allowed a small period to cool slightly (to approximately 80-100 °C) and subsequently placed in the methanol dye solution. Although it was not certain whether it was a result of switching to acetonitrile solvent, or some other artifact of the communal drying oven, this procedure became inadequate. Although αBE-dye still dyed the photoanode the same color, the α-bromines were not consistently preserved. As the α-bromines were crucial to initiation/propagation of the polymer chain, this situation demanded rectification. Eventually, a new procedure was developed. The photoanode was heated at 250 °C in a different, cleaner oven for an hour or so and placed immediately into the acetonitrile dye solution. This procedure consistently yielded a strong organic bromine signal (by XPS) and, more importantly, resulted in polymerization.

The polymerization reaction was also refined. Of particular note, catalyst was added in both its activator and deactivator forms. As discussed previously, it is commonly necessary to compensate for the smaller number of propagating radicals in surface-initiated polymerizations. Deactivator, $Cu(dmb)_2Br_2$, was added to the reaction

solution such that 10% of the catalyst was in the deactivator form. Studies of ATRP of other vinyl monomers suggest that in normal solution phase polymerizations, the ratio stabilizes at approximately 3-5%.[36] In order to compensate for the likelihood of greater radical density at the titania surface, 10% deactivator was initially chosen. After early studies generated concern that the polymerization was not proceeding in a controlled/living fashion, this ratio was increased to 40%. Although excessive levels of deactivator shift the equilibrium of the propagating radical severely to the side of dormancy, thereby greatly slowing the ATRP reaction, priority was given to first achieving a controlled ATRP reaction. Optimization of reaction rate could follow.

Polymerization experiments were also conducted in mixed halide systems. Mixed halide systems, consisting of ATRP reactions where the halide on the initiator does not match the halide of the catalyst, are not new in the literature.[38, 43, 69, 70] Greater control over the polydispersity and controlled/living character of a polymerization may be gained, particularly with bromide-incorporating initiators and chloride-based catalysts. The explanation for this phenomenon lies in the greater bond strength of the C–Cl bond.[33] Prerequisite to a successful ATRP reaction is that the rate of initiation must be fast compared to the rate of propagation.[38, 69] This allows for all polymer chains to begin propagation at approximately the same time, facilitating a low polydispersity and a linear conversion rate with time. As the C–Br bond is more easily broken, initiation with bromide-type initiators occurs quickly, but propagation continues more slowly as chlorine will preferentially react with the active, chain-end radical (due to the greater bond strength of C–Cl).[69]

In this case, mixed-halide systems did not appear to offer any significant advantage, although sophisticated analysis of grown polymer films was not possible due to the cross-linked nature of the film and roughness of the nanocrystalline surface. In fact, as XPS was the primary tool used to characterize the films, mixed-halide systems only obfuscated characterization as inorganic and organic chlorine peaks were not resolved in these films. Mixed-halide systems were therefore abandoned, but not until one important series of experiments had been conducted in such a system.

This series of polymerizations was designed to elucidate whether or not the observed polymerization was indeed proceeding in a controlled/living fashion (i.e., was truly an ATRP reaction). In a mixed-halide system, a film was grown for 20 hours and examined with XPS. No peaks were present for either Ti or Ru, indicating the film thickness had exceeded the escape depth of photoelectrons from both elements. A second film was grown on a new photoanode, but this time film growth was monitored at 2, 4, 10, and 20 hours (**Figure 9**). This was accomplished by removing the photoanode from the reaction solution, rinsing according to the standard protocol, and characterizing with XPS. The photoanode was then returned to the reaction solution. Care was taken to examine a different location on the photoanode each time, in the event that X-rays were detrimental in some way to the organic species on the surface. The XPS spectrum slowly changed over time, finally resulting in a spectrum identical to that of the film grown on the first photoanode in one 20 hour stint.

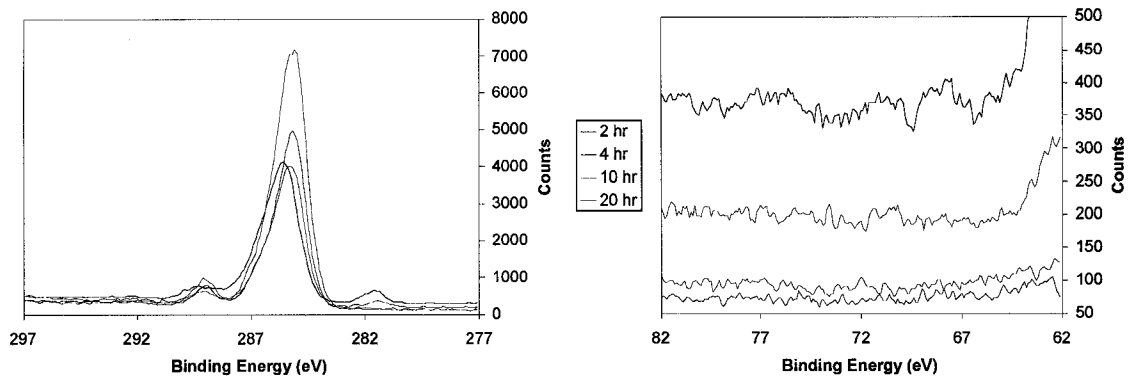

Figure 9. XPS spectra taken throughout a 20 hour polymerization: (left) Ru peak (at ~281 eV) disappears, C peaks increase, (right) Br peak (at ~70 eV) quickly disappears upon initiation, Ti peak at ~62 eV slowly disappears as film grows in thickness. Binding energies have not been corrected.

This result was encouraging for two reasons. Firstly, it indicated that redox polymer films could be consistently grown with approximately reproducible thicknesses. Secondly, it was consistent with a polymerization of "controlled/living" character where the polymer chain is never terminated, but rather is simply dormant when removed from the reaction conditions. Once reintroduced to the appropriate reaction conditions, a controlled/living polymerization may resume. The results of this experiment were consistent with such a process, although it did not rule out the possibility that an uncontrolled radical polymerization was occurring.

As the XPS spectrum was only useful for characterizing film thickness up to the escape depth of Ti and Ru photoelectrons, film growth beyond that point could not be detected. Furthermore, the presence of halide on the terminus of the propagating radical chain (the hallmark of a successfully controlled ATRP) could not be confirmed by XPS in this mixed halide systems due to the fact that the organic chlorine peak was unresolved from the larger inorganic chloride peak in the XPS spectrum. Therefore, the possibility that the film was the result of a short-lived, uncontrolled and "un-living" polymerization

with a slow rate of initiation (on the order of 20 hours) could not be ruled out. In this situation, an initiated polymer chain would uncontrollably propagate and soon terminate, resulting in the appearance of a polymer "island" localized on the surface. As the number of polymer islands steadily increased, the Ti and Ru peaks would be observed to slowly disappear. Unfortunately, later studies indicated that this latter scenario was the more likely (*vide infra*).

Once cobalt redox polymer films could be grown with reasonable control over film thickness, the next step was to test their performance in a DSSC. Two films were grown: one a thick, 20 hour film and the other a thinner, 10 hour film. Both films were characterized with XPS prior to DSSC iV experiments. DSSC experiments using both anodes were performed (**Figure 10**) with a gold counter electrode and a mediator solution of 0.15 M $Co(dtb)_3(ClO_4)_2$, 10% oxidized by $NOBF_4$, with 0.2 M lithium triflate and 0.2 M *tert*-butylpyridine (TBP) in γ-butyrolactone. For comparison, a control photoanode with no cobalt film was also tested. The photoanode with the thicker film performed far worse than the control, primarily due to a dramatically lower current. The thinner film, on the other hand, behaved very similarly to the control, indicating that the film was either behaving ideally as a hole-transport mediator or that film coverage was so inconsistent as to allow the solution-phase mediator unfettered access to the titania surface.

In order to clarify which was the case, a new solution-phase mediator was required, one which was incapable of efficient mediation in the absence of a surface film. During experimentation with the surface passivation of photoanodes, Gregg et al. found that ferrocene may perform adequately as a mediator only when recombination at the

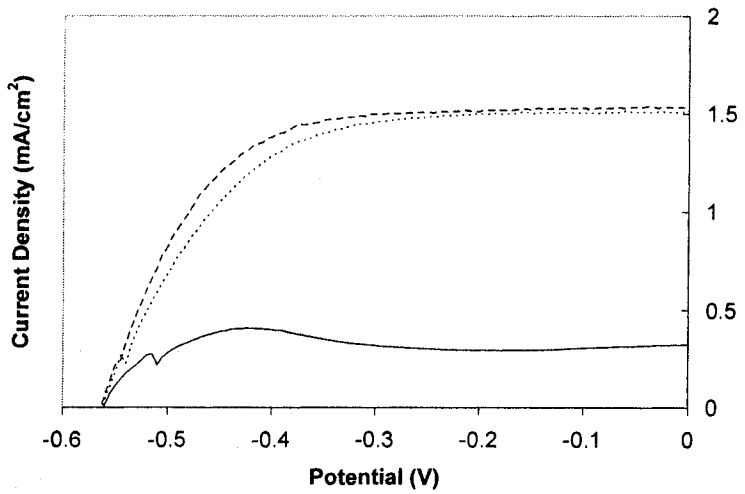

Figure 10. Results of iV experiments with (solid) a thick cobalt film, (dashed) a thinner cobalt film and (dotted) a regular photoanode without a film.

titania surface is inhibited.[18] These studies utilized silanization or electrochemical passivation to reduce recombination, but a successfully grown, thin cobalt redox film should perform similarly. When used as a mediator with an unmodified photoanode, ferrocene yields a very distinctive, very poor iV curve. With proper inhibition of recombination, the iV curve improves dramatically. Therefore, ferrocene is an ideal solution-phase co-mediator that should clearly delineate between photoanodes with and without uniform surface modification. Unfortunately, the reduction potential of ferrocene is not sufficiently negative to reduce a cobalt bipyridine film (0.31 V versus SCE as compared to 0.22 V, respectively).[18, 71] Decamethyl ferrocene (DmFc) has similar electron transfer kinetics and, owing to the ten electron-donating methyl substituents, has a more negative reduction potential of approximately -0.06 V (versus SCE), rendering it capable of reducing the cobalt film.

A mediator solution of 0.15 M DmFc and 0.2 M TBP in 1,2-dichlorobenzene was prepared. The mediator was oxidized to enhance conductivity, but the oxidation

procedure was altered, as $NOBF_4$ is practically insoluble in the solvent. Rather than adding a measured amount of $NOBF_4$ to a large volume of γ-butyrolactone and using 250 μL of this solution to dissolve the mediator, a single grain of NOBF4 was added to the already prepared mediator solution. Although minimally soluble in neat 1,2-dichlorobenzene, $NOBF_4$ was solubilized in the presence of reductant (i.e. the products of the reduction of $NOBF_4$ are soluble in 1,2-dichlorobenzene). The oxidation of DmFc was readily apparent; the initially yellow solution turned green.

The results of the iV experiments indicated that the cobalt films were not functioning ideally. The thicker film photoanode exhibited very poor behavior, with only a small current being generated. The thinner film photoanode proved to be even worse, behaving identically to the unmodified control photoanode (i.e., no photocurrent was observed). At least three possible explanations existed (illustrated in **Figure 11**). Firstly, the cobalt film, at thicknesses sufficient to insulate the titania from solution-phase species, was fatally resistive and preventing proper DSSC function. As little could be done to remedy this problem, it was initially ignored. Secondly, the cobalt film was uniform across the titania surface but was not grafting from exposed regions of FTO glass deep within the titania layer. Due to the high electron density at the FTO surface, perhaps recombination was occurring there at rates great enough to significantly inhibit cell performance.[18] Thirdly, the film was not uniform in coverage on either the titania or the FTO. XPS confirmed the existence of cobalt film on the macroscopic surface of the titania layer but offered little information about the condition of the film inside the pores.

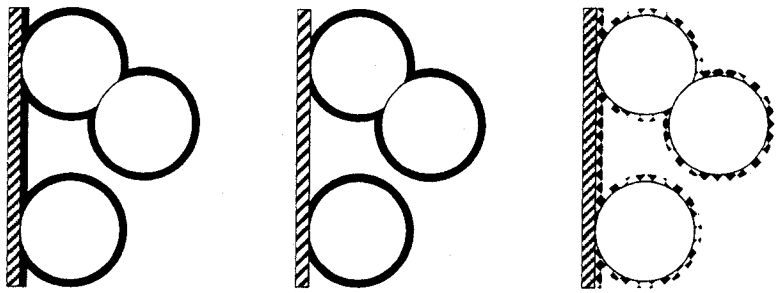

Figure 11. Three possible cobalt film scenarios: (left) film is uniformaly covering all surfaces, (middle) film is covering titania nanoparticles but not FTO glass, (right) film is non-uniform and exposed regions of either titania or FTO are present.

If the second situation were the case, the obvious solution would be to passivate the FTO glass. As the nanocrystalline titania is not electrically conductive until fairly negative potentials are reached, electrochemical polymerization is a convenient method to selectively deposit an insulating film onto the FTO surface. Using a procedure developed by Strein and Ewing and later refined by Gregg et al., an insulating, cross-linked phenol/2-allylphenol copolymer (PPO) can now be easily grown on exposed regions of FTO.[18, 72] The procedure (described above in detail) was performed on photoanodes prior to dye sensitization. After a 10 hour polymerization period, photoanodes were rinsed per usual, characterized with XPS, and evaluated in a iV experiment. Control photoanodes, with PPO but without cobalt film, were also tested. **Figure 12** (left side) shows cyclic voltammetry performed with a photoanode working electrode in a solution of DmFc. The photoanode with PPO film is significantly more insulating than the photoanode without. As can be seen in **Figure 12** (right side), PPO enhanced overall cell performance for both photoanodes (with and without cobalt film) when DmFc was used as the mediator. This result is in good agreement with those previously published by Gregg et al. and is due to the decreased recombination on FTO.[18] However, little difference was observed between photoanodes with and without the

cobalt film, indicating that performance-inhibiting recombination was also occurring on regions of the titania not covered with film.

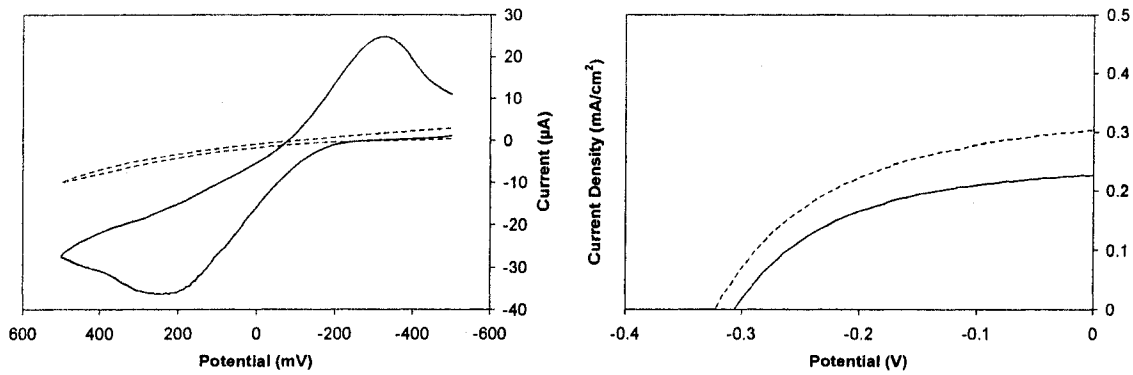

Figure 12. Cyclic voltammetry (left) and iV experiments (right) with DmFc mediator on photoanodes with (dashed) PPO treatment only and (solid) PPO treatment with thinner cobalt film.

Scanning electron microscopy (SEM) was used in an attempt to visualize the cobalt film. Nanocrystalline titania on conducting glass is a reasonably good medium for SEM, due to the sturdy and electron-conducting nature of the surface, and has often been imaged with SEM by other research groups as well as our own (**Figure 13**).[9, 73-76] Photoanodes prepared from typical colloids result in titania spheres with an average diameter of approximately 10-20 nm. As early ATRP efforts resulted in films barely detectable to XPS (a much more sensitive technique), it was generally assumed that the films would not be visible by SEM. However, once XPS no longer detected titanium photoelectrons from the surface, the film thickness was estimated to be on the order of 10 nm (10 nm is an average photoelectron escape depth through an organic matrix). A 10 nm film, applied evenly to the exposed surface of a 10-20 nm sphere, would yield spheres of distinctly larger diameter, perhaps so much so that the film's presence could be visible by SEM.

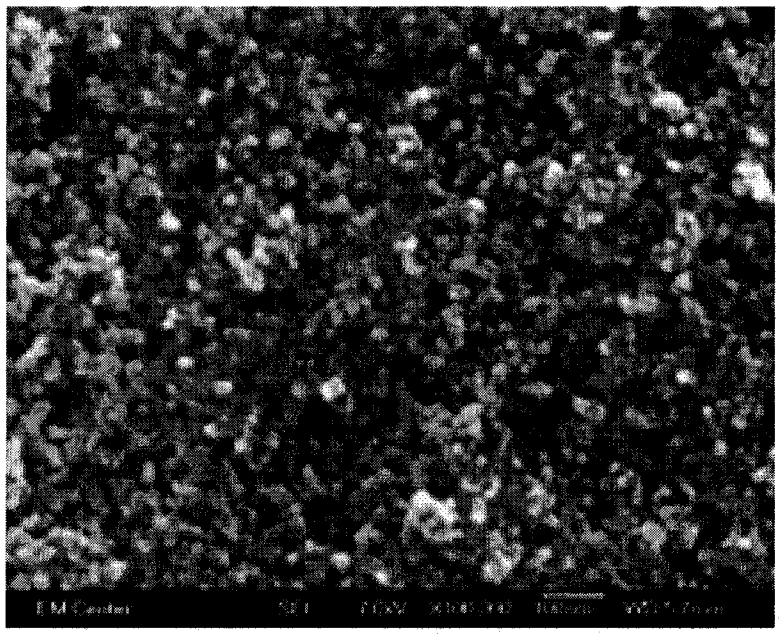

Figure 13. SEM of unmodified nanocrystalline TiO_2 photoanode. Scalebar is 100 nm.

The resulting SEM micrographs are shown in **Figure 14** below. Clearly apparent, a dramatic change in surface morphology has occurred on photoanodes with thicker cobalt films. The film appears to cover the entire macroscopic surface of the titania layer and no pores are visible. The photoanode with a thinner cobalt film, on the other hand, displays distinct regions of polymer as well as regions with no detectable film whatsoever. Fortuitously, a remarkably shallow scratch (most likely less than a micron) was found in the titania layer, allowing for visualization of the inner pore network. No cobalt polymer was visible, indicating both that the polymerization process was not occurring below the macroscopic surface of the titania and that the scratch had been formed after the polymerization reaction. These results strongly suggest that the polymerization process is one of localized, rapid polymerization events that are quickly

and irreversibly terminated, occurring over time until the entire macroscopic surface is covered. It seems unlikely that the process was that of an even, controlled/living polymerization, where slow, uniform film growth would occur.

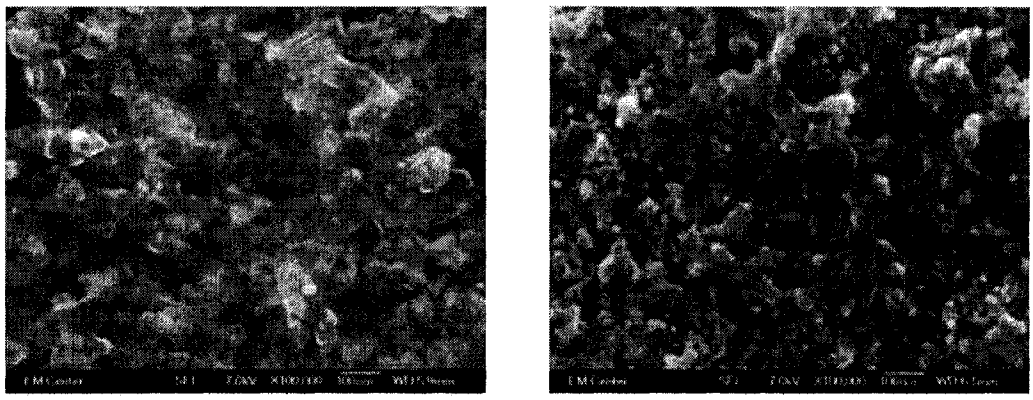

Figure 14. SEM images of TiO_2 photoanodes with (left) a thicker cobalt film and (right) a thinner cobalt film. Note that only the thicker film appears to fully cover the TiO_2 surface. Scalebars are both 100 nm.

Nevertheless, the SEM micrographs in **Figure 14** may provide a small glimmer of hope for the utility of cobalt films in DSSCs. Although only a very small fraction of the total surface area was sampled in the SEM experiments, it appeared that the coverage of the thicker film on the photoanode was complete, i.e. no significant exposed regions of titania remained. Revisiting **Figure 10**, it may be seen that photocurrents were generated across this cobalt film. While it could be that the film's inherent resistivity limited DSSC performance, it could also be that the cell was hampered by a much reduced surface area due to the unavailability of the inner pore network. The SEM image provides a very good indication that the latter possibility was the primary (or at the very least, a strongly contributing) factor. If so, then the obvious solution is to explore ways in which the cobalt film may be grown within the pores and not just on the macroscopic surface of the titania layer.

Recently, several successful methods of growing ordered, mesoporous thin films of titania have been reported.[77-81] These methods differ from the conventional method – which utilizes a titania colloid and results in a random orientation of anatase particles – in that the pore network may be aligned to enhance electron and mediator transport throughout the film. Strategies range from the directed growth of titania nanorods and nanopillars to the ordered stacking of titania nanoparticles. Nearly all employ some type of structure-directing agent, most commonly Pluronic P123 (a tri-block co-polymer available commercially) to form an ordered template for titania growth. In some cases, an additional effect is the enlargement of the pore diameter to truly mesoporous dimensions (defined as pores with 2-50 nm diameters), resulting in pores of 10-20 nm in diameter.[82] In the case of polymer film growth, a larger pore diameter could increase the likelihood that the polymer film would penetrate beyond the macroscopic surface into the inner pore network.[9]

The method of Zukulová et al. was chosen both for its relative simplicity as well as for its demonstrated large pore size.[79] This method utilizes Pluronic P123 to direct the templating of titania nanoparticles. After only a few attempts, films could be made with regions of meso-sized pores. However, significant regions remained without organization – often without any pores whatsoever – and the effort was abandoned.

Conclusions/Future Work

A thin, cobalt redox polymer film was successfully grown in a surface-initiated polymerization. However, it is unlikely that the polymerization reaction proceeded in a controlled/living manner or, in fact, that it occurred by way of an ATRP-type mechanism

at all. SEM and XPS experiments suggest that the polymerization was initiated at the surface by the dye, but that the active radical was typically not well-deactivated, resulting in isolated regions of uncontrolled polymer growth. Over time (approximately 10 hours), these islands of polymer merged, forming a fairly pinhole-free film on the macroscopic surface of the titania layer. Although reproducible, the film impaired photoanode performance in DSSC iV experiments. Whether it did so because of a reduced photoactive surface area or because of an intrinsic electrical resistance on the part of the polymer remains unclear.

It is recommended that further work in this area proceed along two major avenues. Firstly, and most importantly, efforts should be directed to refinement of the surface-initiated polymerization process. The benefits of a controlled/living ATRP reaction (namely slow, uniform growth with a high degree of control over film thickness) could likely address many of the deficiencies of the current polymer film. Secondly, the morphology of the titania layer could be altered to better suit the inclusion of a cobalt film into the pore network. Template-directed assembly of titania nanoparticles or nanotubes are particularly promising techniques which are capable of providing larger, better organized pores to facilitate penetration of polymer into the titania layer.

A variety of strategies for refining the polymerization reaction remain unexplored. As initiation of the reaction is achieved (apparent by the formation of polymer) but is seemingly followed by uncontrolled propagation, attention should be given to the deactivation process. Several suggestions follow.

In most cases, catalyst species for ATRP reactions are prepared *in situ* and, as a result, the exact composition and structure of the catalyst are known in only a few

instances.[83-87] In the process of activating a dormant radical, a copper catalyst abstracts a halogen atom while simultaneously undergoing a one-electron oxidation. Commonly, a change in coordination number accompanies the change in oxidation state for copper coordination complexes. Accordingly, an initially 4-coordinate copper(I) complex may incorporate up to two other ligands into its inner coordination sphere upon oxidation. Free bipyridine in solution could be expected to bind to the copper(II) ion, yielding a stable complex less easily reduced back to copper(I) and thereby inhibiting radical deactivation. However, countering this argument is the fact that successfully controlled ATRP reactions have intentionally been conducted with excess bipyridine.[36, 41, 88]

Nevertheless, to guard against possible side effects from excess bipyridine, preparation and purification of monomer as well as both activator and deactivator forms of the catalyst prior to their use in the polymerization reaction would significantly reduce the chance of free bipyridine in solution (the current polymerization technique deliberately uses excess bipyridine to ensure complete formation of each metal species). An alternate strategy would be to utilize copper complexes with polydentate ligands whose coordination geometry precludes the possibility of an additional bidentate ligand. One way to do this is to utilize a tetradentate ligand which binds in a square planar geometry. As only axial sites remain available for further coordination, a bidentate ligand (requiring adjacent binding sites on the metal) cannot chelate to the copper. Several such copper complexes have been reported to catalyze ATRP reactions, although they still underperform $Cu(bpy)_2X$.[84, 87, 89, 90]

Another possibility is that the density of methacrylate groups on the surface is simply just too high. Although there are only two methacrylate functionalities per

molecule of dye, the monomer, once bound to the dye, would add up to five additional methacrylate groups. As the density of polymerizable groups increases, the concentration of deactivator may become unable to keep the number of active radicals adequately low. Although an unusually high ratio of activator to deactivator was employed (3:2), it may be that the absolute concentration of deactivator was still too low (0.2 mM). It has been found that homogeneous polymerizations conducted in bulk generally result in a concentration of 1 mM deactivator at steady state. Surface-initiated reactions have been reported to require deactivator concentrations of 4.3 mM and 12.8 mM for reactions conducted in bulk and in solution, respectively, in order to achieve controlled/living conditions.[36, 43]

A possible remedy for this situation would be to reduce the concentration of methacrylate groups at the surface through alteration of the monomer. A monomer with fewer methacrylates could easily be prepared. Dialkyl bipyridines with only one alkyl group containing a methacrylate ester would result in a cobalt species with only three total polymerizable functionalities when complexed homoleptically. Synthetically more involved would be the synthesis of a heteroleptic cobalt complex, where two or less bipyridines contain one or two methacrylate esters. The considerable lability of bipyridine ligands chelated to cobalt discourages such an approach, however. Still, as the vast majority of ATRP reactions (both surface-initiated and otherwise) are conducted on monofunctional monomers, it might be prudent to somehow prepare a monofunctional cobalt complex, perhaps one which could be crosslinked after the initial ATRP reaction.

An alternative strategy is to grow a straight-chain polymer using the ligand only, and afterwards cross-link the chains by way of complexation with the metal species. In

addition to reducing the number of methacrylates per monomer, the concentration of monomer could be increased, allowing for an increase in deactivator concentration as well. For solubility reasons, the $Co(dMA)_3(ClO_4)_2$ concentration was not increased beyond 50 mM, thereby limiting the deactivator concentration since a 100:1 or greater monomer-to-catalyst ratio is usually desired.[91, 92] With a change in reaction solvent, the concentration of the substituted bipyridine could likely be made much higher, allowing for correspondingly larger concentrations of deactivator. A natural concern with this strategy is that the introduced cobalt ions would crosslink the polymer at the outer surface of the film to an extent which would prevent further, deeper penetration of cobalt into the film. The resulting film would be cross-linked and (more importantly) redox active only at the outer surface of the film. The cobalt-less inner region of the film would present a significant barrier to conductivity and likely inhibit cell performance. If this was found to be the case, the obvious solution would be to grow films by only a very small amount before cross-linking. A great benefit of the controlled/living nature of ATRP is that several polymerization/crosslinking cycles could be performed if necessary, allowing for the growth of polymer films thicker than the penetration depth of cobalt ion.

A further concern with the direct ATRP of cobalt coordination complexes exists. Cobalt-mediated radical polymerization (CMRP) is another CRP technique, closely related to ATRP. Instead of reversible halogen transfer, association of a cobalt coordination complex with the propagating radical is exploited to temporarily deactivate the growing polymer chain. With their d7 electron configurations, many cobalt(II) complexes act as a stable radical capable of pairing with the active, chain-end radical on the propagating chain.[93, 94] Typical cobalt complexes used are cobalt(II) porphyrins and

variants of bis(acetylacetonate)cobalt(II). Both types share an obvious similarity to the cobalt monomers employed in these ATRP studies. Accordingly, it may be that the cobalt monomer is interacting in some way with the propagating radical or otherwise interfering with proper deactivator function, limiting control in this system.

There are two reasons to expect this to not be the case. Firstly, CMRP catalysts require a "vacant" site in their coordination sphere through which they may interact with the propagating radical. Porphryns and bis(acetylacetonate) species both bind the cobalt in a square planar geometry which leaves both axial sites open; tris(bipyridine) species have no such vacancy. In addition, if the monomer were acting as a radical deactivator, it would be expected to dramatically slow polymerization as the monomer is present in large excess. As slow initiation followed by too rapid polymerization seems to be the case, it is unlikely that the cobalt monomer is behaving in a deactivating capacity. However, a simple test would be to substitute another metal species for the cobalt and observe whether the polymerization reaction is altered. A diamagnetic species (unlikely to interact strongly with free radicals in solution due to a lack of unpaired electrons) such as low-spin iron(II) would make a logical choice.

Finally, it is worth mentioning that while several possibilities remain for the controlled growth of cobalt films using ATRP, it is difficult to conceive that such a film would be of benefit to DSSCs with the current nanocrystalline morphology. Further study of the current literature, in combination with the results presented herein, indicates that the chaotic nature of the randomly deposited film (with randomly oriented and sized pores) is not well-suited for the inclusion of a thin polymer film. Accordingly, it should be noted that any further research of cobalt films by ATRP (perhaps interesting in their

own right) should be conducted with other aims or applications in mind – at least until better morphological control over mesostructured, nanocrystalline films of TiO_2 is realized.

Bibliography

1. Kang, J.; Li, W.; Wang, X.; Lin, Y.; Xiao, X.; Fang, S., Polymer electrolytes from PEO and novel quaternary ammonium iodides for dye-sensitized solar cells. *Electrochimica Acta* **2003,** 48, 2487-2491.

2. Wang, P.; Zakeeruddin, S. M.; Comte, P.; Exnar, I.; Grätzel, M., Gelation of Ionic Liquid-Based Electrolytes with Silica Nanoparticles for Quasi-Solid-State Dye-Sensitized Solar Cells. *Journal of the American Chemical Society* **2003,** 125, (5), 1166-1167.

3. Peter, K.; Wietasch, H.; Peng, B.; Thelakkat, M., Dual-functional materials for interface modifications in solid-state dye-sensitised TiO_2 solar cells. *Applied Physics A - Materials Science & Processing* **2004,** 79, 65-71.

4. Papageorgiou, N., Counter-electrode function in nanocrystalline photoelectrochemical cell configurations. *Coordination Chemistry Reviews* **2004,** 248, 1421-1446.

5. O'Regan, B.; Schwartz, D. T., Efficient dye-sensitized charge separation in a wide-band-gap *p-n* heterojunction. *Journal of Applied Physics* **1996,** 80, (8), 4749-4754.

6. O'Regan, B.; Lenzmann, F.; Muis, R.; Wienke, J., A Solid-State Dye-Sensitized Solar Cell Fabricated with Pressure-Treated P25-TiO_2 and CuSCN: Analysis of Pore Filling and IV Characteristics. *Chemistry of Materials* **2002,** 14, 5023-5029.

7. Senadeera, G. K. R.; Jayaweera, P. V. V.; Perera, V. P. S.; Tennakone, K., Solid-state dye-sensitized photocell based on pentacene as a hole collector. *Solar Energy Materials & Solar Cells* **2002,** 73, 103-108.

8. Nogueira, A. F.; Longo, C.; De Paoli, M.-A., Polymers in dye sensitized solar cells: overview and perspectives. *Coordination Chemistry Reviews* **2004,** 248, 1455-1468.

9. Grant, C. D.; Schwartzberg, A. M.; Smestad, G. P.; Kowalik, J.; Tolbert, L. M.; Zhang, J. Z., Characterization of nanocrystalline and thin film TiO_2 solar cells with poly(3-undecyl-2,2'-bithiophene) as a sensitizer and hole conductor. *Journal of Electroanalytical Chemistry* **2002,** 522, 40-48.

10. Smestad, G. P.; Spiekermann, S.; Kowalik, J.; Grant, C. D.; Schwartzberg, A. M.; Zhang, J.; Tolbert, L. M.; Moons, E., A technique to compare polythiophene solid-state dye sensitized TiO_2 solar cells to liquid junction devices. *Solar Energy Materials & Solar Cells* **2003,** 76, 85-105.

11. van Hal, P. A.; Wienk, M. M.; Kroon, J. M.; Verhees, W. J. H.; Slooff, L. H.; van Gennip, W. J. H.; Jonkheijm, P.; Janssen, R. A. J., Photoinduced Electron

Transfer and Photovoltaic Response of a MDMO-PPV:TiO_2 Bulk-Heterojunction. *Advanced Materials* **2003,** 15, (2), 118-121.

12. Sharma, G. D. S. S.; Roy, M. S., Charge conduction and photogeneration process in hybrid materials of conjugated polymer and dye-sensitized TiO_2 thin-film device. *Journal of Materials Science: Materials in Electronics* **2004,** 15, 69-74.

13. Haque, S. A.; Park, T.; Xu, C.; Koops, S.; Schulte, N.; Potter, R. J.; Holmes, A. B.; Durrant, J. R., Interface Engineering for Solid-State Dye-Sensitized Nanocrystalline Solar Cells: The Use of Ion-Solvating Hole-Transporting Polymers. *Advanced Functional Materials* **2004,** 14, (5), 435-440.

14. Longo, C.; Nogueira, A. F.; De Paoli, M.-A.; Cachet, H., Solid-State and Flexible Dye-Sensitized TiO_2 Solar Cells: a Study by Electrochemical Impedance Spectroscopy. *Journal of Physical Chemistry B* **2002,** 106, 5925-5930.

15. Nusbaumer, H.; Moser, J.-E.; Zakeeruddin, S. M.; Nazeeruddin, M. K.; Grätzel, M., $Co^{II}(dbbip)_2^{2+}$ Complex Rivals Tri-iodide/Iodide Redox Mediator in Dye-Sensitized Photovoltaic Cells. *Journal of Physical Chemistry B* **2001,** 105, 10461-10464.

16. Sapp, S. A.; Elliott, C. M.; Contado, C.; Caramori, S.; Bignozzi, C. A., Substituted Polypyridine Complexes of Cobalt(II/III) as Efficient Electron-Transfer Mediators in Dye-Sensitized Solar Cells *Journal of the American Chemical Society* **2002,** 124, (37), 11215-11222.

17. Cameron, P. J.; Peter, L., M.; Zakeeruddin, S. M.; Grätzel, M., Electrochemical studies of the Co(III)/Co(II)$(dbbip)_2$ redox couple as a mediator for dye-sensitized nanocrystalline solar cells. *Coordination Chemistry Reviews* **2004,** 248, 1447-1453.

18. Gregg, B. A.; Pichot, F.; Ferrere, S.; Fields, C. L., Interfacial Recombination Processes in Dye-Sensitized Solar Cells and Methods To Passivate the Interfaces. *Journal of Physical Chemistry B* **2001,** 105, 1422-1429.

19. Murray, R. W., Polymer Modification of Electrodes. *Ann. Rev. Mater. Sci.* **1984,** 14, 145-169.

20. Pickup, P. G.; Kutner, W.; Leidner, C. R.; Murray, R. W., Redox Conduction in Single and Bilayer Films of Redox Polymer. *Journal of the American Chemical Society* **1984,** 106, 1991-1998.

21. Jernigan, J. C.; Surridge, N. A.; Zvanut, M. E.; Silver, M.; Murray, R. W., Electrical-Field-Driven Electron Self-Exchange in a Mixed-Valent Osmium(II/III) Bipyridine Polymer: Solid-State Reactions of Low Exothermicity. *Journal of Physical Chemistry* **1989,** 93, 4620-4627.

22. White, B. A.; Murray, R. W., Kinetics of Electron Self-Exchange Reactions between Metalloporphyrin Sites in Submicrometer Polymeric Films on Electrodes. *Journal of the American Chemical Society* **1987,** 109, 2576-2581.

23. Jernigan, J. C.; Murray, R. W., Electron Self-Exchanges in an Osmium Polypyridine Redox Polymer in the Absence of Liquid Solvents by Solid-State Voltammetry. *Journal of the American Chemical Society* **1987,** 109, 1738-1745.

24. Ching, S.; Elliott, C. M., Coordination Polymers Based on Bis(bipyridyl)alkane Ligands: Film Preparation and Charge-Transport Characteristics. *Langmuir* **1999,** 15, (4), 1491-1497.

25. Sutin, N., Theory of Electron Transfer Reactions: Insights and Hindsights. In *Progress in Inorganic Chemistry*, Taube, H.; Lippard, S. J., Eds. John Wiley & Sons, Inc.: 1983; Vol. 30, pp 441-498.

26. Ruff, I.; Friedrich, V. J., Transfer Diffusion. I. Theoretical. *Journal of Physical Chemistry* **1971,** 75, (21), 3297-3302.

27. Frank, A. J.; Kopidakis, N.; van de Lagemaat, J., Electrons in nanostructured TiO_2 solar cells: transport, recombination and photovoltaic properties. *Coordination Chemistry Reviews* **2004,** 248, 1165-1179.

28. Abruña, H. D.; Denisevich, P.; Umaña, M.; Meyer, T. J.; Murray, R. W., Rectifying interfaces using two-layer films of electrochemically polymerized vinylpyridine and vinylbipyridine complexes of ruthenium and iron on electrodes. *Journal of the American Chemical Society* **1981,** 103, 1-5.

29. Denisevich, P.; Abruña, H. D.; Leidner, C. R.; Meyer, T. J.; Murray, R. W., Electropolymerization of vinylpyridine and vinylbipyridine complexes of iron and ruthenium: homopolymers, copolymers, reactive polymers. *Inorganic Chemistry* **1982,** 21, 2153-2161.

30. Guadalupe, A. R.; Usifer, D. A.; Potts, K. T.; Hurrell, H. C.; Mogstad, A.-E.; Abruña, H. D., Novel Chemical Pathways and Charge-Transport Dynamics of Electrodes Modified with Electropolymerized Layers of $[Co(V\text{-}terpy)_2]^{2+}$. *Journal of the American Chemical Society* **1988,** 110, 3462-3466.

31. Kamat, P. V.; Bedja, I.; Hotchandani, S.; Patterson, L. K., Photosensitization of Nanocrystalline Semiconductor Films. Modulation of Electron Transfer between Excited Ruthenium Complex and SnO2 Nanocrystallites with an Externally Applied Bias. *Journal of Physical Chemistry* **1996,** 100, 4900-4908.

32. Zaban, A.; Meier, A.; Gregg, B. A., Electric Potential Distribution and Short-Range Screening in Nanoporous TiO_2 Electrodes. *Journal of Physical Chemistry B* **1997,** 101, 7985-7990.

33. Edmondson, S.; Osborne, V. L.; Huck, W. T. S., Polymer brushes *via* surface-initiated polymerization. *Chem. Soc. Rev.* **2004,** 33, 14-22.

34. Zhao, B.; Brittain, W. J., Polymer brushes: surface-immobilized macromolecules. *Progress in Polymer Science* **2000,** 25, 677-710.

35. von Werne, T.; Patten, T. E., Atom Transfer Radical Polymerization from Nanoparticles: A Tool for the Preparation of Well-Defined Hybrid Nanostructures and for Understanding the Chemistry of Controlled/"Living" Radical Polymerizations from Surfaces. *Journal of the American Chemical Society* **2001,** 123, 7497-7505.

36. Matyjaszewski, K.; Miller, P. J., Polymers at Interfaces: Using Atom Transfer Radical Polymerization in the Controlled Growth of Homopolymers and Block Copolymers from Silicon Surfaces in the Absence of Untethered Sacrificial Initiator. *Macromolecules* **1999,** 32, 8716-8724.

37. Matyjaszewski, K., Comparison and Classification of Controlled/Living Radical Polymerizations. In 2000.

38. Patten, T. E.; Matyjaszewski, K., Atom Transfer Radical Polymerization and the Synthesis of Polymeric Materials. *Advanced Materials* **1998,** 10, (12), 901-915.

39. Liu, P.; Tian, J.; Liu, W.; Xue, Q., Surface-initiated atom transfer radical polymerization (ATRP) of styrene from silica nanoparticles under UV irradiation. *Polymer International* **2003,** 53, 127-130.

40. Zhan, B.-Z.; White, M. A.; Fancy, P.; Kennedy, C. A.; Lumsden, M., Functionalization of a Nano-Faujasite Zeolite with PEG-Grafted PMA Tethers Using Atom Transfer Radical Polymerization. *Macromolecules* **2004,** 37, 2748-2753.

41. Matyjaszewski, K.; Xia, J., Atom Transfer Radical Polymerization. *Chem. Rev.* **2001,** 101, 2921-2990.

42. Wang, A., R.; Zhu, S., Control of the Polymer Molecular Weight in Atom Transfer Radical Polymerization with Branching/Crosslinking. *Journal of Polymer Science: Part A: Polymer Chemistry* **2005,** 43, 5710-5714.

43. Huang, W.; Baker, G. L.; Bruening, M. L., Controlled synthesis of Cross-Linked Ultrathin Polymer Films by Using Surface-Initiated Atom Transfer Radical Polymerization. *Angewandte Chemie International Edition* **2001,** 40, (8), 1510-1512.

44. Wang, J.-Y.; Chen, W.; Liu, A.-H.; Lu, G.; Zhang, G.; Zhang, J.-H.; Yang, B., Controlled Fabrication of Cross-Linked Nanoparticles/Polymer Composite Thin Films through the Combined Use of Surface-Initiated Atom Transfer Radical

Polymerization and Gas/Solid Reaction. *Journal of the American Chemical Society* **2002,** 124, 13358-13359.

45. Jiang, C.; Shen, Y.; Zhu, S.; Hunkeler, D., Gel Formation in Atom Transfer Radical Polymerization of 2-(N,N-Dimethylamino)ethyl Methacrylate and Ethylene Glycol Dimethacrylate. *Journal of Polymer Science: Part A: Polymer Chemistry* **2001,** 39, 3780-3788.

46. Ejaz, M.; Yamamoto, S.; Ohno, K.; Tsujii, Y.; Fukuda, T., Controlled Graft Polymerization of Methyl Methacrylate on Silicon Substrate by the Combined Use of the Langmuir-Blodgett and Atom Transfer Radical Polymerization Techniques. *Macromolecules* **1998,** 31, 5934-5936.

47. Xue, D., Unpublished work. In.

48. Dimitrijevic, N. M.; Saponjic, Z. V.; Bartels, D. M.; Thurnauer, M. C.; Tiede, D. M.; Rajh, T., Revealing the Nature of Trapping Sites in Nanocrystalline Titanium Dioxide by Selective Surface Modification. *Journal of Physical Chemistry B* **2003,** 107, 7368-7375.

49. Dong, C.; Ni, X., The Photopolymerization and Characterization of Methyl Methacrylate Initiated by Nanosized Titanium Dioxide. *Journal of Macromolecular Science, Part A - Pure and Applied Chemistry* **2004,** A41, (5), 547-563.

50. Hoffman, A. J.; Mills, G.; Yee, H.; Hoffmann, M. R., Q-Sized CdS: Synthesis, Characterization, and Efficiency of Photoinitiation of Polymerization of Several Vinylic Monomers. *Journal of Physical Chemistry* **1992,** 96, 5546-5552.

51. Hoffman, A. J.; Yee, H.; Mills, G.; Hoffmann, M. R., Photoinitiated Polymerization of Methyl Methacrylate Using Q-Sized ZnO Colloids. *Journal of Physical Chemistry* **1992,** 96, 5540-5546.

52. Kraeutler, B.; Reiche, H.; Bard, A. J.; Hocker, R. G., Initiation of Free Radical Polymerization by Heterogeneous Photocatalysis at Semiconductor Powders. *Journal of Polymer Science: Polymer Letters Edition* **1979,** 17, (8), 535-538.

53. Hoffmann, M. R.; Martin, S. T.; Choi, W.; Bahnemann, D. W., Environmental applications of semiconductor photocatalysis. *Chem. Rev.* **1995,** 95, 69-.

54. Kamat, P. V., Photochemistry on nonreactie and reactive (semiconductor) surface. *Chem. Rev.* **1993,** 93, 267-.

55. Bellobono, I. R.; Morelli, R.; Chiodaroli, C. M., Photocatalysis and promoted photocatalysis during photocrosslinking of multifunctional acrylates in composite membranes immobilizing titanium dioxide. *Journal of Photochemistry and Photobiology A: Chemistry* **1997,** 105, 89-94.

56. Sun, X. J.; Cai, W. M., Titanium dioxide photocatalytic technique at home and abroad. *J. Harbin Institute. Tech.* **2001,** 33, 534.

57. Popović, I. G.; Katsikas, L.; Weller, H., The photopolymerisation of methacrylic acid by coloidal semiconductors. *Polymer Bulletin* **1994,** 32, 597-603.

58. Popović, I. G.; Katsikas, L.; Muller, U.; Velickovic, J. S.; Weller, H., The homogeneous photopolymerization of methyl methyacrylate by colloidal cadmium sulfide. *Macromol. Chem. Phys.* **1994,** 195, 889-.

59. Tada, H.; Hyodo, M.; Kawahara, H., Photoinduced polymerization of 1,3,5,7-Tetramethylcyclotetrasiloxane by TiO_2 Particles. *Journal of Physical Chemistry* **1991,** 95, 10185-10188.

60. Kawai, T.; Sakata, T., Photocatalytic hydrogen production from liquid methanol and water. *J. Chem. Soc., Chem. Commun.* **1980**, 694-695.

61. Stroyuk, A. L.; Granchak, V. M.; Korzhak, A. V.; Kuchmii, S. Y., Photoinitiation of butylmethacrylate polymerization by colloidal semiconductor nanoparticles. *Journal of Photochemistry and Photobiology A: Chemistry* **2004,** 162, 339-351.

62. Klein, C.; Nazeeruddin, M. K.; Di Censo, D.; Liska, P.; Grätzel, M., Amphiphilic Ruthenium Sensitizers and Their Applications in Dye-Sensitized Solar Cells. *Inorganic Chemistry* **2004,** 43, 4216-4226.

63. Zakeeruddin, S. M.; Nazeeruddin, M. K.; Humphry-Baker, R.; Péchy, P.; Quagliotto, P.; Barolo, C.; Viscardi, G.; Grätzel, M., Design, Synthesis, and Application of Amphiphilic Ruthenium Polypyridyl Photosensitizers in Solar Cells Based on Nanocrystalline TiO_2 Films. *Langmuir* **2002,** 18, 952-954.

64. Wang, P.; Klein, C.; Humphry-Baker, R.; Zakeeruddin, S. M.; Grätzel, M., A High Molar Extinction Coefficient Sensitizer for Stable Dye-Sensitized Solar Cells. *Journal of the American Chemical Society* **2005,** 127, 808-809.

65. Kalyanasundaram, K., *Photochemistry of polypyridine and porphyrin complexes.* Academic Press, INC.: San Diego, 1992.

66. Wang, X.-S.; Lascelles, S. F.; Jackson, R. A.; Armes, S. P., Polymers at Interfaces: Using Atom Transfer Radical Polymerization in the Controlled Growth of Homopolymers and Block Copolymers from Silicon Surfaces in the Absence of Untethered Sacrificial Initiator. *Chem. Commun.* **1999**, 1817-1818.

67. Wang, X.-S.; Armes, S. P., Facile Atom Transfer Radical Polymerization of Methoxy-Capped Oligo(ethylene glycol) Methacrylate in Aqueous Media at Ambient Temperature. *Macromolecules* **2000,** 33, (18), 6640-6647.

68. Coullerez, G.; Carlmark, A.; Malmström, E.; Jonsson, M., Understanding Copper-Based Atom-Transfer Radical Polymerization in Aqueous Media. *Journal of Physical Chemistry A* **2004,** 108, 7129-7131.

69. Matyjaszewski, K.; Shipp, D. A.; Wang, J.-L.; Grimaud, T.; Patten, T. E., Utilizing Halide Exchange to Improve Control of Atom Transfer Radical Polymerization. *Macromolecules* **1998,** 31, 6836-6840.

70. Schellekens, M. A. J.; de Wit, F.; Klumperman, B., Effect of the Copper Counterion on the Activation Rate Parameter in Atom Transfer Radical Polymerization. *Macromolecules* **2001,** 34, 7961-7966.

71. Cazzanti, S.; Caramori, S.; Argazzi, R.; Elliott, C. M.; Bignozzi, C. A., Efficient Non-corrosive Electron-Transfer Mediator Mixtures for Dye-Sensitized Solar Cells. *Journal of the American Chemical Society* **2006,** 128, (31), 9996-9997.

72. Strein, T. G.; Ewing, A. G., Characterization of Submicron-Sized Carbon Electrodes Insulated with a Phenol-Allylphenol Copolymer. *Analytical Chemistry* **1992,** 64, 1368-1373.

73. Hagfeldt, A.; Grätzel, M., Molecular Photovoltaics. *Accounts of Chemical Research* **2000,** 33, 269-277.

74. Nazeeruddin, M. K.; Kay, A.; Rodicio, I.; Humphry-Baker, R.; Müller, E.; Liska, P.; Vlachopoulos, N.; Grätzel, M., Conversion of Light to Electricity by *cis*-X_2Bis(2,2'-bipyridyl-4,4'-dicarboxylate)ruthenium(II) Charge-Transfer Sensitizers (X = Cl^-, Br^-, I^-, CN^- and SCN^-) on Nanocrystalline TiO_2 Electrodes. *Journal of the American Chemical Society* **1993,** 115, 6382-6390.

75. Ito, S.; Takeuchi, T.; Katayama, T.; Sugiyama, M.; Matsuda, M.; Kitamura, T.; Wada, Y.; Yanagida, S., Conductive and Transparent Multilayer Films for Low-Temperature-Sintered Mesoporous TiO_2 Electrodes of Dye-Sensitized Solar Cells. *Chemistry of Materials* **2003,** 15, 2824-2828.

76. Barbé, C. J.; Arendsa, F.; Comte, P.; Jirousek, M.; Lenzmann, F.; Shklover, V.; Grätzel, M., Nanocrystalline Titanium Oxide Electrodes for Photovoltaic Applications. *J. Am. Ceram. Soc.* **1997,** 80, (12), 3157-3171.

77. Wu, C.-W.; Ohsuna, T.; Kuwabara, M.; Kuroda, K., Formation of Highly Ordered Mesoporous Titania Films Consisting of Crystalline Nanopillars with Inverse Mesospace by Structural Transformation. *Journal of the American Chemical Society* **2006,** 128, 4544-4545.

78. Adachi, M.; Murata, Y.; Okada, I.; Yoshikawa, S., Formation of Titania Nanotubes and Applications for Dye-Sensitized Solar Cells. *Journal of the Electrochemical Society* **2003,** 150, (8), G488-G493.

79. Zukalová, M.; Zukal, A.; Kavan, L.; Nazeeruddin, M. K.; Liska, P.; Grätzel, M., Organized Mesoporous TiO_2 Films Exhibiting Greatly Enhanced Performance in Dye-Sensitized Solar Cells. *Nano Letters* **2005,** 5, (8), 1789-1792.

80. Jiu, J.; Isoda, S.; Wang, F.; Adachi, M., Dye-Sensitized Solar Cells Based on a Single-Crystalline TiO_2 Nanorod Film. *Journal of Physical Chemistry B* **2006,** 110, 2087-2092.

81. Tang, J.; Wu, Y.; McFarland, E. W.; Stucky, G. D., Synthesis and photocatalytic properties of highly crystalline and ordered mesoporous TiO_2 thin films. *Chem. Commun.* **2004**, 1670-1671.

82. Rouquerol, J.; Avnir, D.; Fairbridge, C. W.; Everett, D. H.; Haynes, J. H.; Pernicone, N.; Ramsay, J. D. F.; Sing, K. S. W.; Unger, K. K., Recommendations for the Characterization of Porous Solids. *Pure and Applied Chemistry* **1994,** 66, (8), 1739-1758.

83. Quebatte, L.; Haas, M.; Solar, E.; Scopelliti, R.; Nguyen, Q. T.; Severin, K., Atom-Transfer Radical Reactions under Mild Conditions with [{$RuCl_2$(1,3,5-$C_6H_3iPr_3$)}] and PCy_3 as the Catalyst Precursors. *Angewandte Chemie International Edition* **2005,** 44, 1084-1088.

84. Kickelbick, G.; Pintauer, T.; Matyjaszewski, K., Structural comparison of Cu^{II} complexes in atom transfer radical polymerization. *New Journal of Chemistry* **2002,** 26, 462-468.

85. O'Reilly, R. K.; Gibson, V. C.; White, A. J. P.; Williams, D. J., Five-coordinate iron(II) complexes bearing tridentate nitrogen donor ligands as catalysts for atom transfer radical polymerisation. *Polyhedron* **2004,** 23, 2921-2928.

86. Gibson, V. C.; O'Reilly, R. K.; Wass, D. F.; White, A. J. P.; Williams, D. J., Polymerization of Methyl Methacrylate Using Four-Coordinate (α-Diimine)iron Catalysts: Atom Transfer Radical Polymerization vs Catalytic Chain Transfer. *Macromolecules* **2003,** 36, 2591-2593.

87. Iovu, M. C.; Maithufi, N. G.; Mapolie, S. F., Evaluation of bis(2-pyridinal)ethylenediimine as ligand for atom transfer radical polymerization of methyl methacrylate: influence of polar solvents. *Polymer International* **2003,** 52, 899-907.

88. Matyjaszewski, K.; Patten, T. E.; Xia, J., Controlled/"Living" Radical Polymerization. Kinetics of the Homogeneous Atom Transfer Radical Polymerization of Styrene. *Journal of the American Chemical Society* **1997,** 119, 674-680.

89. Fournier, D.; Pascual, S.; Fontaine, L., Copper-Mediated Living Radical Polymerization of 2-vinyl-4,4-dimethyl-5-oxazolone. *Macromolecules* **2004,** 37, 330-335.

90. Rademacher, J. T.; Baum, M.; Pallack, M. E.; Brittain, W. J.; Simonsick, W. J., Atom Transfer Radical Polymerization of N,N-Dimethylacrylamide. *Macromolecules* **2000,** 33, 284-288.

91. Wu, X.; Collins, J. E.; McAlvin, J. E.; Cutts, R. W.; Fraser, C. L., Ruthenium Tris(bipyridine)-Centered Linear and Star-Shaped Polystyrenes: Making Atom Transfer Radical Polymerization and Metal Complex Initiators Compatible. *Macromolecules* **2001,** 34, 2812-2821.

92. Johnson, R. M.; Corbin, P. S.; Ng, C.; Fraser, C. L., Poly(methyl methacrylates) with Rutheniuym Tris(bipyridine) Cores via $NiBr_2(PR_3)_2$-Catalyzed Atom Transfer Radical Polymerization (ATRP). *Macromolecules* **2000,** 33, 7404-7412.

93. Lu, Z.; Fryd, M.; Wayland, B. B., New Life for Living Radical Polymerization Mediated by Cobalt(II) Metalloradicals. *Macromolecules* **2004,** 37, 2686-2687.

94. Kaneyoshi, H.; Matyjaszewski, K., Effect of Ligand and n-Butyl Acrylate on Cobalt-Mediated Radical Polymerization of Vinyl Acetate. *Macromolecules* **2005,** 38, 8163-8169.

Chapter 3

A Two Electrode Study of Dye-Sensitized Solar Cells with Cobalt Mediators

Abstract

A suite of DSSC characterization experiments was developed which could be rapidly performed on a standard two electrode sandwich cell. In combination with a novel technique for mediator replacement without cell disassembly, this suite was utilized to probe the influence of a variety of parameters on DSSC functioning in order to elucidate the processes limiting performance in cells mediated by cobalt complexes. The results of this study clearly implicate diffusion of cobalt(III) to the cathode as frequently rate-limiting. Strategies to alleviate this condition include increasing the cobalt(III)

concentration as well as lowering the solvent viscosity. A somewhat unexpected result of the flow-through study is that TiO_2 underlayers or $TiCl_4$ treatments have a surprisingly small effect on the performance of DSSCs, despite their dramatic effect on dark currents. This may be a further indication that diffusion of cobalt(III) – and not recombination across the FTO surface – is performance-limiting in cobalt-mediated DSSCs.

Introduction

Objective

Evaluation of solar cell performance may be accomplished with a variety of experimental techniques. Some methods characterize a DSSC's overall ability to deliver electrical power/current (e.g., iV, IPCE, APCE tests) while others provide insight into specific cell processes (e.g., flash photolysis, IMVS, IMPS – acronyms are either defined below or in the List of Symbols and Abbreviations, page *x*). A combination of both types is useful for a full analysis of a particular DSSC system. Unfortunately, many of these techniques require specialized equipment and unique cell configurations. In our pursuit to optimize and understand cobalt-mediated DSSCs, we sought to assemble a suite of characterization techniques that could be rapidly performed and would yield complementary information regarding the system. Variation of a multitude of cell parameters could then yield insight into the rate-limiting processes of such cells.

iV-type experiments

Perhaps the most common method of cell evaluation is to conduct a current-voltage (iV) experiment, both in the dark and under illumination. In this experiment, the

cell potential is controlled and the current is measured as the potential is scanned across a range of voltages. Several important values may be extracted from this experiment, such as open-circuit voltage (V_{oc}), short-circuit current density (J_{sc}), fill factor (FF), and maximum cell efficiency (η). The standard configuration used when testing DSSCs is commonly referred to as the "sandwich cell" configuration and consists of two electrodes clamped together.[1-3] Due to its experimental simplicity in combination with the wealth of information it yields, the iV experiment was chosen to be the cornerstone of our cell evaluation process. Therefore, other experiments would ideally also use the same sandwich cell configuration so that the entire battery of tests could be performed in rapid succession.

Although iV experiments on DSSCs are generally reported only when conducted under illumination, they may also be performed under dark conditions. Without light, the dark experiment provides some information regarding deleterious electron-hole recombination.[4] In theory, the greater the overpotential required to pass a reverse current, the greater the system's "resistance" to recombination events. However, the usefulness of this experiment is hampered significantly by the variable resistivity of the nanocrystalline TiO_2 layer.[4] In the dark (i.e., without electron injection from the dye-sensitizer), the TiO_2 is highly resistive until potentials are reached which are sufficiently negative as to allow transfer of electrons into the conduction band of the TiO_2. Therefore, until this point is reached, any reverse current must pass through the exposed regions of FTO glass. This situation differs greatly from the standard operating conditions of DSSCs in the light, where recombination may, at least in principle, occur from the high surface area of the TiO_2 layer as well as from the FTO surface.

Consequently, dark curves are infrequently reported in DSSC literature. Nevertheless, the experiment does provide some insight into the system and, in addition, is easily conducted in tandem with the light experiment.

IPCE/APCE experiments

Incident Photon-to-current Conversion Efficiency (IPCE) or Absorbed Photon-to-current Conversion Efficiency (APCE) experiments yield a similar type of information regarding cell performance, although with a few key differences.[5, 6] These two experiments are essentially i-λ experiments wherein the wavelength of illumination is controlled and varied (by means of a monochromator) and the resulting current is recorded. This is in contrast to the iV experiment which is generally conducted using full spectrum (minus the ultraviolet) light from a Xenon arc lamp or similar light source. Also in contrast, the potential of the cell is held at 0V (i.e., short circuit) throughout the experiment. With a well-functioning cell, the shape of the output (from either IPCE or APCE tests) should resemble the absorption spectrum of the dye. Consequently, these tests are frequently used to evaluate dye performance (e.g., injection efficiency).[5]

As our cobalt-based systems utilize the standard N3 dye, there was little incentive to include IPCE or APCE experiments in the battery of tests. In addition, the requirement of a monochromator further reduced the attractiveness of the test. As a result, these experiments were not performed.

OCVD experiments

Recently, Zaban et al. have developed a new sandwich cell experiment that specifically targets recombination of photoinjected electrons from the nanocrystalline titania layer with oxidized mediator.[7, 8] Dubbed the Open Circuit Voltage Decay (OCVD) method, the experimental procedure is fairly simple and – as it also uses the regular sandwich cell configuration – is convenient to integrate into a standard DSSC characterization protocol. As its name implies, the OCVD experiment is conducted by observing the open circuit photovoltage (V_{oc}) decay over time. The cell, maintained at V_{oc}, is brought to steady state conditions (usually requiring only milliseconds) under one sun illumination. After one second, the illumination is ceased. The resulting potential decay is system-dependent and can require from less than a second to several minutes to reach zero volts.

Although experimentally simple, the theory underlying the OCVD experiment is quite complex. As a result, OCVD experiments are capable of yielding significant insight into recombination processes within DSSC systems. Through detailed analysis, as many as eight different parameters may be extracted from a single OCVD curve. A simplified overview of the technique will be presented here (see reference #8 for a more detailed theoretical description).

At open circuit, a photoinjected electron must remain in the conduction band (CB) of the anode or transfer to a reducible species such as the photooxidized dye or the oxidized form of the mediator (i.e., recombine with a photogenerated hole). In reasonably efficient DSSCs, an overpotential exists for recombination at the anode surface which greatly slows the recombination reaction (at least at moderate cell

potentials). As a result, the electron population in the CB will increase when the cell is illuminated. As the Fermi level of the semiconductor anode is a function of the electron population in the CB, an increase (negative shift) of the Fermi level will result. This shift is observed by an increase in cell potential (as V_{oc} is the voltage difference between the Fermi energies of the anode and cathode). The rate of the recombination reaction, however, is potential-dependent. Accordingly, the DSSC will quickly reach an equilibrium-state voltage where the rate of photoinjection equals the rate of recombination. Once illumination ceases, the rate of photoinjection becomes zero. The change in V_{oc} after this point is due solely to recombination, and so OCVD curves directly measure the recombination characteristics of a particular DSSC system.

Several points of clarification are worth mentioning. Firstly, the OCVD experiment is essentially a *dark* experiment as all pertinent data are collected with the light off. Assuming that the reduction of the oxidized dye by mediator is sufficiently fast, the OCVD experiment only measures recombination of photoinjected electrons with oxidized mediator. The assumption of fast dye reduction kinetics is valid in many efficient DSSC systems and greatly simplifies the theoretical description of the OCVD experiment. However, systems where slower kinetics are suspected may not be appropriate for OCVD (e.g., some solid-state systems, particularly dilute mediator solutions, alternative dyes, etc). Secondly, the theory as developed by Bisquert et al. assumes all recombination to occur exclusive at the TiO_2 nanoparticle surface and *not* on any exposed FTO surfaces. With I^-/I_3^- as mediator, this is likely a valid assumption but is not necessarily so for other mediator systems. Thirdly, the OCVD experiment measures relatively slow phenomena on the time scale of a few milliseconds and longer. Other

techniques, (e.g., laser or high frequency domain experiments) are required to measure faster electronic events such as dye injection/reduction.

The rate of recombination measured by OCVD may be reported as an electron lifetime (or "response time"), τ_n. The lifetime of an electron in the CB is potential-dependent and may be calculated using the reciprocal of the slope of the decay curve (at a particular voltage) and normalizing by the thermal voltage:

$$\tau_n = -\frac{k_B T}{e}\left(\frac{dV_{oc}}{dt}\right)^{-1}$$

During a single experiment, V_{oc} typically decays by several hundred millivolts while the lifetime increases exponentially, covering several orders of magnitude. Consequently, τ_n-V_{oc} data is typically displayed on a log-linear plot and theoretical considerations predict three distinct regions: (a) a region of constant τ_n, (b) a region with a linear increase (in log-linear form) of τ_n, (c) a region of increasing τ_n with a parabolic shape.

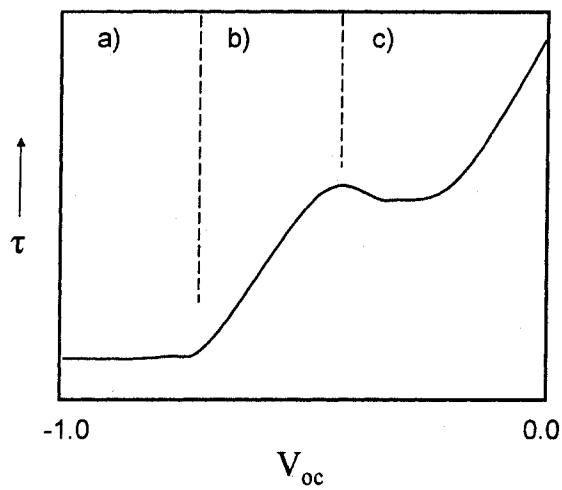

Figure 1. Theoretical behavior of τ_n as a function of V_{oc}. Y-axis is logarithmic, x-axis is linear. (Adapted from reference #8).

In region (a), at high potentials, recombination occurs primarily through reaction of "free" (i.e., mobile, untrapped) CB electrons with mediator. In this region, a significantly greater portion of excited electrons reside in CB states than in bulk trap states (*vide infra*) and are defined by the energy of the lower edge of the CB. As the Fermi energy of the anode decreases, τ_n remains constant as a result of the large capacitance (high density of states, DOS) of the CB.

In region (b), recombination still occurs primarily through free CB electrons, but the capacitance of the bulk traps becomes greater than that of the CB states. Bulk traps are electronic states localized in the interior of the TiO_2 nanoparticle with energy levels just below the lower edge of the CB. These states trap and release electrons only to the CB. As electrons may only react with mediator at the exterior of the nanoparticle, electrons in bulk traps must first be released to the CB and travel to the nanoparticle surface (possibly being trapped and released several times en route) before recombining with mediator. With the majority of excited electrons in bulk trap states, trapping and detrapping rates determine the observed electron lifetime. These rates are mathematically described with an exponential "tailing parameter" and, as a consequence, τ_n responds linearly (in the log-linear format) to decreasing V_{oc}.

At low potentials, region (c), recombination no longer occurs primarily through CB states but rather through surface trap states. Surface traps are similar to bulk traps but with the added feature that electrons in surface traps may be released to mediator species as well as to the CB (i.e., surface traps are in close enough proximity to the nanoparticle surface that they may serve as recombination sites). The rate of the recombination process in this region is therefore dependent on the distribution of surface traps. This

dependence is borne out mathematically as a reciprocal of a Gaussian distribution, and hence τ_n displays a parabolic shape in this region.

Bisquert et al. found excellent agreement between theoretically predicted behavior and experimental results with I^-/I_3^- mediated DSSCs. The OCVD method is simple to perform, strikingly powerful (with appropriate systems), and convenient to include in a DSSC testing protocol as it is conducted on the standard DSSC sandwich cell. For these reasons, we decided to include OCVD in the suite of electrochemical tests.

Current transients

Current versus time experiments ("current transients") are not typically performed on DSSCs. However, it was noticed early on that tris(bipyridine)cobalt-mediated DSSCs exhibit an initial burst of unsustainable current upon exposure to light which then drops to a sustainable level (typically, this level is 50-80% of the initial current) over a few hundred milliseconds (*vide infra*). In order to better characterize this phenomenon, a current transient protocol was developed. Cells, initially in the dark, were exposed to light for one second while held at short circuit. The illumination was then ceased. The current was recorded throughout this period.

Flow-through experiments

In order to compare differing DSSC systems (e.g., systems using 0.3 M mediator with systems using 0.15 M), reproducibility within each system was required. Unfortunately, DSSCs, made up of a disordered nanocrystalline layer and containing multiple processes with competing kinetics, are extremely sensitive to a variety of

factors.[9] As a result, we typically witness significant variance between identical experiments, commonly as great as 15-20%. This statistical noise hampers the ability to detect real differences between DSSC systems. Accordingly, a method was sought to enhance the reproducibility of DSSCs.

For reasons not fully understood, it is our experience that cell performance changes every time a cell is disassembled and reassembled, even when the same anode is used. Furthermore, two anodes, prepared on the same slide and subjected to identical baking and dying conditions, will not yield identical results. A possible explanation for these observations may be supposed by considering the disordered nature of the nanocrystalline titania layer. The nanocrystalline film is essentially a layer of nanometer-diameter spheres piled randomly on top of one another.[10] Within this layer, a network of randomly-distributed pores results. It is reasonable to expect that the pore network may affect the performance of the DSSC (due to varying numbers of dead-ends, closed pores, constrictions, etc...), perhaps by altering the effective mobilities of either the electrons and/or holes, or by influencing the dye loading, or possibly through some other mechanism.[11] Although it would be expected that these types of differences would, on a macroscopic level, average out to yield a homogeneous film, perhaps this is not always the case. If not, it could explain why two otherwise similar anodes yield somewhat different performances and why a single anode, once reassembled, also results in differing behavior (due to improbability of illuminating exactly the same area with both assemblies). Of course, other explanations are possible.

Regardless, it seemed desirable to eliminate this source of error as we strove for greater reproducibility. Several groups have reported using thin spacers to separate the

anode and cathode when sandwiched together.[8, 12, 13] One of the purported rationales for this is to eliminate any shorts which may develop in the areas where the titania directly contacts the cathode.[8] We realized that a spacer could also bestow an ability to replace the mediator solution in the cell without the need for disassembly. Utilizing capillary action, a few μLs of new mediator solution could be drawn into the cell using a Kimwipe placed in contact with the old mediator solution on the other end of the cell. The new mediator solution was drawn into the cell and the old wicked out by the Kimwipe. In this way, the illuminated area could be kept constant and the mediator solution changed. As will be discussed, this turned out to be extremely useful.

Experimental

Synthesis of $Co(dtb)_3(ClO_4)_2$

Typically, three equivalents of 4,4'-di-*tert*-butyl-2,2'-bipyridine ("dtb", obtained from Aldrich Company) were dissolved in a minimum of methanol using heat. One equivalent of $Co(ClO_4)_2 \times 6\ H_2O$ was then added. Although the clear solution turned dark brown immediately upon addition of cobalt, the solution was stirred at reflux for 30-120 minutes to ensure complete complexation. The solution volume was reduced by approximately 80% using rotary evaporation, followed by addition of diethyl ether to precipitate the remaining cobalt complex. The precipitate was filtered and dried in a vacuum oven overnight.

Bulk oxidation to $Co^{III}(dtb)_3(ClO_4)_3$

Bulk oxidation of $Co(dtb)_3(ClO_4)_2$ (500 mg, 0.47 mmol) was performed by addition of a slight excess of $NOBF_4$ to an acetonitrile solution of the cobalt complex. The acetonitrile was removed by rotary evaporation. Thin layer chromatography confirmed the absence of any residual Co^{II} complex. In order to remove the BF_4^- anion, the complex was redissolved in methanol, a large amount of $LiClO_4$ was added, followed by precipitation of the cobalt complex with diethyl ether. The final product was dried overnight in a vacuum oven.

Preparation of TiO_2 photoanodes

Photoanodes were prepared using the standard "doctor-blade" technique.[5] Fluorine-doped tin oxide conducting glass (FTO) was pre-scored, cleaned (Kimwipe/acetone wipe, >30 minutes in a base bath followed by rinses with water, distilled water, and ethanol), dried under a stream of nitrogen, and immobilized using two strips of Scotch tape. The tape also served as a spacer for the spreading of the titania colloid (usually obtained from Solaronix company). After spreading, the colloid was allowed to dry (as judged by the visible change from opaque to transparent) and fired in an oven. The temperature was ramped to 450 °C over ~15 minutes, held for 30-60 minutes, and allowed to cool slowly to room temperature.

In some cases, the photoanodes were then treated with a 0.2 M solution of $TiCl_4$ in Millipore water in a similar manner to the procedure reported by Nazeeruddin and coworkers.[5] A few drops of solution were applied to the surface of the TiO_2 and the entire anode was placed in a high humidity chamber to prevent evaporation of the

solvent. After a variable period of time (specified in the text of the discussion), the anode was removed from the chamber, rinsed with Millipore water, and baked again at 450 °C for at least 30 min.

For a few experiments, a thin layer of compact (i.e., not nanocrystalline) TiO_2 was applied to the conducting side of an FTO substrate prior to deposition of the nanocrystalline film. This underlayer was achieved by use of a sol-gel process.[14] A sol was prepared in 10 mL 200 proof ethanol. To ethanol was added (in sequence, under stirring): 250 uL Millipore water, a few drops HNO_3 (until the pH was approximately 1-2), and 750 uL titanium (IV) isopropoxide. This last addition was performed with the ethanol solution at 0 °C in an ice-water bath. The vial was then sealed with parafilm and allowed to stir at 0 °C for 1-2 hours before being placed in the refrigerator at 4 °C. After aging at least 24 hours (usually 24-25, never more than 72 hours), the sol was removed from the refrigerator and stirred briefly before use. The FTO substrate was cleaned as previously described (base bath, rinsed, dried) and taped on two sides, leaving an exposed area of roughly 12 cm^2. Approximately 1 mL of the Ti sol was applied to the spinning FTO substrate (900 rpm on a Pine Instruments Analytical Rotator) in a steady stream over a period no longer than 15 seconds. The substrate was spun for 1 minute, removed and baked at 450 °C for 30 minutes. Although the thickness of the films was not measured in-house, the procedure is reported to result in 50-60 nm thick films.[14] After cooling, the substrate was then pre-scored before the titania colloid was applied in the manner previously described.

Prior to use in a cell, the photoanodes were reheated to 450 °C for only a few minutes before being allowed to cool to 130 °C. At this point, the still-hot anodes were

immersed in a saturated ethanol (200 proof) solution of *cis*-di(thiocyanato)bis(2,2'-bipyridyl-4,4'-dicarboxylate)ruthenium(II), commonly referred to as N3 dye. After a variable period of time (*vide infra*), the anode was removed from the dye solution, rinsed with ethanol, dried under a stream of nitrogen, and placed in a covered container until use (great care was taken to ensure that anodes never sat out of dye solution for more than a couple of hours before use).

Spacers

Flow-through experiments were conducted on DSSC sandwich cells containing two strips of polyimide tape (with the adhesive removed), one on each side of the cell, between the cathode and photoanode. The thickness of the polyimide spacers was measured with a high-precision micrometer and found to be 25 μm, a value in close agreement with the specifications given by the manufacturer (McMaster-Carr). Spacers of smaller thickness were also attempted. X-ray quality polyester film of 0.00015" thickness (< 4 μm), obtained from Somar Laboratories, Inc., was cut into strips which were used in a manner identical to that described for 25 μm spacers. An intermediate thickness of approximately 8 μm was also attempted by using 4 μm spacers which had been folded back on themselves.

Occasionally in this chapter and more frequently in the following chapters, DSSCs were assembled for one-time use (i.e., without using a flow-through technique to exchange mediator solutions) using the 4 μm spacer. In these instances, the film was cut into a single U-shaped piece rather than into two separate strips simply because a single piece of film is considerably easier to position on the anode. The film was placed on the

titania half of the photoanode, with the open end of the "U" oriented towards the other half of the anode (not covered with titania) so that mediator solution could still be introduced as normal.

Cell assembly

All cell experiments were conducted using a sandwich cell configuration. A thin spacer (either 4 or 25 μm, *vide infra*) was placed on the photoanode followed by the cathode (for flow-through experiments, the cathode was platinum-sputtered-on-FTO glass unless noted otherwise). A few μL's of mediator solution were applied outside the gap between the anode and cathode and were subsequently drawn into the interior of the cell by capillary action. The assembly was then placed into a custom-made cell holder and fixed with a screw clamp. An FTO extension (with conducting copper tape) was clamped to the anode to facilitate electrical connection. The aperture on the cell holder was 0.385 cm^2.

Instrumental

A 75 W Xenon arc lamp was used as a source of illumination. Wavelengths lower than 400 nm were removed with a 400 nm high pass filter, but the light was not collimated. Incident light power was adjusted with the Xenon lamp focus to 1 sun (1000 $W\ m^{-1}$, or 100 $mW\ cm^{-2}$). In cases where lower intensity light was desired, neutral density filters were placed in the light path. A Pentax camera with the back cover removed was utilized as a one second shutter.

Cell experiments were performed with a Kiethley 1400 Sourcemeter interfaced to a personal computer via a National Instruments BNC connector box. All experiments were conducted using specially-written LabVIEW software. One program was written to perform iV experiments (both light and dark) and calculate the cell characteristics (V_{oc}, J_{sc}, FF, η). Another program was used to perform both the OCVD and current transients. Controlling the Keithley sourcemeter with these two programs allowed all four experiments to easily be run in a matter of a couple minutes, greatly facilitating a well-rounded characterization of a particular DSSC system. In most cases, the tests were conducted in the following order: current transient, OCVD, dark iV curve, light iV curve.

Flow-through experiments

Initial introduction of mediator solution was done as customary, with a drop of solution applied to the edge of the cell and capillary action serving to wick the solution into the cell. Subsequently, the mediator solution was replaced using the procedure involving a Kimwipe described above where a drop of new solution, similarly delivered to the edge of the cell, could be drawn into the cell by placing the Kimwipe in contact with the old mediator solution on the other end of the cell. The absorbent Kimwipe removed old solution and wicked new solution into the cell from the other side. For reasons that will be explained, this procedure was repeated three times in succession to ensure complete conversion to the new mediator solution.

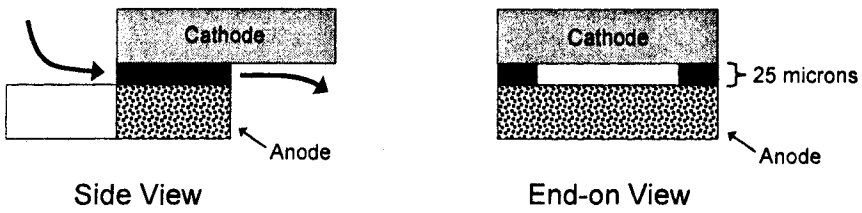

Figure 2. Diagrams illustrating the flow-through technique. Solution was delivered to the left (side view) of the cathode and wicked out by a Kimwipe placed on the right (side view) of the anode. The patterned half of the anode represents the end of the photoanode which is covered by the TiO_2 layer (in reality, the titania is located on the side of the anode facing the cathode).

A few notes are in order to explain the plots from the flow-through study presented in this chapter (these comments pertain only to the flow-through study presented in this chapter and are not universally true for any other experiments presented in this or any other chapter). Except where noted, each figure corresponds to a different photoanode. In general, each photoanode was used for only one DSSC assembly. This was done to assist in reproducibility. Most experiments were conducted with a platinum cathode. Although platinum is not an optimal cathode for cobalt-mediated DSSCs, it is more rugged and consistent that gold cathodes and was chosen for this reason. Unless noted otherwise, all data may be assumed to have been taken with a platinum cathode. It may also be assumed that 25 μm spacers were used, unless explicitly stated otherwise, for reasons to be explained (*vide infra*). All experiments were performed under one sun (AM 1.5) illumination, i.e., 100 mW cm^{-2}.

Within each figure, plot numbers generally correspond to mediator substitutions. For example, plot 1 would be the resulting iV curve after the mediator was replaced (using the wicking procedure) from plot 0. Exceptions to this system will be made obvious. In all cases, data were collected in order of ascending plot number. In situations where data is plotted with discontinuous numbers, it is implicit that unshown

data was collected between the displayed data (e.g., if plots 1 and 7 are displayed, it is true that plots 2-6 were collected before plot 7). This is important to note since the number of mediator substitutions was often a factor in cell performance (*vide infra*).

Transient experiments (current transients, OCVDs) are displayed with a shifted X-axis (the time axis) to coordinate the onset of illumination between each experiment. This is done for ease of visual comparison. With the exception of dark iV experiments, current densities are displayed which normalize for the size of the illuminated area. Dark iV experiments, however, monitor current across the entire photoanode surface rather than just the area illuminated through the cell holder aperture. As this area was not strictly controlled, currents rather than current densities are displayed. It may be roughly approximated that cell size was ~1 cm^2 (making current equal to current density), but each DSSC assembled was slightly different.

Results/Discussion

Flow-through experiments

It was first necessary to establish that the flow-through experiment would provide reliable, reproducible data for valid comparisons between different DSSC systems. To do this, two criteria needed to be met. First, effective replacement of the mediator solution had to be demonstrated and second, the performance of a particular mediator solution needed to be unchanged after replacement with an identical solution (in other words, reproducibility was required). After some experimentation, it was found that the wicking procedure previously described (*vide supra*) was capable of replacing the mediator within the cell as long as the spacer was sufficiently thick. To ensure complete conversion,

three "flushes" (i.e., application of a drop of mediator solution followed by wicking) were performed in sequence. Hereafter, the term "mediator substitution," or just "substitution," will refer to a sequence of three flushes (within this chapter only).

A probable explanation for these two requirements (multiple flushes, thicker spacer) follows. The mediator replacement operation may be considered as a type of liquid/liquid extraction. It is unlikely that all of the old mediator solution is replaced by the new in a single flush. In particular, the solution deep within the pores is almost assuredly less mobile than the solution in the space created by the spacers between the two anodes (referred to hereafter as the "bulk" solution). As a consequence, a flush may replace all or most of the bulk solution but leave that within the pores unchanged. Diffusion between the pore and bulk solutions partially converts the pore solution, but another flush or two is required for full conversion. The requirement of a thicker spacer may be a consequence of the need for a greater volume ratio of bulk/pore solution, or perhaps bulk solution mobility is simply hampered with thinner spacers.

A 25 μm polyimide spacer was found to be sufficient for effective flushing. Both 4 μm and 8 μm spacers were attempted and found to be insufficient, at least over an interval of three flushes. The results for a 25 μm spacer are shown in **Figure 3**. In this plot, a series of iV curves are shown with 5% oxidized cobalt mediator (0.15M), 20% oxidized cobalt mediator (0.15M), and 10% oxidized LiI (0.5 M). It is immediately apparent that, although the cell behavior switches cleanly between each mediator substitution, the cell behavior is not perfectly reproducible between substitutions. Most dramatic is the steadily increasing V_{oc} with each substitution, although I_{sc} drops between some substitutions as well.

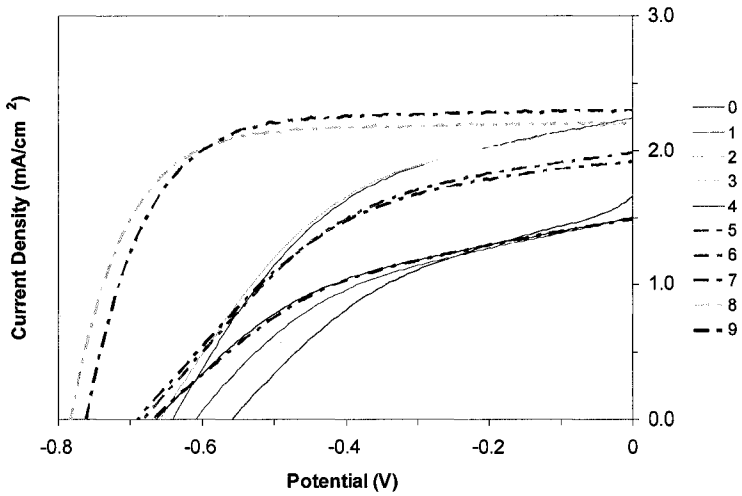

Figure 3. Plot of light iV curves. Plots 0,1,4,5 are 5% Co^{III}, plots 2,3,6,7 are 20% Co^{III}. Plots 8 and 9 are LiI. Cobalt solutions were 0.15 M cobalt complex, 0.2 M LiTriflate, 0.2 M *tert*-butylpyridine (TBP). LiI solution was 0.5 M LiI, 0.05 M I_2.

Figure 4 shows a flow-through experiment conducted with only LiI (0.5 M, 10% oxidized). This plot illustrates two important points. Firstly, the increasing V_{oc} and decreasing I_{sc} is occurring in this system as well, indicating that the phenomenon is likely not unique to the cobalt mediator. Second, the shape of the iV curves are obviously dissimilar to the shapes of the LiI curves in **Figure 3**. This phenomenon was repeatedly observed and warranted further investigation (*vide infra*).

As the changing V_{oc} and I_{sc} did not appear to be due to the mediator solution, a loss of dye was posited. It is frequently observed after cell disassembly that anodes appear lighter in the areas which were exposed to mediator. This trait has been casually observed (i.e., not rigorously tested) to be more pronounced with anodes that have been dyed for longer periods of time (on the order of a days). Although monolayer coverages are typically assumed, it may be that excessively long dying times result in thicker layers

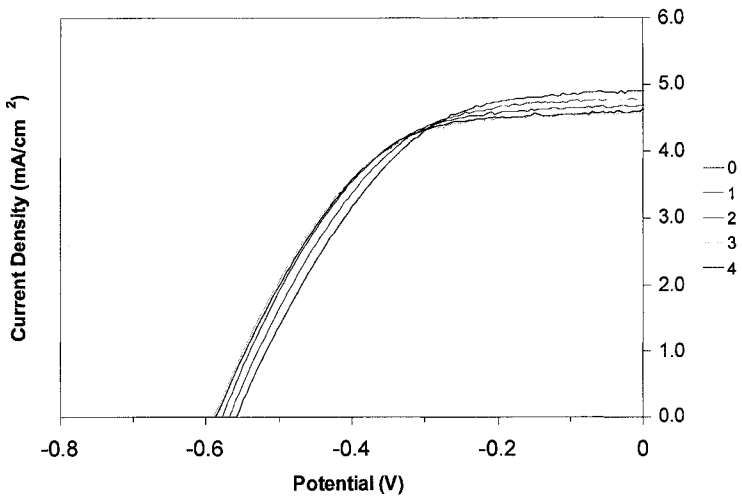

Figure 4. Plot of light iV curves. All plots are LiI. LiI solution was 0.5 M LiI, 0.05 M I_2.

where outer molecules are less strongly bound. With this hypothesis in mind, flow-through experiments were performed with anodes which had been dyed for only three hours. Three hours is generally accepted as a minimum – yet sufficient – time for the formation of a complete monolayer of adsorbed dye.[5, 12] The results are shown in **Figure 5**. Quite clearly, shorter dye times did not cease either the V_{oc} or I_{sc} shifts (although the magnitude of the V_{oc} shift appears smaller in this plot, this was not consistently observed). Interestingly, photoanodes dyed for short times (usually 3 hours) did not generally exhibit the same lightening phenomenon previously described. Accordingly, the three hour dying procedure was continued in subsequent studies.

Treatment of photoanodes with a solution of $TiCl_4$ has been reported to have performance-enhancing effects.[5, 15] The effect of this treatment on reproducibility was examined next. **Figure 6** displays the results with cobalt. Short circuit current is dramatically more stable, although V_{oc} still increases with each mediator substitution. Also noteworthy is the phenomenon that simply waiting two minutes between each series

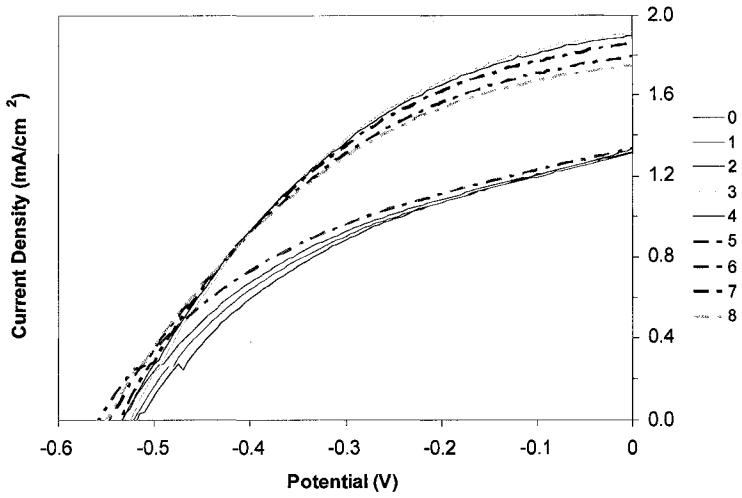

Figure 5. Plot of light iV curves. Plots 0,1,2,6 are 5% Co^{III}, plots 3,4,5,7,8 are 20% Co^{III}. Cobalt solutions were 0.15 M cobalt complex, 0.2 M LiTriflate, 0.2 M TBP.

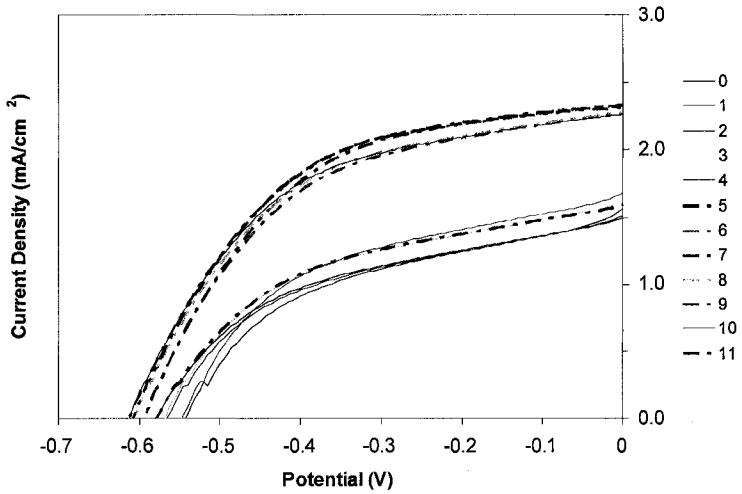

Figure 6. Plot of light iV curves with $TiCl_4$-treated anode. Plots 0-5 are 5% Co^{III}, plots 6-11 are 20% Co^{III}. Even numbered plots are initial iV scans, odd numbered are after two minutes. Cobalt solutions were 0.15 M cobalt complex, 0.2 M LiTriflate, 0.2 M TBP.

of tests (although not all results are shown, the full test protocol was conducted each time) resulted in slightly increased currents. During the wait period, the cell was not under illumination – although it was not rigorously shielded from indirect room lighting.

The current increase occurred irrespective of whether the cobalt solution was 5% or 20% oxidized. **Figure** 7 displays the corresponding current transients. Although in all cases the initial currents are very similar, currents after one second vary significantly. Most notably, 20% oxidized solutions lose current much more gradually than 5%. The two minute wait period also resulted in a slightly larger current after one second. The corresponding OCVD curves of 5% and 20% oxidized solutions are shown in **Figure 8**; however, the curves recorded after the two minute wait period are omitted as they without exception overlaid the original curves. Note that, although V_{oc} steadily increases, the shape of the OCVD curve is unchanging with either substitution or percent of oxidized cobalt (in contrast to the current transients).

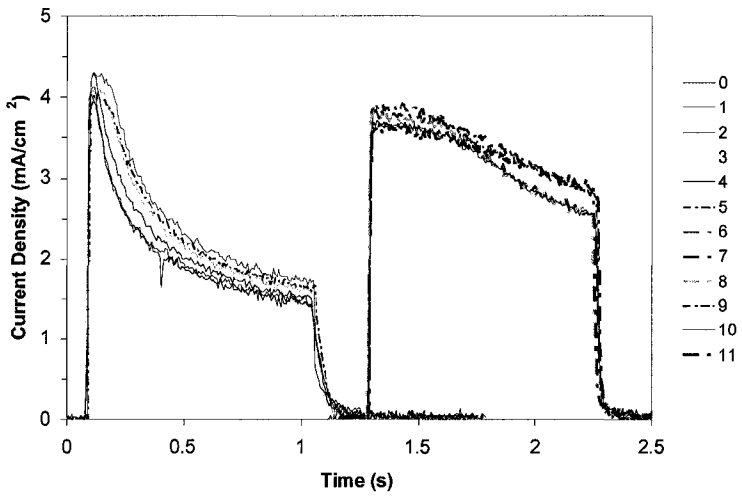

Figure 7. Plot of current transients with $TiCl_4$-treated anode. Plots 0-5 are 5% Co^{III}, plots 6-11 are 20% Co^{III}. Even numbered plots (on left) are initial iV scans, odd numbered (on right) are after two minutes. X-axis has been shifted arbritrarily for each plot. Cobalt solutions were 0.15 M cobalt complex, 0.2 M LiTriflate, 0.2 M TBP.

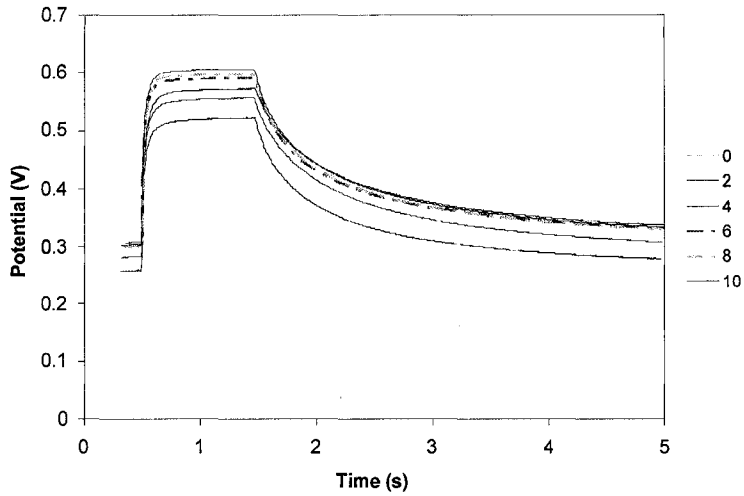

Figure 8. Plot of OCVD curves with $TiCl_4$-treated anode. Plots 0,2,4 are 5% Co^{III}, plots 6,8,10 are 20% Co^{III}. Cobalt solutions were 0.15 M cobalt complex, 0.2 M LiTriflate, 0.2 M TBP.

As briefly covered in Chapter 1, 4-*tert*-butylpyridine (TBP) is commonly used as an additive to mediator solutions (iodide or cobalt-based) due to its tendency to increase V_{oc}.[5, 15] Our standard procedure utilizes 0.2 M TBP in the mediator solution of the cell. Although this concentration should provide a great excess of TBP, the possibility that successive flushes were resulting in increased deposition of TBP (resulting in continually changing performance) was explored. Flow-through experiments were performed on regular (i.e., untreated with $TiCl_4$) anodes using cobalt mediator solutions not containing TBP. **Figure 9** presents data collected on regular anodes without TBP in the mediator solution. Quite clearly, reproducibility of I_{sc} is quite good while V_{oc} steadily increased. Once again, the current increased consistently after a two minute wait in the dark. The corresponding current transients are shown in **Figure 10**.

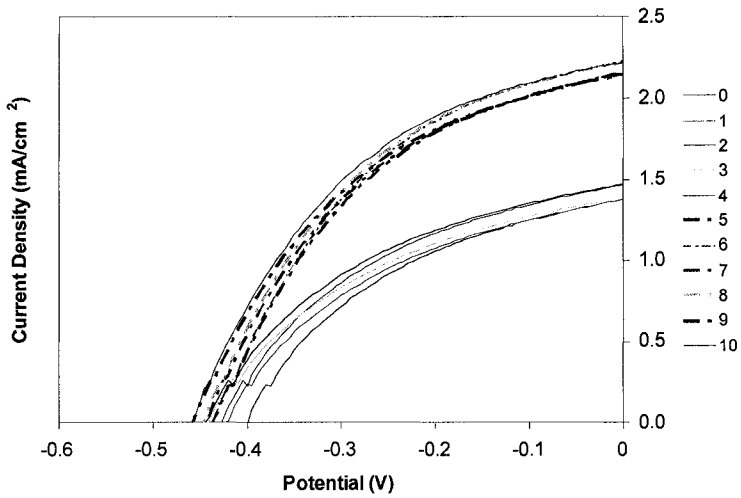

Figure 9. Plot of light iV curves with no TBP. Plots 0-4 are 5% Co^{III}, plots 5-10 are 20% Co^{III}. Plots 2,4,6,8,10 were collected after two minute wait. Cobalt solutions were 0.15 M cobalt complex, 0.2 M LiTriflate.

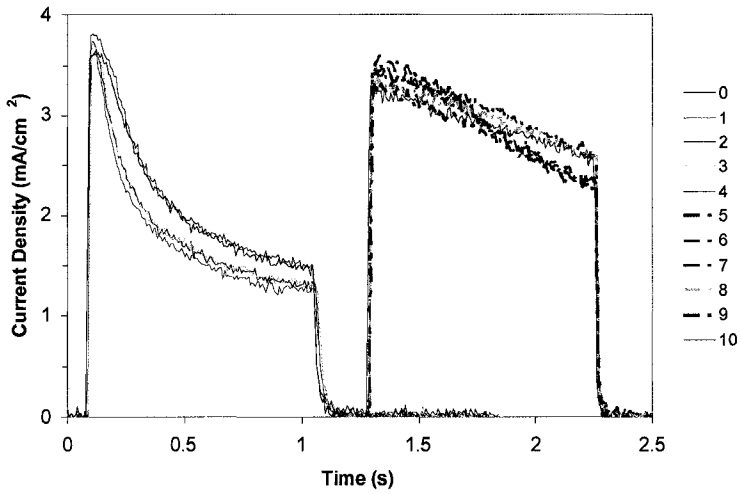

Figure 10. Plot of current transients with no TBP. Plots 0-4 are 5% Co^{III}, plots 5-10 are 20% Co^{III}. Plots 2,4,6,8,10 were collected after two minute wait. Cobalt solutions were 0.15 M cobalt complex, 0.2 M LiTriflate.

Figure 11 shows a more complete flow-through survey with cobalt (5%, 20%, and 30% oxidized) and iodide mediators, all without TBP. Although the increasing V_{oc} is still not understood, reproducibility of the I_{sc} was sufficient that the following may be

safely concluded. Current density increases as the percentage of oxidized cobalt increases. A large increase is observed between 5% and 20% at all voltages. In contrast, the increase is much smaller between 20% and 30%, being manifested primarily at voltages closer to V_{oc} (alternately, it may be stated that FF rather than J_{sc} is improved). This plot also illustrates the change in iodide behavior mentioned previously. As readily seen, the iV curve shifts from high J_{sc} and moderate V_{oc} to moderate J_{sc} and high V_{oc}. This occurrence is consistently observed. **Figure 12** displays the dark iV curves collected immediately prior to each respective light curve. The iodide before and after voltages differ by nearly 200 mV at identical currents. As dark curves primarily measure reverse (recombination) current through regions of exposed FTO, it seems apparent that the FTO surface is being altered in some unobvious way by cobalt mediator solution. From the OCVD transient plot (shown in **Figure 13**) it is likely that recombination across the surface is affected.

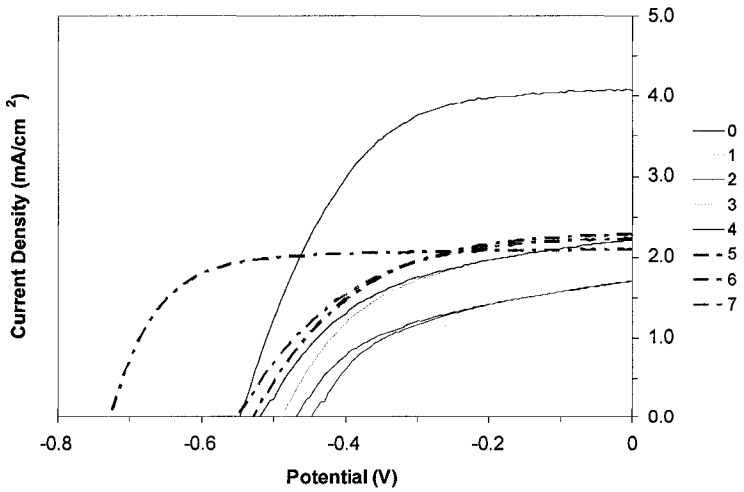

Figure 11. Plot of light iV curves. Plots 1,2 are 10% Co^{III}, plots 3,4 are 20% Co^{III}, plots 5,6 are 30% Co^{III}. Plots 0,7 are LiI. Cobalt solutions were 0.15 M cobalt complex, 0.2 M LiTriflate. LiI solution was 0.5 M LiI, 0.05 M I_2.

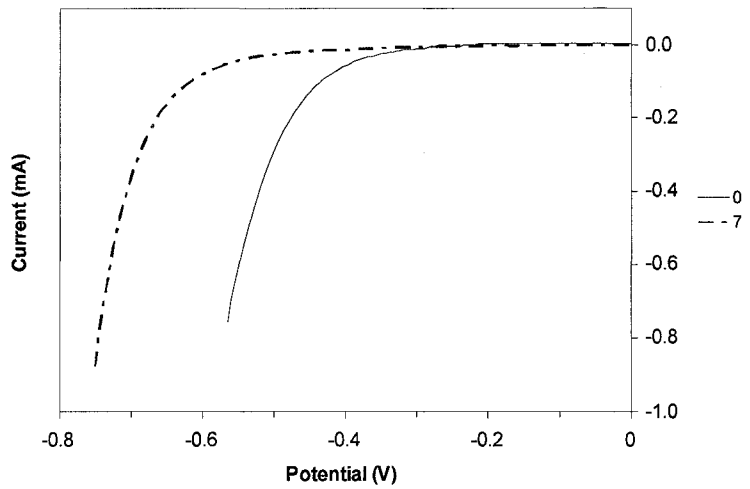

Figure 12. Plot of dark iV curves. Plots 0,7 are LiI. LiI solution was 0.5 M LiI, 0.05 M I_2. Y-axis is current rather than current density.

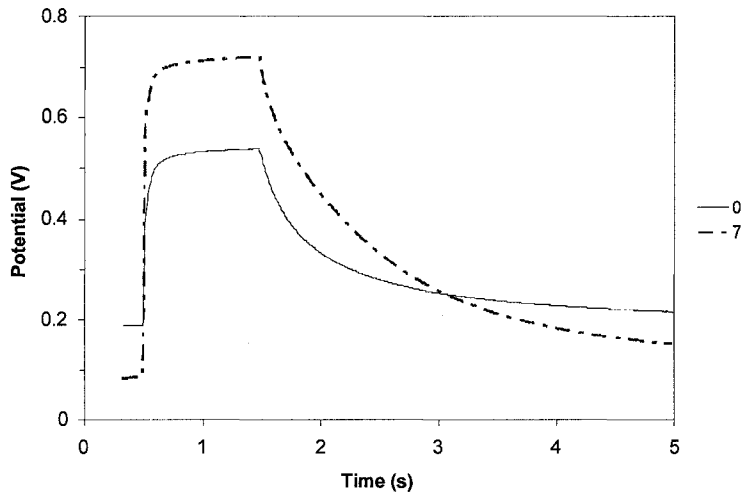

Figure 13. Plot of OCVD curves. Plots 0,7 are LiI. LiI solution was 0.5 M LiI, 0.05 M I_2.

A flow-through study using only iodide was performed next. **Figure 14** illustrates the iV curves. As before (**Figure 4**), the V_{oc} increased and the I_{sc} decreased with each substitution. However, in contrast to results with cobalt (**Figures 6 & 9**), the

iV curves were unaffected by two minutes without illumination. The behavior of the corresponding dark iV curves (**Figure 15**) matches that of the light iV curves with respect to consistently increasing voltages with each substitution.

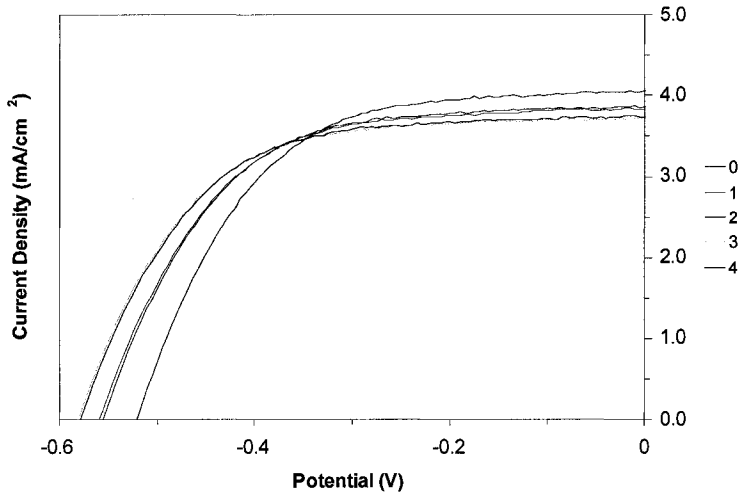

Figure 14. Plot of light iV curves. All plots are LiI. Plots 2,4 are after two minute wait. LiI solution was 0.5 M LiI, 0.05 M I_2.

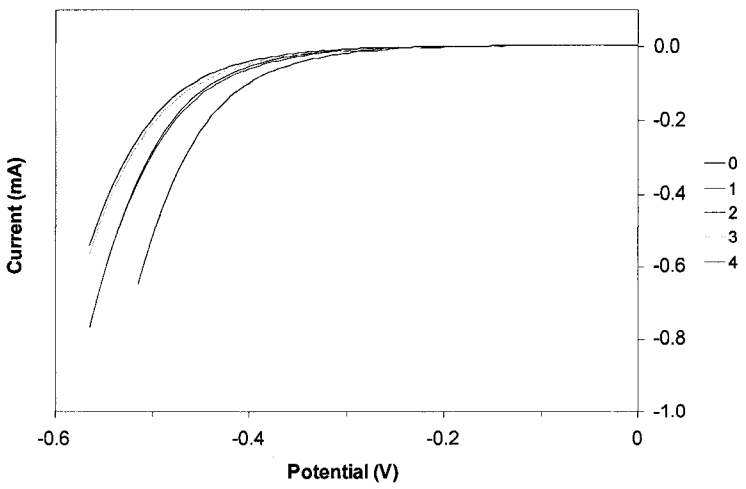

Figure 15. Plot of dark iV curves. All plots are LiI. Plots 2,4 are after two minute wait. LiI solution was 0.5 M LiI, 0.05 M I_2. Y-axis is current rather than current density.

To further investigate this phenomenon, a flow-through study was conducted on a photoanode without the N3 dye. As can be seen in **Figure 16**, each mediator substitution increased the observed voltage by a magnitude comparable to that of a dyed anode.

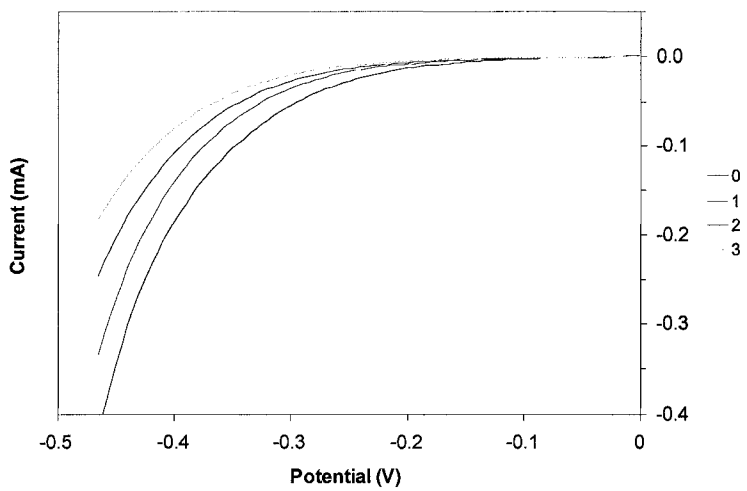

Figure 16. Plot of dark iV curves. All plots are 5% Co^{III}. Cobalt solutions were 0.15 M cobalt complex, 0.2 M LiTriflate, 0.2 M TBP.

As previously mentioned, dark iV curves primarily measure recombination current through exposed FTO surfaces. Accordingly, modification of the FTO surface would be expected to alter the dark response. Treatment with $TiCl_4$ solution deposits a thin layer (a few nanometers or less) of TiO_2 over the entire anode, including the FTO. Similarly, layers of compact (i.e., not nanocrystalline) TiO_2 may be deposited prior to fabrication of the nanocrystalline TiO_2 layer using sol-gel and spin-coating techniques. The effects of both $TiCl_4$ treatment and compact TiO_2 underlayers on the dark iV behavior is displayed in **Figures 17** and **18**, respectively. Note that, in both cases, although the overpotential for reverse current has been shifted negatively by as much as 150 mV, the voltage continues to increase negatively with each substitution. Also of

note, **Figure 17** demonstrates that the two minute wait in the dark does not affect the dark iV curve. Recall that the light iV curve of this DSSC (**Figure 6**, discussed earlier) showed a reproducible current increase after the wait period.

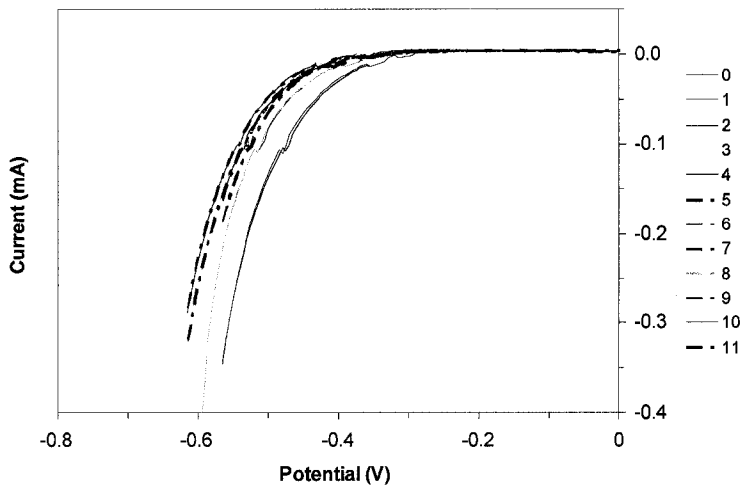

Figure 17. Plot of dark iV curves on $TiCl_4$-treated anode. Plots 0-5 are 5% Co^{III}, plots 6-11 are 20% Co^{III}. Even numbered plots are initial iV scans, odd numbered are after two minutes. Cobalt solutions were 0.15 M cobalt complex, 0.2 M LiTriflate, 0.2 M TBP. Y-axis is current rather than current density.

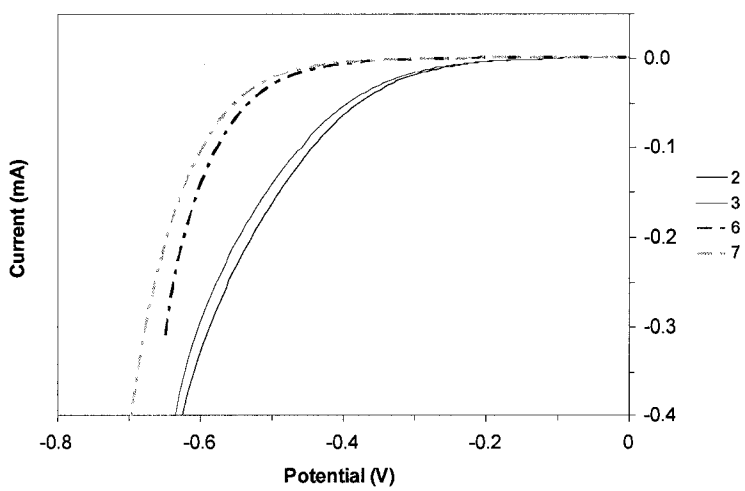

Figure 18. Plot of dark iV curves. Plots 2,3 are with regular anode; plots 6,7 are with a TiO_2 underlayer. All plots are 20% Co^{III}. Cobalt solutions were 0.15 M cobalt complex, 0.2 M LiTriflate, 0.2 M TBP. Y-axis is current rather than current density.

As the voltage was clearly shifted in the dark iV curves (relative to unmodified anodes), one would expect a concomitant shift in the V_{oc} of the light curves. Oddly, this is not clearly the case (**Figures 6** and **18**). Although in all cases (inclusive of those not shown), the V_{oc} is greater with underlayered or $TiCl_4$ treated anodes, the magnitude of the effect is much more subtle and is not obviously larger than the normal variation between anodes. This is especially surprising given the degree to which the OCVDs are altered (**Figure 20**). The extracted electron lifetimes are shown in **Figure 21**. At all voltages, photoanodes without exposed FTO have lifetimes which are greater by approximately an order of magnitude.

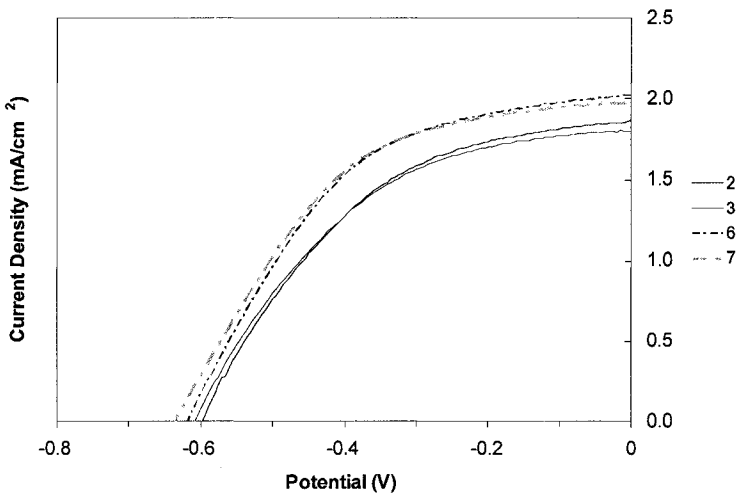

Figure 19. Plot of light iV curves. Plots 2,3 are with regular anode; plots 6,7 are with a TiO_2 underlayer. All plots are 20% Co^{III}. Cobalt solutions were 0.15 M cobalt complex, 0.2 M LiTriflate, 0.2 M TBP.

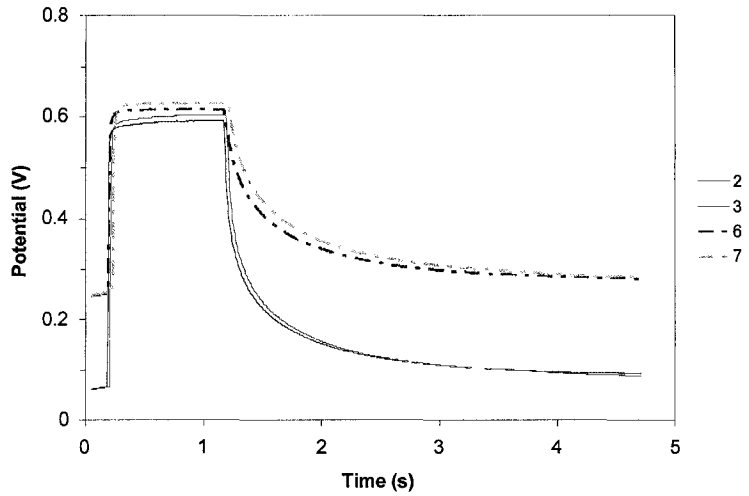

Figure 20. Plot of OCVD curves. Plots 2,3 are with regular anode; plots 6,7 are with a TiO_2 underlayer. All plots are 20% Co^{III}. Cobalt solutions were 0.15 M cobalt complex, 0.2 M LiTriflate, 0.2 M TBP.

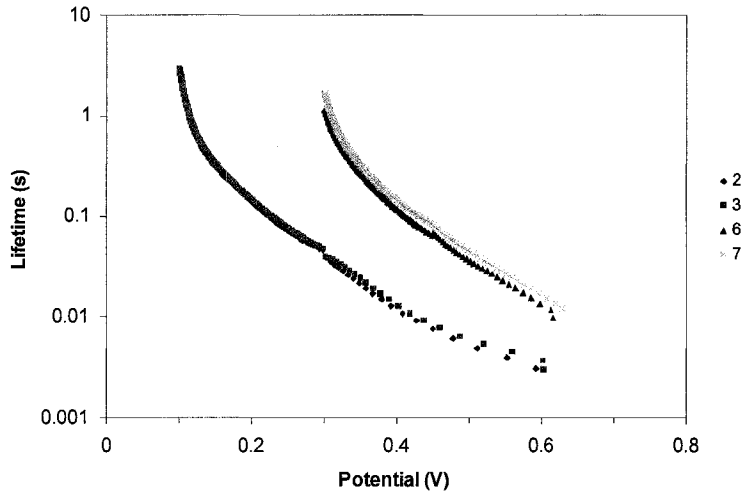

Figure 21. Plot of calculated electron lifetimes for OCVD curves of Figure 20. Note that the Y-axis is a logarithmic scale.

Neither the use of a compact underlayer nor the $TiCl_4$ resulted in a reproducible flow-through cell. Although J_{sc} was typically steady, V_{oc} consistently increased with each successive substitution. Nevertheless, the experiments may provide an important clue as to the rate-limiting step in cobalt-mediated DSSCs. The large shift in both the

dark iV curve and the OCVD was unaccompanied by a proportionately large increase in V_{oc} or J_{sc}. This may indicate that although recombination through exposed regions of FTO occurs in cobalt-mediated DSSCs, it is ultimately not the performance-determining process in these cells. Another ramification of the FTO recombination pathway is that it precludes further analysis of the OCVDs. The theory, as developed by Bisquert et al., relies on the assumption that the primary recombination pathway is through the titania nanoparticles. At this point, even with underlayers or $TiCl_4$ treatment, it is unclear that that is indeed the case. Consequently, the same type of extensive analysis of OCVD curves was not attempted.

Viscosity effects on current transients

Although the origin of the incessantly creeping V_{oc} remains a mystery, a large volume of experiments demonstrate that the concentration of oxidized cobalt has a pronounced effect on cell performance. Current transients suggest that in many systems, a lack of reducible mediator at the cathode hinders cell performance. This conclusion stems from two main observations. One, the cell initially delivers much higher currents than it can ultimately sustain and a drop in current over time results. Two, the sustainable current is improved by higher cobalt(III) concentrations. Slow diffusion of cobalt(III) to the cathode is the obvious first assumption. Initially, cobalt(III) concentrations at both electrodes would be identical to bulk concentrations, but once photocurrent begins to pass, slow diffusion of cobalt(III) would polarize the mediator solution.

If one assumes diffusion-limited transport of cobalt(III) as the rate-limiting step in cobalt-mediated DSSCs, altering the viscosity should have an observable effect. This

may be accomplished in a number of ways. We chose two: by varying the solvent and by heating the mediator solution. Controlling the viscosity through the use of solvents with inherently different viscosities is perhaps the most straightforward method to adjusting the viscosity in a controlled and semi-quantifiable manner but is not without its drawbacks. First, the viscosities of the resulting mediator solutions are only semi-quantifiable as the high concentrations of mediator and additives certainly alter the viscosity from that of the neat solvent. In most cases, this effect is observable by simple visual inspection and so must be considerable. Second, substitution of the solvent affects more than just viscosity. Solvent-specific parameters such as the degree of solvation, Marcus reorganization energy (λ), or reduction potential of the cobalt complex may all be affected to varying degrees. Nevertheless, DSSCs assembled using a selection of appropriate solvents can provide *corroborative* evidence for a diffusion-controlled system. Similarly, heating a system so heavily dependent on a multitude of competing kinetic processes – each possibly temperature dependent – is fraught with the possibility of altering more than just the viscosity of the solvent. Here again, only results consistent with a diffusion-controlled system may be hoped for.

Frequently in our research with cobalt mediators, it has been observed that cell performance improves after continuous exposure to one sun illumination (e.g., **Figure 22**). Out of habit, this exposure is generally conducted with the cell held at short circuit, although cells maintained at open circuit experience similar improvements. Illumination periods as short as two minutes can have considerable effect. The origin of the cell improvement is not fully understood, although a reasonable supposition is that it stems from a temperature increase of the cell due to the illumination. Accordingly, illumination

experiments were conducted in tandem with the temperature experiments in an effort to verify or disprove this hypothesis.

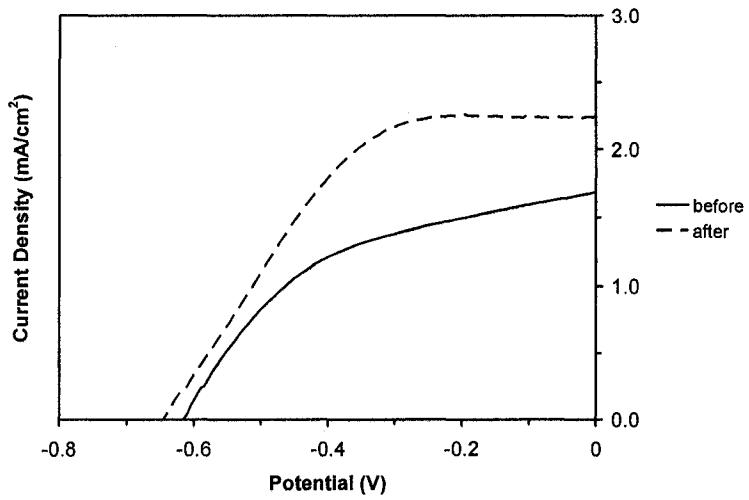

Figure 22. Plot of light iV curves before and after two minute period of illumination at short circuit. Mediator was 5% Co^{III}, 0.15 M cobalt complex, 0.2 M LiTriflate, 0.2 M TBP. Anode had a TiO_2 underlayer.

Solvent effects on current transients

Figure 23 displays the current transients for a flow-through cell with three different mediator solutions. Solutions were identical except for the solvents used. In addition to our standard mediator solvent (γ-butyrolactone, GBL), propionitrile (PN) and propylene carbonate (PC) were used for their widely varying viscosities (at 25 °C): 1.9 cP, 0.294 cP and 2.4 cP, respectively. Comparing the current at one second after exposure (typically equal to the steady state current, although in the case of PC this may not be the case), a clear trend with viscosity emerges. High viscosity resulted in lower sustainable currents, supporting the hypothesis that mass transport of cobalt (III) can be rate-limiting in DSSCs.

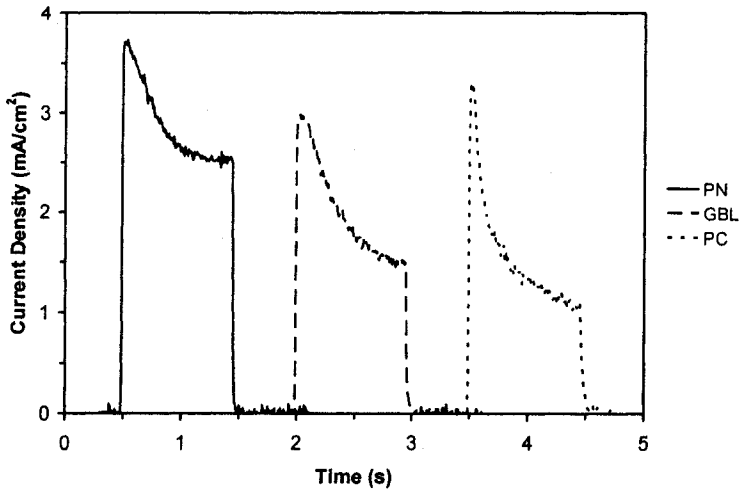

Figure 23. Plot of current transients with solvents of varying viscosity. All mediator solutions were 5% Co^{III}, 0.15 M cobalt complex, 0.2 M LiTriflate, 0.2 M TBP.

Also worthy of note, the behavior of the dark iV curves matched that seen previously, with voltage shifting negatively with each substitution. This observation is particularly perplexing as it further confounds attempts to decipher the shifting voltage. The dark iV curve shifts irrespective of mediator (cobalt/iodide), dying time, lithium ion, *tert*-butylpyridine, or solvent. Although difficult to rationalize, it appears the voltage shift may be due to the flushing process itself.

Temperature effects on current transients

Temperature experiments were conducted with both heating and cooling of the DSSC. For these experiments, conditions were deliberately chosen to maximize the size of the initial current spike relative to the steady state current. Accordingly, the photoanode was treated with $TiCl_4$ for six hours and a nearly saturated solution of cobalt was used (0.3M – noticeably more viscous than 0.15 M solutions) with only a small

amount of oxidized complex (2.5% – an equal amount of Co^{III} as the standard 5% oxidized 0.15 M solution). Heating was accomplished using a heatgun for a period of roughly 15-20 seconds (not strictly controlled). Insertion of the DSSC (still in the cell holder) into a dewar of liquid nitrogen, with the cell holder just touching the N_2 surface, was used to cool the cell. Although temperatures were not rigorously controlled nor recorded, the experiment was intended to yield only qualitative results. Accordingly, this relatively simple manner of conducting the temperature studies was adequate.

Figure 24 displays the resulting current transients. As can be seen, the behavior of the cell could be cycled between large, sharp current spikes at low temperature and smaller, broader peaks at high temperature. **Figure 25** displays the cell behavior when the cell was left to cool on its own. With time (and presumably slow cooling), the cell slowly reverted back to the initial performance. As can be seen, liquid N_2 accelerated this process. Similar behavior resulted when the cell was treated with one sun illumination for two minutes, irrespective of whether the cell was held at short or open circuit (**Figure 26**).

As mentioned briefly in the temperature experiments, 0.3 M solutions of cobalt complex typically exhibit a greater drop in current over time. **Figure 27** displays a comparison between six different DSSCs (six different anodes), three prepared with a solution of 0.3 M cobalt complex and three with a 0.15 M solution. Note that in these cells, a 4 μm spacer was used (rather than the standard 25 μm polyimide spacer) and that the anodes were prepared with a different colloid than the previous studies in this chapter (*vide infra*). In both solutions, the concentration of cobalt(III) was kept roughly constant – only the concentration of cobalt(II) differed (however, this assertion warrants some

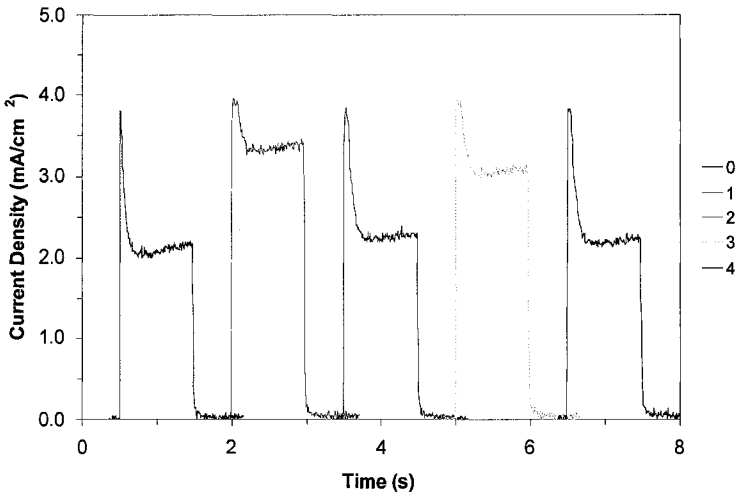

Figure 24. Effect of heat on current transients. Plot 0 is initial, plots 1,3 are after heating, plots 2,4 are after cooling with N_2. Mediator solution was 2.5% Co^{III}, 0.3 M cobalt complex, 0.2 M LiTriflate, 0.2 M TBP. Anode was $TiCl_4$-treated. A 4 μm spacer was used.

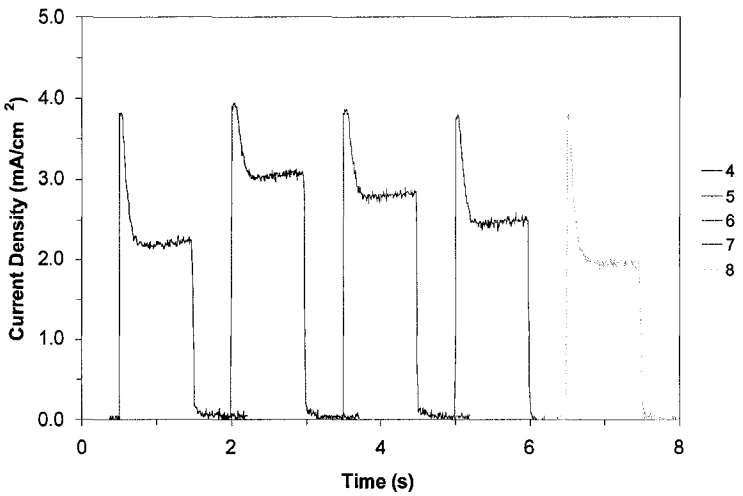

Figure 25. Effect of slow cooling on current transients. Plots 4,8 are after cooling with N_2, plot 5 is after heating, plots 6,7 are after ~1 minute wait period (each). Mediator solution was 2.5% Co^{III}, 0.3 M cobalt complex, 0.2 M LiTriflate, 0.2 M TBP. Anode was $TiCl_4$-treated. A 4 μm spacer was used.

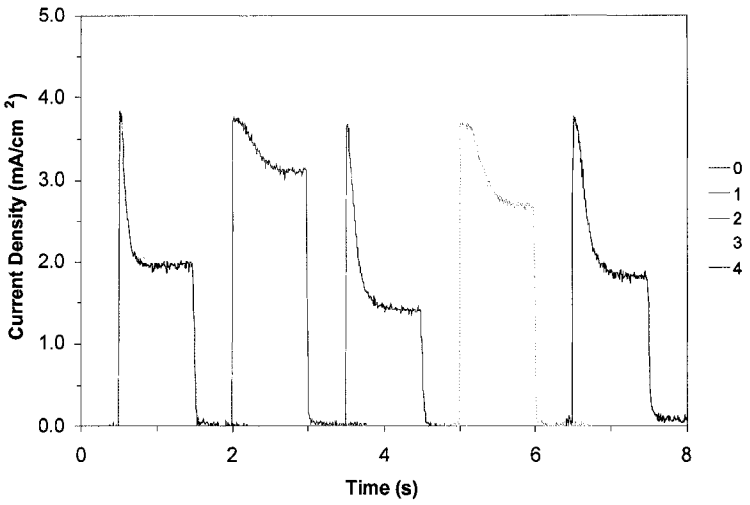

Figure 26. Effect of illumination on current transients. Plot 0 is initial, plots 1,3 are after 2 minutes of illumination, plots 2,4 are after cooling with N_2. Mediator solution was 2.5% Co^{III}, 0.3 M cobalt complex, 0.2 M LiTriflate, 0.2 M TBP. Anode was $TiCl_4$-treated. A 4 μm spacer was used.

amount of skepticism as cobalt(III) concentration was determined through stoichiometric addition of $NOBF_4$ to the mediator solution – a method which is considerably less trustworthy than the method used in the other studies presented here). As cobalt(II) was present in large excess in both solutions, presumably the primary functional difference between the two solutions was in their viscosities. Although this assumption may not be perfect, the advantage of this experiment was that the viscosity could be adjusted without the side effects inherent in the previous viscosity studies (which varied solvent and temperature). The results clearly indicate that the DSSCs with more concentrated mediator solutions were more prone to large current spikes.

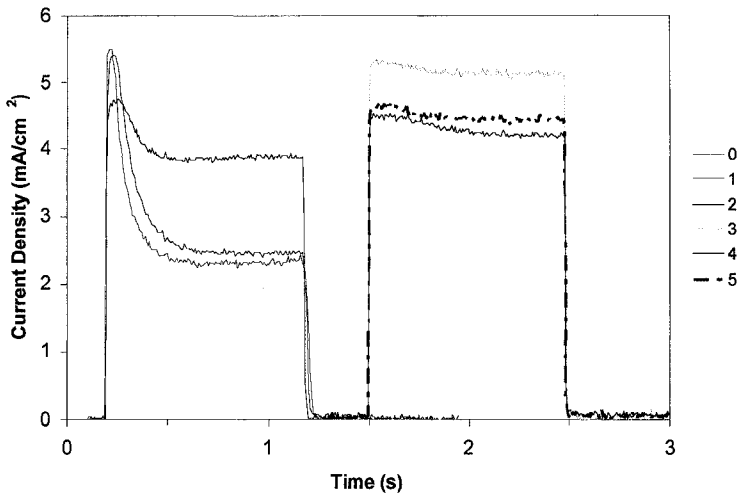

Figure 27. Effect of cobalt concentration on current transients. Plots 0-2 are 0.3 M cobalt complex, plots 3-5 are 0.15 M cobalt. Both solutions were 0.015 M Co^{III} (5% and 10% oxidized, respectively), 0.2 M LiTriflate, 0.2 M TBP. Anodes were $TiCl_4$-treated. A gold cathode and no spacers were used.

Effect of the TiO_2 layer

For the sake of argument, let us assume that diffusion between the two electrodes of the sandwich cell is rate-limiting in cobalt-mediated DSSCs. In experiments with a plastic spacer, there are two distinct regions within the DSSC: the area between the cathode surface and the exterior (or macroscopic) surface of the titania layer, and the network of pores within the nanocrystalline titania layer. Presumably, diffusion through one or both of these regions could be rate-limiting.[16] Two principle differences exist between these two regions. The random network of nanometer-sized pores introduces significant tortuosity for a molecule traveling within the titania layer, whereas the path from the exterior of the layer to the cathode is essentially unobstructed. On the other hand, the entire titania layer is on average only 4 μm thick – in contrast, the distance between the surfaces is on the order of 25 μm (the thickness of the polyimide spacer).

Consequently, it is difficult to predict through which region cobalt complexes would take the longest to travel.[16]

There are a few indications which suggest that diffusion through the porous titania network is at least partially (if not primarily) responsible for the mass-transfer limitation. As previously mentioned, $TiCl_4$ treatment has been found to exacerbate the magnitude of the current spike. $TiCl_4$ treatment deposits a fine layer (on the order of a few nanometers or less) of TiO_2 onto all surfaces of the photoanode (the nanocrystalline TiO_2 as well as any exposed regions of FTO). Any deposition within the TiO_2 layer should result in slightly decreased pore sizes which in turn could, in theory, hamper mobility of electrolyte within the porous network. Although the deposited layer is thin, the constricting effect could be non-negligible as the pore/particle dimensions within the TiO_2 layer are also on the nanometer scale. Supporting this idea is the fact that Barbé and coworkers found that $TiCl_4$ treatment reduces the surface area by roughly 15% on average.[17]

A second observation also lends some credence to the hypothesis that diffusion within the titania layer can be rate-limiting. A study was conducted to determine what conditions were optimal for our DSSCs, both those using iodide and cobalt. In the case of iodide mediated DSSCs, anodes from a colloid prepared by the research group of Professor Carlo Bignozzi were found to be preferable to those prepared from a Solaronix colloid. In contrast, photoanodes prepared from the Solaronix colloid were superior when cobalt complex was used. Scanning electron microscopy (SEM) indicated that the average particle diameter was larger in TiO_2 films prepared from the Solaronix colloid. The micrographs are shown in **Figure 28**. As pore size should correlate with particle

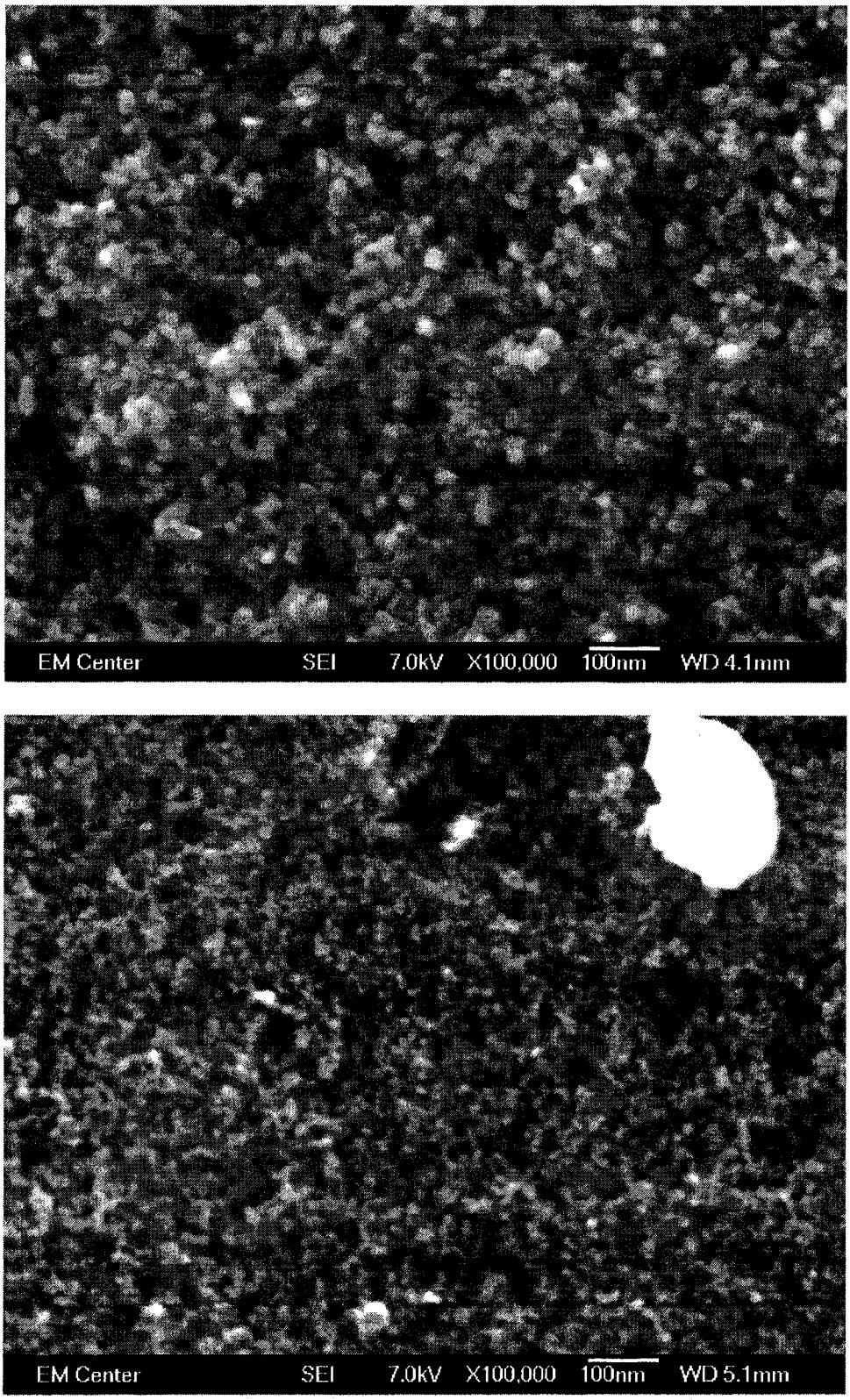

Figure 28. SEM images of titania films prepared from (top) a Solaronix colloid and a (bottom) colloid from the Bignozzi research group. The scale bar is 100 nm for both images.

size, it can be inferred that the pores were also larger on average. Consistent with this finding was the observation that the Solaronix films were visibly less dark when dyed (larger particles should yield films with less total surface area, resulting in less dye adsorption which in turn would render the anode less dark).

Effect of the spacer

While there are indications that the titania layer may affect mediator diffusion through the cell *at times*, it may well be that the thickness of the spacer also influences cell performance. Initial spacer experiments utilized a polyester spacer of 4 μm thickness. **Figures 29** and **30** show the iV curves and current transients, respectively, of DSSCs assembled with and without the spacer. The differences in current are within typical variation for assembled and reassembled cells and indicate that mass-transfer across the 4 μm gap has little or no effect on the maximum current deliverable by the cell.

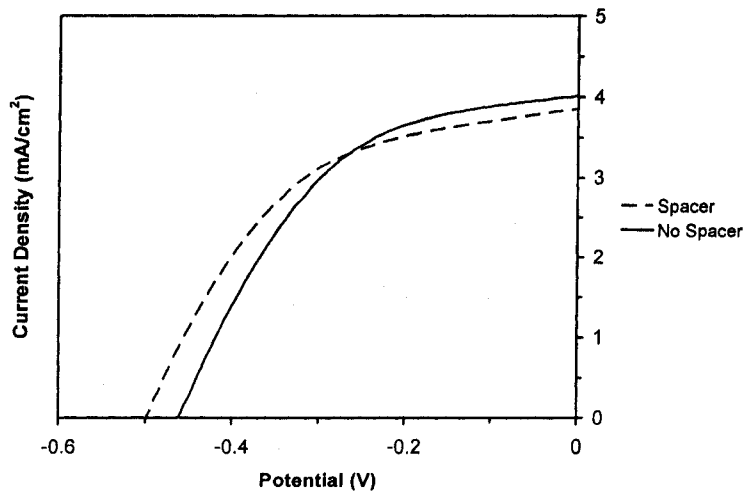

Figure 29. Effect of 4 μm spacer on light iV curves. Mediator solutions were 10% Co^{III} (oxidized by 0.03 M $NOBF_4$), 0.3 M cobalt complex, 0.2 M LiTriflate, 0.2 M TBP. A gold cathode and 4 μm spacers were used.

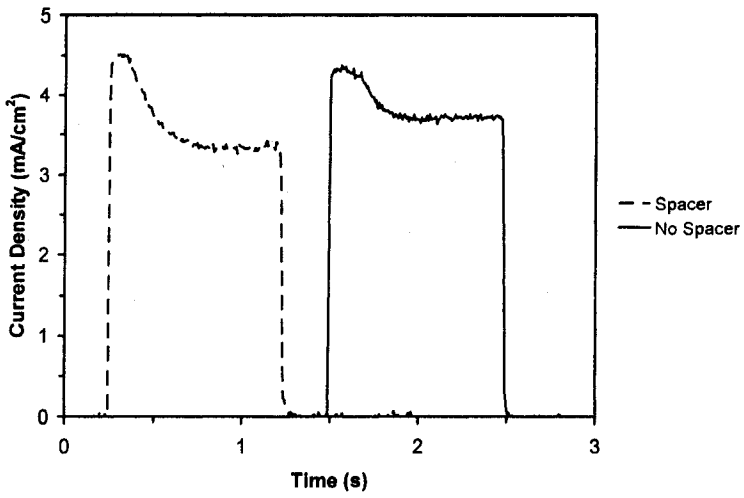

Figure 30. Effect of 4 μm spacer on current transients. Mediator solutions were 10% Co^{III} (oxidized by 0.03 M $NOBF_4$), 0.3 M cobalt complex, 0.2 M LiTriflate, 0.2 M TBP. A gold cathode and 4 μm spacers were used. (1 sun).

Of particular interest is the fact that, even without a spacer, current still drops to a lower steady state value after a few hundred milliseconds. However, in cells with 25 μm spacers, the current drops over a longer timescale, often as great as one second or more. If the drop in current is assumed to be due to mass transport limitations with respect to cobalt(III), then the current would be expected to drop as the diffusion layer (the region where analyte concentrations are altered from their bulk values) grows thicker. In thin cells (such as the DSSC), the current decrease should continue until the diffusion layer reaches the opposite side of the cell, at which point the current will reach a steady state value. The fact that the current stabilizes after a greater length of time with larger spacers is consistent with the supposition that diffusion is performance limiting in cobalt-mediated DSSCs.

Furthermore, three electrode experiments (detailed in the following chapter) were performed using cells which were identical but for the thickness of the spacer. In all

cases, cells with 25 μm spacers gave reduced currents. This finding supports the assertion that diffusion is performance-limiting in 25 μm cells but unfortunately may also indicate that the design of the flow-through study presented in this chapter introduced (or, at the very least, exaggerated) a mass transport limitation which may or may not be present in thinner cells. This idea is further discussed below.

Conclusions

The flow-through study presented here provides insight into cobalt-mediated DSSCs with a degree of rigor not previously possible. A multitude of processes must coordinate within DSSCs for successful light conversion and the kinetics of each are impacted by an incredible number of factors in oftentimes subtle and not so obvious ways. Accordingly, it is important to remove as many variables as possible when making comparisons. Flow-through mediator replacement provides a manner in which to remove the inescapable performance changes which occur upon disassembly and reassembly. Coupled with the suite of four complementary sandwich cell evaluation techniques, the flow-through study has yielded information as to the limitations of cobalt-mediated cells and offered suggestions for how to improve them.

The most unambiguous result from these studies is that diffusion of cobalt(III) is often rate-limiting in cobalt-mediated DSSCs. Methods to alleviate this include increasing the cobalt(III) concentration as well as lowering the solvent viscosity. The latter strategy may be accomplished by any number of methods, including application of heat or light as well as through selection of solvent. Consistent with Murphy's Law, utilization of both strategies in tandem is complicated by the solubility characteristics of

cobalt(III) complexes. Propionitrile, a solvent with low viscosity and reasonably low vapor pressures (important in unsealed cells), reaches saturation at relatively low cobalt(III) concentration (approximately 0.01 M, or ~7% of a 0.15 M cobalt solution). Few other solvents with low viscosities have been attempted. The results of this study, however, suggest that a more extensive solvent search might be warranted.

Although diffusion of cobalt(III) clearly limits performance in DSSCs with 25 μm spacers, it is less certain that this is the case in DSSCs with either thinner or no spacers. As previously discussed, 25 μm spacers appear to limit maximum attainable currents. There are a few signs, however, that diffusion is still a problem in thinner cells. Firstly, as demonstrated in **Figure 30**, current spikes are still observed in these cells. In addition, the current spike and overall cell performance (as measured by a light iV experiment) can be improved with two minutes of illumination in DSSCs with 4 μm spacers (data not shown). In fact, in these cells illumination is often capable of removing the current spike altogether.

A somewhat unexpected result of the flow-through study is that TiO_2 underlayers or $TiCl_4$ treatments have a surprisingly small effect on the performance of DSSCs. Considering the large voltage shifts observed in the dark iV curves, one would expect a marked improvement in the light iV curves, at least with V_{oc} and perhaps FF. However, this is not the case. Light iV curves did not significantly improve with either technique. This may be a further indication that diffusion of cobalt(III) – and not recombination across the FTO surface – is performance-limiting in cobalt-mediated DSSCs.

Other behaviors were observed during the course of the flow-through study. Although their origins at the moment are less well understood, they provide hints as to

other phenomena within the cell and may serve as a guide for future attempts to design DSSCs. The observation that LiI behavior is altered when an anode is exposed to cobalt mediators is particularly interesting. The dramatic increase in V_{oc} and decrease in J_{sc} are consistently observed. As the dark iV curve is affected, one would initially suspect a mechanism involving exposed regions of FTO. Yet $TiCl_4$ treatment does not alter the effect of cobalt mediators on LiI behavior in any way. Regardless, it would appear that the cobalt mediator itself is responsible for the altered LiI behavior. If so, adsorption of the cobalt complex (or a decomposition product) is likely as the effect remains once the cobalt solution is removed. As LiI currents were significantly decreased, it may be that cobalt adsorption onto a surface limits the maximum current deliverable by the cell. Although only speculation is possible at this point, it seems clear that a better understanding of how cobalt complex alters the cell could assist efforts to improve cobalt-mediated DSSCs.

The tendency of J_{sc} to decrease and V_{oc} to increase with flushing is also curious. As the V_{oc} increase occurred in all situations, it can only by deduced that it is somehow a consequence of the flushing process itself. On the other hand, it was possible to eliminate the change in J_{sc} by either $TiCl_4$ treating the photoanode or removing *tert*-butylpyridine from the mediator solution. Initially, it would seem that a continual increase in TBP adsorption with each flush was responsible for the J_{sc} decrease. Either removing TBP or modifying the anode surface with $TiCl_4$ treatment (presumably altering TBP's tendency to adsorb, in this scenario) would then be sensible solutions to the problem. Inconsistent with this scenario, however, is the fact that the J_{sc} decrease was also observed in DSSCs mediated by a LiI solution not containing TBP.

Lastly, the reproducible increase in currents after a two minute period without illumination is odd. This occurred in cells with or without TBP, with or without $TiCl_4$ treatment. Only current was affected – V_{oc}, OCVDs and dark iV curves were unaffected – and no such increase was observed with LiI mediated cells. Furthermore, current transients indicated that steady-state currents and not initial currents were improved. This observation may indicate that either a change in viscosity or cobalt(III) concentration is somehow occurring. A plausible explanation for how or why has yet to be found.

Future Experiments

At this point, the flow-through survey has likely yielded as much information as it can. Three possible exceptions exist. As will be discussed in Chapter 4, platinum is not an ideal cathode for use in cobalt-mediated DSSCs. Although DSSCs with platinum cathodes exhibit similar J_{sc} and V_{oc} characteristics, the FF is consistently worse than for DSSCs with the best gold cathodes. The extent to which platinum is affecting the results of the flow-through survey is unknown at this time. Conceivably, it could be useful to repeat the experiments using a gold cathode. The danger of such an endeavor is that the integrity of the gold cathode may well be subject to change during the course of the study. Unfortunately, the electron transfer kinetics across gold surfaces to cobalt complexes seem to be strongly influenced by factors not currently understood, making their behavior seem erratic. Nevertheless, it might be a good idea to try.

As alluded to earlier, there currently exists a limit to the concentration of cobalt(III) attainable with our common DSSC solvents. With higher viscosity solvents,

this limit is around 30% (maybe slightly greater). With propionitrile, it is much lower. It very well could be worth the time to find a relatively low viscosity solvent in which cobalt(III) complexes are more soluble. Very likely, a change in the counterion (currently ClO_4^-) could increase the solubility of the cobalt complex. Once a more soluble mediator system was found, flow-through experiments would be advisable.

It also might be valuable to adapt the flow-through experiment so that a thinner spacer could be used. Although 4 μm and 8 μm spacers were found insufficient for complete mediator substitution (*vide supra*), it would be of benefit to conduct flow-through studies with a spacer which did not introduce or exacerbate diffusion limitations within the cell. Possibly, the number of flushes could be increased (most probable with the 8 μm spacer), although this would exaggerate the phenomena within the cell which appear flush-dependent (increasing V_{oc}, decreasing J_{sc} in certain conditions, etc...). It is also possible that a more creative solution could be found.

It may be worth attempting XPS or other surface-sensitive experiments to try and determine how cobalt complexes could be altering the DSSC (as discussed with LiI changing iV behavior).

Finally, future research into DSSCs may well include the development of novel mediator systems. Flow-through experiments are clearly useful in comparing mediators and should be used to evaluate these novel systems.

Bibliography

1. Grätzel, M., Perspectives for dye-sensitized nanocrystalline solar cells. *Prog. Photovoltaics* **2000,** 8, (1), 171-185.

2. Cahen, D.; Hodes, G.; Grätzel, M.; Guillemoles, J. F.; Riess, I., Nature of Photovoltaic Action in Dye-Sensitized Solar Cells. *Journal of Physical Chemistry B* **2000,** 104, 2053-2059.

3. Ellingson, R. J.; Asbury, J. B.; Ferrere, S.; Ghosh, H. N.; Sprague, J. R.; Lian, T. Q.; Nozik, A. J., Dynamics of Electron Injection in Nanocrystalline Titanium Dioxide Films Sensitized with [Ru(4,4'-dicarboxy-2,2'-bipyridine)$_2$(NCS)$_2$] by Infrared Transient Absorption. *Journal of Physical Chemistry B* **1998,** 102, 6455-6458.

4. Gregg, B. A.; Pichot, F.; Ferrere, S.; Fields, C. L., Interfacial Recombination Processes in Dye-Sensitized Solar Cells and Methods To Passivate the Interfaces. *Journal of Physical Chemistry B* **2001,** 105, 1422-1429.

5. Nazeeruddin, M. K.; Kay, A.; Rodicio, I.; Humphry-Baker, R.; Müller, E.; Liska, P.; Vlachopoulos, N.; Grätzel, M., Conversion of Light to Electricity by *cis*-X$_2$Bis(2,2'-bipyridyl-4,4'-dicarboxylate)ruthenium(II) Charge-Transfer Sensitizers (X = Cl$^-$, Br$^-$, I$^-$, CN$^-$ and SCN$^-$) on Nanocrystalline TiO_2 Electrodes. *Journal of the American Chemical Society* **1993,** 115, 6382-6390.

6. Ferrere, S., New Photosensitizers Based upon [Fe(L)$_2$(CN)$_2$] and [Fe(L)$_3$] (L = Substituted 2,2'-Bipyridine): Yields for the Photosensitization of TiO_2 and Effects on the Band Selectivity. *Chemistry of Materials* **2000,** 12, 1083-1089.

7. Zaban, A.; Greenshtein, M.; Bisquert, J., Determination of the Electron Lifetime in Nanocrystalline Dye Solar Cells by Open-Circuit Voltage Decay Measurements. *ChemPhysChem* **2003,** 4, 859-868.

8. Bisquert, J.; Zaban, A.; Greenshtein, M.; Mora-Seró, I., Determination of Rate Constants for Charge Transfer and the Distribution of Semiconductor and Electrolyte Electronic Energy Levels in Dye-Sensitized Solar Cells by Open-Circuit Photovoltage Decay Method. *Journal of the American Chemical Society* **2004,** 126, 13550-13559.

9. Bisquert, J.; Cahen, D.; Hodes, G.; Rühle, S.; Zaban, A., Physical Chemical Principles of Photovoltaic Conversion with Nanoparticulate, Mesoporous Dye-Sensitized Solar Cells. *Journal of Physical Chemistry B* **2004,** 108, 8106-8118.

10. Hagfeldt, A.; Grätzel, M., Molecular Photovoltaics. *Accounts of Chemical Research* **2000,** 33, 269-277.

11. Benkstein, K. D.; Kopidakis, N.; van de Lagemaat, J.; Frank, A. J., Influence of the Percolation Network Geometry on Electron Transport in Dye-Sensitized Titanium Dioxide Solar Cells. *Journal of Physical Chemistry B* **2003,** 107, 7759-7767.

12. Würfel, U.; Wagner, J.; Hinsch, A., Spatial Electron Distribution and Its Origin in the Nanoporous TiO_2 Network of a Dye Solar Cell. *Journal of Physical Chemistry B* **2005,** 109, 20444-20448.

13. Nusbaumer, H. Alternative Redox Systems for the Dye-Sensitized Solar Cell. Doctor of Philosophy, École Polytechnique Fédérale de Lausanne, Lausanne, 2004.

14. Smestad, G. P.; Spiekermann, S.; Kowalik, J.; Grant, C. D.; Schwartzberg, A. M.; Zhang, J.; Tolbert, L. M.; Moons, E., A technique to compare polythiophene solid-state dye-sensitized TiO_2 solar cells to liquid junction devices. *Solar Energy Materials & Solar Cells* **2003,** 76, 85-105.

15. Schlichthörl, G.; Huang, S. Y.; Sprague, J.; Frank, A. J., Band Edge Movement and Recombination Kinetics in Dye-Sensitized Nanocrystalline TiO_2 Solar Cells: A Study by Intensity Modulated Photovoltage Spectroscopy. *Journal of Physical Chemistry B* **1997,** 101, 8141-8155.

16. Papageorgiou, N.; Liska, P.; Kay, A.; Grätzel, M., Mediator Transport in Multilayer Nanocrystalline Photoelectrochemical Cell Configurations. *Journal of the Electrochemical Society* **1999,** 146, (3), 898-907.

17. Barbé, C. J.; Arendsa, F.; Comte, P.; Jirousek, M.; Lenzmann, F.; Shklover, V.; Grätzel, M., Nanocrystalline Titanium Oxide Electrodes for Photovoltaic Applications. *J. Am. Ceram. Soc.* **1997,** 80, (12), 3157-3171.

Chapter 4

Development and Results of an Improved Thin Cell, Three Electrode Experiment

Abstract

A novel three electrode DSSC experiment, modified from two existing techniques, was devised and implemented in order to study cathode behavior in cobalt-mediated DSSCs. The new experiment incorporated a split photoanode in conjunction with a customized potentiostat circuit to allow for simultaneous monitoring of cathode potential, photoanode potential and cell current while still maintaining the thin electrode separation of the standard sandwich cell configuration. Interestingly, DSSCs with poor cathodes, characterized by decreased photocurrent and/or fill factor, exhibited only

modest charge transfer overpotentials (or none at all) on the cathode. Even more perplexing, mass transfer overpotentials were not observed, even in clearly diffusion-limited cases. Whether these results are due to a deficiency in the experiment or are a consequence of the DSSC system being extremely sensitive to very small overpotentials is still uncertain.

Introduction

Objective

The standard electrochemical DSSC evaluation technique is the iV experiment conducted under light conditions.[1-3] While very useful for describing overall cell performance, it yields little information on cathode or electrolyte behavior.[4] Specifically, the existence of an overpotential on the cathode (due to either cathode or electrolyte limitations) cannot be detected with iV experiments as only two electrodes are used.[4] Introduction of a third electrode with a constant potential (i.e. a reference) into the system allows the potentials of both the photoanode and cathode relative to the reference to be recorded throughout a iV scan, enabling the detection of an overpotential on the cathode.[4, 5] Although non-trivial to perform, a three electrode experiment was considered valuable as both mass transfer and charge transfer overpotentials were suspected with cobalt-based mediator systems in DSSCs.

Energetic description of iV experiments

In order to understand iV experiments (two or three electrode), a brief discussion of the thermodynamics within a DSSC during the scan is in order. **Figure 1** (left) depicts

an energy diagram overlaid onto a physical representation of a DSSC in the dark. Without illumination, the cell passes no current and is therefore at equilibrium.[6] The potential (i.e. the Fermi energy) of both electrodes is determined by the concentration ratio of oxidized/reduced mediator in accordance with the Nernst equation, shown below.[5, 6]

$$E = E^{0'} - \frac{RT}{nF} \ln\left(\frac{C_R^*}{C_O^*}\right)$$

where E is the measured potential of the electrode or redox couple, $E^{0'}$ is the formal potential of the couple, R is the ideal gas constant, T is temperature, *n* is the number of electrons transferred per redox reaction, F is the Faraday constant, C^* is the bulk concentration of the oxidized or reduced species (denoted by the subscript).

Upon illumination, equilibrium conditions no longer exist and the potential of the photoanode may be varied independently of the mediator solution. On the other side of the cell, if ideal conditions are assumed (described below), the cathode will remain fixed at the potential of the mediator, which in turn will deviate only minimally (if at all) from the dark potential.[6] At all times, the cell potential (E_{cell}) is dictated by the difference between the cathode and photoanode Fermi energies.

The relative energies within an illuminated DSSC at open circuit are shown in **Figure 1** (right). At open circuit, no current is allowed to flow between the cathode and photoanode. Photoinjected electrons will remain in the conduction band of the photoanode (encompassing the conduction bands of both the titania or fluorine-doped tin oxide (FTO) layers) until recombining with either the oxidized dye or oxidized mediator.[7] As the Fermi energy of the photoanode (strictly speaking, a quasi-Fermi energy) is determined directly from the population of electrons in its conduction, the Fermi energy

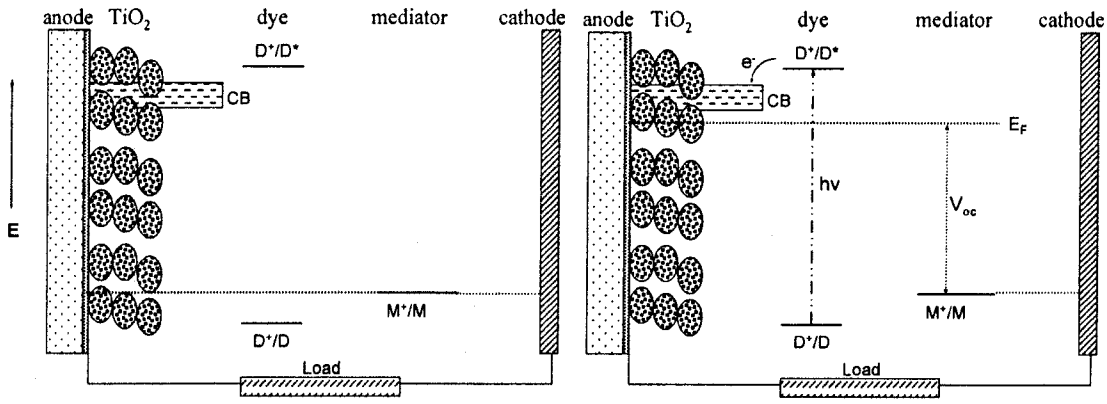

Figure 1. Energy diagrams of: (left) a DSSC in the dark, (right) an illuminated DSSC at open circuit.

will initially rise as electrons are injected into the conduction band.[7] The rate of recombination, which is driving force dependent, will increase as the Fermi level rises until the cell reaches its maximum potential, at which point the rates of photoinjection and recombination are equal.[8] The difference between the photoanode and cathode potentials at this point is the open circuit potential (V_{oc}).

During an iV experiment, the cell potential is scanned from open to short circuit. Ideally, the cathode potential will remain virtually constant and it will be the photoanode potential that changes (**Figure 2**, left).[5] At short circuit, the Fermi energies of the photoanode and cathode are equal ($E_{cell} = 0$) and the cell is passing its maximum current. If electrolyte or cathode behavior is not ideal, an overpotential (η) at the cathode may exist when the cell passes current (**Figure 2**, right), resulting in a negative shift of the Fermi energy of the cathode.[4] Either a charge transfer (η_{CT}) or a mass transfer (η_{MT}) overpotential is possible (*vide infra*) and would negatively affect DSSC performance by decreasing the observed fill factor (FF) and usually the short circuit current (I_{sc}) as well.

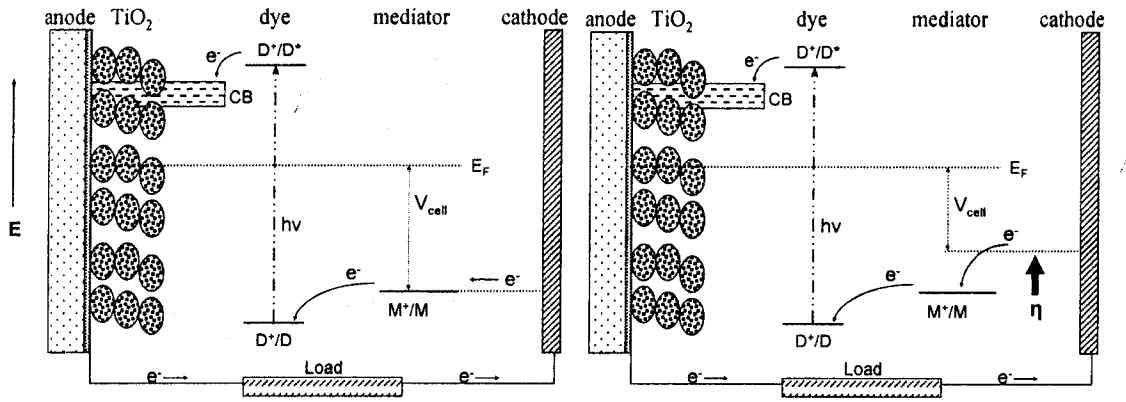

Figure 2. Energy diagrams of a DSSC midway through a iV scan where: (left) the cathode functions ideally, (right) a cathodic overpotential exists.

Unfortunately, without a reference electrode, an overpotential at the cathode is impossible to detect as there are numerous causes for a low FF or I_{sc}. However, if a reference with a constant – and ideally a known (although this is not strictly required) – potential is introduced to the system, detection of a cathodic overpotential becomes possible.[4, 5] **Figure 3** depicts the situation for two systems where the potential of the reference is equal to V_{oc} of the photoanode (any constant potential is acceptable, but the reasons for picking this potential will become clear later in the chapter). In both cases, as the potential of the photoanode is varied from open to short circuit, its potential relative to the reference ($E_{PA,ref}$) changes from zero to a large and positive number (in contrast, E_{cell} changes from a large and positive number to zero). In the ideal case (left), the potential of the cathode relative to the reference ($E_{DC,ref}$) is positive and constant throughout the scan. However, in a non-ideal cell (**Figure 7**) $E_{DC,ref}$ will be less positive when current passes than at open circuit due to the overpotential at the cathode. A plot of electrode potential ($E_{PA,ref}$ and $E_{DC,ref}$) versus cell potential is shown in **Figure 9** (right) for both an ideal and non-ideal DSSC.

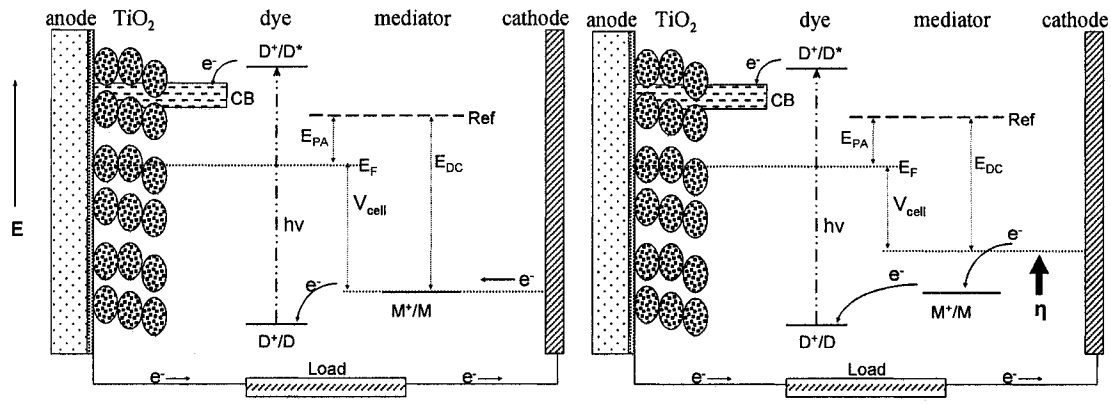

Figure 3. Energy diagrams of a DSSC containing a reference electrode where: (left) the cathode functions ideally, (right) a cathodic overpotential exists.

Cathodic overpotentials in DSSCs

A suitable mediator/cathode combination requires, first and foremost, sufficiently fast electron transfer kinetics so as to allow for moderately large currents with little or no overpotential (η). According to Butler-Volmer theory, in the absence of mass-transfer effects (i.e. the surface concentrations of each redox species are equal to the bulk concentrations, $\frac{C_{O(x=0)}}{C_O^*} = \frac{C_{R(x=0)}}{C_R^*} = 1$), the ability of a redox-active species/electrode system to deliver large currents is directly proportional to both the charge transfer (or "kinetic") overpotential, (η_{CT}), and the exchange current, i_0 – which is in turn dependent on the standard heterogenous rate constant, k^0 – of the system.[9]

$$i = i_0 \left[\frac{C_{O(x=0)}}{C_O^*} e^{-\alpha f \eta} - \frac{C_{R(x=0)}}{C_R^*} e^{(1-\alpha) f \eta} \right]$$

In a DSSC, overpotentials at the cathode are undesirable as they represent a voltage loss within the cell. Therefore, an ideal mediator will have a high k^0 on its respective cathode, allowing the system to be able to supply large currents at small overpotentials. Although

the k^0 of a specific mediator on a particular cathode can be determined experimentally outside of a DSSC sandwich cell, it is difficult to know what value of k^0 is sufficient to ensure ideal performance under operating conditions. A three electrode measurement is an ideal method for directly elucidating whether or not a kinetic overpotential exists at the cathode and requires no estimation of ideal k^0 values.

There exists another mechanism by which an overpotential at the cathode could occur. Butler-Volmer theory also predicts that even in the case of large exchange currents, a concentration (or "mass transfer") overpotential (η_{MT}) could arise if the system reaches the mass-transfer-limited current.[9] In this situation, mass-transfer limitations will cause the ratio of oxidized/reduced species (O/R ratio) to shift at the surface of the electrode ($\frac{C_{O(x=0)}}{C_O^*} \neq \frac{C_{R(x=0)}}{C_R^*} \neq 1$ in the above equation), due to the lack of availability of one of the redox species (O, in the case of reduction at the cathode). As electrode potential is dependent on the concentration of oxidized and reduced species, a change in the O/R ratio at the cathode will be accompanied by a Nernstian shift in potential at that electrode. Although the sandwich cell geometry is specifically designed to minimize η_{MT}, the tortuosity of the mediator's path through the highly chaotic and porous photoanode cannot be avoided. In addition, viscosity may play a role as most mediator solutions are saturated with electrolyte. It is, therefore, desirable to ascertain the extent to which a concentration overpotential exists.

Previous three electrode experiments with DSSCs

The standard cell configuration used for iV experiments is commonly referred to as the "sandwich cell" configuration and consists of two electrodes clamped together.[1-3]

The distance between electrodes is thus on the order of microns and is intentionally kept small to minimize the effects of molecular diffusion on cell performance (i.e. minimize η_{MT}).[4] While this geometry may be optimal for cell performance, it does not allow for easy integration of a reference electrode.[4]

Nevertheless, several groups have sought to determine the actual potentials present in the cell under operation in light conditions.[4, 5, 10-12] The most common strategy involves using a spacer to increase the distance between electrodes, allowing for inclusion of a reference electrode.[5, 10-12] Tubing is used to connect the cell chamber (the region between electrodes) to an exterior electrolyte chamber in which a reference electrode is placed. As implemented by Meyer et al., data was collected "manually" using a variable resistor, two voltmeters and an ammeter.[5] While this procedure successfully allows for simultaneous monitoring of both the cathode and photoanode potentials relative to a reference, it is slow and requires large volumes of redox mediator. In addition, the spacer alters the regular dimensions of the cell by dramatically increasing the distance between electrodes.

Zaban et al. developed an ingenious approach to this experiment by splitting the photoanode lengthwise into two, electrically isolated halves.[4] One half is connected to the working electrode of a potentiostat and behaves as a normal photoanode. The other half is connected to the reference electrode. As the potentiostat prohibits current from flowing through the reference, this half of the photoanode is maintained (under illumination) at the cell's V_{oc} and acts as a reference. The drawback to this method is that conventional potentiostats do not output the potential of the auxiliary electrode. As a result, two separate current-voltage curves must be collected in sequence (one

incorporating the reference and one without it) and compared. Any dissimilarity between the shapes of the two iV curves indicates that an overpotential exists. Unfortunately, quantification of the overpotential is impossible with this method. In addition, two separate scans are required and it must be assumed that the cell behavior is the same for each scan. The benefits of this approach are that the thin sandwich cell configuration is maintained, standard electrochemical instrumentation is used, and only small amounts of mediator are required.

Experimental

Spacer experiments

Photoanodes were prepared according to a standard procedure. Fluorine-doped tin oxide (FTO) conducting glass was cleaned for >30 minutes in a base bath, rinsed with H_2O, distilled H_2O, and 95% ethanol, and dried under a stream of nitrogen. The titania colloid (obtained from Solaronix Co.) was spread using a doctor blade method and subsequently fired in an oven at 450 °C for at least 30 minutes. At this point, the photoanodes were allowed to slowly cool to room temperature (generally requiring 4-5 hours). Individual anodes were partitioned from the batch photoanode and were reheated to 450 °C before immersion in the N3 dye solution.

The Teflon® spacer was machined to the following dimensions: 25 mm X 13 mm X 3 mm. A 10 mm diameter circle was cut into the bottom half, running through the entire thickness of the spacer. Two enclosed 1.5 mm channels were bored from the top of the spacer down to the circle. Modification of the Teflon® surface was performed to promote surface adhesion of a plastic layer to both the front and the back side of the

spacer. The spacer was brought into an inert atmosphere glovebox and immersed in a solution of anthracene and sodium metal in THF for approximately 30 seconds. The previously white Teflon® spacer, surface now reduced, appeared dark brown. After drying, the spacer was removed from the glovebox, placed between two poly(ethylene) sheets and clamped between two glass microscope slides. The assembly was heated moderately with a heatgun until the plastic on both sides appeared smooth. The assembly was placed under a stream of water which both cooled the glass slides and disrupted any adhesion between the slides and the plastic. Once the excess poly(ethylene) was cut away, the laminated spacer was fitted with two 2" Teflon® plastic tubes, the opposite ends of which had been previously heat-sealed onto a dulled hypodermic needle. The tubing was inserted into the 1.5 mm channels (from the top) and glued into place with Torr Seal® two-part epoxy.

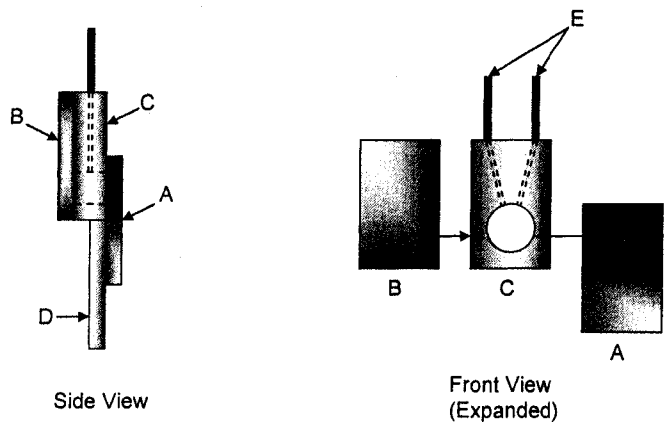

Figure 4. Diagram of the spacer experiment. A – Photoanode, B – Cathode, C – Spacer, D – FTO extension for anode, E – Teflon® tubes (needles not shown). Dotted lines represent features not visible on the surface.

Current-voltage experiments were performed as follows. An expanded DSSC was assembled by sandwiching the spacer between the photoanode and cathode. Once

clamped together, an enclosed chamber was created by the spacer between the photoanode and cathode that was only accessible by the 1.5 mm channels. An open syringe barrel was inserted onto one of the spacer needles. A second syringe (with plunger), filled with mediator solution, was inserted onto the other. Mediator solution was pumped through the cell carefully (so as to minimize the formation of air bubbles) until overflow was observed in the first syringe barrel. Finally, a reference electrode was placed into the overflow syringe.

Initially, data collection was performed according to the method of Meyer et al., using a variable resistor, amperometer, and two voltmeters (or one voltmeter used twice per resistor setting).[5] Later measurements, however, were taken with a more sophisticated, computer-integrated system that enabled faster data collection and digital output. The cell potential was controlled by a PAR Model 175 Universal Programmer in conjunction with a PAR Model 173 Potentiostat. Data was recorded by a computer equipped with a National Instruments PCI-6014 DAQ board, outfitted with a BNC-2110 connector block and controlled by a custom-designed Labview 6.1 software program. The potential of the photoanode relative to the reference ($E_{PA,ref}$) and the current were output from the potentiostat. The potential of the cathode was monitored by directly wiring the cathode to the BNC connector block. Although effective, the cathode potential is not directly controlled in the experiment and can reach voltages significantly greater than the maximum voltage tolerated by the data acquisition system. Consequently, the system is at some risk in this configuration – indeed, one input was ruined during the course of this experimentation.

Split photoanode experiments

Photoanodes were prepared as previously described (Chapter 3), utilizing the standard doctor blade technique. After baking at 450 °C and cooling to room temperature, a linear groove roughly bisecting the photoanode area was cut through the TiO_2 and FTO layers using a small grinding wheel mounted in a Dremel tool affixed to a solid support. The photoanode was then guided underneath the spinning Dremel tool in a fashion analogous to a wooden board being cut on a table saw. The height of the Dremel tool was carefully adjusted to yield a gap depth on the order of a few hundred microns. The resistance across the resulting gap was consistently greater than 350 MΩ. The photoanode was then either $TiCl_4$ treated (*vide infra*) or heated once again to 450 °C, cooled to ~120 °C, and immersed in N3 dye solution.

Later experiments also employed a "$TiCl_4$ treatment," which was performed after the photoanode was split. This treatment, modeled after a procedure developed by Barbé et al., consisted of the following procedure.[13] Once the photoanode had cooled, several drops of a 0.2 M solution of $TiCl_4$ in water were applied to the surface of the TiO_2 portion of the photoanode. The photoanode was then allowed to sit in a high relative humidity chamber for at least 12 hours. During this period, it was important that the solution on the anode surface not evaporate to dryness. Afterwards, the photoanode was rinsed with Millipore water, blown dry under a stream of N_2, and baked at 450 °C for 30 minutes.

A split extension for the photoanode was constructed using regular (i.e. not FTO or other conducting glass) and two strips of copper tape. The two strips were applied to

either side of the glass piece and, once clamped onto the photoanode, allowed for both halves of the photoanode to be connected to the potentiostat with alligator-type clips.

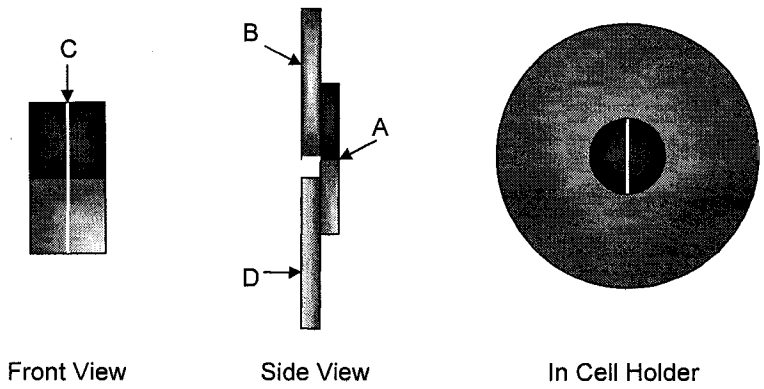

Figure 5. Three views of the split photoanode. Front View – split anode only. Side View – assembled with cathode and split FTO extension. In Cell Holder – illustrating the area under illumination, A – split anode, B – cathode, C – insulating gap, D – split FTO extension.

Initially, split photoanode experiments were conducted in the manner of Zaban et al., using a conventional potentiostat system with two output signals.[4] A PAR Model 173 potentiostat with a PAR Model 175 Universal Programmer was used in either two- or three-electrode mode to control the voltage across the cell. Current and voltage signals were recorded with a custom-designed Labview 6.1 software program using the same computer data acquisition system as previously described in "Spacer Experiments".

Later, current-voltage curves were measured using a locally constructed operational amplifier potentiostat circuit, designed to directly control the potential difference between the cathode and photoanode. The instrument was configured similarly to a conventional (albeit much simplified) potentiostat, save that the auxiliary electrode feedback loop consisted of a single 1000 Ohm resistor and did not include the reference electrode. The reference electrode potential was still monitored with a voltage

follower and referenced to instrument ground (see **Figure 6** for the complete wiring diagram). This allowed direct control of the potential across the cell (auxiliary versus working electrode) while still allowing for determination of electrode potentials versus the reference. A PAR Model 175 Universal Programmer was used to vary the potential across the cell (scan rate was 50 mV/s unless otherwise noted). Use of the same computer data acquisition system previously described in "Spacer Experiments" allowed photoanode potential ($E_{PA,ref}$), cathode potential ($E_{DC,ref}$), cell potential ($E_{cell} = E_{PA} - E_{DC}$), and current to be recorded simultaneously at all points throughout a single scan.

Some experiments also employed the use of thin (on the order of microns) spacers to keep electrical shorts to a minimum. As most experiments did not utilize a spacer, their use will be explicitly stated. Two different thicknesses (4 μm and ~25 μm) were used, each of which is described in detail in the experimental section of Chapter 3.

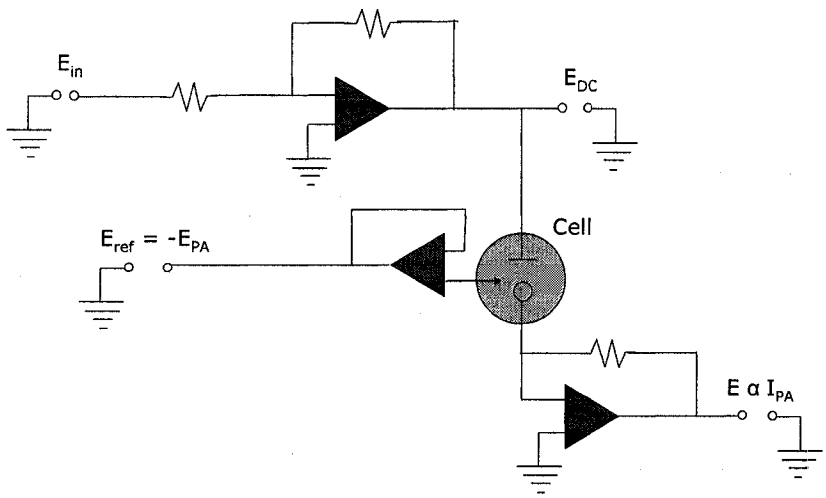

Figure 6. Schematic of custom-designed potentiostat circuit used for three electrode experiments. All resistors are 1000 Ohms. Note that the cell directly controls the potential of the cathode (T-shaped electrode in cell) versus the photoanode (circular electrode in cell); the latter electrode is held at instrument ground. The arrow electrode is the reference half of the photoanode.

Four electrode experiments

A variation of the split photoanode experiment was performed. In addition to a split photoanode, the gold counter electrode was also divided into two halves using a Dremel tool. Experiments were conducted exactly as with the split photoanode experiments previously described, but with one additional feature. The arrangement of the three electrodes used (working, reference, and auxiliary electrodes) could be easily altered, without cell disassembly, by simply changing the wiring of the cell. For example, the cathode half opposite the photoanode could be used as the auxiliary, creating a relatively efficient sandwich cell. Alternatively, the other cathode half (diagonally across from the photoanode) could be used to impose a massive solution resistance/mass transfer condition on the cell. Similarly, the location of the reference could be varied.

Osmium-complex cathode modification

FTO electrodes modified with dichloro-bis(4,4'-dicarboxylic acid-2,2'-bipyridine)osmium(II) were prepared by first soaking the FTO electrodes in a KOH-saturated isopropanol base bath for 20 minutes. The electrodes were then rinsed with tap water, de-ionized water, and 95% ethanol and dried under a nitrogen stream. The electrodes were placed in a solution of Alconox® in de-ionized water in an ultrasonic cleaner for 15 minutes, rinsed with millipore de-ionized water, and dried under a nitrogen stream. Next, the electrodes were soaked in electronics-grade isopropanol, placed in the ultrasonic cleaner for 15 minutes, and dried under a nitrogen stream. Finally, the electrodes were cleaned with an air plasma for 45 minutes. Osmium modification of the

patterned electrodes was accomplished by placing them in a solution of dichloro-bis(4,4'-dicarboxylic acid-2,2'-bipyridine)osmium(II) in absolute ethanol. The Petri dish containing the electrodes and osmium complex was sealed with parafilm, wrapped in aluminum foil, and agitated overnight on a Lab-Line Maxi Rotator 4631. The osmium-modified electrodes were then rinsed with absolute ethanol and dried under a nitrogen stream.

Unmodified FTO electrodes underwent a cleaning procedure identical to the osmium-modified electrodes.

Mediator solutions

Cobalt complexes and mediator solutions were prepared as described previously (Chapter 3), except in a limited number of cases. Where specified, the desired ratio of oxidized-to-reduced mediator was achieved through the stoichiometric addition of an oxidizing agent ($NOBF_4$) to the mediator solution. In all other cases, it may be assumed that the ratio of oxidized-to-reduced mediator was determined using previously bulk oxidized cobalt(III) complex (as described in Chapter 3).

Glassy carbon counter electrodes

The counter electrode, purchased from Alfa Aesar, was 3 mm thick, Type 2 glassy carbon, cut into an rectangle of approximately 1 cm by 2 cm. Immediately prior to each use, the electrode was polished on 600-C grit sandpaper (lending a dull, obvious scratched appearance to the previously glassy carbon surface). Performances of thusly polished carbon electrodes were found to be improved over either unpolished glassy

carbon (dramatically worse) or alumina polished glassy carbon (still retaining a glassy appearance). When assembled in DSSCs, an insulating plastic spacer (~1mm thickness) was placed on the back side of the electrode (between the sandwich cell and the clamp of the cell holder) to prevent shorting of the cell to the cell holder and did not affect cell performance in any other way.

Development of the Three Electrode Experiment

Spacer experiments

Three electrode experiments were conducted utilizing the previously described Teflon® spacer between the electrodes and mediated by the I^-/I_3^- redox couple in an effort to reproduce previously published results.[5] Initially, the experiment was performed as described by Meyer et al., with cell potential being controlled through the manual adjustment of a variable resistor connecting the cathode and photoanode. Although this method worked, data collection was slow. Consequently, a computer-controlled system was devised which dramatically decreased the time required to perform the experiment while yielding significantly more data points.

The resulting data are shown in **Figure 7**. These data are in good agreement with the results of Meyer et al. and indicate that the experiment was functioning properly. As can be seen, the cathode potential ($E_{DC,ref}$) is roughly constant while the photoanode potential steadily decreases (becomes more negative) as the cell potential increases. Iodide is therefore behaving well as a mediator in these cells. It is apparent, however, that $E_{DC,ref}$ is not *perfectly* constant, being considerably more negative (by ~150 mV) at short circuit than at open circuit (E_{cell} = 671 mV), indicating that an overpotential exists.

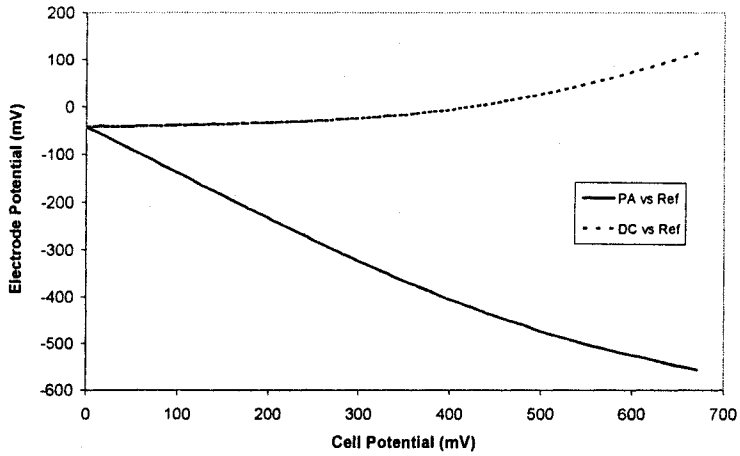

Figure 7. Results of a three electrode experiment performed using the Teflon spacer. In addition to the spacer, the cell consisted of a platinum cathode and a N3-dyed photoanode. The mediator comprised 100 mM LiI and 25 mM I_2 in acetonitrile.

Considering the increased thickness of the cell with a spacer (3 mm), this is likely due to a mass transfer limitation within the cell.

Further investigation with spacers in the cell was discontinued for several reasons. Firstly, the increased thickness of the cell is obviously a poor simulator of typical sandwich cell conditions and almost certainly contributes to a mass transfer limitation within the cell.[4] Even worse, preliminary experiments performed by our collaborators in Italy indicated that the solution resistance of such a large cell was likely to be considerably greater for cobalt-based mediators than with I^-/I_3^-.[14] Secondly, the experiment requires large volumes of mediator which would have been practically prohibitive for many of our cobalt-based mediators which are synthesized in-house on relatively small scales.

Split photoanode experiments

The split photoanode approach developed by Zaban et al., was adopted for its crucial advantage: the sandwich cell configuration is maintained. This allows for a realistic distance between electrodes and drastically smaller volumes of mediator to be used.[4] However, while data collection was considerably easier than with the spacer experiment, interpretation of data was problematic, as electrode potentials were not recorded directly and therefore had to be inferred from iV curve shape (explained below). The experimental procedure was as follows. A iV experiment was performed with the potentiostat in two-electrode mode followed by a iV experiment in three-electrode mode. The two-electrode mode of a potentiostat is attained by shorting the reference and auxiliary electrode wires together. In this mode, the potentiostat behaves like a sourcemeter and simply biases the working electrode against the auxiliary electrode (which is also acting as the reference electrode). Conducting the experiment in two-electrode mode was equivalent to conducting a standard iV light experiment. In three-electode mode, the reference wire of the potentiostat was connected to the non-operational side of the photoanode and the instrument behaved as a typical potentiostat. After adjusting for the difference in reference electrode potential, the two iV curves were compared. Any difference in shape between the two- and three-electrode mode curves indicates that an overpotential exists at the cathode (*vide infra*).

Zaban et al. found that with I^-/I_3^-, the two electrode mode consistently yielded lower photocurrents throughout the scan, a phenomenon which they attributed to "a negative shift of the counter electrode with respect to the open circuit conditions."[4] Although this explanation is likely valid when comparing a poor cathode to a better

cathode, it is difficult to understand why a change in reference potential should affect the maximum current deliverable by the DSSC. However, it is logical that an overpotential at the cathode should affect the FF (i.e., the shape of the iV curve) observed between two- and three-electrode modes. *The reason for this is that the three-electrode curve is a plot of current vs. photoanode potential rather than cell potential.* The opposite is true in the case of the two-electrode curve (i.e., the standard two-electrode iV curve is a plot of current vs. cell potential).

The fact that 2- and 3-electrode mode iV curves utilize two different potentials for their x-axis is directly responsible for the differing iV curve shapes (when overpotentials are present at the cathode). If a cathodic overpotential is required to pass current, then any change in cell potential that is accompanied by a change in current will result in a change in the potential of *both* electrodes. Consequently, for a given change in current, the photoanode will experience a potential change that is *less* than the change in E_{cell}. This effect will only be manifested in regions where a change in E_{cell} results in a change in current and will be most dramatic at voltages close to open circuit. In these regions, larger current gains with smaller potential changes will result in better FFs. Hence, three-electrode mode iV curves are predicted to have better FFs than two-electrode mode curves in DSSCs where cathodic overpotentials are present, with the magnitude of the difference being roughly proportional to the size of the overpotential.

The results of a split photoanode experiment with iodide are shown in **Figure 8**. Once the potential axis of the three-electrode curve is shifted arbitrarily to allow for easy visual inspection, it can be seen that the three-electrode curve displays a slightly higher current between 150 and 400 mV. The difference is extremely small, however, indicating

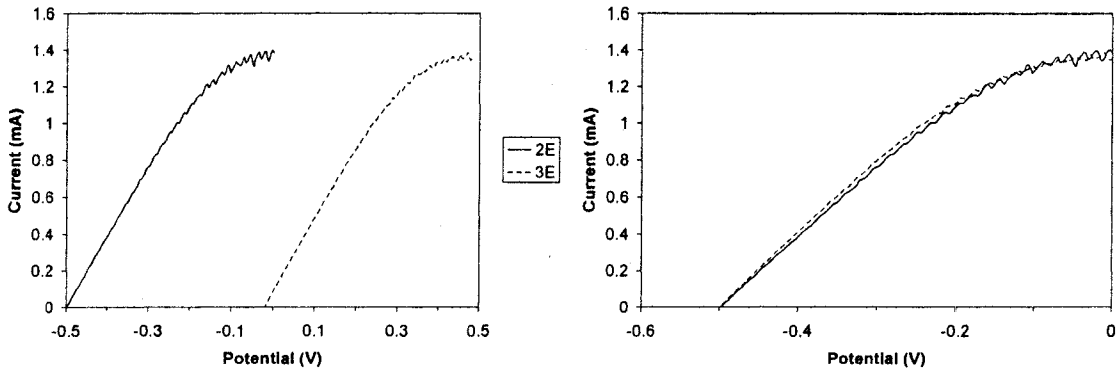

Figure 8. Results of a three electrode experiment using a split photoanode and a standard potentiostat: (left) the original iV curves as collected, (right) the three electrode curve has been shifted so that the two open circuit potentials match. The cell consisted of a platinum cathode and a N3-dyed photoanode with a TiO_2 layer of "2 scotch" thickness (~6 μm) and a compact TiO_2 underlayer. The mediator comprised 0.5 M LiI and 0.05 M I_2 in γ-butyrolactone. No spacers of any kind were used in this experiment.

that the overpotential at the platinum cathode is negligible for all practical purposes. *Note that currents rather than current densities are reported. The location of the insulating gap within the illuminated area (see* ***Figure 5****) was not possible to reliably control;* ergo *the area of the photoanode was not constant nor easily calculated. Accordingly, all split photoanode iV curves will be displayed with current (unadjusted for area) and comparison of currents between different cells is generally not possible.*

At this point, a new instrumental setup was designed which would both simplify the operation of the experiment as well as yield quantitative information about the magnitude of any overpotentials present on the cathode. The computer-integrated data collection system developed for the spacer experiment was implemented so that data could be plotted in the same manner and quantitative values for η could be realized. The customized potentiostat circuit shown in **Figure 6** was utilized. The primary motivation for the new apparatus was to eliminate any possibility that instrumental complexity was complicating the experiment in some unforeseen way. However, an added benefit of the

new potentiostat circuit was that the cell potential could be directly controlled – as opposed to before when some amount of calculation was required to ensure that the potential scan (of $E_{PA,ref}$) encompassed the proper range of potentials for E_{cell} – which made performing the experiment faster and more facile.

In order to evaluate the new instrumental setup, an overpotential at the cathode was simulated by introducing a variable resistor into the circuit. The resistor was placed in series between the cathode and the potentiostat. Increasing the resistance results in an increasing potential drop across the resistor (at a given current) and should mimick the effects of either η_{CT} or η_{MT}. In addition to confirming the design of the new instrument, this experiment provided insight into how cathodic overpotentials would affect cell performance. **Figure 9** (left) shows how the iV curve was affected by added resistance. The FF was affected most dramatically, although short circuit current (I_{sc}) was also lowered somewhat. **Figure 9** (right) displays the behavior of the electrode potentials during the iV scans. Added resistance resulted in a potential drop at short circuit (y-intercept) as compared to open circuit (E_{cell} = 456 mV). In accordance with Ohm's Law, the potential drop doubled when the resistance doubled. Also of note, the greatest changes in cathode potential occurred in the regions of greatest current change. As expected, the electrode potentials at V_{oc} were unchanged by added resistance. Although none of these observations are surprising, the experiment was helpful in confirming that the instrument was functioning properly.

One surprising phenomenon was noticed, however, during the course of these (and other) experiments. It was found that the x-intercept of the $E_{PA,ref}$ curve (corresponding to V_{oc} of the cell) did not always correlate with the V_{oc} as measured in the

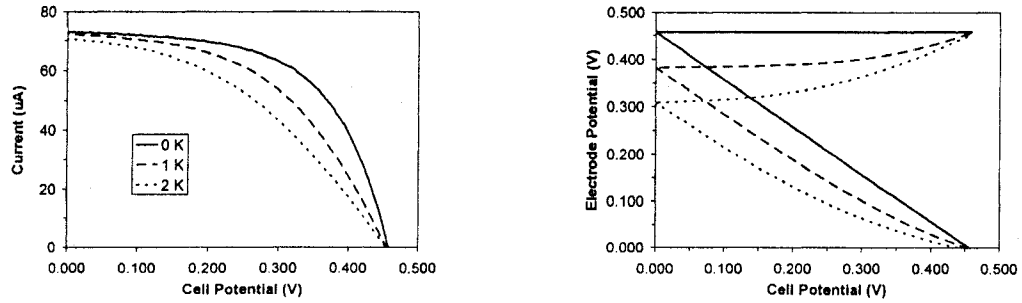

Figure 9. Results of added resistance (1 kΩ and 2 kΩ) on cell performance. A gold cathode and a two week old (note the low currents) N3-dyed photoanode were used. The mediator solution comprised 0.15 M cobalt complex (10% oxidized by $NOBF_4$), 0.2 M lithium triflate, 0.2 M TBP.

iV experiment. This unexpected behavior was subsequently explained when a voltage difference was measured between the reference and photoanode halves of the DSSC (using a voltmeter while the cell was under illumination), indicating that V_{oc} was not the same for each half. Subsequent investigations indicated that the inhomogeneity of the incident light beam was responsible. The beam was not collimated nor defocused in any way, resulting in an uneven distribution in light power across the illuminated area. Localized "hot spots" existed and resulted in a slightly increased V_{oc} (generally only higher by 30 mV or less). As a test, the split cell was rotated such that the two halves of the anode were exposed to different parts of the light beam. A concurrent shift in V_{oc} was observed with each change in orientation, confirming the existence of local hot spots.

If the reference and photoanode open circuit potentials are not identical, the x-intercept of the $E_{PA,ref}$ curve (vs. E_{cell}) no longer corresponds to V_{oc} for the cell. Although not a significant problem, compensation for this effect was desired for ease of interpretation and so that comparisons could be made between cells. Accordingly, all plots of electrode potential versus cell potential have had their y-axis shifted so that the x-intercept matches V_{oc} for the photoanode. Effectively, this shift simply means that all

electrode potentials are versus the open circuit potential of the photoanode half and not that of the reference half. Validating this claim is that the magnitude of the vertical axis shift corresponds to the potential difference measured between the two halves at open circuit (in cases where this potential was measured). In fact, initially the y-axis was always shifted by the measured value, but it was soon realized that the V_{oc} of the iV curve was consistently identical (without exception) to the x-intercept of the electrode potential curve after the y-axis shift. Hence, for all curves shown here, the y-axes were simply shifted by an amount corresponding to difference in V_{oc} values (i.e. the difference in potentials was not measured) so that the x-intercepts matched.

A variation on the split photoanode experiment (as described above) was designed with the intent of ascertaining the extent to which a mass transfer overpotential would affect the measured cathode potential. The cathode was also divided in half (electrically), resulting in a sandwich cell with four electrodes. This "four electrode experiment" allowed standard split photoanode experiments (using only three of the four electrodes) to be conducted with several different electrode arrangements. The idea behind the experiment was to artificially impose a mass transfer condition on the cell and monitor the response, thereby testing the system in a new but analogous fashion as the variable resistor test.

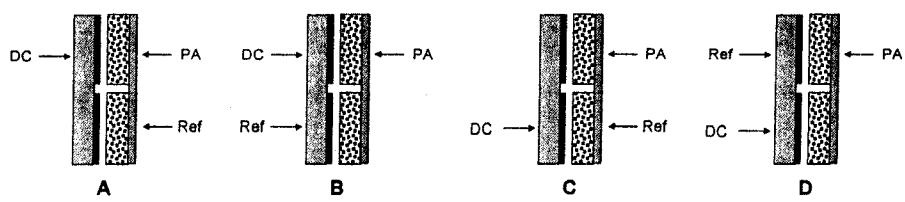

Figure 10. Four possible electrode configurations for a four electrode DSSC (not to scale).

The three configurations tested are shown pictorially in **Figure 10**. Arrangement **A** results in a relatively efficient DSSC with minimal mass transfer effects. The reference electrode is the other half of the photoanode, making this situation basically identical to that of the "standard" split photoanode (with regular cathode) experiment just presented. Arrangement **B** is similar but the location of the reference has been switched to the gold electrode not being used as a cathode. Arrangements **C** and **D** have serious mass transfer/solution resistance problems between the anode and cathode. The difference between the two arrangements is in the location of the reference. In Arrangement **C**, the reference is once again the other half of the photoanode. In Arrangement **D**, the reference has been switched to be the other half of the gold cathode. Although the potential of this reference is not identical to that of the photoanode reference, it should still be constant throughout the experiment which is all that is required. After adjusting for the different reference potential (by shifting the y-axis so that the x-intercepts match) comparisons between experiments conducted in any of the arrangements can be readily made.

A series of experiments were conducted on a single four electrode DSSC, wired in each of the arrangements described. The cell was not disassembled in any way between each wiring configuration, and care was taken to disturb the cell as little as possible during the rewiring. The results are shown in **Figure 11**. It is immediately apparent that mass transfer/solution resistance effects are severely hampering the cell when the cathode and photoanode are not directly opposite each other (Arrangements **C** and **D**). It can also

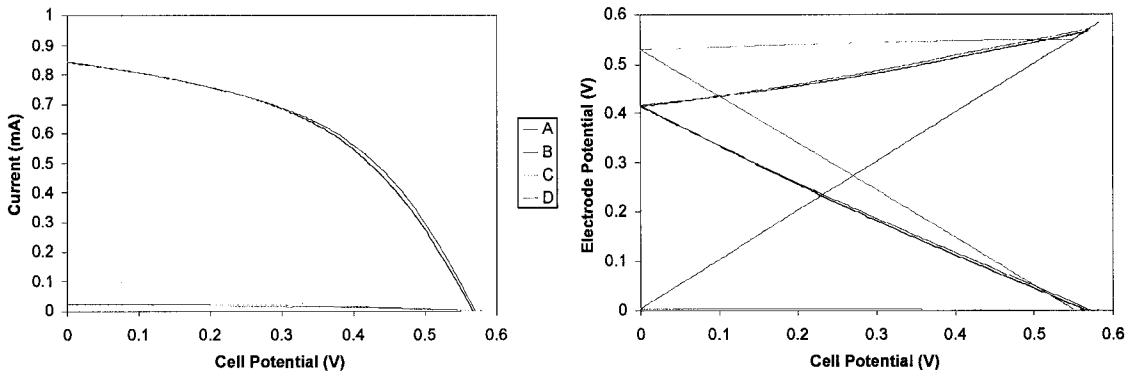

Figure 11. Results of four electrode experiments with a split gold cathode and a split N3-dyed photoanode. Plot titles refer to the arrangements as described in the text. A 4 μm spacer was employed. The mediator solution was composed of 0.15 M total cobalt complex, 10% cobalt(III), 0.2 M lithium triflate and 0.2 M TBP.

be seen that the location of the reference makes little difference when the current-carrying electrodes are opposite (Arrangements **A** and **B**).

Interestingly, when the current-carrying electrodes are not directly opposite, the location of the reference impacts the observed electrode behavior to very large degree. The likely reason for this is that, in Arrangements **C** and **D**, the location of the reference drastically changes which electrode is nearest the reference. Electrodes opposite the reference are significantly closer than those on the same side of the cell. As solution resistance may be modeled as a resistor across the cell from anode to cathode (see **Figure 12**), it makes sense that the potential drop across the resistor depends on where along the resistor the measurement is made (in a manner analogous to the way a simple variable resistor operates). In Arrangement **C**, the reference is very close to the cathode and little potential drop (overpotential) is registered. In Arrangement **D**, however, there is a large difference in potential between the cathode and the reference as the reference is much closer to the photoanode (i.e. significantly more solution resistance lies between the reference and the cathode).

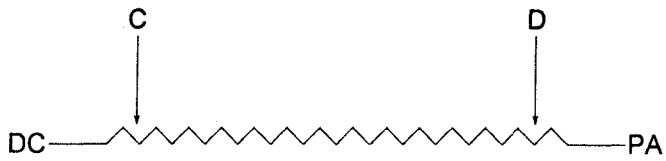

Figure 12. Representation of effect of reference placement in a system with significant solution resistance. Arrow **C** models Arrangement **C**, Arrow **D** likewise models Arrangement **D**.

Unfortunately, it is not clear how useful the results of these experiments are. In the case of large solution resistance, reference electrode placement is clearly important. Yet the standard three electrode split photoanode experiment places the cathode directly opposite the photoanode – an arrangement that results in very little solution resistance. Perhaps noteworthy is the observation that the cathode is *also* directly opposite the reference in a standard split photoanode experiment, meaning that the reference is closer to the cathode than the photoanode. On the other hand, neither η_{CT} nor η_{MT} can be modeled as a resistor across the cell, so the location of the reference should not impact the ability of the system to measure overpotentials.

Results/Discussion

Reproducibility test

The principle reason for designing a three electrode experiments was to ascertain the effect of overpotentials at the cathode on cell performance. To do this, comparisons were needed between DSSCs with various types of cathodes and various cell thicknesses. Unlike comparisons between differing mediator solutions, the cells would have to be disassembled and reassembled in order to change the conditions (cathode, thickness of

spacer, etc...). Unfortunately, it has been our observation that cell behavior typically changes somewhat every time the cell is reassembled. A reproducibility test was performed to gauge the magnitude of this effect.

Figure 13 (left) shows the iV curves from split photoanode experiments performed with identical conditions. The same photoanode, cathode, and cobalt mediator solution were used for each curve, although a new spacer was used with each assembly (all were 4 μm in thickness and all were cut from the same original sheet of polyester – ostensibility lending greater confidence that all spacers were the same thickness). With each disassembly, the photoanode and cathode were rinsed with acetonitrile and dried with GUST dusting spray. The DSSC was assembled and a new drop of the same cobalt mediator solution was applied and wicked into the cell. The location of the insulating gap within the aperture (determining the relative areas of the photoanode and reference halves) was reproduced as closely as possible, with the area of the photoanode occupying approximately two-thirds of the total aperture and the reference occupying the remainder.

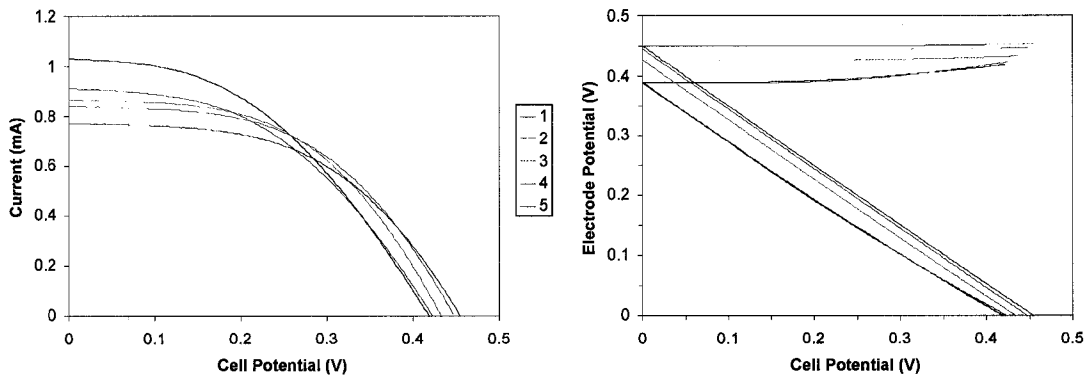

Figure 13. Results of a series of five assemblies with a single photoanode and a gold cathode. The mediator solution was 0.15 M total cobalt complex (20% cobalt(III)), 0.2 M lithium triflate without any TBP. A 4 μm spacer was employed.

As can be seen, V_{oc} and I_{sc} changed over time in a manner consistent with the changes observed in the two electrode, flow-through experiments (Chapter 3), i.e. V_{oc} increased after two assemblies and I_{sc} probably decreased (an approximation, as changes due to varied areas of illumination are certainly also present). **Figure 13** (right) shows the behavior of the electrodes during each scan. Initially, significant (~30 mV) overpotentials occurred at short circuit (E_{cell} = 0 mV) and then decreased after two assemblies to smaller drops of ~5 mV. Oddly, no such change in overpotential was observed in the experiments which are described in the following. Consequently, it is difficult to lend much weight to this trend.

Cell thickness survey

A series of split photoanode experiments was conducted on cobalt-mediated DSSCs of varying thicknesses. The intent was to gauge the extent to which mass transfer effects alter cell behavior, with the assumption that mass transfer overpotentials would be larger for DSSCs with thicker spacers (see Chapter 3). Representative results are shown in **Figure 14.** The open circuit voltage is similar for the first two assemblies (as expected), but rather than increasing with the third assembly, V_{oc} declines somewhat. This contradicts the baseline V_{oc} shift expected from the reproducibility studies described above, but can perhaps be explained by the fact that no spacer was used in this assembly. Accordingly, electrical shorts – occurring at points of contact between the two electrodes – may have existed and could have served to lower V_{oc}.

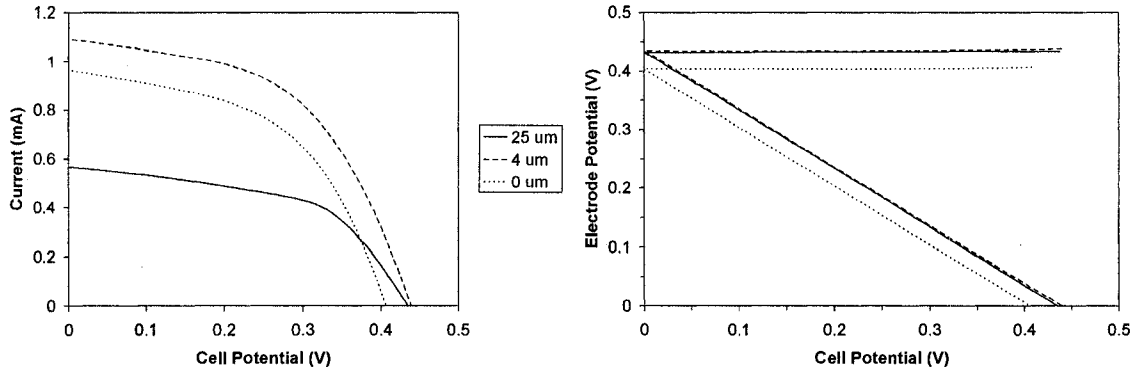

Figure 14. Typical results when the spacer thickness is varied. A gold cathode was used. The mediator solution was 0.15 M total cobalt complex (20% cobalt(III)), 0.2 M lithium triflate without any TBP.

The lower current passed with the 25 μm spacer is worthy of note. Several surveys were performed (with Au and Pt counter electrodes, with and without $TiCl_4$ treatment) and significantly lower currents (generally about half of thinner cells) were consistently observed with the 25 μm spacer. Although the photoanode area was not strictly controlled, it was kept very similar (and certainly was never half of the normal area). In addition, were the phenomenon due to unintentional variations in anode area, it would not have always occurred – which it did. The logical conclusion is that the 25 μm spacer lowers the photocurrent, due most likely to increased mass transfer problems or solution resistance. Consequently, one would expect to see a mass transfer overpotential in the cell. Oddly, no such overpotential was observed (**Figure 12**, right). In all three cases, the potential at short circuit was only 2-3 mV less than at open circuit. This confusing result is particularly difficult to explain and warrants further discussion (*vide infra*).

Cathode surveys

The performances of four different cathode materials in cobalt-mediated DSSCs were evaluated with a series of split photoanode experiments. The survey was conducted twice, with a different photoanode for each survey. A 4 μm spacer was employed and the cells were disassembled and reassembled as before. The iV curves are shown in **Figure 15** (left). In addition to the expected increase of V_{oc} with each cell assembly, it can be seen that the platinum counter has a notably worse FF. Glassy carbon and gold have similarly shaped profiles and FTO is, as expected, terrible. Looking at the plot of the electrode potentials (**Figure 15**, right), only the FTO electrode has significantly alter behavior. The overpotentials at short circuit are 4, 3, 0, and 191 mV for gold, platinum, carbon, and FTO cathodes, respectively. Considering that in the simulated overpotential experiment (*vide supra*), a decrease in FF was observed in conjunction with a significant overpotential at the cathode (~150 mV per 1 kΩ added resistance), it is surprising that no overpotential was observed with the Pt cathode and its significantly worse FF.

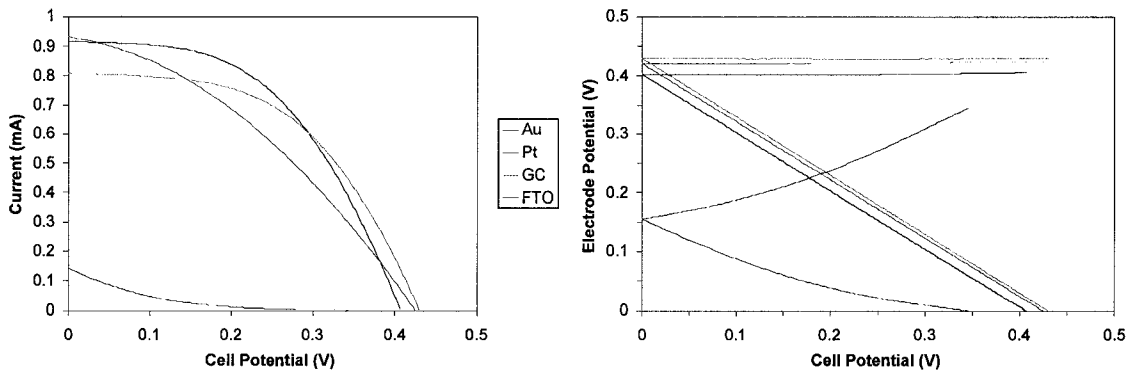

Figure 15. Results of the cathode survey with cobalt mediator. A 4 μm spacer was employed. The mediator solution was 0.15 M total cobalt complex (20% cobalt(III)), 0.2 M lithium triflate without any TBP.

The glassy carbon cathode behaved very similarly to gold. In standard two electrode iV experiments (of controlled area), the carbon cathode resulted in light iV curves of qualitatively very similar shape but less current (by approximately 10%, **Figure 16**). This effect (also seen in carbon cathode DSSCs mediated by iodide, *vide infra*) is attributed to a lack of back-reflected light in these cells due to the much higher light absorbance by the black carbon electrode rather than suboptimal electrode transfer kinetics at the carbon surface.

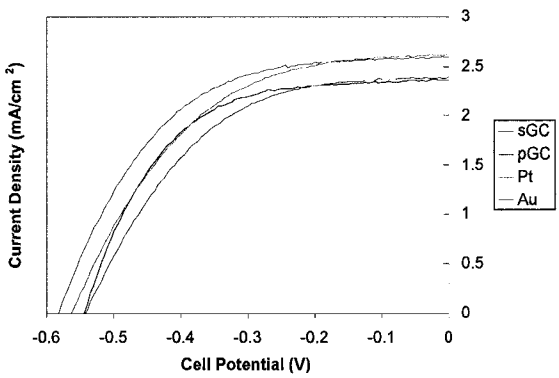

Figure 16. Results of a two electrode cathode survey with cobalt mediator. Two different glassy carbon electrodes were used, one sanded with 600-C grit sandpaper (sGC) and the other polished with alumina powder (pGC) immediately before use. A 4 μm spacer was employed. The mediator solution was a three day old 0.15 M total cobalt complex (20% cobalt(III)), 0.2 M lithium triflate with TBP added that day.

A brief cathode survey was also conducted on DSSCs mediated with I^-/I_3^-. Typically, only platinum cathodes are used with iodide as very few other conductors exhibit sufficient electron transfer kinetics for the reduction of I_3^- and are stable in the presence of I_2. Nevertheless, comparisons between iodide and cobalt mediators were desired and so a brief cathode survey was conducted on Pt, glassy carbon, and FTO cathodes. The glassy carbon electrode – fabricated for the cobalt studies – was included in the survey as a few studies have shown carbon to be a potentially useful cathode

material in DSSCs. The experiments were conducted as with the cobalt mediators; the results are shown in **Figure 17**. Platinum and glassy carbon counter electrodes performed very well, exhibiting low cathodic overpotentials. FTO, on the other hand, proved to be an almost ideal "worst case scenario" for reduction of I_3^-, with basically all of the potential change during the scan associated with the change in potential of the cathode (~346 mV overpotential).

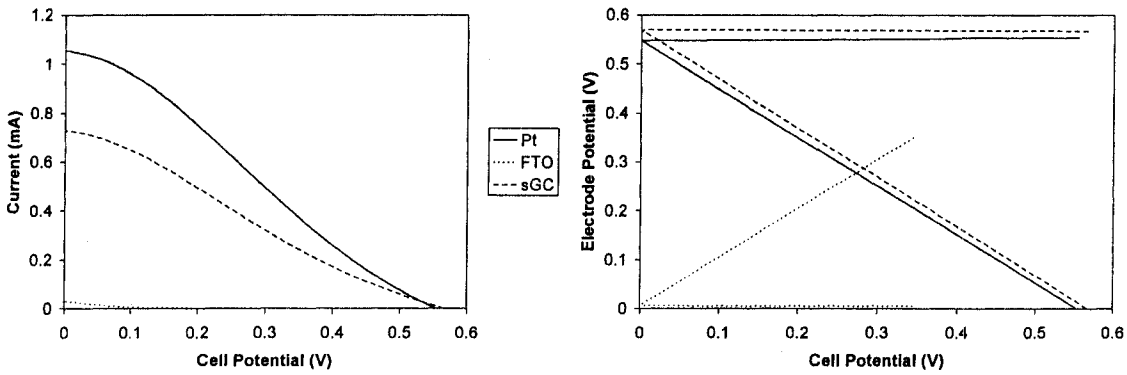

Figure 17. Results of the cathode survey with iodide mediator. A 4 μm spacer was employed. The mediator solution was 0.15 M LiI, 0.015 M I_2 (resulting in 10% oxidized), 0.05 M lithium triflate without any TBP.

Osmium-modified cathodes

In research conducted by group members other than myself, it has been discovered that FTO or ITO (indium/tin oxide transparent conducting glass) electrodes become catalytic towards the oxidation and/or reduction of tris(bipyridine) cobalt complexes when their surfaces are modified by certain transition metal coordination complexes.[15-17] This effect has been exploited to develop transparent cathodes for use in cobalt-mediated DSSCs, either singly or in optical tandem (i.e. stacked).[17] Stacked cells provide the opportunity to increase photocurrent through decreased electron diffusion

pathlength as well as through increased light absorption due to the use of two spectrally-complimentary, dyed photoanodes.

Osmium bipyridine complexes possess a reduction potential sufficiently negative so as to be capable of reducing cobalt(III) bipyridine complexes, even when adsorbed onto the surface of FTO glass (approximately as a monolayer). Such osmium-modified cathodes appear to function well in cobalt-mediated DSSCs. The split photoanode experiment was conducted in order to more quantitatively evaluate their performance. Experiments were performed on a single photoanode, disassembled and reassembled as before – except that less effort was made to reproduce the relative areas of the reference and photoanode with each assembly. **Figure 18** (left) displays representative iV curves of cells with gold, osmium-modifed, and regular FTO cathodes incorporating a 4 μm spacer. As before, unmodified FTO yields very little current. After osmium modification, however, the cell yields currents very comparable to that of cells with gold. It can be seen that the fill factor was slightly worse with the osmium-modified cathode, a feature which was repeatedly observed. **Figure 18** (right) shows the electrode behavior throughout the course of each scan. The gold cathode required very little overpotential (<1 mV), whereas the osmium-modified cathode displayed a slight overpotential of 10 mV. The difference in FF observed between gold and osmium-modified cathode iV curves would lead one to expect η to be greater for the latter cathode, but considering the range of overpotentials commonly observed for a single cathode material, it is difficult to say if an overpotential of 10 mV is experimentally significant in this case. Of course, the difference in behavior between modified and unmodified FTO is quite striking, underscoring the dramatic surface dependence of cobalt bipyridine complexes.

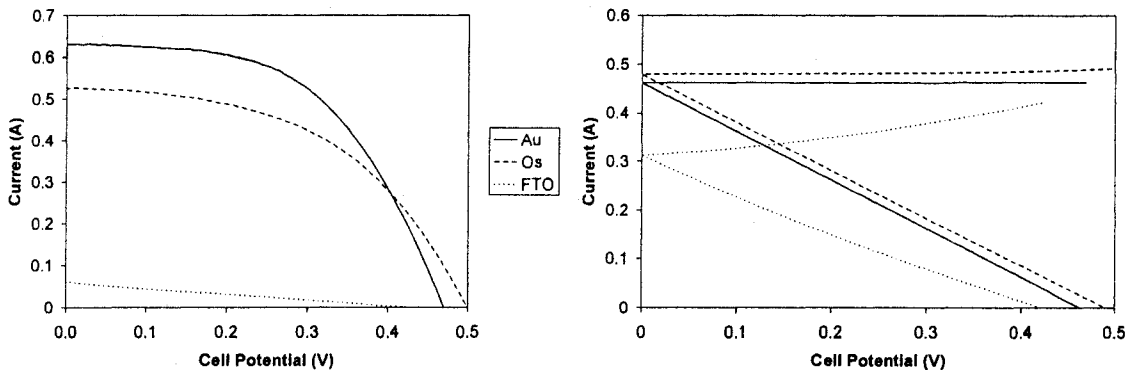

Figure 18. Results of a cathode survey including an osmium-modified FTO cathode. A 4 μm spacer was employed. The mediator solution was 0.2 M cobalt complex (10% oxidized by $NOBF_4$), 0.2 M lithium triflate and 0.2 M TBP.

Conclusions

A novel three electrode DSSC experiment, modified from two existing approaches, was devised and implemented in order to study cathode behavior in cobalt-mediated DSSCs. The new experiment incorporates a split photoanode in conjunction with a customized potentiostat circuit and allows for simultaneous monitoring of cathode potential, photoanode potential and cell current while maintaining the thin electrode separation of the standard sandwich cell configuration. Extensive testing of the system was conducted (with alternative four electrode geometries, utilizing resistors to simulate overpotentials as well as by selection of cathodes known to have both slow and fast heterogenous electron transfer kinetics) and the results were in good agreement with theoretical predictions (presented in the introduction). Once deemed to be functioning properly, the new technique was used in a systematic study of cobalt mediator behavior in DSSCs with different cathode materials and variable spacer thicknesses.

Unfortunately, the impact of this study is uncertain, due primarily to two surprising observations. Firstly, a clear trend was observed where 25 μm spacers lowered currents in the cells, almost certainly due to mass transfer limitations imposed by the greater distance between electrodes. Surprisingly, however, no significant overpotential was observed on the cathode. Secondly, platinum cathodes consistently performed worse in cobalt-mediated DSSCs, evidenced primarily by a decreased fill factor. As slower electron transfer kinetics are almost surely to blame, it was again surprising that no overpotential was measured on the cathode. Given these two observations, it would appear that the three electrode experiment is incapable of detecting either mass transfer or charge transfer overpotentials (η_{MT} or η_{CT}, respectively), except in cases where η_{CT} is extremely large, such as with FTO cathodes.

Any explanation for this apparent failure of the three electrode experiment must lie in one of two categories: either the experiment is incapable of detecting subtle overpotentials or the aforementioned phenomena occur without a corresponding change in cathode potential. All things considered, each conclusion would be completely unexpected and, accordingly, both warrant further discussion.

Experimental flaws

Considering the success of the control experiments, coupled with the fact that overpotentials can be reliably observed on FTO cathodes, it seems unlikely that the three electrode apparatus is not functioning properly. Extensive effort was made to preclude easy-to-overlook sources of error, such as improper grounding or poor electrical connections. The use of a custom-made, simplified potentiostat circuit not only allowed

for straightforward control of cell potential but was also intended to reduce the chance of any unexpected quirk in the circuitry of a conventional potentiostat/galvanostat (e.g., PAR 173) from interfering with the experiment in some unforeseen way. Therefore, considering the care with which this much-simplified instrument has been examined and utilized, the only possible problem with the experiment must be in its *design*. In particular, the arrangement of the electrodes within the electrochemical cell (in this case, within the DSSC) could be a source of error.

In any sort of electrochemical experiment, the location of the reference electrode is of utmost importance.[9] As observed with the four electrode experiments, the location of the reference drastically impacted the measured cathode behavior. Specifically, it was confirmed that the reference electrode is much closer to the surface opposite than to the surface laterally proximal (i.e., the surface on the same electrode but on the other side of the insulating gap). In the case of the normal three electrode setup, this fact means that the reference electrode is significantly closer to the dark cathode than to the photoanode. However, it is difficult to understand what sort of influence this arrangement should have. As the photoanode is also directly opposite the cathode, no significant solution resistance is expected as the distance across the cell is very small (4 μm across the spacer plus ca. 4 μm through the titania layer). Accordingly, the variable resistor arguments presented in the case of the four electrode experiments should not apply. In addition, the fact that overpotentials are observable (in the case of FTO) strongly suggests that the cell geometry is not fundamentally flawed.

Unusual electrochemistry

The second possibility is that neither mass transfer nor charge transfer overpotentials of any significant size occur in cobalt-mediated DSSCs, even with large spacers or suboptimal cathode materials. Although this result runs counter to standard Butler-Volmer type theories of electrochemical behavior, in the absence of any design flaws in the experiment (an assumption, for now), there is no other option.

Unsurprisingly, rationalizing how mass transfer and charge transfer resistances may exist without corresponding overpotentials is not a simple task. Despite significant effort, few reasonable hypotheses have been found. As will be discussed in the next chapter, it may be that surprisingly small overpotentials strongly affect cell performance yet are too small to be reliably detected by the split photoanode experiment. This explanation is still not completely satisfactory, but for the moment is about all that can be said. Clearly, an answer exists, but finding it will require further research, creativity, and time.

Bibliography

1. Grätzel, M., Perspectives for dye-sensitized nanocrystalline solar cells. *Prog. Photovoltaics* **2000,** 8, (1), 171-185.

2. Cahen, D.; Hodes, G.; Grätzel, M.; Guillemoles, J. F.; Riess, I., Nature of Photovoltaic Action in Dye-Sensitized Solar Cells. *Journal of Physical Chemistry B* **2000,** 104, 2053-2059.

3. Ellingson, R. J.; Asbury, J. B.; Ferrere, S.; Ghosh, H. N.; Sprague, J. R.; Lian, T. Q.; Nozik, A. J., Dynamics of Electron Injection in Nanocrystalline Titanium Dioxide Films Sensitized with [Ru(4,4'-dicarboxy-2,2'-bipyridine)$_2$(NCS)$_2$] by Infrared Transient Absorption. *Journal of Physical Chemistry B* **1998,** 102, 6455-6458.

4. Zaban, A.; Zhang, J.; Diamont, Y.; Melemed, O.; Bisquert, J., Internal Reference Electrode in Dye-sensitized Solar Cells for Three-Electrode Electrochemical Characterizations. *Journal of Physical Chemistry B* **2003,** 107, 6022-6025.

5. Oskam, G.; Bergeron, B. V.; Meyer, G. J.; Searson, P. C., Pseudohalogens for Dye-Sensitized TiO_2 Photoelectrochemical Cells. *Journal of Physical Chemistry B* **2001,** 105, 6867-6873.

6. Bisquert, J.; Cahen, D.; Hodes, G.; Rühle, S.; Zaban, A., Physical Chemical Principles of Photovoltaic Conversion with Nanoparticulate, Mesoporous Dye-Sensitized Solar Cells. *Journal of Physical Chemistry B* **2004,** 108, 8106-8118.

7. Zaban, A.; Greenshtein, M.; Bisquert, J., Determination of the Electron Lifetime in Nanocrystalline Dye Solar Cells by Open-Circuit Voltage Decay Measurements. *ChemPhysChem* **2003,** 4, 859-868.

8. Bisquert, J.; Zaban, A.; Greenshtein, M.; Mora-Seró, I., Determination of Rate Constants for Charge Transfer and the Distribution of Semiconductor and Electrolyte Electronic Energy Levels in Dye-Sensitized Solar Cells by Open-Circuit Photovoltage Decay Method. *Journal of the American Chemical Society* **2004,** 126, 13550-13559.

9. Bard, A. J.; Faulkner, L. R., *Electrochemical Methods : fundamentals and applications*. 2nd ed. ed.; John Wiley & Sons, Inc.: 2001.

10. Yan, S. G.; Hupp, J. T., Energetics of Electron Transfer at the Nanocrystalline Titanium Dioxide Semiconductor/Aqueous Solution Interface: pH Invariance of the Metal-Based Formal Potential of a Representative Surface-Attached Dye Couple. *Journal of Physical Chemistry B* **1997,** 101, 1493-1495.

11. Kamat, P. V.; Bedja, I.; Hotchandani, S.; Patterson, L. K., Photosensitization of Nanocrystalline Semiconductor Films. Modulation of Electron Transfer between Excited Ruthenium Complex and SnO2 Nanocrystallites with an Externally Applied Bias. *Journal of Physical Chemistry* **1996,** 100, 4900-4908.

12. Kuciauskas, D.; Freund, M. S.; Gray, H. B.; Winkler, J. R.; Lewis, N. S., Electron Transfer Dynamics in Nanocrystalline Titanium Dioxide Solar Cells Sensitized with Ruthenium or Osmium Polypyridyl Complexes. *Journal of Physical Chemistry B* **2001,** 105, 392-403.

13. Barbé, C. J.; Arendsa, F.; Comte, P.; Jirousek, M.; Lenzmann, F.; Shklover, V.; Grätzel, M., Nanocrystalline Titanium Oxide Electrodes for Photovoltaic Applications. *J. Am. Ceram. Soc.* **1997,** 80, (12), 3157-3171.

14. Caramori, S.; Bignozzi, C. A., Private communication. In 2003.

15. Elliott, C. M.; Caramori, S.; Bignozzi, C. A., Indium Tin Oxide Electrodes Modified with Tris(2,2'-bipyridine-4,4'-dicarboxylic acid) Iron(II) and the Catalytic Oxidation of Tris(4,4'-di-tert-butyl-2,2'-bipyridine) Cobalt(II) *Langmuir* **2005,** 21, (7), 3022-3027.

16. Xue, D.; Elliott, C. M.; Gong, P.; Grainger, D. W.; Bignozzi, C. A.; Caramori, S., Indirect Electrochemical Sensing of DNA Hybridization Based on the Catalytic Oxidation of Cobalt (II). *Journal of the American Chemical Society* **2007,** 129, (7), 1854-1855.

17. Scott, M. J.; Nelson, J. J.; Caramori, S.; Bignozzi, C. A.; Elliott, C. M., Cis-Dichloro-bis(4,4'-dicarboxy-2,2'-bipyridine)osmium(II)-Modified Optically Transparent Electrodes: Application as Cathodes in Stacked Dye-sensitized Solar Cells. *Inorganic Chemistry (submitted for publication)* **2007**.

Chapter 5

A Consideration of the Origins of Mass Transfer Limitations in Dye-Sensitized Solar Cells Mediated by Cobalt Complexes

Abstract

The possibility of mass transfer limitations in typical cobalt-mediated DSSCs was examined from a theoretical standpoint. Although conventional electrochemical models do not predict mass transfer of cobalt(III) to be a problem, actual DSSCs are likely more complicated than standard models of relatively simple systems. Two hypotheses were developed and examined. The first supposed that catalytic "islands" on the cathode were responsible for observed photocurrents but were simply not sufficiently numerous to provide adequate surface area for cobalt(III) reduction. However, experiments using

cathodes intentionally fabricated to behave in this manner (catalytic gold nanoclusters on relatively inert FTO glass) did not support this hypothesis. The second hypothesis reasoned that diffusion of cobalt(III) through the mesoporous titania layer of the cell was hampered by the layer's small pore size, tortuosity, or both. Preliminary experiments using a modified rotating disk electrode indicate that this is very likely the case. Although further research is required to accurately quantify the effect, initial considerations and results suggest that the effective diffusion coefficient (uncorrected for porosity) of cobalt bipyridine complexes through mesoporous titania films is on the order of 1×10^{-7} cm^2 s^{-1} or less.

Introduction

By far, the most substantial result of the flow-through, two electrode study presented in Chapter 3 was that a mass transfer limitation exists at the cathode in cobalt-mediated DSSCs. Unfortunately, this conclusion was not supported by the results of the three electrode experiment detailed in Chapter 4, although some confusion still lingers as to the interpretation and validity of the data. While attempting the difficult task of reconciling mass transfer limitations without a concurrent η_{MT}, it was realized that standard electrochemical theory predicted that mass transfer should *not* be a problem in DSSCs of 4 μm thickness with 0.03 M cobalt(III). The purpose of this chapter will be to describe two possible models that may explain this behavior and to present results from preliminary experiments designed to evaluate the validity of each. Further experiments will also be suggested.

Formulation of the problem

The passage of current at an electrode is governed by the concentration profile of the redox active species in solution.[1] In the absence of convection and migration (conditions which are true in an unstirred electrochemical cell with excess supporting electrolyte – typically the case), the flux of a redox active species may be described by Fick's laws of diffusion.[1] Fick's first law relates the flux of a species O to the concentration gradient along a 1-dimensional axis perpendicular to an electrode surface:

$$-J_O(x,t) = D_O \frac{\partial C_O(x,t)}{\partial x}$$

where $J_O(x,t)$ is the flux of an oxidized species through point x at time t per second per cm^2 of area normal to the x-axis. D_O is the diffusion coefficient (units of $cm^2\ s^{-1}$) of the oxidized species and $\frac{\partial C_O(x,t)}{\partial x}$ is its concentration gradient, with x increasing away from the electrode surface.

As cell currents are known and the thickness of the DSSC may be approximated, it is possible to calculate a concentration gradient of cobalt(III) under steady state conditions by assuming a linear gradient across the cell during steady state. Using an experimentally obtained value of 5 mA cm^{-2} for the current density, assuming a relatively small and conservative value of D_O of 4 x 10^{-6}, approximating the distance between cathode and anode to be 4 μm (accurate with regards to the 4 μm spacer, but neglecting the complicated matter of diffusion within the titania layer of the photoanode), and keeping in mind the relation that flux (J_O) is equal to $\frac{i}{FA}$ for a one electron reduction (i is current, A is area, and F is the Faraday constant), it can be estimated that the cobalt(III)

concentration should only change by 0.005 M across the entire distance of the cell. As one cobalt(III) will be generated at the photoanode for every cobalt(III) reduced at the cathode, the concentration of cobalt(III) at the cathode will be reduced by the same amount that it is increased at the photoanode, meaning that the estimated cobalt(III) concentration change will be shared by both cathode and photoanode. Accordingly, the cobalt(III) concentration at the cathode will only drop by one half of 0.005 M, or 0.0025 M.

This is a very interesting result. In a 20% oxidized DSSC with 0.15 M total cobalt concentration, a drop of 0.0025 M is only a change of ~8%. In order for the current to be mass transfer limited, the cobalt(III) concentration must be driven down to practically zero at the cathode surface (i.e., a drop of 100%).[2] Even in the case of 5% oxidized solutions, the calculated concentration drop is still only a 33% decrease. Of course, these calculations only considered diffusion across the 4 μm gap created by the plastic spacer. In an actual DSSC, some degree of diffusion within the titania layer is required, although to what extent is difficult to ascertain (*vide infra*). However, even if cobalt(III) were required to diffuse through the entire thickness of the layer (typically 4 μm), the drop in concentration would only be greater by a factor of two. Even in this case, the decreases in cobalt(III) concentration would only be 16% and 66% (for 20% and 5% oxidized solutions, respectively), which is *still* not great enough to result in a diffusion-limited current. Consequently, these quick calculations predict that cobalt-mediated DSSCs should *not* exhibit a mass transfer limitation (see **Figure 1** on page 199).

Hypotheses

Considering that initial spikes in the current transients are consistently observed, the above calculation presents something of a conundrum. All explanations for this dilemma must lie in one of two categories: either the model used for the calculations is flawed or the initial current spike is not due to mass transfer limitations. The latter possibility seems unlikely, given the results of Chapter 3 and the difficulty of finding other reasonable hypotheses. Furthermore, Nusbaumer et al. observed similar current transient behavior with DSSCs mediated by their cobalt complex, which they likewise ascribed to diffusion limitations.[3,4] An alternative explanation has been proposed for qualitatively similar behavior in another type of DSSC, although its relevance to cobalt-mediated DSSCs is unlikely, given the differences in cell components, observed behavior (the current declined over ~15 minutes as opposed to hundreds of milliseconds) and the nature of the hypothesis proposed.[5]

Therefore, if the assertion that mass transfer issues exist in cobalt-mediated DSSCs is correct, it must be that the situation within the DSSC is decidedly more complex than the simple model originally considered. One likely factor, initially neglected for simplicity's sake, is the diffusion of cobalt(III) within the nanocrystalline titania layer. Considering the high degree of tortuosity within the mesoporous titania layer, it is reasonable to believe that diffusion of cobalt(III) is hindered to a significant degree within this layer. One study, conducted on the smaller I_3^- ion, found that the effective diffusion coefficient through a similar (although not identical) pressed and sintered titania membrane was nearly an order of magnitude smaller than the diffusion

coefficient through bulk solution.[6] Interestingly, another study found that the effective diffusion *of charge* through the nanocrystalline layer was not significantly hindered in I^-/I_3^- mediated DSSCs, perhaps indicating that this system conducts holes in a manner more complicated than simple diffusion.[7]

Unfortunately, consideration of diffusion within the titania layer is extremely complex. As illumination occurs from the photoanode side of the cell and the light intensity is significantly attenuated across the cell, it may be expected that the concentration of photogenerated holes (i.e., oxidized dye molecules) is highest in the interior of the titania layer (closest to the FTO substrate and farthest from the cathode).[2] Nevertheless, holes will be generated, to some degree, throughout the entire thickness of the titania layer, ostensibly requiring mass transport of cobalt(III) throughout the entire titania layer.[7] In reality, the average diffusion length of the cobalt(III) complex is probably a balance between several factors. For example, it could be expected that cobalt(III) generation (by oxidation of cobalt(II)) would be weighted towards the interior of the titania layer due to the distribution of oxidized dye, thereby increasing the average cobalt(III) diffusion distance to the cathode. On the other hand, the tortuosity of the titania layer and the greater pathlength for cobalt(II) to reach the interior may counterbalance the oxidized dye distribution and decrease the average diffusion length of cobalt(III). Accordingly, determining the impact of the titania layer on mediator performance is no simple matter.

Papageorgiou et al. developed a method for evaluating the effective diffusion coefficient of I_3^- within DSSCs which should be generally applicable to any redox mediator.[7] Unfortunately, the technique relies heavily on calculation and theory in

conjunction with experiment. Accordingly, a few assumptions are necessary and may greatly impact the final result. Nevertheless, the technique could yield a valuable estimate as to whether mass transfer through the titania is the rate-limiting factor in cobalt-mediated DSSCs.

Although this experiment has not been performed with cobalt tris(bipyridine) complexes to date, an approximate diffusion coefficient may be estimated by considering the sustainable currents in a DSSC without a plastic spacer (without a spacer, the photoanode and cathode are pressed directly against each other and therefore the distance between them is negligibly small). This is tantamount to assuming that, even with a spacer present, the bulk of the concentration change occurs within the titania layer (i.e., the gradient is much larger in this layer). Using Fick's first law as before, but this time assuming a linear concentration gradient of 0.06 M over 4 μm (a typical titania film layer thickness) and solving for D_o, a value of approximately 3×10^{-7} is calculated for DSSCs with maximum currents densities of 3-5 mA cm^{-2}. This number is about an order of magnitude smaller than typical values for diffusion through bulk solution, in agreement with the results of the I_3^- diffusion study (Kebede/Lindquist) previously mentioned.[6] However, it is only a very crude estimate, especially given the unlikely assumption of a linear concentration gradient throughout the entire thickness of the titania layer.

Nevertheless, the hypothesis that mass transfer through the titania layer may be rate-limiting in cobalt-mediated DSSCs appears to have significant merit. In particular, it allows for the concentration gradient at the cathode to be smaller than expected while simultaneously allowing the absolute concentration of cobalt(III) to be driven down to nearly zero. Barring any unforeseen effects at the cathode (*vide infra*), Fick's first law

should hold and the cobalt(III) concentration gradient must be close to that calculated earlier for typical current densities (5 mA cm^{-2}). With a significantly smaller effective diffusion coefficient through the titania layer, the concentration gradient may be dramatically larger than would otherwise be the case. As illustrated in **Figure 1**, this allows the cobalt(III) concentration to be driven down to practically zero at the cathode, which is required if the diffusion of cobalt(III) is to be rate-limiting in these cells.

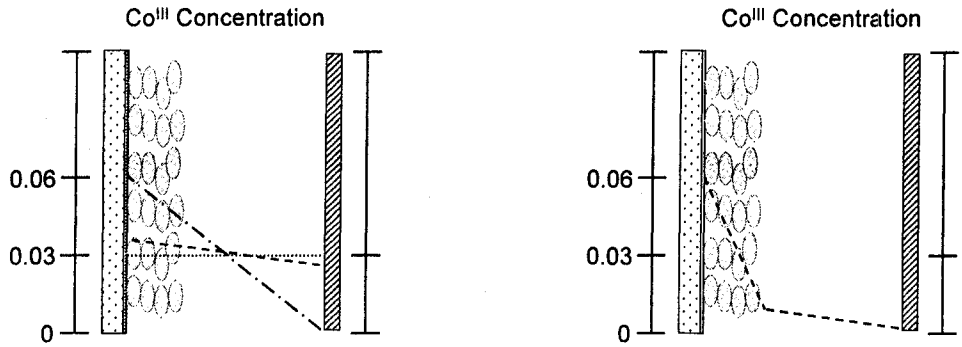

Figure 1. Diagrams illustrating possible concentration profiles of cobalt(III) in DSSCs if *(left)* the effective diffusion constant is continuous throughout the cell and *(right)* the effective diffusion constant is dramatically smaller through the TiO_2 layer. *Left figure:* profile in the dark (dotted line), during operation, according to Fick's law estimate (dashed line), required gradient for mass transport limitations during operation (dotted/dashed line). *Right figure:* estimated profile, note that the concentration gradient at the cathode is the same as in left figure (dashed line), but the concentration is much lower. *Both figures:* concentration axis is in molarity.

An alternative hypothesis is that the cathode surface is not uniform with regards to the reduction of cobalt(III) complexes. Fick's first law assumes a planar, uniform electrode surface so that only diffusion away from the cathode (i.e., along the x-axis) needs to be considered.[1] If, however, the surface is not uniform, then diffusion along the y- and z-axes may be relevant and may contribute to mass transfer effects which would not otherwise be predicted. As mentioned in the introductory chapter, a variety of observations have indicated that the electrochemical reduction of cobalt(III) bipyridine

complexes may be best thought of as a catalytic process. If true, then the inhomogeneity of the cathode surface may be manifested as regions which are highly catalytic towards the reduction of cobalt(III) complexes (characterized by very fast heterogeneous electron transfer characteristics) and regions which are much less catalytic. The end result of which may be that the effective surface area of the cathode is much smaller than the actual surface area, a situation which could certainly lead to mass transfer limitations even in configurations with small interelectrode distances.

Although this hypothesis was originally conceived as a thought experiment, there are reasons to suspect that only a small portion of the cathode is actually catalytic to cobalt(III) reduction. Firstly, as discussed at length in the introductory chapter, the electrochemical behavior of cobalt complexes is notably unconventional and clearly surface dependent. Indeed, if their behavior were not so unusual, cobalt complexes would almost certainly be very poor mediators in DSSC. Accordingly, it makes little sense to treat the cathode as a traditional electrode surface *a priori* when considering cobalt(III) behavior. Furthermore, preliminary experiments using a novel laser scanning system to probe localized iV characteristics in DSSCs (somewhat analogous to scanning, electrochemical microscopy, or SECM), performed by Scott and coworkers, indicate that the current profile across the illuminated area is often not uniform when gold cathodes are used in cobalt-mediated DSSCs.[8] In particular, regions of significantly more current were frequently found. While it was not possible to deconvolute the influence of the photoanode from that of the cathode in this scanning laser experiment, it certainly provides credibility to the possibility that the cathode is not uniformly catalytic to cobalt(III) reduction.

Reduced surface area experiments

One approach to evaluate whether catalytic zones on the cathode can result in the DSSC behavior typically observed with standard cathodes is to intentionally fabricate cathodes with such characteristics. If these cathodes, with deliberately reduced surface areas, behaved similarly to standard gold cathodes, then it would seem highly likely that the surface of standard gold cathodes is also only partially active.

Fortunately, the research group of Professor Prieto contains expertise with a standard technique for controllably depositing gold nanoclusters onto silica surfaces. With this technique, gold nanoclusters (with an average diameter of ~30 nm) are electrostatically attracted to a thin film of poly(lysine) previously applied to the silica surface. The electrode is baked in an oven to remove the organic componenents, leaving a silica surface with nanometer-sized regions of gold. Depending on conditions used, the coverage of the surface may be easily varied from 1-2 nanoclusters per micron to a maximum of 10-15. Assuming that the poly(lysine) would likewise adhere to the oxide surface of FTO (a very probable assumption), this technique presented a route to FTO cathodes with surfaces comprising large regions of FTO on the surface (inactive to cobalt(III) reduction) and small, catalytic islands of gold. This provided an ideal platform for testing the possibility that the surface of standard gold cathodes are only partially active.

Electrochemistry through titania films

In order to investigate the possibility that diffusion of cobalt(III) through the titania film was unusually slow and thereby limiting DSSC performance, a means of characterizing the effective diffusion constant through the film was desired. Multiple electrochemical techniques are, at least in principle, well-suited for the task and, in some cases, may yield very accurate, quantitative values for the diffusion coefficient. Initially, however, a relatively simple experiment was desired which would qualitatively indicate whether or not diffusion through the film is hindered with respect to free stream diffusion through bulk solution. Rotating disk electrochemistry was chosen.

Rotating disk electrochemistry is a hydrodynamic (i.e., utilizing stirring) technique which uses a rotating disk electrode (RDE) to both stir the solution and act as the working electrode.[1] Its primary advantage lies in the fact that laminar flow across the RDE surface occurs upon stirring and results in a undisturbed layer of solution between the electrode surface and the bulk solution (the "hydrodynamic boundary layer") of predictable thickness. The hydrodynamic boundary layer thickness, δ, is a function of rotation rate and as such may be reliably controlled. When the surface of an RDE is covered by a electrochemically inert, permeable membrane (such as a nanocrystalline titania film at positive potentials), two unstirred layers result: the region within the film and a region outside the film known as the hydrodynamic boundary layer. If a change in potential at the RDE is accompanied by a change in the equilibrium concentrations of an electroactive species (e.g., species O is reduced to R), current will pass and a diffusion layer will grow from the RDE surface. Once the diffusion layer reaches the stirred solution (traversing across both the film and the hydrodynamic boundary layer), steady-

state conditions will develop as the bulk concentrations of O and R are maintained within the stirred solution. The time for the system to reach steady-state therefore depends on both the titania film thickness and δ. If both thicknesses are known, then the time for an RDE system to reach equilibrium can yield valuable information about the rate of diffusion across both layers.

Experimental

Gold nanocluster cathodes

FTO electrodes (approximately 2 cm^2 in area) were rigorously cleaned using the following procedure. They were soaked for 30-60 minutes in a base bath, rinsed with distilled water, sonicated in an aqueous solution of Alconox detergent for 15 minutes, rinsed with Millipore water, sonicated in electronics grade isopropanol for 15 minutes, blown dry with a stream of nitrogen and finally treated with an air plasma for 45 minutes or greater. Once clean, poly(lysine) (Poly-L-Lysine, 0.1% w/v, Ted Pella) was applied using a drop-coating type procedure. A few drops of poly(lysine) solution were delivered to the horizontal FTO substrate, allowed to stand for one minute and carefully removed by diluting with distilled, deionized water and subjecting the substrate to a gentle stream of nitrogen. The FTO substrate was allowed to stand for at least five minutes until fully dry. A few drops of a colloidal dispersion of gold nanoclusters in water (30 nm average diameter, 0.24 nM, Ted Pella) was applied and allowed to stand for a variable period of time, ranging from approximately 5 seconds to 10 minutes. Although the relationship is clearly not linear, longer periods of time generally result in increased gold loading on the surface, although saturation apparently does occur as no further increases were observed

in periods greater than 10 minutes. After the appropriate time, the gold colloid was very gently blown off of the substrate using a light nitrogen stream. Finally, the cathodes were baked at 450 °C for 1 hour. Characterization of the cathodes before and after the bake was performed using scanning electron microscopy (SEM).

Testing of cathodes

Testing of cathodes was done by performing a series of experiments on a DSSC sandwich cell utilizing the cathode, a standard titania photoanode, a 4 μm spacer and a mediator solution containing $Co(dtb)_3(ClO_4)_2$ (oxidized to either 5% or 20% using previously oxidized-in-bulk $Co(dtb)_2(ClO_4)_3$) and 0.2 M lithium triflate. Photoanode fabrication, cell assembly, and testing were all conducted as described in Chapter 3.

Rotating disk elecrode (RDE) fabrication

A RDE, modified so as to comprise a typical 4 μm titania layer and an electroactive FTO surface (see **Figure 2**), was fabricated in the following manner. A standard photoanode (prepared as described in previous chapters, but broken to minimize the area of the uncovered "half") was covered with a thin (~15 μm) piece of polyethylene, sized to cover the entire titania layer but with a hole cut in the center (roughly circular with a diameter of approximately 5 mm). A piece of Teflon® non-adhesive tape (Saunders Corp. Teflon® Tape 5-111, 0.005" thick) was placed over the anode (to prevent adhesion of the polyethylene to the microscope slide), covered by a microscope slide, and the whole assembly (anode-polyethylene-Teflon®-glass) was clamped together and placed in an oven at ~190 °C for 5-10 minutes. Afterwards, the

assembly was removed from the oven and taken apart. The photoanode, with the melted polyethylene firmly affixed and covering all but the center of the titania, was glued to a commercially-made RDE (Pine Instruments) using Torr Seal® high vacuum grade, two-part epoxy. A small wire was attached to the FTO portion of the anode using conductive silver paint and Torr Seal® was used to cover all of the exposed conductive surfaces at the anode (excepting the circular region of titania in the center of the anode). The other end of the wire was attached to the upper contact of the RDE using silver paint and the entire wire was wrapped securely to the RDE shaft using standard, "pipe-thread type" Teflon® tape.

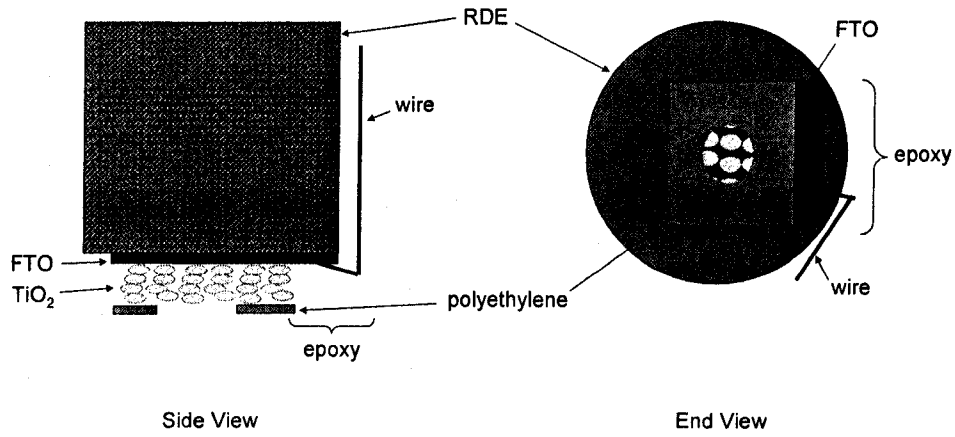

Figure 2. Two views of the tip of the modified RDE.

RDE experiments

RDE experiments were conducted using a Pine Instruments Analytical Rotator with modified and unmodified rotating disk electrodes (Pine Instruments). A specially designed electrochemical cell (previously made in-house[9]), containing two chambers separated by a glass frit, was used to prevent reduced material at the platinum counter

electrode from contaminating the working electrode (RDE). The cell also contained a fixed silver wire for use as a quasi-reference. The electrolyte solution consisted of 0.1 M $TBAPF_6$ and approximately 0.25 mM $Fe(terpy)_2(ClO_4)_2$, where TBA = tetra(*n*-butyl)ammonium and terpy = 2,2':6',2''-terpyridine. A BAS 100 B Potentiostat-Galvanostat controlled by BAS 100 W software on a personal computer was used to perform cyclic voltammetric and chronoamperometric experiments.

Results/Discussion

Reduced surface area experiments

Cathodes were prepared which possessed a significantly reduced surface area of gold in order to examine whether the surface of regular gold cathodes is only partially active towards the reduction of cobalt(III). Cathodes consisting of gold nanoclusters sporadically distributed across a FTO substrate were fabricated with two different gold loadings: "light" (average of 1-2 clusters per 1 μm^2) and "heavy" (approximately 10 clusters per μm^2). Very roughly, light loadings correspond to 0.3% of the total surface being covered by gold, with heavy loadings estimated at approximately 1.4% surface coverage. **Figure 3** shows a typical SEM micrograph of a heavily loaded cathode.

DSSC cell experiments were conducted using these cathodes and cobalt mediators. Representative iV curves are shown in **Figure 4** (left). Quite clearly, photocurrents are much reduced in the cells with the gold nanocluster cathodes in comparison to the cell with a regular gold cathode. The corresponding current transients are also shown for these cells (**Figure 4**, right). As can be seen, the height of the initial current spike relative to the steady state current was approximately the same in all cases.

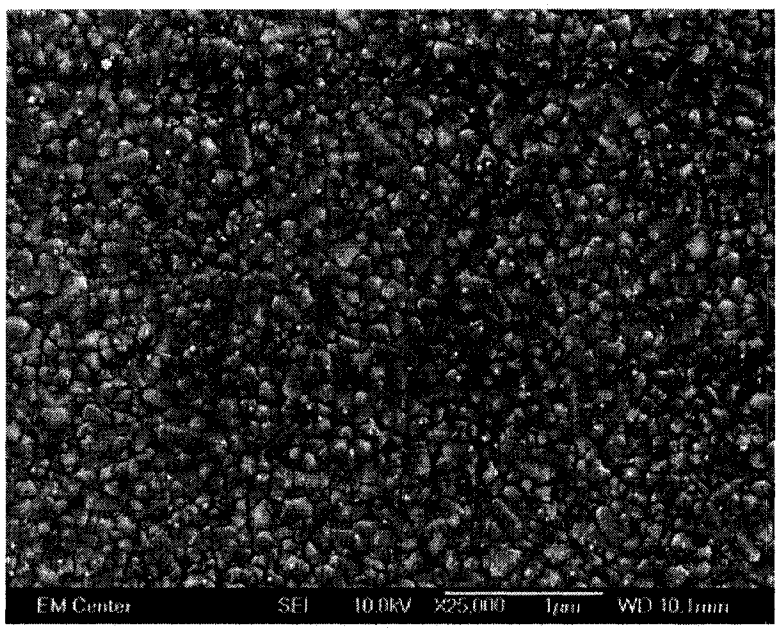

Figure 3. SEM micrograph of a "heavily" loaded FTO cathode with gold nanoclusters. The gold nanoclusters are the white spheres in the image. Scalebar is 1 μm.

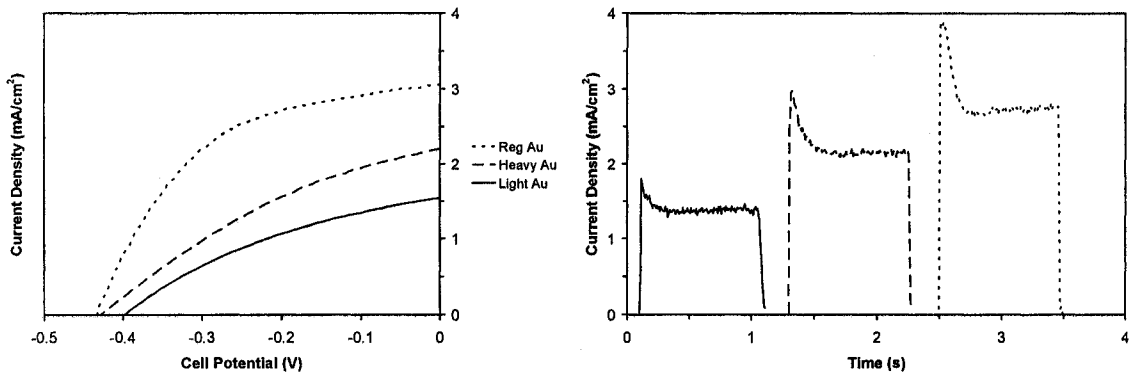

Figure 4. Results of DSSC experiments with gold nanocluster cathodes. Cobalt solution was 0.15 M total cobalt complex (5% oxidized) and a 4 μm spacer was employed.

Two major points are clearly illustrated by these experiments. Firstly, even when the active area of the cathode is reduced to 0.3% of normal, the cell current is only reduced by a factor of 2 or 3. The remarkably disproportionate current decrease may indicate that the surface of regular gold cathodes (completely covered by gold) is actually

only partially active in the reduction of cobalt(III). Alternatively, it may be that cell currents are typically so low that only small active areas are needed, meaning that reductions in surface area must be particularly dramatic to display any effect whatsoever. Secondly, if the current spike is caused by insufficient cathode surface area, decreasing the surface area would be expected to exacerbate the effect. Clearly, this is not the case, as the current spike is unchanged by lowering the active surface area. Considering these two points, it seems most likely that the current spike is *not* due to a scarcity of active cathode area, regardless of whether or not the typical gold cathodes are active on their entire surface.

Split photoanode experiments

As the reduced area cathodes presented an intermediate case (less photocurrent than gold cathodes but more than bare FTO) not previously available, three electrode/split photoanode experiments were conducted using the lightly loaded gold nanocluster cathode. These experiments were conducted exactly as described in Chapter 4, using a 4 μm spacer, 0.15 M total cobalt complex (5% oxidized) and 0.2 M lithium triflate. The results are shown below in **Figure 5**.

As previously observed, photocurrents were reduced with the gold nanocluster cathode by a factor of approximately two (keeping in mind that the area is not strictly controlled). Interestingly, the potential difference between short and open circuit (i.e., the overpotential on the cathode) is only ~15 mV, surprisingly small considering the dramatic effect of the cathode on current. In agreement with previous results, the regular gold cathode experienced no potential change during the experiment.

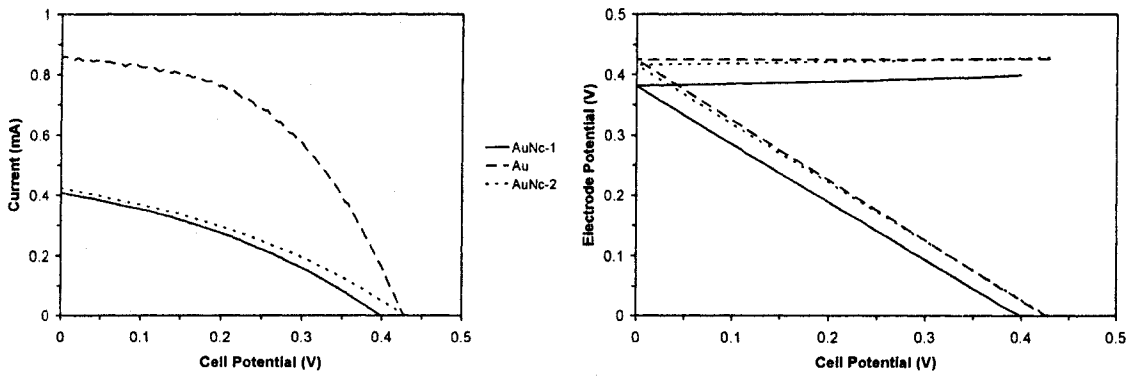

Figure 5. Split photoanode experiments using a reduced area gold nanocluster cathode (AnNc) and a regular gold cathode (Au). "AuNc-1" and "AuNc-2" refer to the first and second cell assembly using the same AuNc cathode. All assemblies used the same photoanode and were conducted in the order: AuNc-1, Au, AuNc-2.

Although the discussion presented in the previous chapter still stands, these experiments, in conjunction with the results of bare FTO and osmium-modified FTO, may suggest that surprisingly small overpotentials (< 15 mV) greatly affect the current characteristics of the DSSC. In the case of platinum (which generally exhibits a poorer FF), the overpotential may be so small as to be beyond the detection limit of the experiment, perhaps due to the electrode arrangement within split photoanode cells. Further confounding the issue is that, so far, only *charge transfer* overpotentials (specific to the cathode material) seem to be at all observable. Mass transfer overpotentials still seem completely undetectable to the split photoanode technique, as no mass transfer limited cases (cells with 25 μm spacers and presumably most cells with gold cathodes, *vide infra*) have displayed any overpotential in these experiments. The reason for such selectivity remains in question.

Diffusion through titania films

Given the findings of the reduced area cathode experiments, the most probable explanation for the apparent mass transfer limit in cobalt-mediated DSSCs was that diffusion through the mesoporous titania was rate limiting. In order to lend credence to this hypothesis, RDE experiments were conducted in an effort to qualitatively evaluate whether the diffusion constants of metal bipyridine species are suppressed within titania films.

A modified RDE was constructed which was essentially a spinning photoanode possessing a reduced area of titania-covered FTO – all other conductive surfaces were covered by an insulating material. In order to properly measure the diffusion coefficient through the film, it was necessary to ensure that the electroactive species traversed the entire thickness of the film. In our system, this was easily accomplished by selectively using positive potentials so that only the FTO surface (or regions of the titania film *very* close to it) was electrochemically active (titania is insulating except at potentials negative of its flatband potential).[10, 11] However, it was necessary to replace the cobalt complex with another metal species of comparable size but faster heterogeneous electron transfer kinetics on FTO (cobalt mediators are practically inert on FTO). $Fe(terpy)_3(ClO_4)_2$ is fairly close in size – admittedly, it is lacking the bulky *tert*-butyl groups of the $Co(dtb)_3(ClO_4)_2$ – and exhibits very reversible (i.e. fast) electron transfer kinetics on FTO. Hence, this iron complex was chosen.

RDE experiments with an unmodified, glassy carbon RDE were performed for comparison purposes. Two cyclic voltammograms using this electrode are shown in **Figure 6**. The stirred solution voltammogram is nearly identical to that of the unstirred

solution for the first part of the scan (beginning at 500 mV until ca. 1100 mV) but then deviates significantly. The deviation is due to the point in time where the diffusion layer had crossed the hydrodynamic boundary layer and reached the stirred solution. At this point, a steady-state concentration gradient was reached and the faradaic current leveled off (ignoring charging current).

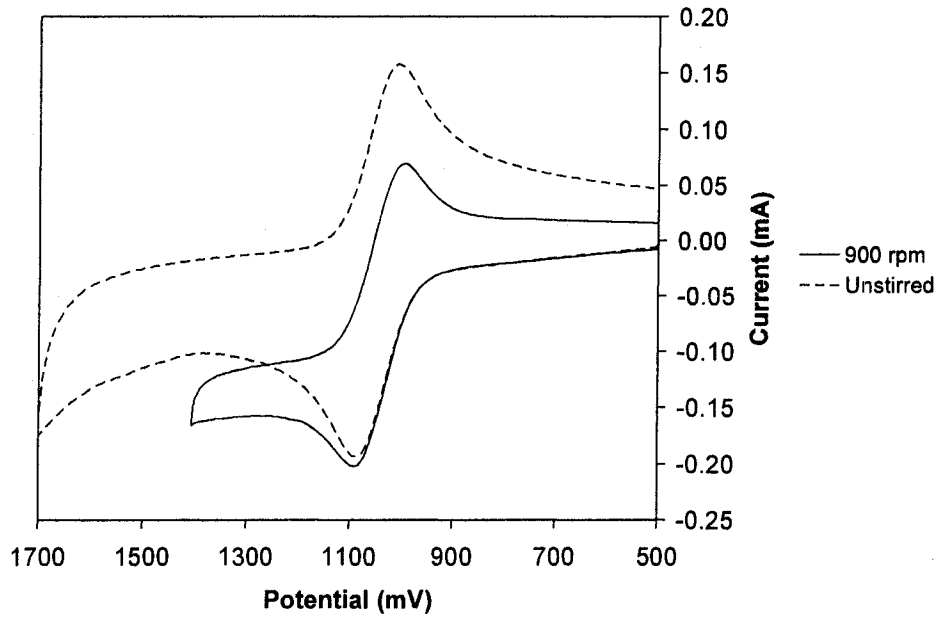

Figure 6. Cyclic voltammograms of stirred (at 900 rpm) and unstirred RDE experiments using an unmodified glassy carbon disk working electrode and $Fe(terpy)_3(ClO_4)_2$. Scan rate was 1000 mV s^{-1}. Potentials have been shifted to account for the drifting potential of the silver wire quasi-reference.

The time elapsed from onset of faradaic current (occurring at approximately 900 mV) to the point where the slope of the stirred solution voltammogram begins to deviate from the unstirred (~1135 mV) can be calculated by dividing the voltage change (235 mV) by the scan rate (1000 mV/s). The resulting time (0.235 seconds) can be used to estimate the thickness of the hydrodynamic boundary. Using the one-dimensional

random-walk model (" the drunken sailor problem"), the thickness of the diffusion layer can be estimated by the root-mean-square equation:

$$l = \sqrt{2Dt}$$

where l represents the diffusion layer thickness, D is the diffusion coefficient in units of $cm^2\ s^{-1}$, and t is time in seconds.[1] Using the observed time of 0.235 seconds and a standard diffusion coefficient of 1×10^{-5} (a reasonable assumption as the diffusion coefficient for $Co(dtb)_3(ClO_4)_2$ has been experimentally determined to be very nearly this value[12]), a value of 22 μm is calculated. Although the root-mean-square equation is not exact, it provides a good approximation for the thickness of the diffusion layer when it came into contact with the stirred solution.

This value should also correspond to δ, the thickness of the hydrodynamic boundary. Accordingly, a calculation of δ can serve to cross-check the previous calculation by using the equation:

$$\delta = 1.61 D_O^{1/3} \omega^{-1/2} \nu^{1/6}$$

where D_O is the diffusion coefficient of species O, ω is the angular frequency of rotation (s^{-1}) and ν is the kinematic viscosity of the solvent ($cm^2\ s^{-1}$).[1] Using the same value for D as before, 0.0045 for the kinematic viscosity of acetonitrile with 0.1 M supporting electrolyte and converting the stirring rate (900 rpm) into angular frequency ($\omega = 2\pi 900/60$), a value of 21 μm is obtained. This is in good agreement with the value calculated by the root-mean-square approximation and demonstrates the usefulness of cyclic voltammetry with a RDE to estimate diffusion layer characteristics.

Figure 7 displays cyclic voltammograms collected using the modified RDE at the same stir rate as before (900 rpm). As can be seen, very little difference exists between

the stirred and unstirred voltammograms (excepting the periodic noise in the stirred voltammogram due most likely to suboptimal electrical contact with the RDE), indicating that the diffusion layer did not extend past the hydrodynamic boundary layer on the timescale of the experiment. In these voltammograms (stirred and unstirred), the scan rate was 500 mV s^{-1}. As the onset of faradaic current is at roughly 900 mV and the positive sweep ended at just over 1600 mV, 1.4 seconds elapsed (700 mV divided by 500 mV s^{-1}) without the diffusion layer reaching the stirred solution.

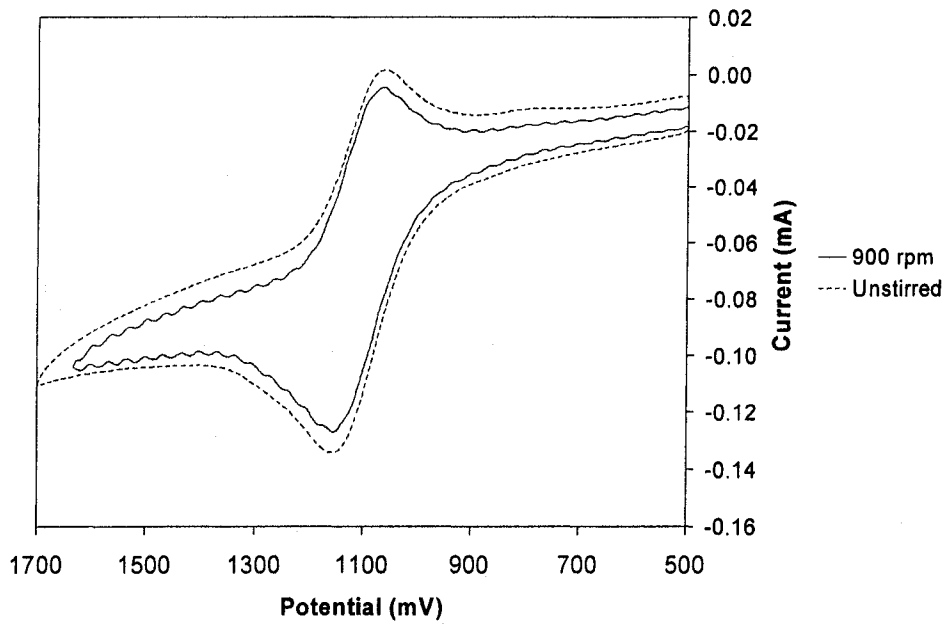

Figure 7. Cyclic voltammograms of stirred (at 900 rpm) and unstirred RDE experiments using a modified titania-on-FTO working electrode and $Fe(terpy)_3(ClO_4)_2$. Scan rate was 500 mV s^{-1}. Potentials have been shifted to account for the drifting potential of the silver wire quasi-reference.

This is a very noteworthy result. For a rotating electrode with a non-electroactive, porous film covering an electroactive surface, steady state should be reached once the diffusion layer reaches a thickness equal to the film thickness plus δ.[1] In this case, the

titania film thickness was 4 μm and δ was approximately 21 μm, assuming that the modified electrode surface (not perfectly planar) behaved similarly to the more nearly ideal unmodified RDE. Therefore, in comparison to the unmodified RDE, the diffusion layer of the modified RDE at steady state should be about 25% larger. Accordingly, everything else being equal, the time to reach steady state should have been increased by 56% ($l \alpha t^{1/2}$ in the root-mean-square equation). As steady state was reached in 0.235 seconds for the unmodified RDE, only 0.37 seconds should have been required for the modified RDE. Instead, even after 1.4 seconds, the modified RDE had still not attained a steady state. Clearly, this indicates that something is different with this electrode.

Barring any unforeseen and undesirable effects of the slightly less-than-ideal electrode surface (*vide infra*), this result almost certainly indicates that the diffusion constants of metal polypyridine complexes inside the mesoporous titania film are significantly less than in bulk solution. After all, the thickness of the diffusion layer is a function of time and diffusion constant only – so any variations in the thickness must be due to variations in the diffusion constant. Although the experiment is not rigorous enough to confidently extract a value for the diffusion constant, it qualitatively indicates that the actual value within the mesoporous film is significantly lower than in bulk solution. Furthermore, this experiment lends support to the hypothesis that mass transfer of cobalt(III) is frequently rate-limiting in operating DSSCs.

Admittedly, the surface of the modified electrode was not perfectly planar (crucial to predictable laminar flow characteristics), but it is unlikely that conditions were so far from ideal as to so dramatically alter the time needed to reach steady state. Nevertheless, it must be remembered that the polyethylene insulator was approximately 15 μm thick

originally (after baking at 190 °C, the plastic appeared to have melted and thinned somewhat). As the hole in the plastic was roughly 5 mm in diameter, it is likely that the insulator only significantly increased the hydrodynamic boundary layer at the edges, but it clearly would have had some effect (**Figure 8**). Also potentially problematic is the fact that, at the edge of the electrode, Torr Seal® disrupted the otherwise smooth surface, protruding by as much as a few millimeters past the electrode surface. Although the flow appeared laminar (no obvious bubbles, vortex, or disturbance) at the electrode surface, it is difficult to estimate the degree to which the Torr Seal® irregularity disrupted the normally very predictable flow profile.

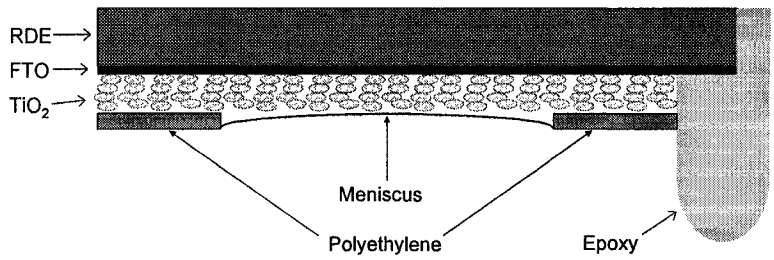

Figure 8. Side view of the tip of the modified RDE showing possible influences on the flow profile across the surface. Note that this is not to scale. Actual thicknesses were approximately: TiO_2 (4 μm), polyethylene (10-15 μm), epoxy (2-3 mm).

For the sake of argument, it could be assumed that the non-ideal surface of the RDE was completely responsible for the delay in reaching steady state due to an unexpectedly large hydrodynamic boundary layer thickness. In this case, the actual thickness of the film plus δ can be estimated. In an effort to better quantify the time needed to reach steady-state, voltammetry experiments were conducted at slower scan rates. Unfortunately, although the effects of stirring could be seen at low scan rates (250 mV s^{-1} or less), it was difficult to reliably determine the point when the diffusion layer

reached the stirred solution. Probably, this is due to a non-uniform thickness of δ across the electrode surface caused by the slight protrusion of the polyethylene layer. Nevertheless, a lower limit for the hydrodynamic boundary layer thickness can be estimated by assuming that steady state would have been reached just after the region observed in the cyclic voltammogram shown in **Figure 7**. In this case, assuming an unaltered diffusion coefficient and that the time needed to reach steady state was 1.4 seconds or greater, δ must have been 53 μm or greater.

This result is only a factor of two larger than the value predicted for an ideal RDE system and is therefore not wholly out of the realm of possibility, especially given the imperfect surface of the modified RDE. However, this is a lower limit to the possible thickness. Furthermore, assuming a meniscus-shaped hydrodynamic boundary layer (due to the polyethylene layer, **Figure 8**), the calculated distance of 53 μm corresponds to the thinnest portion of the layer, the point the diffusion layer would have reached first. Lying in the center of the exposed titania film, this point is least likely to have been affected by the polyethylene film and therefore least likely to deviate dramatically from the predicted hydrodynamic boundary layer thickness.

Considering these two points, it seems unlikely that the imperfections of the RDE are great enough to offset the experimental result that diffusion through mesoporous titania is dramatically slow. An upper boundary to the diffusion constant can be approximated by again using 1.4 seconds (from **Figure 7**) and assuming that the hydrodynamic boundary layer thickness was the same as observed with the glassy carbon RDE, which required 0.235 seconds for the diffusion layer to traverse. With the modified RDE, the extra time needed to reach steady state (~1.15 s) is due to the movement of the

diffusion layer through the 4 μm thick titania film. Inserting 1.15 s and 4 μm into the root-mean-square equation, a diffusion constant of 7×10^{-8} cm^2 s^{-1} is calculated. As the time to reach steady state was a lower estimate, 7×10^{-8} is an upper estimate to the diffusion constant of metal polypyridines through the mesoporous titania layer.

Conclusions/Future Work

After further consideration and experimentation, the results detailed in this chapter support the hypothesis that the mass transfer of cobalt(III) complex may frequently be limiting the performance of DSSCs mediated by cobalt compounds. As described in Chapter 3, the current spike commonly witnessed in current transients of cobalt-mediated DSSCs is clearly affected by solution viscosity and cobalt(III) concentration, consistent with this hypothesis. Although a mass transfer limitation would not be expected for a simple thin layer cell of 4 μm under the same conditions, further work has shown that the mesoporous nature of the titania film very likely complicates diffusion across this layer. In particular, preliminary experiments conducted using a RDE modified to comprise an electroactive FTO surface covered by a mesoporous titania film indicate that diffusion is dramatically slowed for metal polypyridine complexes, perhaps by as much as 2-3 orders of magnitude. Qualitatively, this result agrees with the work of Kebede and Lindquist, who found that the diffusion constant of I_3^- is decreased by about an order of magnitude through roughly similar titania membranes.[6] Furthermore, it has been demonstrated in this chapter that a mass transfer limitation arising from a lack of catalytic sites on the cathode is unlikely.

Additional experiments are warranted in order to quantify and further substantiate the mass transfer limitation of cobalt-mediated DSSCs. The RDE experiments detailed in this chapter were only preliminary. In particular, questions remain regarding the flow profile across the irregular and non-planar surface of the modified RDE. As discussed, it appears unlikely that the profile was altered to the extent that the conclusions regarding the diffusion coefficient are wrong, but extraction of a reliable value from the data is likely not possible at present. The estimated value of 7×10^{-8} (an upper limit) is relatively close to that predicted by the consideration of actual currents observed in DSSCs (3×10^{-7}) as discussed in the introduction to this chapter. Considering that the latter number was arrived at under the assumption of a linear concentration gradient across the titania layer (unlikely, as discussed), the two numbers are actually in fairly good agreement. Nevertheless, future work should be directed towards electrochemical experiments designed to more accurately determine the value of the effective diffusion coefficient through mesoporous titania films.

Several methods may be envisioned. Obviously, initial efforts should be directed towards the fabrication of a more planar RDE. The rotating disk experiment has been shown to be promising in this regard and if the flow profile can be improved, then it should be possible to more reliably extract a value for the diffusion coefficient. Alternatively, thin cell experiments offer an conceptually simpler method by which to control the thickness of the unstirred portion of the bulk solution (i.e., the thin layer cell equivalent to the hydrodynamic boundary layer thickness). Through the use of a spacer and a regular (or modified) DSSC sandwich cell configuration, the two thicknesses of the titania and bulk solution layers may be easily controlled. In point of fact,

chronoamperometry on a thin layer cell was briefly attempted before switching to the RDE experiments. For reasons not entirely clear (possibly due to less than ideal electron transfer kinetics on the titania-covered gold electrode), the experiments were not successful. Future work on thin layer cells is advised, as they could very well provide a second reliable means to confirm future values for the diffusion coefficient of metal polypyridine complexes. Thirdly, the experimental/theoretical technique developed by Papageorgiou and coworkers provides a method to more accurately account for the influence of porosity on the effective diffusion coefficient and is therefore also recommended.[7]

Lastly, in the event that mediator transport is proven to be rate-limiting, the challenge will be to alleviate the problem. As proposed in Chapter 3, finding a less viscous solvent in which cobalt(III) complexes are soluble is an obvious first approach. Other strategies are less obvious. In principle, creation of a thin cobalt layer on the surface of the photoanode (serving to control the electron transfer kinetics at the titania surface) could allow for the use of a second redox couple, one with faster diffusion through mesoporous titania, to shuttle the photogenerated hole through the film to the cathode. However, as detailed in Chapter 2, creation of a thin cobalt layer on the photoanode surface is a formidable challenge. Another strategy is to alter the morphology of the nanocrystalline titania in such a way as to facilitate faster ionic transport through the film. Ordered mesoporous films and titania nanorods offer two ways in which the pores may be aligned to provide more direct, less tortuous paths through the titania layer.[13-18] Increasing the average pore size may also increase the effective diffusion coefficient through the film.

Whatever the best solution turns out to be, the cobalt-mediated DSSC is clearly a very complex system with a variety of parameters which have not yet been optimized. With so many variables and so many possibilities, it is impossible to say whether this type of solar cell will ever become commercially viable. But clearly, regardless of the outcome, much can be learned from its study regarding surface-dependent electron transfer kinetics, diffusion through porous films, and thin layer electrochemistry in general.

Bibliography

1. Bard, A. J.; Faulkner, L. R., *Electrochemical Methods : fundamentals and applications*. 2nd ed. ed.; John Wiley & Sons, Inc.: 2001.

2. Papageorgiou, N.; Liska, P.; Kay, A.; Grätzel, M., Mediator Transport in Multilayer Nanocrystalline Photoelectrochemical Cell Configurations. *Journal of the Electrochemical Society* **1999,** 146, (3), 898-907.

3. Nusbaumer, H.; Moser, J.-E.; Zakeeruddin, S. M.; Nazeeruddin, M. K.; Grätzel, M., $Co^{II}(dbbip)_2^{2+}$ Complex Rivals Tri-iodide/Iodide Redox Mediator in Dye-Sensitized Photovoltaic Cells. *Journal of Physical Chemistry B* **2001,** 105, 10461-10464.

4. Nusbaumer, H. Alternative Redox Systems for the Dye-Sensitized Solar Cell. Doctor of Philosophy, École Polytechnique Fédérale de Lausanne, Lausanne, 2004.

5. Robel, I.; Subramanian, V.; Kuno, M.; Kamat, P. V., Quantum Dot Solar Cells. Harvesting Light Energy with CdSe Nanocrystals Molecularly Linked to Mesoscopic TiO_2 Films. *Journal of the American Chemical Society* **2006,** 128, 2385-2393.

6. Kebede, Z.; Lindquist, S.-E., The obstructed diffusion of the I_3^- ion in mesoscopic TiO_2 membranes. *Solar Energy Materials & Solar Cells* **1998,** 51, 291-303.

7. Papageorgiou, N.; Barbé, C.; Grätzel, M., Morphology and Adsorbate Dependence of Ionic Transport in Dye Sensitized Mesoporous TiO_2 Films. *Journal of Physical Chemistry B* **1998,** 102, 4156-4164.

8. Scott, M. J.; Woodhouse, M.; Parkinson, B. A.; Elliott, C. M., submitted for publication. *Journal of the Electrochemical Society* **2007**.

9. Salzer, C. A. Ion transport, sensing applications, and redox gradient formation : an electrochemical study of electronically conducting polymers. Colorado State University, Fort Collins, 2002.

10. Gregg, B. A.; Pichot, F.; Ferrere, S.; Fields, C. L., Interfacial Recombination Processes in Dye-Sensitized Solar Cells and Methods To Passivate the Interfaces. *Journal of Physical Chemistry B* **2001,** 105, 1422-1429.

11. Zaban, A.; Meier, A.; Gregg, B. A., Electric Potential Distribution and Short-Range Screening in Nanoporous TiO_2 Electrodes. *Journal of Physical Chemistry B* **1997,** 101, 7985-7990.

12. Elliott, C. M.; Caramori, S.; Bignozzi, C. A., Indium Tin Oxide Electrodes Modified with Tris(2,2'-bipyridine-4,4'-dicarboxylic acid) Iron(II) and the Catalytic Oxidation of Tris(4,4'-di-tert-butyl-2,2'-bipyridine) Cobalt(II) *Langmuir* **2005,** 21, (7), 3022-3027.

13. Wu, C.-W.; Ohsuna, T.; Kuwabara, M.; Kuroda, K., Formation of Highly Ordered Mesoporous Titania Films Consisting of Crystalline Nanopillars with Inverse Mesospace by Structural Transformation. *Journal of the American Chemical Society* **2006,** 128, 4544-4545.

14. Adachi, M.; Murata, Y.; Okada, I.; Yoshikawa, S., Formation of Titania Nanotubes and Applications for Dye-Sensitized Solar Cells. *Journal of the Electrochemical Society* **2003,** 150, (8), G488-G493.

15. Zukalová, M.; Zukal, A.; Kavan, L.; Nazeeruddin, M. K.; Liska, P.; Grätzel, M., Organized Mesoporous TiO_2 Films Exhibiting Greatly Enhanced Performance in Dye-Sensitized Solar Cells. *Nano Letters* **2005,** 5, (8), 1789-1792.

16. Jiu, J.; Isoda, S.; Wang, F.; Adachi, M., Dye-Sensitized Solar Cells Based on a Single-Crystalline TiO_2 Nanorod Film. *Journal of Physical Chemistry B* **2006,** 110, 2087-2092.

17. Tang, J.; Wu, Y.; McFarland, E. W.; Stucky, G. D., Synthesis and photocatalytic properties of highly crystalline and ordered mesoporous TiO_2 thin films. *Chem. Commun.* **2004**, 1670-1671.

18. Kato, T.; Hayase, S., Quasi-Solid Dye Sensitized Solar Cell with Straight Ion Paths. *Journal of the Electrochemical Society* **2007,** 154, (1), B117-B121.